

2011

Self-healing polymers - the importance of choosing an adequate healing monomer, and the olefin metathesis polymerization of agricultural oils

Timothy C. Mauldin
Iowa State University

Follow this and additional works at: <https://lib.dr.iastate.edu/etd>

 Part of the [Chemistry Commons](#)

Recommended Citation

Mauldin, Timothy C., "Self-healing polymers - the importance of choosing an adequate healing monomer, and the olefin metathesis polymerization of agricultural oils" (2011). *Graduate Theses and Dissertations*. 10299.
<https://lib.dr.iastate.edu/etd/10299>

This Dissertation is brought to you for free and open access by the Iowa State University Capstones, Theses and Dissertations at Iowa State University Digital Repository. It has been accepted for inclusion in Graduate Theses and Dissertations by an authorized administrator of Iowa State University Digital Repository. For more information, please contact digirep@iastate.edu.

**Self-healing polymers – the importance of choosing an adequate healing monomer, and
the olefin metathesis polymerization of agricultural oils**

by

Timothy C. Mauldin

A dissertation submitted to the graduate faculty
in partial fulfillment of the requirements for the degree of

DOCTOR OF PHILOSOPHY

Major: Chemistry

Program of Study Committee:
Michael R. Kessler, Co-Major Professor
Malika Jeffries-EL, Co-Major Professor
Aaron D. Sadow
Javier Vela
Arthur H. Winter

Iowa State University

Ames, Iowa

2011

Copyright © Timothy C. Mauldin, 2011. All rights reserved.

TABLE OF CONTENTS

ACKNOWLEDGEMENTS	vi
ABSTRACT	vii
CHAPTER 1: GENERAL INTRODUCTION	1
1.1 Introduction	1
1.2 Dissertation organization	2
1.3 Background and literature review	4
1.3.1 Olefin Metathesis	4
1.3.2 Agricultural oils as a renewable resource in polymer development.....	6
1.4 References	8
CHAPTER 2: SELF-HEALING POLYMERS AND COMPOSITES	11
2.1 Abstract	11
2.2 Introduction	11
2.3 Types of Self-healing	14
2.3.1 Crack-filling healing.....	14
2.3.2 Diffusion.....	35
2.3.3 Bond Reformation	38
2.3.4 Virgin Property Strengthening.....	51
2.4 Virgin property reduction.....	57
2.5 Healing evaluation.....	60
2.6 Practical applications of self-healing polymers	66
2.6.1 Healing in coatings vs. bulk composites	66
2.6.2 Healing in the presence of structural reinforcements	67
2.7 Conclusions	69
2.8 References	70
CHAPTER 3: LATENT CATALYTIC SYSTEMS FOR RING-OPENING METATHESIS-BASED THERMOSETS	86
3.1 Abstract	86
3.2 Introduction	86
3.3 Experimental	87

3.3.1 Materials	87
3.3.2 $(H_2IMes)(PMe_3)(Cl)_2Ru(=CHPh)$	87
3.3.3 General DSC Technique	88
3.4 Isoconversional Model-Free Approach	89
3.5 Results and Discussion	90
3.6 Conclusions	100
3.7 Acknowledgements	101
3.8 References	101
CHAPTER 4: ENHANCED BULK CATALYST DISSOLUTION FOR SELF-HEALING MATERIALS	102
4.1 Abstract	102
4.2 Introduction	102
4.3 Experimental	106
4.3.1 General considerations	106
4.3.2 Synthesis of phenyl vinyl ether	107
4.3.3 Synthesis of $(PCy_3)_2Cl_2Ru=C(H)OPh$	107
4.3.4 Synthesis of N,N-dimethyl-5-norbornene-2-carboxamide	107
4.3.5 Dissolving Grubbs' Catalyst in solvent	108
4.3.6 Dissolving Grubbs' Catalyst in monomer	109
4.4 Results and Discussion	109
4.4.1 Healing monomer library dissolution parameters	109
4.4.2 Catalyst dissolution parameters	113
4.4.3 Model Validation	116
4.5 Conclusions	123
4.6 Acknowledgements	123
4.7 References	123
CHAPTER 5: A MODIFIED RHEOKINETIC TECHNIQUE DESIGNED TO ENHANCE THE UNDERSTANDING OF MICROCAPSULE-BASED SELF-HEALING POLYMERS	127
5.1 Abstract	127
5.2 Introduction	127

5.3 Experimental	130
5.3.1 General Considerations.....	130
5.3.2 Rheometer bottom plate modification	130
5.3.3 Rheology procedure.....	131
5.4 Results and Discussion.....	132
5.5 Conclusions	139
5.6 Acknowledgements	140
5.7 References	140
CHAPTER 6: RING-OPENING METATHESIS POLYMERIZATION OF A MODIFIED LINSEED OIL WITH VARYING LEVELS OF CROSSLINKING	143
6.1 Abstract	143
6.2 Introduction	143
6.3 Experimental	146
6.4 Results and Discussion.....	147
6.4.1 Structural characterization of Dilulin™	147
6.4.2 Microphase Analysis	151
6.4.3 Crosslink Efficiency	155
6.4.4 Crosslink Density	157
6.4.5 Thermal Stability	158
6.5 Conclusions	159
6.6 Acknowledgements	159
6.7 References	160
CHAPTER 7: BLOCK COPOLYMERS DERIVED FROM THE ACYCLIC DIENE METATHESIS (ADMET) POLYMERIZATION OF A MODIFIED VEGETABLE OIL.....	163
7.1 Abstract	163
7.2 Introduction	163
7.3 Experimental	164
7.3.1 General Considerations.....	164
7.3.2 Synthesis of ethane-1,2-diyl bis(undec-10-enoate)	164
7.3.3 ADMET Polymerization.....	165

7.3.4 Ring-opening polymerization of lactide	166
7.4 Results and Discussion.....	166
7.5 Conclusions	170
7.6 Acknowledgements	171
7.7 References	171
CHAPTER 8: GENERAL CONCLUSIONS.....	172
8.1 General Discussions	172
8.2 Recommendations for future research.....	173
8.3 References	175
APPENDIX A: SUPPLEMENTARY INFORMATION FOR CHAPTER 4	176
A.1 Calculation of Norbornene's Group Contributions	176
A.2 Calculation of E_T for norbornene	176
A.3 Calculation of E_D for norbornene	176
A.4 Calculation of E_P for norbornene	177
A.5 Calculation of E_H for norbornene	178
A.6 Summary	178
A.7 References	178
APPENDIX B: SUPPLEMENTARY INFORMATION FOR CHAPTER 5.....	179
APPENDIX C: SUPPLEMENTARY INFORMATION FOR CHAPTER 6.....	181
APPENDIX D: DIFFERENTIAL SCANNING CALORIMETER-BASED CURING KINETIC ANALYSES OF THE RING-OPENING METATHESIS POLYMERIZATION OF SUBSTITUTED NORBORNENYL DERIVATIVES.	183
D.1 Introduction	183
D.2 Experimental	183
D.2.1 General Considerations.....	183
D.2.2 General DSC technique	184
D.3 Results	185
D.4 Conclusions	186
D.5 References	186

ACKNOWLEDGEMENTS

First and foremost, I would like to extend my heartfelt appreciation to my advisor, mentor, and friend Dr. Michael R. Kessler for the opportunity to perform my graduate studies in his research group, and for his steadfast direction and encouragement throughout. Everything presented herein originated from his ingenuity and wise tutelage. I would also like to express thanks to my co-advisor, Dr. Malika Jeffries-EL. Her synthetic expertise—which I believe is matched by very few—has saved this research from the grasps of peril on numerous occasions, and her constant energy and enthusiasm throughout good or bad fortune has served as sense of inspiration for my own personal development. Drs. Aaron Sadow, Javier Vela, Arthur Winter, Richard Larock, and Victor Lin's time and guidance while serving on my advisory committee is also greatly appreciated.

I would like to thank the many graduate students, postdoctoral researchers, research scientists, visiting researchers, and undergraduate students who have provided personal and professional support throughout the course of my graduate studies. In particular, Dr. Xia Sheng, Dr. Wonje Jeong, Dr. Xing Liu and Dr. Jong Keun Lee were instrumental in guiding me through the massive learning curve experienced in my first years as a young graduate student. Dr. Jong Keun Lee deserves special acknowledgement for inviting me to perform research in his labs for two months at the Kumoh National Institute of Technology (KIT) in South Korea through a NSF/KOSEF joint fellowship, the experience during which leaves a lasting impression on me to this day. Undergraduate students Karan Haman, Elease McLaurin, Josh Leonard, Mark Rogalski and Mitch Rock, with whom I have worked in varying capacities, are also thanked for their technical and intellectual contributions to this work. In addition to the above, friends and fellow officemates Dr. Prashanth Badrinarayanan, Dr. Eduard Stefanescu, Dr. Gökür Tütüncü, Dr. Mesut Varlioğlu, Louis Charles, Peter Hondred, Rui Ding and Wilber Lio, among others, all deserve many thanks for creating an enjoyable working environment.

Finally, I would like to thank my family for their support and encouragement throughout graduate school and all other endeavors.

ABSTRACT

Modern society's immense and ill-fated reliance on petrochemical-based polymeric materials will likely necessitate a shift in polymer production paradigms in the near future. The work presented herein attempts to address this issue via a two-pronged approach. First, efforts to improve the duration of composite materials by incorporation of a self-healing function are discussed, the fruitful application of which can potentially reduce or eliminate the massive carbon footprints associated with the repair/replacement of damaged materials. And second, polymeric materials derived predominately from natural and renewable feedstock—namely vegetable oils—are developed.

Early microcapsule-based self-healing materials utilized dicyclopentadiene-filled microcapsules and Grubbs' olefin metathesis catalyst to initiate the healing mechanism. However, the patent-protected catalyst, made from the precious metal ruthenium and sometimes costly ligands, will likely never be inexpensive and therefore limit large-scale applications. Hence, clever approaches to reduce the healing catalyst loading in self-healing polymers are of great interest. To this end, our efforts have revolved around solving the problem of the relatively inefficient use of Grubbs' catalyst during the healing mechanism. Given that the mismatch of the olefin metathesis polymerization and Grubbs' catalyst dissolution (in monomer) kinetics is a known cause of this inefficient use of the catalyst, we attempted to tune the "latency" (i.e. pot life) of the olefin metathesis polymerization to ensure more complete dissolution of catalyst in monomer. In an alternative approach to improving efficient catalyst dissolution, we developed a simple model to predict relative dissolution rates of Grubbs' catalyst in a small library of healing monomers. This model was shown experimentally to be able to aid in the selection of, for example, reactive monomer additives that can yield impressive improvements in catalyst dissolution at small loadings. Furthermore, we have recently developed a novel rheokinetic technique designed to mimic the self-healing mechanism. This new analytical technique allows for collection of copious amounts of information related to the self-healing mechanism (e.g. healing kinetics, rheological and mechanical changes of polymerizing healing agents, adhesive interactions between healing agent and polymer matrix, etc.) to be extracted from a single experiment.

New polymers derived from renewable feeds were synthesized via olefin metathesis polymerization techniques, which are ideally suited to react with the unactivated olefins (i.e. non-styrenic, non-acrylated, non-conjugated, etc.) prominent in most vegetable oils. Various vegetable oils were modified to contain norbornenyl functional groups via the high-pressure Diels-Alder addition of cyclopentadiene to their olefins to yield ROMP-reactive monomers. These monomers, polymerized in the presence of Grubbs' catalyst and the occasional comonomer, were able to yield highly crosslinked thermosets with ambient temperature storage moduli, glass transition temperatures and decomposition temperatures comparable to their currently-used, petrochemical-based counterparts. Other research thrusts in this area have focused on the development of renewable thermoplastic polymers. Vegetable oils were chemically modified to yield a series of α,ω -dienes, from which polymers were formed via acyclic diene metathesis (ADMET). The resulting polymers were shown to have unique material properties, comparable to that of other biopolyesters (poly(lactic acid), poly(glycolides), poly(caprolactones), etc.) and common, petrochemical-derived polyesters.

CHAPTER 1: GENERAL INTRODUCTION

1.1 Introduction

The past half-century has seen a materials revolution, as polymer-based materials are rapidly supplanting their metal, wood, ceramic, etc. counterparts in a wide variety of applications. Unfortunately, this trend conflicts with another budding trend in modern society: the reduction of our reliance on the petrochemical industry, of which the vast majority of polymers are ultimately derived. In addition to problems related to their feed source, the ultimate fate of used polymeric materials is of grave concern. The Environmental Protection Agency estimates that municipal solid waste generation—consisting of roughly 20% mixed plastic goods—has nearly tripled in the last 50 years [1]. Management of this growing amount of polymer waste comes at the cost of massive energy outputs and carbon dioxide emissions; for example, it is estimated that 52.8 million BTU's of energy is expended and 1.5 metric tons of carbon dioxide emissions are released for every ton of polymer waste that is processed [2]. These figures do not include the frequent additions to the especially destructive plastic waste reservoirs in the natural environment, such as the Great Pacific Garbage Patch [3], which is estimated to contain from 10^7 - 10^8 tons of polymer-rich waste [4]. One approach to mitigating these problems is to improve product lifetime of polymeric materials. Longer product lifetimes would intuitively reduce both the amount of polymer waste produced and the amount of feedstock required to replace the products with new material. Polymers containing inherent self-healing capabilities, through embedded healing additives, [5] are attractive options to extend product lifetimes. However, self-healing polymers are still in their infancy, and many questions need to be answered before these materials can be used commercially. Of specific interest is the kinetics of the healing, which is dominated by a complex and poorly understood combination of individual kinetic events occurring throughout the self-healing mechanism. Thus, the main thrust in this thesis is to gain a better understanding of the factors that affect the kinetics of self-healing polymers, and how healing kinetics influences the overall quality of healing.

In addition to improving the lifetime of polymer-based materials, finding alternative sources (i.e. not petroleum-based) for polymer precursor chemicals can help alleviate some

of the aforementioned problems. Vegetable oils, which are available in massive quantities in the agricultural reservoir of the American Midwest, are prime candidates as renewable resources to achieve this goal. Thus, the work presented in this thesis discusses the development and characterization of several novel materials derived mostly from vegetable oil precursors.

1.2 Dissertation organization

This work is organized into main chapters, which are each manuscripts that have either been published in scholarly journals, or will be submitted at a future date.

Chapter 1 gives a general introduction that outlines a background for olefin metathesis chemistry, which is an underlying theme for much of the work presented in this thesis. Specific focus will be placed on olefin metathesis polymerization techniques: ring-opening metathesis polymerization (ROMP) and acyclic diene metathesis (ADMET) polymerization. Additionally, an introduction to one of the two main topics of this thesis—vegetable oils as a renewable resource for the polymer and composite material industries—will be described.

Chapter 2 also serves as an introduction chapter, outlining recent advances in the second topic of this thesis: the field of self-healing polymers and composites. This chapter was separated from the current, general introduction chapter on the basis that it was written, and is currently published, as a critical review paper. The specific self-healing mechanism studied throughout the course of the work presented herein, self-healing polymers based on the delivery of encapsulated liquids, is discussed most heavily, but other self-healing mechanisms are also highlighted.

Chapter 3 presents work to develop olefin metathesis catalysts with tunable degrees of “latency.” This work is intended to serve as tool for the optimization of reaction shelf-life in self-healing polymers, which, as described in more detail in chapter 2, must be tuned to be in balance with a number of other kinetic parameters in the self-healing mechanism. We also envision that this work will have broad applications for tuning the reaction shelf-life of monomer/catalyst solutions for a variety of polymer processing techniques (e.g. reaction-injection molding, prepreg preparation, etc.).

Chapter 4 outlines efforts to develop and test a model to predict relative dissolution rates of Grubbs' olefin metathesis catalyst in a variety of ROMP-active monomers, of which efficient kinetics is of paramount importance in self-healing polymers. The concept of solubility parameters, otherwise well-known in the realms of coating technology and polymer physics as a means to predict solvent/solute mixing, was slightly modified to develop this model.

Chapter 5 discusses a novel rheokinetic technique designed to study the polymerization reaction of healing monomers in an environment that mimics that of the self-healing mechanism. This new analytical technique was shown to be a quick and simple alternative to the often laborious, tedious and material-intensive experiments performed in the past to study self-healing polymers. Initial work with this technique has already revealed a number of previously unobserved and unknown phenomena affecting the self-healing mechanism, the knowledge of which may drastically change potential applications for self-healing polymers.

Chapter 6 begins the second topic of this thesis, which involves the synthesis and characterization of novel polymers derived from the olefin metathesis polymerization of oleochemicals. This chapter discusses new polymers made from the ring-opening metathesis polymerization of a modified linseed oil with a comonomer. Interesting and complex property changes were observed in these materials that were dependent on the extent of crosslinking; reasons for these property changes were investigated and discussed.

Chapter 7 involves the synthesis and characterization of a new, telechelic unsaturated biopolyester made from the acyclic diene metathesis polymerization of a modified castor oil. The endgroups of these polymers were used to grow poly(lactic acid), also a bio-based polymer, to form an ABA-triblock copolymer derived almost completely from renewable resources.

Chapter 8 gives a series of general conclusions drawn from this thesis and provides suggestions for future work.

1.3 Background and literature review

1.3.1 Olefin Metathesis

Olefin metathesis is a chemical reaction characterized as a “shuffling” of the sp^2 carbons of double bonds (Figure 1). Since its first observation in the late 1950's, this reaction has garnered much popularity in both academia and industry [6, 7], and has found many practical uses in organic synthesis and polymer chemistry, eventually culminating in the 2005 Nobel Prize for its study and development [8-10]. The reaction is facilitated by a metal-carbene complex, and proceeds through a metallocyclobutane intermediate, as shown in Figure 1.1. Metals commonly used for olefin metathesis are molybdenum, ruthenium and tungsten, and less commonly titanium and rhenium.

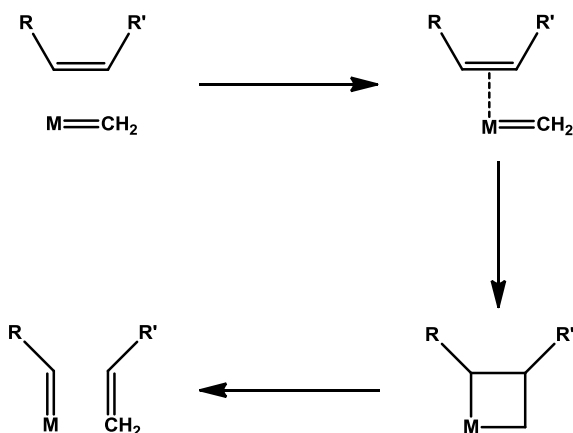


Figure 1.1. Olefin metathesis mechanism with a metal carbene.

Depending on the substrate and reaction conditions, olefin metathesis can be demarcated into several distinct reaction types; several of the more widely-used reaction types—ring-closing metathesis (RCM), ring-opening metathesis polymerization (ROMP), acyclic diene metathesis (ADMET), and enyne metathesis (EM)—are shown in Figure 1.2. RCM and EM find most utility in organic synthesis, while ROMP and ADMET are most often used as polymerization techniques. Though both ROMP and ADMET utilize the same overriding chemistry, the polymerization mechanisms are fundamentally different. ROMP is a chain-growth living polymerization that has gained much popularity as a route to complex

copolymer architectures, surface functionalization, and some structural polymers [11-15]. ADMET is a step-growth polymerization technique that has been most useful for forming well-defined telechelic polymers and precision-functionalized polyethylene [16-19].

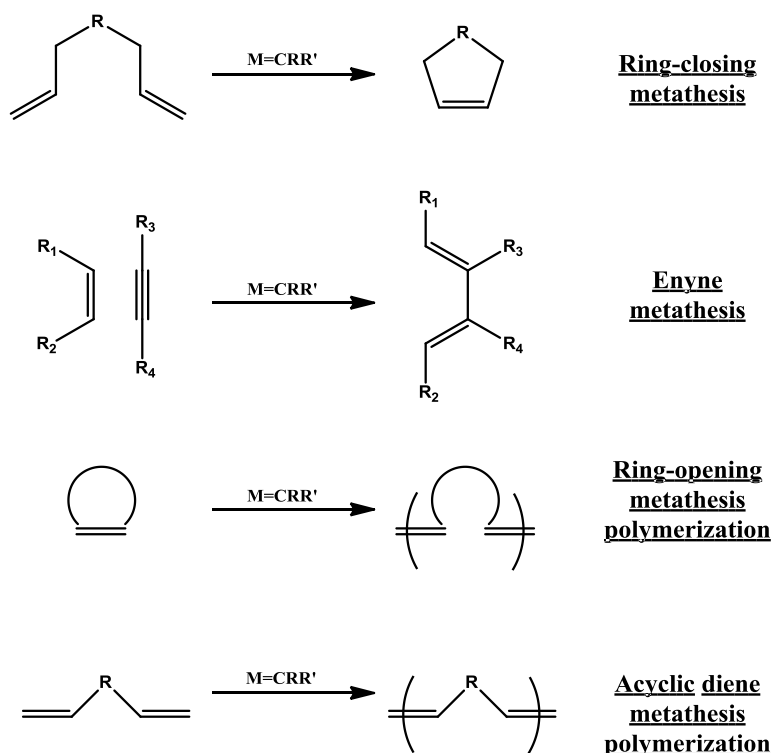


Figure 1.2. Common reaction types

Most catalysts used for olefin metathesis fall in to three categories: Schrock-type molybdenum catalysts [20, 21]; Grubbs'-type ruthenium catalysts [22-24]; and others loosely referred to as ill-defined catalysts, usually consisting of "simpler" metal halides and co-catalysts, in which the metal-carbene is generated *in-situ*. Grubbs'- and Schrock-type catalysts are known for their well-defined structures (Figure 1.3), well-known catalytic cycles, and superior reactivity, and as such is almost exclusively used in academia. But the latter group of ill-defined catalysts composes much of what is used in industrial implementations of olefin metathesis, most likely due to their relatively cheaper costs, relative to the well-defined catalysts. Grubbs'-type catalysts, in particular, have received much attention for their relative/oxygen insensitivity and functional group tolerance, being

able to react in the presence of most types of acids, alcohols, aldehydes, ketones, esters, amides, and moderate reactivity in tertiary amines [25]. Recent advances have even offered Grubbs-type catalysts with reactivity paralleling (or in some cases surpassing) the once dominant Schrock catalysts [26].

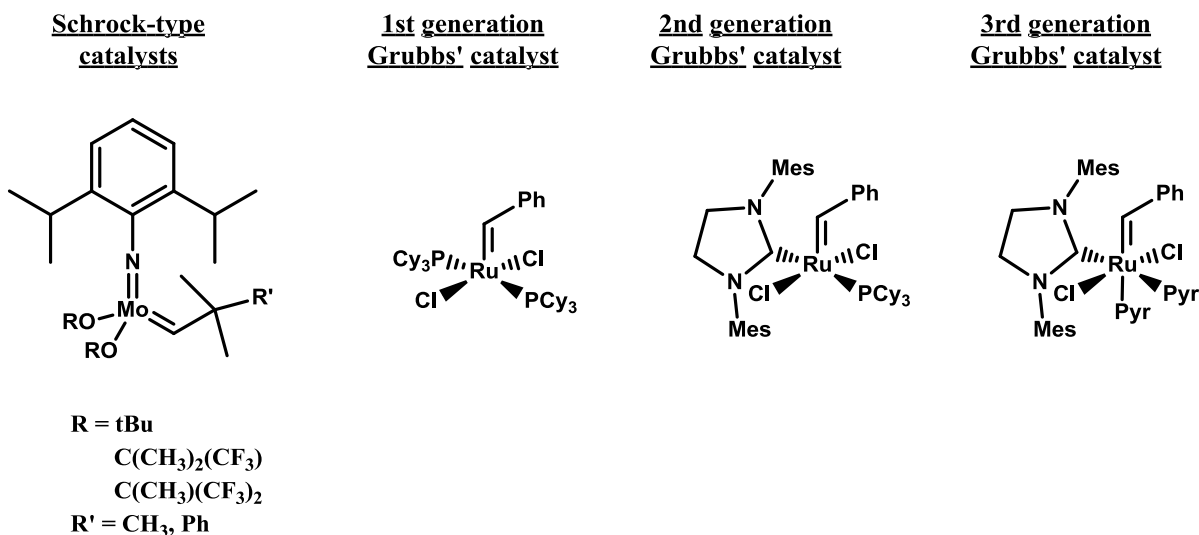


Figure 1.3. Well-defined olefin metathesis catalysts.

1.3.2 Agricultural oils as a renewable resource in polymer development

In recent years there has been extensive interest in materials derived from bio-based sources, especially those resulting from abundant and renewable agricultural oils, in an effort to reduce our dependency on conventional petroleum-based polymers. Historically, vegetable oils already have a place in the polymer market, albeit mostly for use in the paint and coating industry [27-28] for their ability to react with oxygen and act as drying agents, but a mass of recent work has shown that derivatives of these vegetable oils can form bulk polymers and composites with structural applications that have similar or better thermal/mechanical properties than their petrochemical counterparts [29-30]. Vegetable oil-based materials also have the advantage of lower cost, minimal VOC emissions, and the promise of biodegradability.

Most common vegetable oils consist of a triglyceride with three fatty acid-based ester chains. Individual fatty acid chains are often linear, ranging from 14 to 22 carbons in length,

and usually contain anywhere from 0-3 double bonds. This high degree of unsaturation gives these macromolecules potential for functionalization and subsequent polymerization to form a highly crosslinked polymer matrix. Oils from different agricultural sources rarely have identical chemical structures, but have a distribution of often many fatty acid chains throughout their triglycerides. Table 1.1 shows the fatty acid distributions commonly observed in a number of vegetable oils and animal fats. Polymers have been made from soybean [31-34], corn [35], tung [36-37], linseed [38-41], and castor oil [42-43], among others, and many approaches to polymerization have been utilized including cationic [44-46], free radical [47-48], thermal [49-50], UV-initiated [51] and ring-opening polymerization [52]. Strangely, transition metal-based catalysts have yet to assert themselves as a force in vegetable oil bulk polymerization, despite the continual development of novel catalyst complexes that can produce high-yielding, stereoregular, regioregular, monodisperse and living polymers, often under mild reaction conditions.

Table 1.1. Fatty acid distribution in common plant and animal oils [53].

Main fatty acid contents in different oils

Fatty acid	[#C: #DB*]	Canola oil	Corn oil	Cottonseed oil	Linseed oil	Olive oil	Soybean oil	Tung oil	Fish oil†
Palmitic	16:0	4.1	10.9	21.6	5.5	13.7	11.0	—	—
Stearic	18:0	1.8	2.0	2.6	3.5	2.5	4.0	4	—
Oleic	18:1	60.9	25.4	18.6	19.1	71.1	23.4	8	18.20
Linoleic	18:2	21.0	59.6	54.4	15.3	10.0	53.3	4	1.10
Linolenic	18:3	8.8	1.2	0.7	56.6	0.6	7.8	—	0.99
α -elaeostearic acid	—	—	—	—	—	—	—	84	—
Average #DB/triglyceride.	—	3.9	4.5	3.9	6.6	2.8	4.6	7.5	3.6

*#C stands for number of carbon atoms in chain and #DB stands for the number of double bonds in that chain.

Olefin metathesis is an ideal technique for reaction with vegetable oils. Olefin metathesis reacts with the “unactivated” (i.e. non-conjugated, non-acrylic, non-styrenic, etc.) double bonds prominent in vegetable oils, which are otherwise inactive towards most types of addition polymerization. The functional group tolerance of Grubbs’-type olefin metathesis catalysts is also extremely useful for reactions that may be spiked with fatty acids, glycerol, water, etc. One of the earliest reports of the use of olefin metathesis for the modification of vegetable oils comes from van Dam et al. in 1972 [54], but these and most subsequent reports were focused on small molecule synthesis. Olefin metathesis as a route to form polymer from vegetable oil sources is a relatively new field, with most work stemming from the

groups led by Meier [55-62], Larock [63-68], and Kessler [69-71]. The former has primarily focused on ADMET and ATMET (acyclic triene metathesis) of vegetable oil, while the latter two have mostly, but not exclusively, performed ROMP of modified vegetable oils.

1.4 References

- [1] *Municipal Solid Waste Generation, Recycling, and Disposal in the United States: Facts and Figures for 2009*; EPA-530-F-010-012; Washington D.C., 2010.
- [2] Calculated via the Environmental Protection Agency's Waste Reduction Model (WARM) software, available from: <http://www.epa.gov/warm> (accessed September 1, 2011).
- [3] Day, R.H.; Shaw, D.G. and Ignell, S.E. Proceedings of the Second International Conference on Marine Debris, Honolulu, HI, April 2-7 1989; Shomura, R.S. and Godfrey, M.L. eds.
- [4] Moore, C.; Moore, S.L.; Leecaster, M.K. and Weisber, S.B. *Mar. Pollut. Bull.* 2001, **42**, 1297.
- [5] For a more detailed description of self-healing polymers with embedded healing additives, see chapter 2 of this thesis.
- [6] Rouhi, A.M. *Chem. Eng. News* **2002**, 80, 34.
- [7] Rouhi, A.M. *Chem. Eng. News* **2002**, 80, 29.
- [8] Schrock, R.R. *Angew. Chem. Int. Ed.* **2006**, 45, 3748-3759.
- [9] Chauvin, Y. *Angew. Chem. Int. Ed.* **2006**, 45, 3741-3747.
- [10] Grubbs, R.H. *Angew. Chem. Int. Ed.* **2006**, 45, 3760-3765.
- [11] Bielawski, C.W. and Grubbs, R.H. *Prog. Polym. Sci.* **2007**, 32, 1-29.
- [12] Nguyen, S.T.; Johnson, L.K. and Grubbs, R.H. *J. Am. Chem. Soc.* **1992**, 114, 3974-3975.
- [13] Maughon, B.R. and Grubbs, R.H. *Macromolecules* **1997**, 30, 3459-3469.
- [14] Hillmyer, M.A.; Lepetit, C.; McGrath, D.V.; Novak, B.M. and Grubbs, R.H. *Macromolecules*, **1992**, 25, 3345.
- [15] Hillmyer, M.A. and Grubbs, R.H. *Macromolecules*, **1993**, 26, 872.
- [16] Lindmarkhamberg, M. and Wagener, K.B. *Macromolecules*, **1987**, 20, 2949.
- [17] Wagener, K.B.; Boncella, J.M. and Nel, J.G. *Macromolecules*, **1991**, 24, 2649.
- [18] Baughman, T.W. and Wagener, K.B. *Adv. Polym. Sci.*, **2005**, 176, 1.
- [19] Schwendeman, J.E.; Church, A.C. and Wagener, K.B. *Adv. Synth. Catal.*, **2002**, 344, 597.
- [20] Schrock, R.R.; Murdzek, J.S.; Bazan, G.C.; Robbins, J.; DiMare, M. and O'Regan, M. *J. Am. Chem. Soc.* **1990**, 112, 3875-3886.
- [21] McConville, D.H.; Wolf, J.R. and Schrock, R.R. *J. Am. Chem. Soc.* **1993**, 115, 4413-4414.
- [22] Wu, Z.; Nguyen, S.T.; Grubbs, R.H. and Ziller, J.W. *J. Am. Chem. Soc.* **1995**, 117, 5503-5511.
- [23] Dias, E.L.; Nguyen, S.T. and Grubbs, R.H. *J. Am. Chem. Soc.* **1997**, 119, 3887-3897.
- [24] Schwab, P.; Grubbs, R.H. and Ziller, J.W. *J. Am. Chem. Soc.* **1996**, 118, 100-110.

- [25] Trnka, T.M. and Grubbs, R.H. *Acc Chem. Res.* **2001**, *34*, 18-29.
- [26] Scholl, M.; Ding, S.; Choon, W.L. and Grubbs, R.H. *Org. Lett.* **1999**, *1*, 953-956.
- [27] Wexler, H. *Encycl. Polym. Sci. Technol.* 1966, *5*, 216.
- [28] Gallagher, E.C. ASTM Special Technical Publication 1972, STP 500, 53-70.
- [29] Li, F.; Larock, R. C. *Polym. Mater. Sci. Eng.* 2002, *86*, 379-380.
- [30] Li, F.; Larock, R. C. In *Natural Fibers, Biopolymers, and Their Biocomposites*; Mohanty, A.K.; Misra, M.; Drzal L.T., Eds.; CRC Press: Boca Raton, FL, 2005, pp 727.
- [31] Li, F.; Hanson, M.V.; Larock, R.C. *Polymer* 2001, *42*, 1567-1579.
- [32] Li, F.; Larock, R.C. *J. Appl. Polym. Sci.* 2001, *80*, 658-670.
- [33] Li, F.; Larock, R. C. *J. Polym. Sci., Part B: Polym. Phys.* 2000, *38*, 2721-2738.
- [34] Li, F.; Larock, R. C. *J. Polym. Sci., Part B: Polym. Phys.* 2001, *39*, 60-77.
- [35] Li, F.; Hasjim, J.; Larock, R.C. *J. Appl. Polym. Sci.* 2003, *90*, 1830-1838.
- [36] Li, F.; Larock, R.C. *J. Appl. Polym. Sci.* 2000, *78*, 1044-1056.
- [37] Li, F.; Larock R.C. *Biomacromolecules* 2003, *4*, 1018-1025.
- [38] Motawie, A.M.; Hassan, F.A.; Manich, A.; Aboul-Fetouh, M.E.; El-din, A.F. *J. Appl. Polym. Sci.* 1995, *55*, 1725-1732.
- [39] Meneghetti, S.M.P.; de Souza, R.F.; Monteiro, A.L.; de Souza, M.O. *Prog. Org. Coat.* 1998, *33*, 219-224.
- [40] Tuman, S.J.; Chamberlain, D.; Scholsky, K.M.; Soucek, M.D. *Prog. Org. Coat.* 1996, *28*, 251-258.
- [41] Henna, P.; Andjelkovic, D. D.; Kundu, P. P.; Larock, R. C. *J. Appl. Polym. Sci.* 2007, *104*, 979-985.
- [42] Yin, Y.; Yao, S.; Zhou, X. *J. Appl. Polym. Sci.* 2003, *88*, 1840-1842.
- [43] Cassidy, P.E.; Schwank, G.D. *J. Appl. Polym. Sci.* 1974, *18*, 2517-2526.
- [44] Khot, S.N.; Lascala, J.J.; Can, E.; Morye, S.S.; Williams, G.I.; Palmese, G.R.; Kusefoglu, S.H.; Wool, R.P. *J. Appl. Polym. Sci.* 2001, *82*, 703-723.
- [45] Li, F.; Perounoud, A.; Larock, R. C. *Polymer* 2001, *42*, 10133-10145.
- [46] Andjelkovic, D. D.; Valverde, M.; Henna, P.; Li, F.; Larock, R. C. *Polymer* 2005, *46*, 9674-9685.
- [47] Frankel, E.N. *Prog. Lipid Res.* 1980, *19*, 1-22.
- [48] Valverde, M.; Andjelkovic, D. D.; Kundu, P. P.; Larock, R. C. *J. Appl. Polym. Sci.* 2008, *107*, 423-430.
- [49] Wang, C.; Erhan, S. J. *Am. Oil Chem. Soc.* 1999, *76*, 1211-1216.
- [50] Kundu P.; Larock, R. C. *Biomacromolecules* 2005, *6*, 797-806.
- [51] Thames, S.F.; Yu, H. *Surf. Coat. Technol.* 1999, *115*, 208-214.
- [52] Eren, T.; Kuesefoglu, S.H.; Wool, R. J. *J. Appl. Polym. Sci.* 2003, *90*, 197-202.
- [53] Sharma, V. and Kundu, P.P. *Prog. Polym. Sci.*, **2006**, *31*, 983.
- [54] van Dam, P.B.; Mittelmeijer, M.C. and Boelhouwer, C. *J. Chem. Soc. Chem. Commun.*, **1972**, *22*, 1221.
- [55] A. Rybak, M. A. R. Meier, *ChemSusChem* 2008, *1*, 542.
- [56] H. Mutlu, M. A. R. Meier, *Macromol. Chem. Phys.* 2009, *210*, 1019.
- [57] P. A. Fokou, M. A. R. Meier, *J. Am. Chem. Soc.* 2009, *131*, 1664.
- [58] P. A. Fokou, M. A. R. Meier, *Macromol. Rapid Commun.* 2010, *31*, 368.

- [59] L. Montero de Espinosa, J. C. Ronda, M. Galia, V. Cadiz, M. A. R. Meier, *J. Polym. Sci. A.: Polym. Chem.* 2009, 47, 5760.
- [60] L. Montero de Espinosa, M. A. R. Meier, J. C. Ronda, M. Galia, V. Cadiz, *J. Polym. Sci. A.: Polym. Chem.* 2010, 48, 1649.
- [61] P. A. Fokou, M. A. R. Meier, *Macromol. Rapid Commun.* 2008, 29, 1620.
- [62] U. Biermann, J. O. Metzger, M. A. R. Meier, *Macromol. Chem. Phys.* 2010, 211, 854.
- [63] Refvik, M. D.; Larock, R. C.; Tian, Q. *J. Am. Oil Chem. Soc.* **1999**, 76, 93.
- [64] Larock, R. C.; Tian, Q. *J. Am. Oil Chem. Soc.* **2002**, 79, 479.
- [65] Henna, P.; Larock, R. C. *J. Appl. Polym. Sci.* **2009**, 112, 1788-1797.
- [66] Xia, Y.; Lu, Y.; Larock, R. C. *Polymer* **2010**, 51, 53-61.
- [67] Henna, P. H.; Larock, R. C. *Macromol. Mater. Eng.* **2007**, 292, 1201-1209.
- [68] Henna, P.; Larock, R. C.; Kessler, M. *Macromol. Mater. Eng.* **2008**, 293, 979-990.
- [69] Haman, K.; Badrinarayanan, P. and Kessler, M.R. *ACS Appl. Mater. Interfaces*, **2009**, 1, 1190.
- [70] Jeong, W.; Mauldin T.C.; Larock, R.C. and Kessler, M.R. *Macromol. Mater. Eng.*, **2009**, 294, 756.
- [71] Mauldin, T.C.; Haman, K.; Sheng, X.; Henna, P.; Larock, R.C. and Kessler, M.R. *J. Polym. Sci., Part A: Polym. Chem.*, **2008**, 46, 6851.

CHAPTER 2: SELF-HEALING POLYMERS AND COMPOSITES

A paper published in *International Materials Reviews**

Timothy C. Mauldin¹ and Michael R. Kessler²

2.1 Abstract

Inspired by the unique and efficient wound-healing processes in biological systems, several approaches to develop synthetic polymers that can repair themselves with complete, or nearly complete, autonomy have recently been developed. This paper aims to survey the rapidly expanding field of self-healing polymers by reviewing the major successful autonomic repairing mechanisms developed over the last decade. Additionally, we discuss several issues related to transferring these self-healing technologies from the laboratory to real applications, such as virgin polymer property changes as a result of the added healing functionality, healing in thin films vs. bulk polymers, and healing in the presence of structural reinforcements.

Keywords: Self-healing; Self-repairing; Autonomic; Polymer; Composite; Polymer-matrix composite

2.2 Introduction

The past half-century has witnessed a dramatic increase in the use of polymers and polymer matrix composites (PMC's), which are rapidly supplanting their metal, ceramic and wood counterparts. Perhaps one of the best examples of this polymer insurgency is the recent completion of the Boeing 787 airplane, widely-publicized as the first major airliner to be constructed mostly of PMC's [1]. But while the exponential growth of composites in the aerospace market looks promising as a microcosm for the continuing growth of the polymer industry as a whole, problems arise when exchanging different material types that exhibit

* Reprinted with permission of *International Materials Reviews*.

¹ Department of Chemistry, Iowa State University, Ames, IA 50011, USA.

² Department of Materials Science and Engineering, Iowa State University, Ames, IA 50011, USA.

inherently different failure behavior. For example, failure of PMC's generally results from delamination, fiber-matrix debonding, fiber fracture and/or microcracking of the brittle polymer matrix [2,3]. This is in contrast to, for example, the metal parts that the PMC's are replacing, which are typically tougher and used without reinforcement. So in order for the potential of polymer composites (such as high strength-to-weight ratio, corrosion resistance, versatility in manufacturability, part count reduction, good vibration damping, etc.) to be fully realized, methods to prevent or arrest these common polymer failure modes must be developed.

Traditionally, failure in PMC's is approached with the mindset of managing damage and/or designing materials to better withstand thermal and mechanical loads. However, conventional approaches to managing failure in PMC's (such as damage detection [4], damage prediction [5, 6], protective coatings, and manual repair/replacement [7, 8]) are limited in that they all require some type of manual intervention, which can be costly and time-consuming. And while the numerous approaches to improve PMC's tolerance to thermal and mechanical stresses (either by optimizing or developing new polymer matrices and structural reinforcements) have indeed proven fruitful, simple property optimization cannot free any material from its fate of a finite lifetime.

Instead, given that all PMC's will inevitably fail, perhaps we should entertain the idea of shifting the current paradigm away from simply improving materials to be less susceptible to damage. In other words, a stronger material can only delay catastrophic failure and not prevent it, and that failure could potentially be of great consequence. Surely nature would agree with this mentality, as the protective skin and shell materials of many flora and fauna are significantly weaker than the synthetic composite materials used for structural applications [9]. Instead, nature incorporates her structural materials with sufficient mechanical integrity for its intended applications and handles external damage by implementing advanced, autonomic repairing mechanisms to quickly and efficiently clot and heal cell tissue. In this sense, the "product lifetime" of natural, biological materials often greatly exceeds that of synthetic polymers and composites. So perhaps a shift towards nature's mentality in material design would also be well suited for man-made applications.

To this end, scientists and engineers have taken their cue from nature and, starting from the early 1990's, began creating synthetic mimics of living biological systems. These self-healing polymers emulate biological systems to varying extents, with some being completely autonomic, and some requiring external stimuli to undergo the healing event. Here, we review recent work to develop, optimize and evaluate these numerous approaches to impart a self-healing function to polymers and composites. Additionally we will discuss in detail various issues related to incorporating self-healing materials into real applications, such as virgin property reduction, healing in films/coatings vs. bulk composites, and healing in the presence of structural fiber reinforcements.

The inherent multidisciplinary nature of the field of self-healing polymers, along with the diversity of the different self-healing methodologies, has left some ambiguity on how to best categorize self-repairing systems. For example, some have suggested an organization based on the underlying chemistry involved in the healing process [10], the degree of biomimicry [11], the type of material being healed (e.g. thermoplastic polymers, thermoset polymers, composites, metals, etc.) [12,13], the physical phase of the healing additive (solid vs. liquid) [14], the external stimuli required to initiate healing event [15], and the intrinsic or extrinsic nature of the healing [16]. This ambiguity, which is a direct consequence of the multidisciplinary nature of the field, will likely not be resolved here, but given the spirit of autonomic healing, we organize the different self-healing techniques with the mechanism by which the healing occurs. This organizational approach allows the many fundamentally different self-healing techniques to fall into four different categories: 1) healing by crack-filling adhesion, 2) healing by diffusion, 3) healing by bond reformation, and 4) virgin property strengthening in response to stress (Table 2.1). Healing via crack-filling adhesion is the original and probably most well-studied approach to self-healing and will be discussed first.

Table 2.1. Organizational structure of the different self-healing mechanisms.

Healing Mechanism (section)	Types of healing (section)
Crack-filling Healing	Microencapsulated healing agents
	Phase-separated healing agents
	Healing agents in hollow fibers
	Microvascular networks
Diffusion	Thermoset/thermoplastic blends
	Dangling chain diffusion
	Viscoelastic healing
Bond Reformation	Thermally-reversible
	UV-initiated
	Metal-ligand dissociation/association
	Supramolecular assembly
Virgin Property Strengthening	Mechanophores

2.3 Types of Self-healing

2.3.1 Crack-filling healing

Most of the concerted effort to develop polymers and composites that exhibit autonomic repair has revolved around crack-filling mechanisms, in which fluid substances fill damage volumes and heal with various different chemical and/or physical processes. These crack-filling substances, which can include liquid monomers, liquid catalysts, thermoplastic polymers, organic or inorganic film formers, or solvent solutions, are often referred to as “healing agents,” and this nomenclature will be used herein. It is important to consider the advantages of crack-filling healing, as opposed to the healing mechanisms presented later in this review that require intimate contact (in some cases, contact on the molecular level) of damage surfaces. Crack-filling eliminates the need to close cracks, which otherwise may be difficult for stiff structural polymers and composites. Even if an easy route to crack closure was possible in real applications, this could hardly be considered truly autonomic healing since it would require both damage detection and some extent of manual intervention (e.g. applying pressure). And while it probably can be argued that the healing

mechanisms requiring contacting damage surfaces are capable of repairing small-sized cracks without the need for external closure, it is at least reasonable to presume that crack-filling mechanisms are better suited for healing a wider range of damage volumes. Obviously, this is contingent on a sufficient supply of healing agent to entirely fill cracks, which can be accomplished by optimizing the amount of healing agent present in the polymers.

2.3.1.1 Microencapsulated healing agents

One of the first successful techniques to impart a completely autonomic self-healing function to polymers was the incorporation of liquid healing agent-filled microcapsules and catalyst (either as a solid particle or a separately encapsulated liquid) into the polymer matrix. In this approach, which is described schematically in Fig. 2.1, cracks propagate through the polymer matrix, rupturing several of the microcapsules. Capillary action then drives the liquid monomer out of the broken capsules and onto the crack surface where it comes into contact with the catalyst, which is either embedded in the crack plane (solid catalyst) or also released from ruptured microcapsules (liquid catalyst). Upon contact with the catalyst, the healing agent polymerizes and adheres the two crack faces together [17].

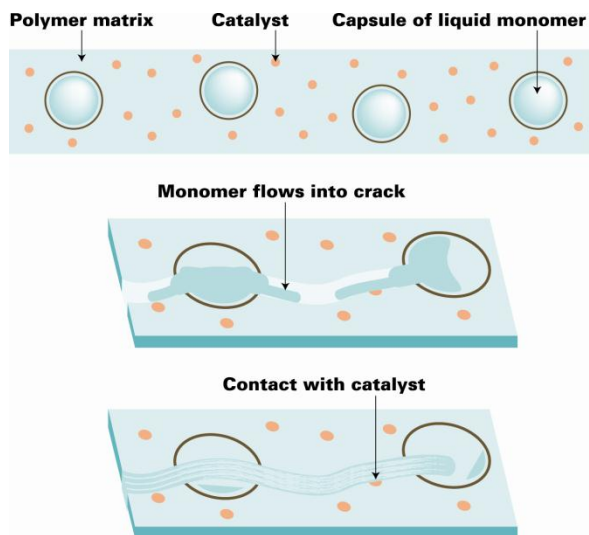


Figure 2.1. Microcapsule-based self-healing technique with a liquid, encapsulated monomer and a solid catalyst.

The key to realizing a successful microcapsule-based self-healing system lies with carefully choosing a healing agent/catalyst combination with the requisite features to be compatible with the healing mechanism. For example, the healing agent and the catalyst must have a long shelf life and be stable to the composite processing conditions without undergoing decomposition, uncatalyzed polymerization, or leaching out of the microcapsule shell. Furthermore, once the microcapsules rupture the healing agent must have a sufficiently low viscosity to flow out of the capsules and completely fill the crack volume in a reasonable timeframe, good wetting properties on the crack surface, and minimal loss of the healing agent from the crack plane through, for example, volatilization or diffusion into the polymer matrix. And finally, the healing agent must have rapid catalyst dissolution (or for liquid catalysts, rapid mixing) and polymerization kinetics, low shrinkage upon polymerization, and the resulting polymer should have good mechanical and adhesive properties.

Preliminary systems used styrene/polystyrene blends [18] and phenolic-based resins [19] in their microcapsules with varying results, but the healing chemistry found to most completely fulfill this daunting set of healing agent requirements is the ring-opening metathesis polymerization (ROMP) [20-22] of dicyclopentadiene (DCPD) with the popular ruthenium-based olefin metathesis catalyst Bis(tricyclohexylphosphine) benzyldiene ruthenium dichloride, colloquially referred to as “Grubbs’ catalyst” [23-27]. In this reaction, the highly-strained olefin of DCPD coordinates to the ruthenium catalyst, followed by a cycloaddition with the ruthenium-carbene to form a metallocyclobutane intermediate, and finally a cycloreversion to open dicyclopentadiene’s strained ring and add an ultimate unit to the growing polymer chain (Fig. 2.2). In addition to being a cheap, readily available byproduct of the petroleum industry, DCPD is particularly attractive as a healing agent because it contains a second cyclic olefin that can act as a crosslinking site, producing a polymer with good mechanical properties.

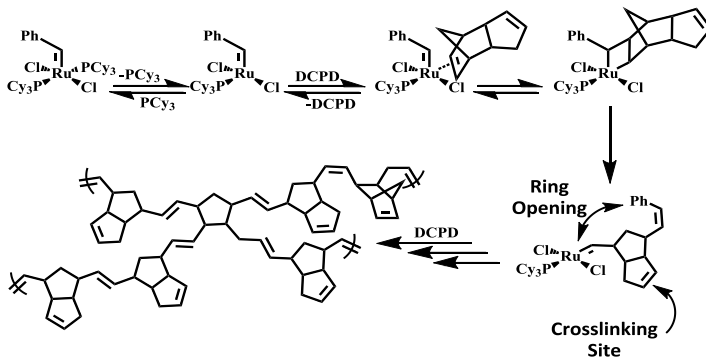


Figure 2.2. Polymerization mechanism of DCPD with Grubbs' catalyst.

White *et al.* first reported using DCPD/Grubbs' catalyst in a self-healing system [28], in which DCPD was encapsulated in a poly(urea-formaldehyde) shell and embedded with the catalyst in an epoxy matrix. It was shown that, after failure, the self-healing polymer could recover up to 75% of its virgin fracture toughness. And by optimizing various parameters (catalyst and microcapsule size and loading), it was found that up to 90% toughness recovery could be achieved [29]. In addition to healing large cracks, fatigue lifetime of these systems could be improved to over 30 times longer than that of a polymer without a self-healing functionality, and under certain conditions (low applied stress and short rest periods) fatigue crack growth was indefinitely retarded [30-32].

Most utilizations of the DCPD/Grubbs' catalyst-based healing agent system have been used to heal structurally dissimilar polymer matrices (predominately epoxies, but other polymers have also been healed, such as PMMA bone cement [33, 34], epoxy vinyl esters [35], and poly(styrene-*b*-butadiene-*b*-styrene) [36]). Given that most living organisms ultimately repair their damaged cell tissue with structurally similar (often identical) tissue material, these ROMP-based healing systems are not entirely biomimetic. So intuitively, a healing chemistry that produces a polymerized healing agent structurally similar or identical to the polymer matrix it heals would be of some benefit, not only as a means to better mimic nature, but also to increase the interfacial compatibility between the adhesive (healing agent) and substrate (crack surface). Therefore, two different types of matching polymer matrices/healing agents—based on epoxies and poly(dimethylsiloxane) (PDMS) polymers—were developed and are discussed below.

One of the first successful attempts to match a healing agent to its epoxy matrix was done by Rong *et al.*, in which a diglycidyl ether bisphenol-A (DGEBA)-based epoxy resin was encapsulated in a urea-formaldehyde microcapsule and, along with a commercially available capsulated imidazole hardener, embedded in an epoxy matrix made from the same DGEBA epoxy resin as in the microcapsules [37]. Healing with this system showed promising results, with just over 100% recovery in fracture toughness. Further improvements were achieved by replacing the capsulated imidazole with an epoxy-soluble imidazole, $\text{CuBr}_2(2\text{-MeIm})_4$, dissolved into the epoxy matrix during fabrication [38]. Using this soluble hardener, significantly lower loadings of epoxy/imidazole healing agents were able to yield better toughness recovery after failure (111%) than with the discrete, capsulated imidazole. Extensive work has been conducted to test the versatility of this system towards glass fiber-reinforced composites subject to long storage times (up to 18 months) [39] and different types of damage (mode I fracture vs. impact) [40-42]. All conditions showed good healing capabilities, with healing recoveries ranging from 60% (mode I fracture of composites aged for over two months) to over 100% (low-energy impact damage of composites with minimal post-fabrication ageing time). However, one disadvantage to all epoxy-based self-healing systems using an imidazole hardener was the need for external heat to polymerize the healing agent, generally requiring a curing cycle after the damage event at temperatures from 120-140 °C.

In order to develop a more autonomic epoxy-based self-healing system (i.e. without the need for external heat), more aggressive hardeners were used. These hardeners included a mercaptan, encapsulated separate from the epoxy and used as a two-capsule system [43], and the cationic initiator $\text{BF}_3 \cdot \text{OEt}_2$, which was either encapsulated and used as a two-capsule system [44] or dispersed throughout the polymer matrix via diffusion from $\text{BF}_3 \cdot \text{OEt}_2$ -absorbed short sisal fibers [45]. Both hardener types cured the epoxy healing agent rapidly at ambient or sub-ambient temperatures and resulted in good healing—80% recovery of impact strength and 104.5% recovery of fracture toughness—at low microcapsule loadings (~5 wt. %).

Keller *et al.* investigated healing in a PDMS elastomer with a healing agent that, when polymerized, is identical to the polymer matrix [46, 47]. In this system a two-capsule

healing agent was used: the first capsule contained a vinyl-functionalized PDMS resin and a platinum catalyst, and in the second capsule was a liquid initiator containing a hydrosiloxane copolymer diluted with 20% solvent to reduce its viscosity. Both components were encapsulated in urea-formaldehyde shells. Upon rupture of the microcapsules and release of the two shell materials into the damage area, the platinum catalyst adds the Si-H bonds of the hydrosiloxane copolymer across the vinyl groups of the PDMS resin to cure and heal damage. This system was shown to heal tear damage by recovering 70-100% of tear strength and significantly retard fatigue crack growth. Additionally, it was recently proposed, as a modification to the logistics of this healing chemistry, to use a heterogeneous platinum catalyst supported on a glass fiber to initiate the hydrosilylation of the siloxane polymers [48]. While glass fibers would likely not be used in an elastomer matrix, this concept could be applied to a structural composite, allowing both polysiloxane polymers to be incorporated into one microcapsule, thus eliminating any issues related to mixing of two microcapsule components. These fibers have been shown to quickly and efficiently catalyze hydrosilylation, but have not yet been incorporated into a self-healing system.

Other PDMS self-healing polymers using different healing chemistries have been developed as well. For example, a tin-catalyzed condensation polymerization of polysiloxane-based healing agents was able to heal puncture damage sufficiently enough to withstand 101.3 kPa of pressure without leakage [49].

“Healing” has been defined thus far as the post-damage recovery of structural integrity through some type of polymerization. However, not all polymers are intended for structural applications. Paints and primers, for example, are used primarily for their ability to coat and protect other materials, such as metals that commonly rust and corrode if exposed to ambient temperature and humidity. Thus, in these applications, “healing” can also be defined as recovery of corrosion inhibition [50, 51]. While corrosion inhibition can indeed be recovered by applying conventional, polymerization-based healing to polymer coatings, many have also investigated the deposition of corrosion and rust inhibiting film-formers into areas of damage. Similar to the previously discussed self-healing systems, microcapsules have been shown to successfully deliver these film-forming compounds (which have included organic molecules, organic salts [52], and inorganic salts [53]) to the damaged

regions of coatings and subsequently inhibit metal corrosion and rusting. Another intuitive delivery approach was recently developed by Shchukin and coworkers where the film-forming compounds were incorporated into thin layers of polyelectrolytes, which were either directly coated on the metal surface or layered on SiO₂ nanoparticles embedded in a coating [54-56]. Once the coating in these systems is damaged and the metal surface is revealed, the onset of corrosion mechanisms changes the local pH in the defect region, thereby distorting the polyelectrolyte layers' adhesion and depositing the film-former on the metal surface.

Healing agent/catalyst optimization

Much effort has been dedicated to optimizing existing microcapsule-based self-healing that uses ROMP healing agents. A large amount of this effort has been focused on improving the kinetics of healing, which is a crucial factor when deciding the appropriate applications for self-healing polymers that may be subject to constant or frequent stress. Perhaps the most straightforward approach to this is to improve the polymerization rate of the healing agent, but a healing agent's bulk polymerization rate does not necessarily correlate to the rate of healing, since the complex healing mechanism is a function of numerous other kinetic parameters (e.g. bulk polymerization rates, catalyst dissolution kinetics, mobility of the healing agent on the crack surface, mobility of dissolved catalyst throughout liquid healing agent). For example, DCPD/Grubbs catalyst achieves a maximum room temperature degree of cure in 7-8 hours [57], but self-healing polymers using DCPD and Grubbs' catalyst as a healing agent system reaches a maximum healing in the range of 12-15 hours [58].

Two ROMP-based monomers that have received significant attention as more rapid healing agents are ethylidene norbornene (ENB) and the *exo*-isomer of DCPD. DCPD is most easily obtained as the commercially available *endo*-isomer, and all ROMP-based self-healing systems discussed thus far have also used this isomer. However, the *exo*-isomer, which can be prepared from *endo*-DCPD in a two-step isomerization process [59], is known to undergo ROMP nearly 20-times faster than its *endo*-counterpart [60]. So unsurprisingly, when *exo*-DCPD was incorporated into a self-healing polymer steady-state healing was reached after only about 30 minutes—nearly 20 times faster than the time required to fully heal with the *endo*-isomer [61]. However, increasing the bulk polymerization rate by using

exo-DCPD as a healing agent came at the expense of significantly decreasing the quality of healing. This was found to be a result of a mismatch between the bulk polymerization and catalyst dissolution kinetics, causing polymer to be formed only intermittently on the self-healing crack surface, localized around the catalyst particles. An analogous effect was observed with epoxy-based healing agents, in which rapidly curing epoxy/hardener combinations also formed non-continuous films of polymer in the crack volume, resulting from a mismatch of polymerization and epoxy/hardener mixing kinetics [43, 44], if the epoxy- and hardener-filled microcapsules were poorly distributed throughout the polymer matrix [62]. Some approaches to reduce the severity of these kinetic mismatches, and consequently increase both the quality and speed of healing, will be discussed later in this section.

Ethylidene norbornene, a monomer also active towards the ROMP chemistry, is particularly attractive as a healing agent because it is a cheap, commercially available chemical with an extremely rapid bulk polymerization rate; the time to reach maximum room temperature cure for ENB is nearly an order of magnitude faster than *endo*-DCPD with an order of magnitude lower loading of catalyst [63-65]. Liu *et al.* first investigated the feasibility of ENB and ENB/DCPD blends as healing agents using a quick and convenient rheokinetic technique developed to simulate a self-healing polymer [66, 67]. In this technique, a rheometer's bottom plate was coated with a layer of epoxy polymer containing embedded Grubbs' catalyst (which was polished to reveal the catalyst on the epoxy surface), and the healing agent was injected between the top and modified bottom parallel plates (Fig. 2.3). This approach, with dissolution and diffusion of the catalyst in the healing agent occurring concurrently with polymerization, encompasses all of the different kinetic phenomena occurring during the self-healing mechanism. ENB was shown to reach maximum cure in this simulative self-healing environment in about 25 minutes, and blends of ENB and *endo*-DCPD were able to effectively merge the rapid healing kinetics of ENB with the good mechanical properties of polyDCPD.

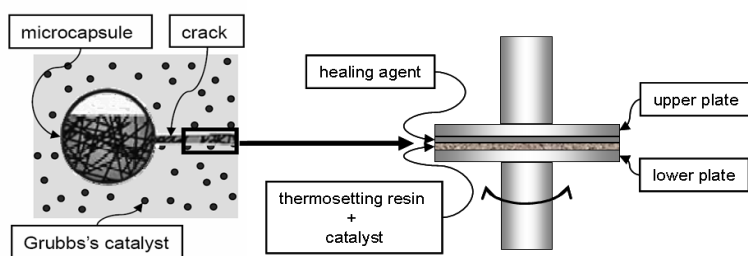


Figure 2.3. Rheokinetic test method designed to mimic self-healing. Reprinted with permission from reference [67].

To complement these kinetic optimizations of ROMP-based self-healing polymers, a concerted effort is currently underway in our labs to improve the mechanical properties of polymerized healing agents. Sheng *et al.* developed several custom, ROMP-active crosslinking agents that, when blended with other self-healing ROMP monomers (*endo*-DCPD, *exo*-DCPD or ENB), significantly increases storage modulus (12% increase at 20.3 wt.% crosslinker loading), glass transition temperature (~ 30 °C increase at 16.7 wt.% crosslinker loading), and crosslink density (62% decrease in molecular weight between crosslinking sites at 19.6% crosslinker loading) of the resulting polymers [68, 69]. Also, Jeong *et al.* have reported one of the first approaches towards improving mechanical properties of healing agents using nano-fillers [70]. In this work, multi-walled carbon nanotubes (MWNT) were chemically modified with a ROMP-active norbornenyl-group, and addition of these functionalized-MWNT to DCPD showed massive improvements in tensile toughness ($>900\%$), relative to neat polyDCPD, at nanotube loadings (0.4 wt. %) low enough to not significantly increase the viscosity of the liquid healing agent. More specifically, the strain to failure in these systems increased from 5.75% for neat polyDCPD to 51.8% for the composite, resulting in a corresponding toughness increase of 2.44 MPa to 25.0 MPa. The functionalized-MWNTs also showed excellent long-term dispersion in liquid DCPD and ENB [71], and moderately improved modulus, glass transition temperature, and crosslink density of both polymerized healing agents.

One downside to microcapsule-based self-healing is the non-negligible detrimental effects the embedded microcapsules and catalyst impart to the virgin mechanical properties of the composite. Details related to this virgin property reduction will be discussed later, but

in order to partially offset this effect, it is of interest to optimize self-healing systems to require lower loadings of healing additives to achieve high degrees of healing. Rule *et al.* showed that self-healing polymers with smaller crack volumes requires lower amounts of microcapsules with smaller capsule diameters to achieve full healing [72], so a method to reduce the size of cracks could presumably decrease the amount of necessary healing components. One technique that could fulfill this requirement is the embedment of shape memory alloys or polymers, which has been shown in the past to adequately facilitate crack closure [73-78]. Kirkby *et al.* recently incorporated shape memory alloy wires into self-healing polymers, which showed that *in-situ* crack closure, resulting from activation of the shape memory wires, did indeed reduce the necessary loadings of healing components to achieve maximum healing efficiencies, and the heat generated from the wires also assisted in curing the healing agent faster and to a higher degree of cure [79, 80].

In spite of all the great improvements to self-healing polymers described above, perhaps the largest drawback of using ROMP-based self-healing is economics—the Grubbs' catalyst uses ruthenium, a precious metal that will likely never be inexpensive. One way this problem can be addressed is by using the monomers described above with faster healing kinetics (such as ENB and *exo*-DCPD), which require lower loadings of catalyst to achieve high degrees of cure in a reasonable time period. Additionally, increasing the rate of catalyst dissolution in healing agent, either by treating the catalyst particles to have a larger surface area [81] or selecting catalysts and healing agents with inherently matching chemical compatibilities [82, 83], is known to reduce the amount of catalyst required in a self-healing polymer. Also, Rule *et al.* showed that by encasing Grubbs' catalyst in a protective wax shell, a 10-fold decrease in catalyst loading can achieve similar healing to an unprotected catalyst [84]. This resulted from both the especially small catalyst particle size in the wax increasing the surface area of catalyst available for the healing agent to dissolve and the wax casing protecting the catalyst from decomposition at the hands of incompatible polymer matrix resins. The development of this wax encasing technique also allowed other ROMP-catalysts, with significantly lower air stability and lower functional group tolerance (but also lower price) compared to Grubbs' catalyst, to be incorporated into self-healing polymers [85].

Microcapsule optimization

One of the crucial factors related to engineering self-healing polymers is the development of adequate microcapsules. The encapsulation technique should, ideally, be simple and user-friendly, and the liquid healing agent should be chemically inert to the microencapsulation conditions. The healing agent should not leach out of the capsules over time, nor should any other components destructively permeate into the microcapsule. The capsules should be robust enough to withstand handling and fabrication of self-healing composites, but fragile enough to break and subsequently release core material once the self-healing polymer is fractured. And finally, these capsules should also have a compatible outer shell wall to promote good adhesion to the surrounding polymer matrix.

The encapsulation of DCPD in a poly(urea-formaldehyde) shell was among the first reports of microcapsules for self-healing materials [86] (Fig. 2.4), and many variations of this seminal fabrication technique, as well as mechanical testing of the resulting microcapsules, have since been reported [87, 88]. One significant improvement to the DCPD-filled UF capsules was the development of a procedure to produce nano-sized microcapsules [89] (Fig. 2.4), which is important, for example, when fabricating thin self-healing coatings. In other reports, epoxy matrix/microcapsule adhesion was enhanced by grafting either silane-coupling agents [90] or epoxy functional groups [91] to the surface of the urea-formaldehyde capsules. One especially interesting variant of these systems was a binary capsule consisting of a large, DCPD-filled microcapsule ($\sim 140 \mu\text{m}$) with smaller capsules ($\sim 1.4 \mu\text{m}$) containing a second, different liquid at the periphery of the larger capsule [92] (Fig. 2.4). In this work, the common plasticizer dibutylphthalate was encapsulated in the smaller, peripheral capsules, and preliminary results have shown some potential for encapsulating a liquid initiator in these peripheral capsules, thus potentially eliminating the need for a two-part self-healing system [93].

Additional improvements to encapsulating ROMP-based monomers involve the use of stronger shell wall materials. In one example, a technique was developed to encapsulate DCPD in melamine-formaldehyde polymer shells [94], which was shown to produce capsules with stronger shell materials that rupture at larger deformations than the urea-formaldehyde systems [95]. Recently, Liu *et al.* developed an approach to encapsulate a

blend of ENB and ROMP crosslinkers in a ternary melamine-urea-formaldehyde shell wall [96] (Fig. 2.4). This fabrication was a very user-friendly technique (unlike other microencapsulation procedures, external control of pH was not necessary) that produced a narrow size distribution of capsules without any of the non-capsule polymer debris that plague many of the abovementioned fabrication techniques. These microcapsules also had a very rough outer surface and showed significantly higher thermal stability (300 °C) and less core material permeability when compared to their urea-formaldehyde capsule counterparts.

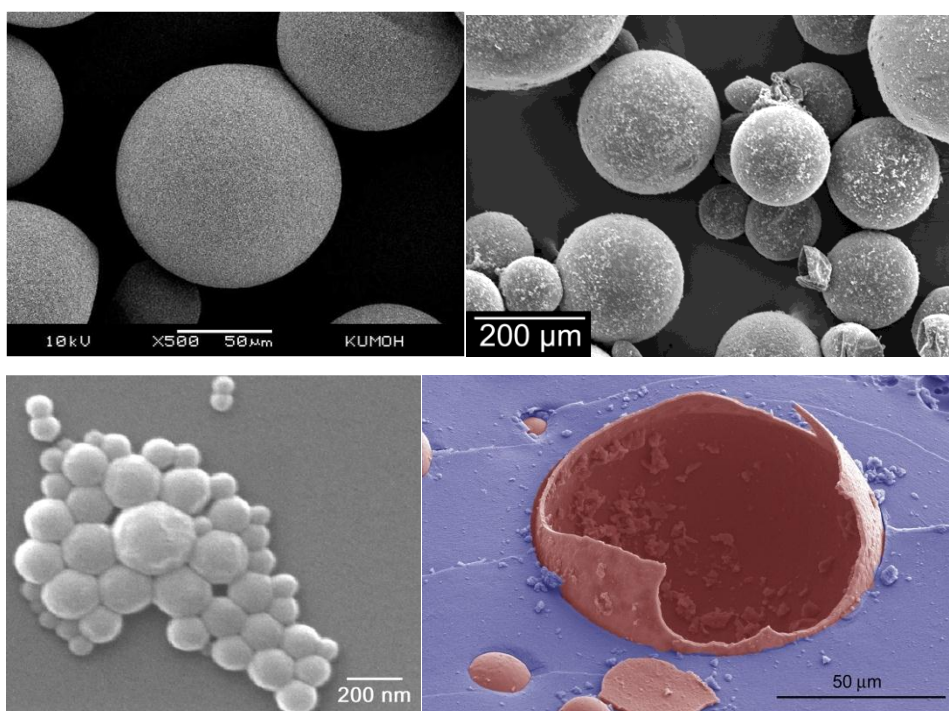


Figure 2.4. Clockwise from top-left: ENB and crosslinker-filled MUF capsules [96]; DCPD-filled UF capsules with smaller, peripherally decorated microcapsules [92]; a ruptured, DCPD-containing UF capsule embedded in a fractured self-healing polymer's crack plane; and DCPD-filled nano-sized capsules [89].

There are numerous reports of microcapsules for self-healing polymers containing epoxy resins. With some exceptions, most of these reports have encapsulated bisphenol-derivative epoxies in urea-formaldehyde shells [97-100]. One improvement to these systems was the use of a UV-curable epoxydiacrylate shell material, which utilizes a quicker and

more efficient fabrication technique that produces microcapsules with properties comparable to, or better than, the urea-formaldehyde systems (Fig. 2.5) [101]. A moisture-sensitive epoxy hardener, $\text{BF}_3 \cdot \text{OEt}_2$, was also encapsulated with this UV-curable shell material using a novel technique that avoids the hardener's decomposition, which would otherwise occur very rapidly as most types of encapsulation procedures necessarily use aqueous chemicals. In this technique, carbon dioxide bubbles were encapsulated in the shells, followed by evacuation of the CO_2 from the capsule, and diffusion the $\text{BF}_3 \cdot \text{OEt}_2$ into the empty core (Fig. 2.5) [102].

A plethora of other resins have been encapsulated in different shell wall materials, all of which show promise for self-healing applications. For example: solvent/epoxy solutions (Fig. 2.5) [103], solvent/carbon nanotube suspensions [104], and liquid paraffin wax [105] have been encapsulated in urea-formaldehyde shells; Styrene [106, 107] and polythiol epoxy hardeners (Fig. 2.5) [108] have been encapsulated in melamine-formaldehyde shells; reactive amines have been encapsulated in polyureas [109], and diisocyanate resins were encapsulated in polyurethane shells [110].

Other optimizations of self-healing microcapsules include variations in healing agent delivery technique, such as work by Kirk *et al.* where, instead of microcapsules, epoxy and hardener were absorbed into nanoporous silica, which was then incorporated into a polymer [111]. Also, Pastine *et al.* recently reported the development of phototriggerable microcapsules, which "burst" upon exposure to ultraviolet (UV) radiation [112]. These capsules could possibly be used to maximize the amount of healing agent released into a surface crack (for example, in a self-healing coating or film) upon exposure to artificial or even natural (solar) UV light.

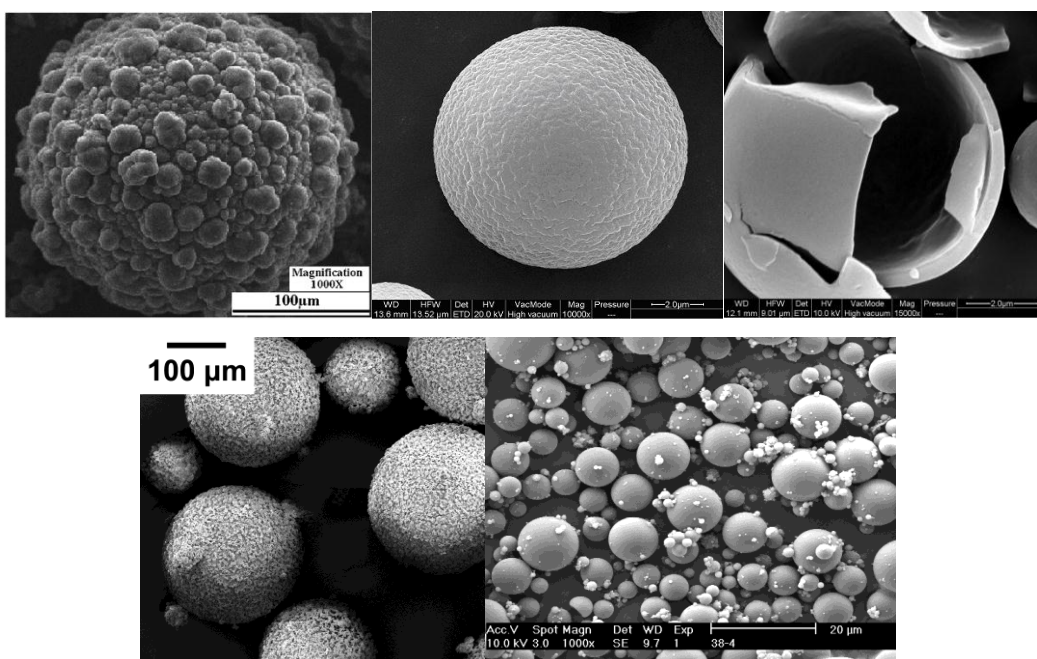


Figure 2.5. Clockwise from top-left: epoxy-filled urea-formaldehyde capsules [99]; epoxy in UV-curable epoxydiacrylate shells [101]; BF_3OEt_2 -filled epoxydiacrylate microcapsule after rupture [102]; polythiol-filled melamine-formaldehyde capsules [108]; urea-formaldehyde shell microcapsule filled with an epoxy/solvent solution [103].

2.3.1.2 Phase-separated healing agents

An alternative to storing healing agent in microcapsules is the incorporation of healing agents directly into the polymer matrix as a phase-separated component. One key difference between this approach and the microcapsule systems is that the protection afforded by the capsule shell is lost, therefore necessitating long-term inertness between the healing agent and the matrix resin/polymer. But even though this brings about stricter healing agent requirements than that of the microcapsule-based healing agents, these phase-separated systems offer the potential of reduced fabrication time (i.e. no need for encapsulation procedures) and generally simpler processing. *Zako et al.* were the first to demonstrate healing with phase-separated healing agents. In their work, solid epoxy prepolymer healing particles (Toa-Gosei AP-700), with a melting point of 383-413 K and a mean diameter of 105 μm , were incorporated into a fiber-reinforced polymer matrix [113, 114]. After damage to

the matrix, these composites were heated above the melting point of the epoxy prepolymer, which then caused the epoxy particles exposed on the fracture surface to melt and fill the damaged region. Upon cooling, the epoxy healing agent cures to heal the polymer, showing nearly full recovery of stiffness and even an increased fatigue lifetime, relative to the virgin material.

Cho *et al.* demonstrated self-healing of a vinyl ester matrix containing both encapsulated and phase-separated healing agents [115]. In this system, a mixture of hydroxyl end-functionalized polydimethylsiloxane and polydiethoxysiloxane healing agents were incorporated into the matrix as the phase-separated component, and a solution of an organotin polycondensation catalyst was used in embedded microcapsules. Healing in this system was relatively less efficient (24% recovery of fracture toughness) than others, but the healed regions showed excellent corrosion resistance, chemical stability and passivating ability, which are of paramount importance to the paint and coating industries [116].

Meure *et al.* introduced a slightly different methodology by using phase-separated particles of a thermoplastic polymer, polyethylene-co-methacrylic acid (EMAA) [117]. After fracture and a subsequent heating cycle, the EMAA polymer infiltrated the damage regions and restored 85% of the virgin polymer's fracture toughness (critical stress intensity factor). One especially interesting aspect of the EMAA healing agent is a built-in pressure-based delivery system resulting from bubbles present in the phase-separated EMAA particles. These bubbles, likely filled with water resulting from reactions between the EMAA particles and the polymer matrix resin during fabrication [118], expand during the heating/healing cycle to force the healing agent into cracks (Fig. 2.6).

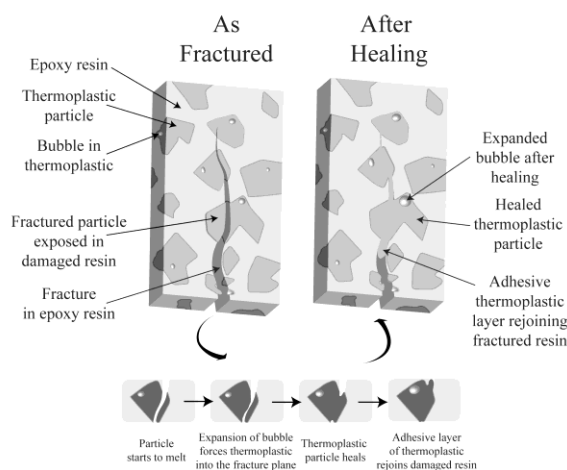


Figure 2.6. Phase-separated EMAA particles exhibiting a pressure-driven healing effect when heated to its melt. Reprinted with permission from reference [117].

Another thermoplastic polymer used as a phase-separated healing agent is Poly(ϵ -caprolactone) (PCL) [119]. PCL forms a miscible blend with uncured epoxy resin, but during the epoxy's curing reaction, the PCL undergoes a reaction-induced phase separation to yield a polymer with an ordered “bricks-and-mortar” morphology with spheres of epoxy polymer (bricks) interpenetrated with a network of PCL (mortar) (Fig. 2.7, left). After damage and a short heating cycle, the PCL melt was able to infiltrate damage and either completely recover or surpass some virgin mechanical properties (Fig. 2.7, right). This system is especially promising for its simple processing, micron-scale distribution of phase-separated PCL, and, interestingly, many of the material properties of the polymer are dominated by that of the thermoset epoxy “bricks.”

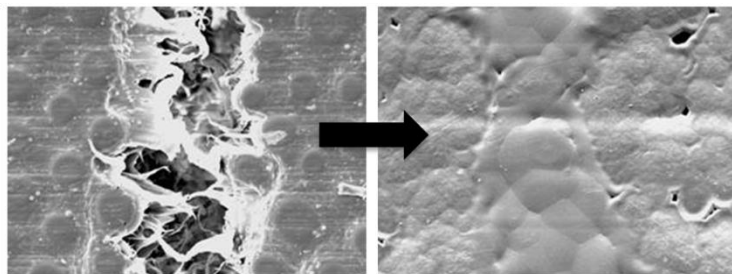


Figure 2.7. Epoxy polymer with intermingling, phase-separated PCL after damage (left) and after a heating cycle (right). Reprinted with permission from reference [119].

2.3.1.3 Healing agents in hollow fiber

One drawback for many of the systems described above is that small, localized volumes of healing agent limits repeated healing of one damage site. Storage vessels capable of supplying volumes of healing agent significant larger than expected crack sizes could potentially address this problem, but increasing the size of the types of storage vessels described above could drastically diminish the virgin properties of the polymer in which they are embedded. To solve these problems, significant effort has been dedicated to incorporating healing agents into hollow fibers, which can be used both as a structural reinforcement and as a large storage vessel. Once failure occurs in composites filled with these resin-infused fibers, fibers rupture and healing agent(s) can diffuse into the damaged regions (Fig. 2.8). These hollow fibers have been filled either through open ends, with either capillary action or vacuum assistance, or through surface pores, which need to be covered after resin infusion (Fig. 2.9).

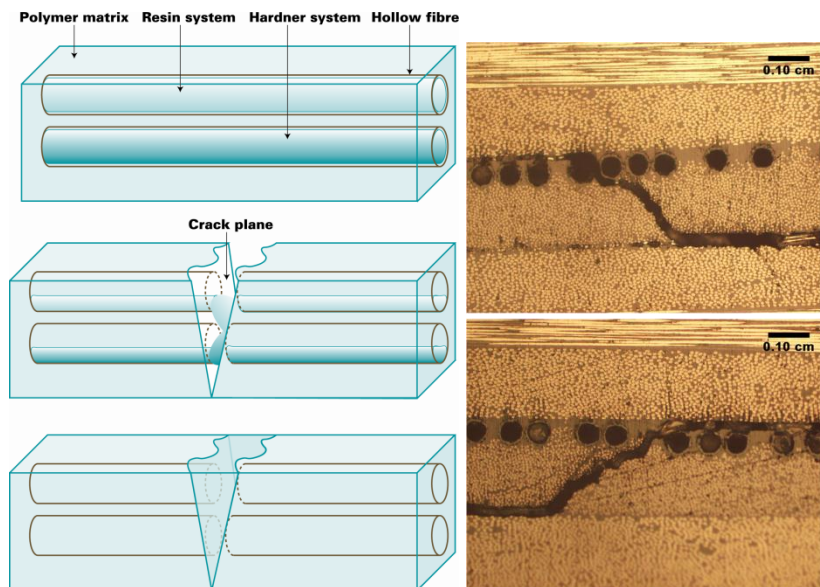


Figure 2.8. Self-healing concept using hollow fiber storage vessels (left) and ruptured hollow vessels containing healing agent (right). Images reprinted with permission from reference [133].

Earlier generations of composites with resin-filled fibers were reported by Dry *et al.* [120-123] and Motuku *et al.* [124] to rupture in response to damage and adequately release healing agent. The quality of healing, however, was limited by poor healing agent reactivity and especially large fiber sizes that frequently acted as initiation sites for failure. Modifications to these early fibers have been reported by Dry *et al.* to adequately heal composites in short time periods [125-127], but the differences between these more recent reports and the earlier systems are not described in detail. Resin-filled fibers with diameters small enough to impart some structural reinforcement to the polymer matrix were used by Bleay *et al.* [128], but the healing agent chemistry in these systems generally required harsh curing conditions (vacuum and heat).

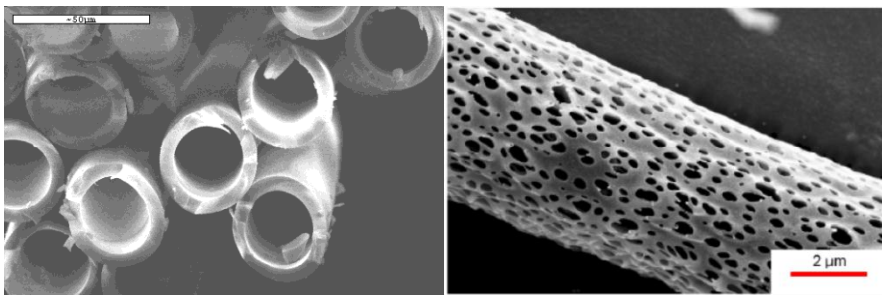


Figure 2.9. Hollow fibers with open ends (left) [133], and hollow fibers with open surface pores (right) [136].

Bond and coworkers developed a technique to manufacture hollow borosilicate glass fibers with variable degrees of hollowness, internal diameters, external diameters and lengths [129]. After targeting the optimal parameters for self-healing applications (fiber hollowness: 50-55%, external diameter: 60 μm , internal diameter: 40 μm), these fibers were filled with a two-part epoxy resin and, in some cases, a UV fluorescent dye. Early work incorporated these fibers into reinforced polymers as groups of consecutive orthogonal plies, which showed that, after applying load, the UV dye from the fractured fibers can sufficiently fill fracture and delamination areas to aid in damage visualization [130,131]. Additionally, after a short healing time, epoxy resin/hardener was able to flow out of the fibers and cure, recovering nearly 75% of the flexural strength lost after damage. This system was further optimized by intermingling the filled hollow fibers at optimal pitch spacings within E-glass

or carbon fiber plies, resulting in both negligible virgin property reduction and nearly full recovery of flexural [132-134] and compression-after-impact strength [135].

A number of different types of healing agents have been reported to sufficiently heal when incorporated into hollow fibers. In one approach, Liu *et al.* reported a coating that can heal its ability to act as a water permeation barrier [136]. In this work hollow, water-degradable poly(lactic acid) (PLA) fibers were filled with a metal oxide precursor healing agent, TiCl_4 , and subsequently incorporated into sub-surface polymer layers of multilayer films. Once damage penetrated deep enough in the multilayer film to reach the PLA layers, atmospheric moisture degraded the PLA fibers, releasing TiCl_4 into the damaged region. On contact with ambient humidity, the healing agent oxidizes to a TiO_2 film to form an effective water permeation barrier. Another healing agent reported to adequately self-heal a polymer when infused in hollow fibers is DCPD, otherwise well-known in the realm of microcapsule-based self-healing [137]. A commercially available borosilicate glass tube (external diameter: 125 μm , degree of hollowness: 64%) was filled with either DCPD or a suspension of functionalized-MWNT [70] in DCPD by capillary action, sealed at both ends, and coated with Grubbs' catalyst at its exterior walls. After damage and a short waiting time, healing with DCPD was able to recover 90% of its virgin tensile strength, with even higher values of strength recovery possible at low loadings of the functionalized-MWNT.

2.3.1.4 Microvascular networks

Infusing larger storage vessels, such as the hollow fibers described above, with healing agent will likely result in multiple healing events of one damage site, but the total volume of liquid in each fiber is still finite. A logical progression to supplying even larger volumes of healing agent to damage sites is through a series of healing agent-filled interconnected channels, which could potentially be linked to an external, refillable liquid pump to deliver a constant supply of healing agent. Healing with connected networks of healing agent is mechanistically similar to that of the hollow fiber approach, and it is perhaps the most biomimetic self-healing system that will be presented in this review since the network of channels is visually and conceptually similar to the vascular systems of many

plants and animals (Fig. 2.10). Appropriately, connected networks of flowing healing agent have been coined “microvascular” networks.

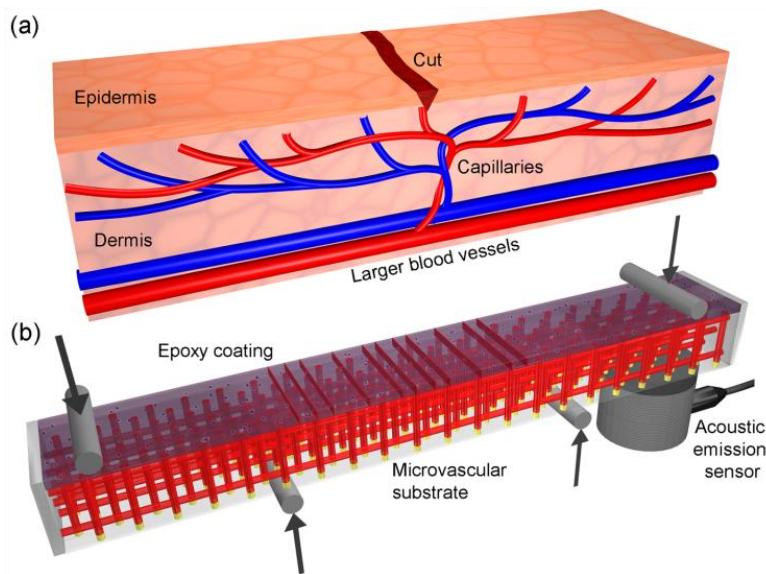


Figure 2.10. Microvascular-based self-healing concept: a) A capillary network in the outer skin layer with a cut and b) schematic of an epoxy specimen containing a microvascular network, loaded in a 4-point bending configuration monitored with an acoustic-emission sensor. Reprinted with permission from reference [149].

Connecting channels of storage vessels adds several degrees of complexity not present in most other self-healing techniques. Bejan and coworkers have addressed some network design parameters by calculating optimal two and three dimensional vascular architectures that efficiently deliver healing agent to multiple damage sites with maximum flow properties [138-143]. Williams *et al.* complemented this work with calculations to determine optimal network sizes and architectures to enhance the reliability (e.g. minimizing the negative effects of network leakage and blocking) and applicability (e.g. minimum mass penalties, pumping power requirements, etc.) of microvascular self-healing systems [144, 145]. However, the complexity of many of these optimal design conditions for microvascular systems would likely require extremely sophisticated fabrication techniques that are currently technologically unavailable or too elaborate to be practical. Therefore,

only a few vascular architectures described in these reports have been experimentally demonstrated.

A fabrication technique utilizing a robotic direct-write assembly to develop a scaffold of fugitive wax was used to construct microvascular networks. The fugitive wax scaffold was infused with an epoxy/hardener resin system, which was subsequently cured, and the wax removed at elevated temperatures to create a well-defined network in the evacuated microchannels [146-148]. Initial self-healing work using this fabrication technique contained Grubbs' catalyst embedded in the epoxy matrix and DCPD flowing through the microvascular network, which showed up to 70% recovery of fracture toughness after damage in a 4-point bending protocol [149, 150]. Substantial healing was observed for up to 7 damage/healing cycles, after which point healing diminished, presumably due to consumption of the embedded Grubbs' catalyst that cannot be replenished as easily as the DCPD flowing through the network channels. This prompted Toohey *et al.* and Hansen *et al.* to change the healing chemistry from a system using a solid catalyst to a two-part liquid healing agent—an epoxy and an amine hardener—with each part flowing through segregated vascular networks [151, 152]. Over 60% recovery of fracture toughness was achieved for up to 16 intermittent damage/healing cycles and 50-100% recovery of fracture toughness was achieved for 30 damage/healing cycles with adjacent and interpenetrating networks, respectively.

In another work, microvascular networks were added to composite sandwich structures by embedding PVC tubes horizontally into a polymethylacrylimide closed-cell foam, drilling vertical holes at appropriate locations into the foam through the tubes to form vascular networks, and sandwiching the resulting samples with an E-glass/epoxy composite skin [153, 154]. After impact damage, vascular networks filled with a premixed epoxy/hardener were able to fully restore the undamaged sandwich structure's flexural load and compression-after-impact (CAI) strength. When epoxy and hardener were separately added to segregated vascular channels (in which mixing of the two components must occur after they diffuse out of the networks into damage regions) full recovery of virgin properties also occurred, but only when both filled networks were ruptured.

2.3.2 Diffusion

The subsections below discuss self-healing mechanisms based on molecular diffusion of a mobile species to create chemical or physical adhesive linkages. An important distinction can be made between these systems and the crack-filling adhesives: essentially, the diffusion-based healing mechanisms in the subsections below all require the transport of the mobile species from one damage surface to another, as opposed to the crack-filling systems that fill the space between damage surfaces with a healing agent. This distinction brings about several issues not present with the crack-filling systems, such as both the necessity for crack closure and application of an external stimulus to drive the movement of the mobile species.

2.3.2.1 Healing via a thermoset/thermoplastic miscible blend

Hayes and coworkers developed a self-healing approach based on a thermoset/thermoplastic blend. A thermoplastic polymer (polybisphenol-A-co-epichlorohydrin) chosen to form a homogenous blend with the thermoset, both before and after curing, was dissolved into the thermoset epoxy resin, and E-glass/epoxy composites were fabricated with conventional layup techniques [155]. After tensile or impact loading, significant decreases in delamination area and increases in extension at failure, fracture toughness, and impact strength were observed after a short heat treatment at temperatures ranging from 100-140 °C, resulting from the thermoplastic polymer melt diffusing through and filling the damage region. The extent of healing varied with different thermoplastic polymer loadings and healing temperatures, with optimal conditions showing about 70% recovery of virgin properties and significant, but slightly diminishing, healing with repeated damage/healing cycles [156].

2.3.2.2 Dangling chain diffusion healing

Another diffusion-based healing technique utilizes interactions between “dangling chains” of polymer, branching off of the main polymer backbone, across damage surfaces to heal. After diffusion, these dangling chains can heal a polymer either by physical (mechanical interlocking) or chemical (reactions) interactions. One such polymer was

fabricated by eliminating the sol fraction of a weak polyurethane sol-gel just beyond its sol-gel critical point [157, 158]. Elimination of the sol near the critical point allowed the polyurethane gel to have a high enough crosslink density to maintain mechanical integrity, but a sufficient number of dangling chains available for healing. After cutting these polymers with a razor blade the two damage surfaces were brought into contact, which allowed for topological interactions (interdiffusion of dangling chains) between the damage surfaces to effectively heal damage. The extent of healing was found to be strongly dependant on the number and length of the dangling chains, and samples containing optimized chain parameters demonstrated the ability to recover nearly 80% of their virgin tear strength after only 10 minutes of room temperature healing time.

Given that the gels discussed above have relatively weak mechanical properties (which was actually a necessity to produce the dangling chain molecular mobility required to facilitate room-temperature curing), their application base is limited. Rahmathullah *et al.* investigated the ability of thermoset epoxy/amine polymers, which are often used for structural applications, to heal via topological diffusion mechanisms [159]. Fractured halves of compact tension test specimens were brought into intimate contact with each other, clamped at either high or low pressures, and healed with a heat treatment of 185 °C for one hour. Elevated healing temperatures were required to bring the epoxy into its rubbery state, which allowed for enhanced molecular mobility of the topological polymer chains. In cases where the polymer was initially fabricated with a stoichiometric ratio of epoxy and amine, significant diffusion across the crack plane occurred to recover up to 50-60% of the maximum load-at-failure, which was repeatable over numerous damage/healing cycles. In cases where the epoxy/amine ratio was not stoichiometric, over 100% recovery of virgin properties was possible due to unreacted epoxy groups diffusing through the damaged areas and undergoing various epoxy ring-opening polymerization reactions at the crack interface.

Caruso *et al.* also demonstrated healing of epoxy/amine matrices with residual reactive groups [160]. Various solvents were selected and encapsulated in urea-formaldehyde microcapsules, which were embedded in the polymer matrix. Upon fracture, the microcapsules would rupture and transport solvent into the damage region, which acted to increase local molecular mobility at the crack surfaces and assist in the diffusion of residual

reactive groups. This solvent-assisted diffusion allowed the residual epoxy/amine groups to heal below the bulk polymer's glass transition temperature (in the case of this work, at room temperature), resulting in over 80% recovery of fracture toughness. This system was later improved upon by including epoxy resin solutes in the microcapsules, which allowed for full recovery of the virgin material fracture toughness [161].

2.3.2.3 Viscoelastic healing

Kalita and coworkers demonstrated a healing technique that takes advantage of the inherent viscoelastic behavior of polymers. Thin films of commercially-available poly(ethylene-*co*-methacrylic acid) (EMAA), either neutral or partially ionized, were subject to high-energy impact or sawing damage, after which point the damage was autonomically healed to withstand pressures of up to 3 MPa [162, 163]. This healing was attributed to a viscoelastic response of the EMAA, facilitated by a transfer of energy from the damage event to temporarily bring the damaged region of polymer into a melt. More specifically, the transfer of energy during impact or sawing elicited a localized melt of the damage region that allowed the inherently elastic response of EMAA to physically close deformations. Subsequently, the viscous behavior of the polymer melt allowed for diffusion of polymer chains to seal the damage site. This healing mechanism was shown to be applicable only when the damage event was of high enough energy to bring the local damage region into the melt. Also, healing was only observed over a defined temperature range, -30-60 °C, since at lower temperatures the damage event could not transfer enough energy to heat the polymer above its melt temperature, and at higher temperatures the damage energy was dispersed more easily throughout a larger area of polymer, also resulting in a failure to heat the localized damaged region into a melt.

Studying the detailed mechanism of this viscoelastic healing has proven difficult as the healing response occurs almost instantaneously (attempts to visually monitor the healing were unsuccessful, even with high-speed camera analysis capable of 4000 frames/sec [162]). To address this problem, a quasi-static test method was developed to mimic the high-impact ballistic damage in which a pre-heated, disc-shaped object was rapidly (10^3 - 10^5 mm/min) pulled through the EMAA polymer in a controlled manner [164]. This technique allowed for

the contribution of the elastic and viscous components of the healing process to be monitored independently. It was proposed that the ionic clusters along the EMAA chain enhances healing, relative to neutral EMAA, by increasing the elastic modulus and therefore aiding in efficient damage closure. The viscous component of healing was improved by heating the localized damage region to higher temperatures and maintaining the heat for longer times [165].

2.3.3 Bond Reformation

Polymers with controlled reversible polymerization processes have shown great potential for self-healing. These unique polymers, sometimes called “mendomers” or “dynamers,” contain specific bonds that are reversible in response to a generally mild external stimulus (e.g. heat, light, acidic or basic conditions, etc.). This unique characteristic has profound implications for self-healing polymers: a bulk mendomer has the potential to repeatedly heal itself in such a way that the virgin material is fully restored, even at the molecular level. A great number of different mendomers have been reported in the literature, so the entire scope of these reversible polymers is too great to fully address here; interested parties are directed to several recent reviews that give due credit to the breadth of this field [166-170]. Instead, we focus our discussion only on reversible polymers that have been shown to heal bulk damage in solid state polymers.

By employing rational molecular design, the reversible bonds in mendomers can be engineered to behave as “weak links” that preferentially break in response to stress, preserving the intactness of the irreversible bonds. This is especially important for self-healing applications—if large scale damage can translate to the molecular level exclusively as cleavage of the “weak links,” then molecular structure can be completely restored upon employing the external stimuli to reform these broken “weak links.” However, it is probably unreasonable to expect macroscopic damage of a bulk polymer to occur exclusively through these “weak links” (although we admit that, to the best of our knowledge, there have been no literature reports to confirm or refute this claim). For this reason, many of the polymers presented in this subsection have only been shown to heal after a depolymerization/polymerization cycle, which allows intact “weak links” at the damage site

to break and subsequently reform with “weak links” on opposite damage surfaces. Also, the depolymerization step can provide additional molecular mobility for the “weak links” to partially fill the crack volume and diffuse into opposite crack surfaces to find bonding partners.

One inherent limitation in these systems is that applying the required external stimulus to initiate the depolymerization/polymerization cycle of damaged monomers requires manual intervention, and the healing is therefore not fully autonomic. However, clever solutions to this problem have recently started appearing in the literature. For example, monomers requiring thermal stimuli can be heated by passing electrical currents through reinforcing graphite fibers [171, 172], although incorporation of these fibers still cannot be considered truly autonomic healing without an efficient detection system that can locally heat damage regions. Also, monomers requiring UV irradiation to reverse bonding can potentially receive this external stimulus via sunlight. But there are still significant questions that need to be addressed before the sun can be considered a feasible self-healing UV-source, such as how to exclusively expose sunlight to damage regions in order to not constantly depolymerize “healthy” polymer.

2.3.3.1 Thermally reversible self-healing

For a large number of polymers that heal via bond reformation, heat is the external stimulus that begins the healing process. The reason for this ubiquity can perhaps be attributed to the fact that a thermally-reversible chemistry—the Diels-Alder (DA) reaction (between a diene and a dienophile)—is ideal for self-healing for a number of reasons. First, when a good diene and dienophile pair are chosen (such as furan and maleimide derivatives, respectively), the DA reaction can occur at room temperature without the need for any external reagents or solvents, which is an invaluable quality when preparing bulk polymers. Additionally, the controlled retro Diels-Alder (rDA) reaction of furan/maleimide-derived polymers occurs in the temperature range of approximately 90-120 °C, which is low enough such that thermal degradation will not compete with the cycloreversion, but high enough for some structural applications. And finally, the DA-adduct is often believed to act as the “weak link” during failure, cycloreverting to reform the diene and dienophile preferentially

to random bond scission. This implies that, should the “broken” diene and dienophile parts be brought together again in a solid-state DA reaction, damage can be repaired on the molecular level.

Chen *et al.* developed thermoset polymers based on the Diels-Alder reaction between the multi-furan and multi-maleimide monomers shown in Fig. 2.11, which resulted in a polymer with tensile, compressive and flexural mechanical properties similar to commercially available epoxies and unsaturated polyesters [173]. Original reports demonstrated that this polymer, when fractured in a compact tension protocol, could be heated to above 120 °C and recover 57% of its original fracture load upon cooling (Fig. 2.11). Using differential scanning calorimetry (DSC) and solid state ^{13}C NMR spectroscopy healing was observed to predominately result from the solid state DA reaction, and this healing was repeatable for multiple damage events [174]. Later reports showed that full recovery of virgin mechanical properties could be achieved for repeated damage events when fracture surfaces were accurately aligned and clamped with 0.35 MPa of pressure during healing [175]. Healing of polymers with structurally different multi-furan and multi-maleimide monomers have also been met with similar levels of success [176-178].

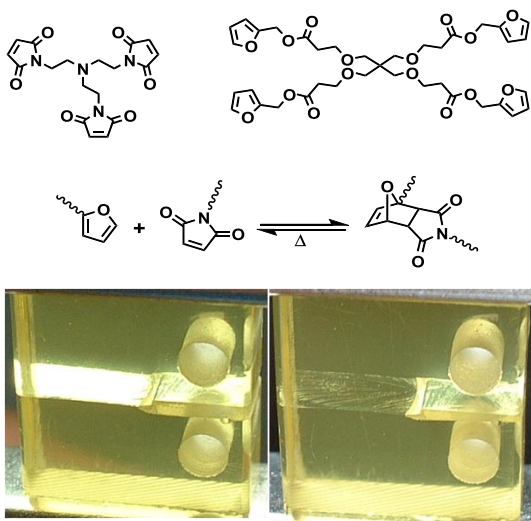


Figure 2.11. Chemical structures of a thermally reversible, DA-based thermoset polymer with the generalized DA reaction between a substituted furan and a substituted maleimide (top). A compact tension specimen comprised of this polymer after damage (bottom left) and after a heat treatment (bottom right). Images reprinted with permission from reference [173].

Murphy *et al.* have developed a series of self-healing DA-based monomers that use cyclopentadiene (CPD) as both the diene and dieneophile. In this novel approach, a macrocyclic derivative of DCPD, which is the DA adduct of two molecules of cyclopentadiene, was synthesized using several short organic linkers in such a way that the rDA reaction of the macrocycle would yield an α,ω -bis(cyclopentadiene) [179]. Upon cooling to below rDA temperatures, this linear molecule will preferentially undergo intermolecular DA reactions, as opposed intramolecular cyclization, to form the polymer backbone (Fig. 2.12). These resins are unique in that the one-component monomer greatly simplifies polymer fabrication, relative to multi-part resins that require homogeneous mixing of two or more liquids or solids. Healing efficiencies varied with the different mendomers shown in Fig. 2.12, but all systems showed full recovery of compression strength over several damage/healing cycles, as high as 60% recovery of fracture strength, and visual disappearance of both fracture and indentation damage after heating at or above 120 °C [171, 172].

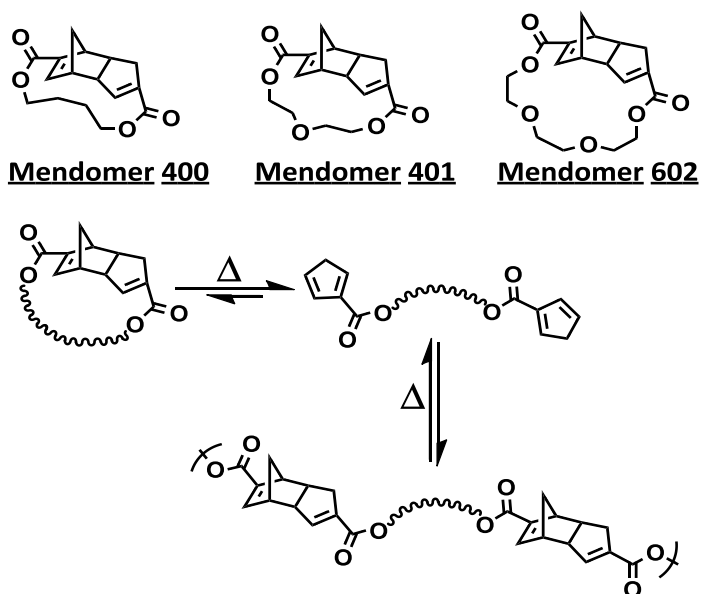


Figure 2.12. Three mendomers (above), which form a self-healing polymer after a heat treatment (below).

While the above systems show great potential for healing at the molecular level, the economic drawback of scaling up synthesis of these custom-made DA monomers would likely outweigh the benefit of healing, at least for large-scale, industrial applications. One recently investigated approach to reduce the economic severity of thermally-reversible healing is to functionalize well-known polymers, made from resins that are already cheap and commercially available in massive quantities, with DA-based thermally-reversible crosslinks. And in addition to healing, when these crosslinks are “broken” at elevated temperatures via the rDA reaction, the resulting functionalized resins and polymers can be recycled using standard thermoplastic processing technology. To this end, several well-known polymers (such as polyamides [180], polyketones [181], PMMA [182-185], and polyesters [186, 187]) have been functionalized with pendant or telechelic furan groups and crosslinked with small bis- or tris-maleimides. The functionalized resins were either commercially available or obtained in 1-2 step syntheses from commercially available resins. All crosslinked polymers were shown to have thermal and mechanical properties superior to their non-crosslinked polymer counterparts, and after a heat treatment to cleave the crosslinking groups, they could be processed using standard solution or melt processing techniques. Crack-healing behavior was observed in all systems, with nearly full recovery of virgin material properties possible after the rDA/DA heat treatment.

In addition to the thermoplastic polymers above, epoxy resins have also been prepared with thermally-reversible furan/maleimide crosslinks (Fig. 2.13). Since epoxies traditionally behave as thermosets, these polymers are unlike the DA-crosslinked thermoplastics above in that they likely will never have the ability to be melt or solution processed, but they can still function to heal damage. In one example of this work, Tian *et al.* synthesized a furan-functionalized diepoxide resin that, when cured with an anhydride hardener and crosslinked with a commercially-available bismaleimide, possessed thermal and mechanical properties similar to or better than traditional epoxy resins [188]. After damage and a 20 minute heating cycle at ≥ 119 °C a decrease in crack size was qualitatively observed.

Peterson *et al.* developed a thermally-reversible epoxy gel, which was intended for use as a crack-filling healing agent (similar to the above microcapsule or phase-separated healing agents) that could be added to a traditional, unfunctionalized polymer matrix as a

secondary phase [189, 190]. The healing agent was synthesized from a furan-functionalized epoxy prepolymer in *N,N'*-dimethylformamide (DMF) solvent, which was crosslinked with a commercial bismaleimide to form the gel. The addition of this thermally-reversible healing agent gel was hypothesized to allow for a self-healing polymer matrix that does not contain thermally reversible crosslinks (and would therefore not lose mechanical integrity while heating), but maintain the ability to repeatedly heal on the molecular level (through the discreet gel-phase filling damage regions). The initial reports of this technique focused mainly on manually applying healing agent gel to the crack surfaces of fractured specimens, which demonstrated the ability to partially heal the polymer for at least five damage/healing cycles.

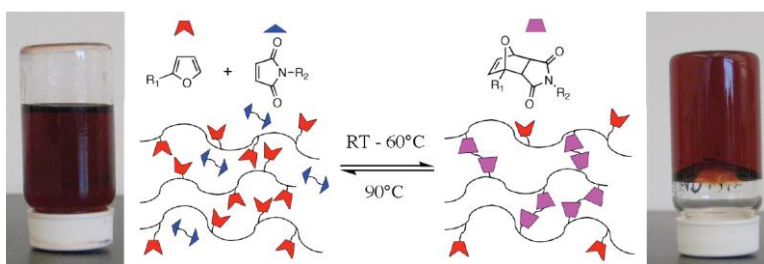


Figure 2.13. Self-healing with thermally-reversible, maleimide-furan crosslinks. The right inverted vial shows a polymer gel with crosslinks that can be cleaved at elevated temperatures to form a liquid polymer solution (left inverted vial). Reprinted with permission from reference [189].

2.3.3.2 UV-initiated self-healing

Conceptually similar to the thermally-reversible systems, bond reformation of damaged polymers can also be achieved by employing UV light as an external stimulus. One type of chemistry identified by Cho *et al.* as suitable for this type of healing is the [2+2] cycloaddition of cinnamoyl groups. Several tricinnamates were synthesized and photoirradiated to form cyclobutane-containing crosslinked polymer films, and it was observed by FTIR, UV/vis spectrophotometry, fluorescence spectrometry and fluorescence microscopy that after crack damage of these films, the cyclobutyl groups at the damage regions cyclorevert to reform cinnamoyl functionalities (Fig. 2.14) [191]. After 10 minutes

of re-irradiation with UV light, the cinnamoyl groups were able to recyclize to recover as high as ~25% of the virgin film's flexural strength [192]. This relatively low quality of healing may limit cinnamate-based polymers to film or coating applications, for which mechanical integrity is not always a primary concern. Furthermore, the most appealing UV sources (e.g. sunlight) may have small penetration depths unable to reach damage deeper than the small sample thicknesses typical of polymer films.

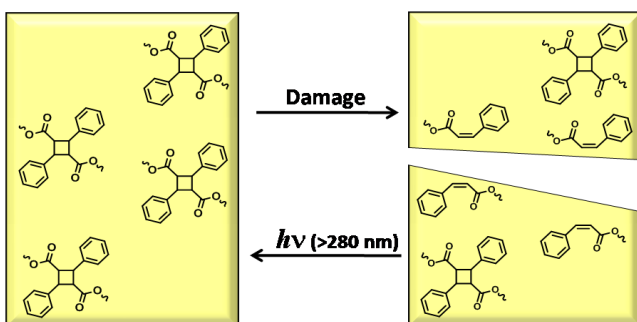


Figure 2.14. UV-based healing of cracks in cyclobutane-containing polymers of tricinnamates. Adapted from reference [192].

Polyurethanes incorporating a chitosan-based crosslinker were also shown to heal in the presence of ultraviolet light [193]. Chitosan is a partially deacetylated derivative of the polysaccharide chitin, which is the primary structural component of anthropod exoskeletons and available in massive quantities worldwide. In these polymers, a commercially-available chitosan saccharide was first functionalized with pendant 4-membered ring oxetane groups and subsequently cured with a trifunctional isocyanate and a polyethylene glycol chain extender to form a crosslinked polyurethane network. After damage and exposure to UV light, these polyurethane films were found to effectively heal scratches (Fig. 2.15). Through a series of control tests and ATR-FTIR and IRIR-imaging of damaged regions, the authors hypothesized a two-step healing mechanism. First, mechanical damage opened the oxetane pendant rings to create two reactive ends. Then, exposure to UV radiation cleaved urea linkages in the chitosan backbone, which combined with the oxetane reactive ends to form new crosslinks. This healing mechanism was qualitatively observed to both close and seal scratch damage. One promising feature of this system is that rapid healing (~30 minutes) of

micron-sized cracks is possible using UV light of similar wavelength and power density as the sunlight that reaches Earth's surface, but detailed information not present in this initial report (such as the polyurethanes virgin mechanical properties, quality of healing, and repeatability of healing) should be addressed before the practicality of this technology can be judged.

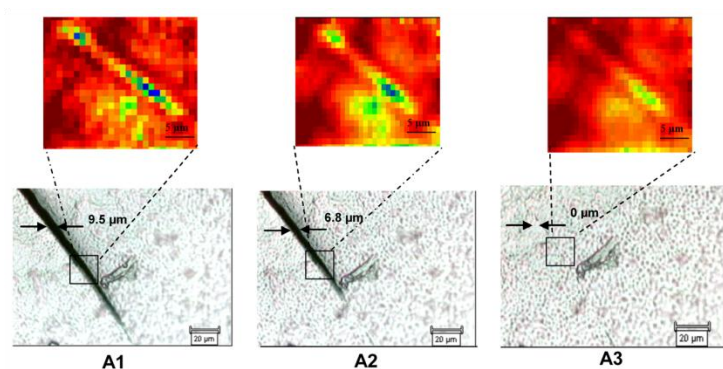


Figure 2.15. IR (above) and optical (below) images of oxetane-substituted chitosan crosslinked polyurethane during healing of crack damage. UV exposure times: A1) 0 min, A2) 15 min, A3) 30 min. Reprinted with permission from reference [193].

2.3.3.3 Metal-ligand dissociation/association healing

As mentioned earlier, ideal design of polymers that heal via bond reformation lies with the placement of “weak link” moieties, sacrificial bonds designed to break in response to stress, thereby preserving the generally irreversible organic covalent bonds. And with the appropriate chemistry, these “weak links” can recombine to reform the virgin polymer network and heal damage. Coordination polymers, which contain metal-ligand bonds in their backbone, may satisfy these requirements given that metal-ligand bonds are generally known to be much more labile than their organic covalent counterparts, but, if the metal and ligand are chosen wisely, have a high enough thermodynamic affinity to rapidly re-associate.

As an important segue from molecular design to the demonstration of self healing in a bulk polymer, a detailed understanding of the precise mechanochemical (i.e. chemical response to mechanical stress) dissociation of metal-ligand bonds in coordination polymers is required. Knowing how mechanical force affects metal-ligand bonding motifs is vital to

ensure that the reversible “weak link” in the polymer backbone is indeed preferentially broken during failure. As mentioned earlier, while macroscopic damage will probably not exclusively break these weaker bonds, it is intuitive that “weak links” with weaker bond strengths and higher densities throughout the polymer backbone can better preserve the integrity of the irreversible bonds they are designed to protect. Yet despite the complexity of this effect, with potential implications towards quality and repeatability of healing, the precise mechanochemical response of the “weak links,” relative to the irreversible bonds in the polymer, has gone largely overlooked in the bond reformation self-healing systems described outside of this sub-section. But with regards to the mechanochemical bond cleavage in coordination polymers, which has been extensively studied, metal-ligand bonds are generally known to break at much lower mechanical loads than the polymer’s irreversible covalent bonds. In one example, Kersey *et al.* studied the mechanical behavior of a palladium/pyridine-based coordination polymer using single-molecule force spectroscopy [194]. Separate PEG polymers were attached to both the tip of an AFM probe and a SiO₂ substrate, which were end-capped with pyridine-based ligands. The substrate was then flooded with a DMSO solution of a bispalladium complex, and the pyridine ligands coordinated to the metal to form polymer extending from the AFM probe to the sample surface (Fig. 2.16). When the functionalized AFM probe was retracted to the contour length of the polymer, bond rupture was consistently observed to occur through metal-ligand dissociation. Solutions of polymer-functionalized N-heterocyclic carbene ligands have also been shown to efficiently cleave from silver and ruthenium complexes when subject to ultrasound-induced mechanical stress [195, 196], which is especially noteworthy given that these carbene ligands are known to be excellent σ -donors, often leading to high metal-ligand bond strengths [197-199]. In other work, Paulusse *et al.* synthesized diphosphine telechelic poly(tetrahydrofuran) polymers, and the phosphine endgroups were complexed to palladium or platinum halides to yield polymers with multiple metal coordination sites along the polymer backbone [200-202]. Stress was applied to a solution of the metal-phosphine coordination polymers via ultrasonication, and chain scission was observed to occur predominantly through metal-phosphine dissociation.

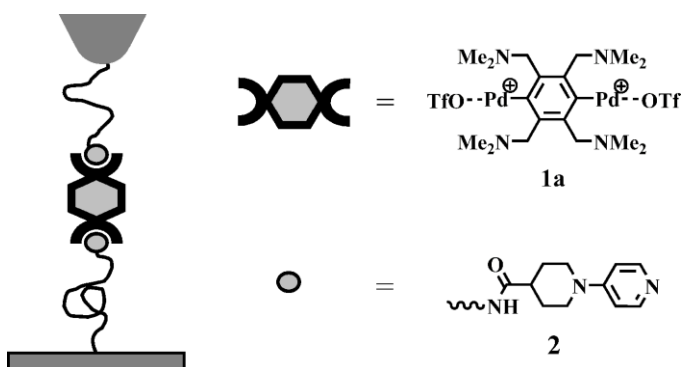


Figure 2.16. Single-molecule force spectroscopy of a coordination polymer containing pyridine-palladium bonds in an AFM instrument. Reprinted with permission from reference [203].

Bulk healing of coordination polymers has been demonstrated with several different systems. In one example, linear polymers with pyridine pendant groups were crosslinked with bis-palladium or bis-platinum complexes to form hybrid polymer gels, which were observed to rapidly undergo ligand dissociation and reassociation in response to shear stress [203]. Varghese *et al.* synthesized lightly-crosslinked, hydrophilic polymer gels containing carboxyl groups that could be healed by dipping fractured gels into a CuCl_2 solution [204]. When the damage surfaces are brought into contact, the carboxylate groups on the polymer chain effectively coordinate to the copper complex, resulting in significant recovery of mechanical properties. Williams and coworkers developed conducting organometallic polymers comprised of bis-N-heterocyclic carbenes and nickel, palladium or platinum metals [205]. These polymers exhibited conductivities on the order of $10^{-3} \text{ S cm}^{-1}$, and, after immersion in DMSO vapor at $150 \text{ }^\circ\text{C}$ for two hours to facilitate the metal-ligand association, were qualitatively observed to heal microcracks [206].

2.3.3.4 Healing via supramolecular assembly

Polymers made from supramolecular self-assembly have also been shown to exhibit self-healing behavior. The connectivity in these polymers partially relies on non-covalent interactions (e.g. hydrogen bonding, π - π stacking, etc.), which surely satisfies the

omnipresent molecular design requirement of a “weak link” throughout the polymer backbone.

Montarnal *et al.* reported the bulk synthesis of a hydrogen bonding supramolecular polymer by first reacting dimeric or trimeric fatty acid derivatives with diethylenetriamine, followed by subsequent reaction with urea [207]. This synthetic technique provided a batch of different monomers containing numerous hydrogen bond donors and acceptors (Fig. 2.17) that formed a supramolecular polymer through molecular recognition of these hydrogen bonding sites. Variations in the ratio of reactants were able to produce materials with a wide-array of properties ranging from polymers behaving like semi-crystalline thermoplastics to elastomers to associating liquids [208], although self-healing tests were only conducted on an elastomer-like material with a glass transition temperature of 28 °C. When this elastomer was fractured and the damage surfaces brought together, nearly full recovery of the virgin material's elongation at break was achieved after 180 minutes. Healing was only able to fully recover virgin properties when the fracture surfaces of broken specimens were brought into contact with each other immediately after fracture, with maximum possible healing decreasing at longer waiting times. This was attributed to the fact that broken hydrogen bonding groups eventually find partners within the broken part, leaving less hydrogen donors and acceptors available to associate with those across damage surfaces [209]. Kundu *et al.* developed a supramolecular hydrogel consisting of an oligomeric electrolyte, poly(pyridinium-1,4,-diyl-iminocarbonyl-1,4-phenylenemethylene chloride), which was able to quickly recover the virgin gel's shear modulus after destruction of the network under high shear stress [210]. Based on the unlikelihood of π - π stacking of the aromatic groups in the oligomer backbone, due to the positive charge on the main chain, and an activation energy for gel reformation (-10.4 ± 0.6 kJ/mol) being significantly lower than expected for hydrogen bonding through water or amide groups, the authors proposed that the healing took place through chlorine ion-mediated hydrogen bonding with water.

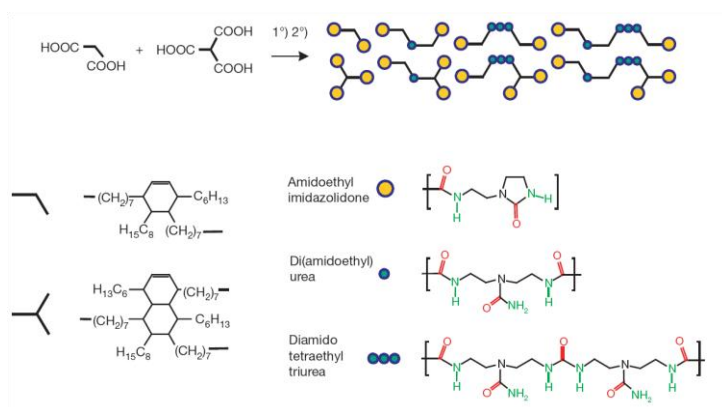


Figure 2.17. Synthetic scheme of a self-healing, supramolecular elastomer. Red bonds are hydrogen acceptor groups, and green bonds are hydrogen donor groups. Reprinted with permission from reference [209].

Greenland *et al.* and Burattini *et al.* developed healable supramolecular self-healing polymers formed with π - π stacking interactions [211, 212]. These materials consisted of a blend of low molecular weight polymers—a chain-folding polydiimide and a pyrenyl end-capped polyamide or polysiloxane—that assembled to form flexible, self-supporting films with glass transition temperatures higher than 100 °C. Rapid and reversible self-assembly of the electron-poor aromatic groups along the backbone of the polydiimide and the electron-rich telechelic pyrenyl groups (Fig. 2.18) was observed through model compound studies, computational modeling, and ^1H NMR, UV-vis, and fluorescence spectroscopy. When solution-cast films were cut, the broken pieces brought together, and healed at elevated temperatures, full and repeatable recovery of tensile modulus was possible in about 5 minutes at 50 °C and only a few seconds at 80 °C. This healing was also qualitatively observed by ESEM to close and seal microcracks, albeit only above ambient temperatures, while control tests with the polydiimide and a phenyl end-capped polymer (as opposed to the telechelic pyrenyl group) exhibited no healing (Fig. 2.19). This control test was vital to rule out viscous behavior of the polymer melt as a major contributor to healing. Instead, healing was attributed to a disruption of the π - π stacking interactions at elevated temperatures that allowed the polymer to fill the damage region and reform the π - π non-covalent interactions upon cooling. This was confirmed by rheometric analysis of the films, which showed a

significant drop-off in modulus and melt-viscosity above a critical temperature, which in the case of this work was c.a. 40 °C [213].

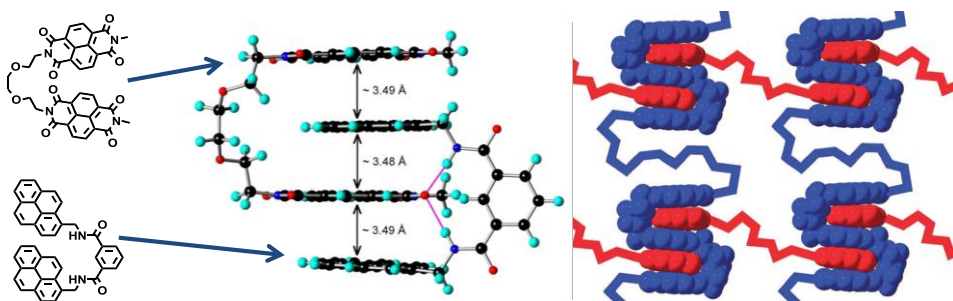


Figure 2.18. π - π stacking interactions of electron-rich and electron-poor aromatic groups in a model compound (left) and a supramolecular polymer (right). Reprinted with permission from references [211, 213].

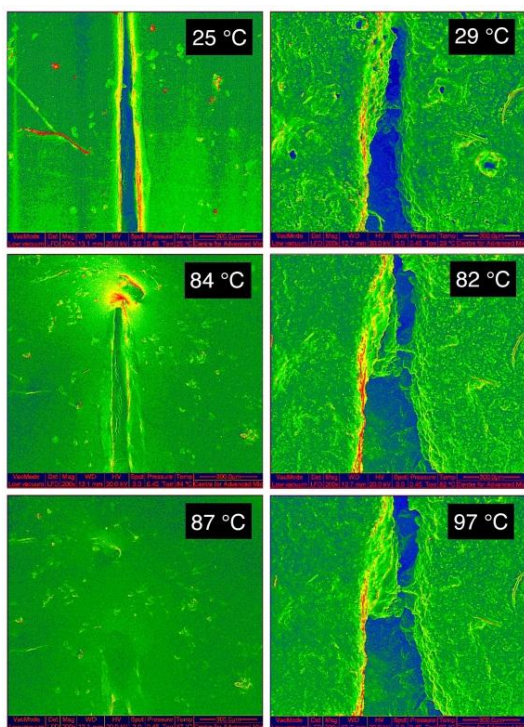


Figure 2.19. Healing in a polydiimide/pyrenyl end-capped polyamide supramolecular polymer (left) and a control polydiimide/phenyl end-capped polyamide (right) at various temperatures. Reprinted with permission from reference [213].

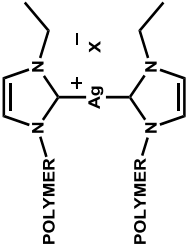
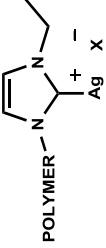
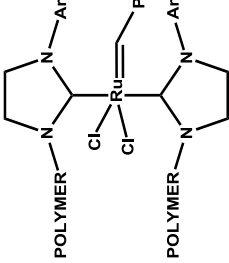
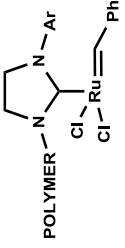
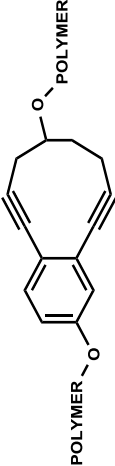
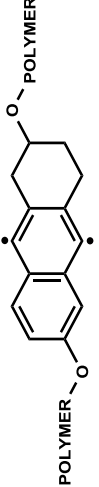
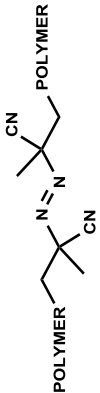
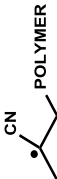
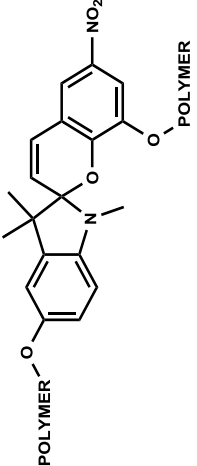
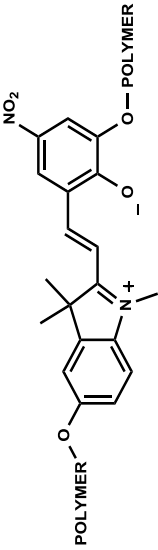
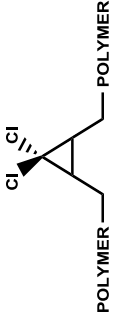
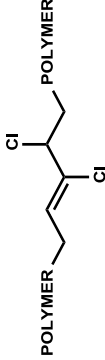
2.3.4 *Virgin Property Strengthening*

A drastically different methodology relatively new to the field of self-healing polymers is the development of materials that apply local strengthening mechanisms in response to stress, but prior to virgin material failure. These polymers incorporate mechanophores (mechanochemically active units) along their backbone that are designed to remain dormant when unperturbed, but impart additional polymerization and/or chemical crosslinking to localized portions of the bulk polymer that are under stress. While this research is still in its early stages, and to date bulk polymers that conclusively demonstrate virgin property strengthening have yet to be reported, the current efforts to develop these systems are discussed below. We will mainly focus our discussion of mechanophore chemistry on current efforts to impart a virgin property strengthening mechanism to bulk polymers; several good reviews encompassing a larger scope of mechanochemistry are available elsewhere [214-216].

Many mechanophores are designed to generate active metal catalysts when placed under stress. In fact, the coordination polymers mentioned above (that heal via reversible metal-ligand association/dissociation) can potentially be used as mechanophores [194-196, 200-202, 203, 205, 206], assuming the force-induced dissociation of their metal-ligand bonds activates an otherwise dormant precatalyst. Sijbesma and coworkers have reported two mechanophore-linked polymers that satisfy this requirement [196]. In the first case, solutions of silver complexes of polymer-functionalized N-heterocyclic carbenes were able to efficiently catalyze the transesterification of vinyl acetate and benzyl alcohol after sufficient ultrasound-induced force was applied to cleave one of the metal-carbene bonds (Mechanophore 1 in Table 2.2). And second, solutions of ruthenium biscarbene complexes with polymer-functionalized ligands were able to initiate olefin metathesis reactions, both ring-closing metathesis and ring-opening metathesis polymerization, after stress-induced ligand dissociation (Mechanophore 2 in Table 2.2). These reports have only focused on the catalysis of small molecules in solution, and have not yet been used to demonstrate self-strengthening. It would be interesting to determine if the ultrasound stress-induced chemistry of metal catalyst mechanophores like these can translate into virgin property strengthening of bulk polymers, potentially by triggering crosslinking reactions on nearby polymer chains.

Mechanophores that form stable, well-defined radicals under stress are especially attractive for self-strengthening applications. In unsaturated polymers, for example, if well-defined radicals can be mechanochemically formed prior to material failure, they can potentially crosslink neighboring double bonds through radical polymerization. One type of chemistry investigated for this purpose is the Bergman cyclization of enedynes to form arene diradical intermediates, which are known to produce high molecular weight polymer in the presence of common unsaturated monomers [217, 218]. The Bergman cyclization is generally known as a thermally activated rearrangement that, when done on a strained 10-membered ring enediyne, often occurs under mild heating conditions. But COGEF (CONstrained Geometries simulating External Force) modeling has predicted that under mechanical load the enediyne ring can be distorted towards its cycloaromatization transition state, lowering the activation barrier enough to spontaneously cyclize at ambient temperatures (Mechanophore 3 in Table 2.2) [219]. In an attempt to empirically prove this model, enediyne rings were incorporated into bulk poly(methyl methacrylate) as a crosslinker, and the crosslinked polymer was swelled with methyl methacrylate monomer. It was hypothesized that, if the dimensional expansion of the swollen polymer provided adequate force to elongate the enediyne crosslinks enough to spontaneously cyclize, the resulting cyclized adducts could initiate detectable amounts of polymerization of the methyl methacrylate monomer. However, after failing to detect any significant polymerization of the liquid methyl methacrylate, it was concluded that swelling provided inadequate mechanical force to induce the spontaneous cyclization. In other work, radicals were generated from the ultrasound-induced homolytic extrusion of nitrogen from an azo-functionalized poly(ethylene glycol) (Mechanophore 4 in Table 2.2) [220]. This mechanochemistry was not demonstrated in a bulk polymer, and the ability of the resulting radicals to initiate vinyl polymerization was not evaluated, but considering the efficiency of the radical formation and the structural similarity of these azo moieties to that of the well-known radical vinyl initiator azoisobutylnitrile (AIBN), this mechanophore may be useful to initiate radical crosslinking mechanisms in bulk unsaturated polymers.

Table 2.2. Mechanophores and the processes initiated by their force-induced activation.

	Mechanophore	Force-activated mechanophore	Process	Referen
1			Transesterification	196
2			Olefin metathesis	196
3			Radical polymerization	217-219
4			Radical Polymerization	220
5			Visual color change, fluorescence	221, 222
6			None	225

Although the ongoing development of different mechanophores does indeed look promising for future applications, several issues related to shifting the technology from solution-based systems under ultrasound-induced forces to bulk polymers under macroscopic damage must first be addressed. For example, while ultrasound-induced stress activation of the polymer-linked mechanophores mentioned above has been well-documented, it is not known how well this behavior will translate to bulk polymers. In fact, there is very little precedent at all for the precise mechanochemical transformations of any type of mechanophore in a bulk polymer under mechanical load. In one of the few promising examples, PMA- and PMMA-linked spiropyran mechanophores were developed that, when placed under load, undergoes a reversible electrocyclic ring-opening reaction to form the corresponding merocyanine (Mechanophore 5 in Table 2.2) [221]. This reaction was not designed to initiate any additional polymerization or crosslinking mechanisms, but a marked fluorescence and visual color change of the activated mechanophore allows for an easy approach to map the mechanochemical transduction throughout a polymer. And indeed, when bulk polymers containing the spiropyran mechanophore were fabricated, both tensile and compression load induced a color change concentrated at regions of high stress (e.g. Fig. 2.20 shows a yellow-to-red color change at the neck region of a dogbone specimen, which becomes more prominent at higher tensile loads) [222]. But while this precedent does bode well for the prospect of incorporating reactive, self-strengthening mechanophores into bulk polymers, it is still unknown exactly how these different mechanophores would respond to macroscopic stress or how effective their solid-state strengthening mechanisms would be.

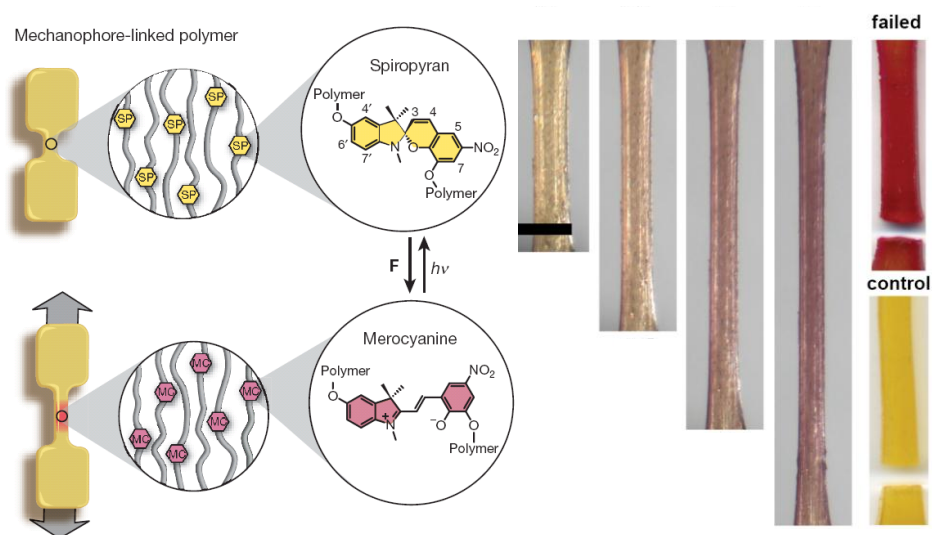


Figure 2.20. A bulk PMA-linked spiropyran dogbone specimen under tensile stress, which mechanically-converts the spiropyran moiety to the red-colored merocyanine at increasing loads. Reprinted with permission from reference [222].

The desired periodicity of mechanophores along a polymer backbone may also differ in bulk polymers. In many of the studies utilizing ultrasound-induced forces, only one mechanophore is placed near the center of the polymer chain. This is done predominately for analytical reasons—the presence of only one mechanophore greatly simplifies data interpretation, and the solvodynamic shear stress resulting from ultrasonication is generally localized near the center of the polymer [223, 224]. But in bulk polymers, stress distribution along polymer chains may follow different trends, and surely crosslinked polymers, without a traditional midpoint, would not greatly benefit from specific mechanophore placement. Hence, it is prudent to carefully weigh the advantages of varying the number of mechanophores present in a polymer. Lower densities of mechanophores along a polymer backbone, such as in many of the reports using ultrasonication, may lessen the scale-up obstacles of synthetically-challenging mechanophores. Furthermore, sparse placement of mechanophores along the backbone would probably reduce their affect on the virgin properties of the polymer and allow for conventional processing techniques to be used. However, higher densities along a polymer chain would intuitively increase the amount of mechanophores activated under stress, thus increasing initiation sites for additional

polymerization and crosslinking. Lenhardt and coworkers have taken the first steps towards answering these questions by investigating the activity of higher densities of non-scissile mechanophores in a single polymer chain [225]. In their work, reaction of polybutadiene with aqueous NaOH in chloroform conveniently afforded abundant quantities of gem-dichlorocyclopropane mechanophores (as high as 72% conversion of olefins to cyclopropyl groups) along the backbone of the polymer. When subjected to ultrasound-induced force, these mechanophores undergo electrocyclic ring opening to form 2,3-dichloroalkenes (Mechanophore 6 in Table 2.2), which, due to the high density of mechanophores, was easily monitored by $^1\text{H-NMR}$ (Fig. 2.21). The utility of the resulting dichloroalkenes mostly lies with their ability to map stress distribution along the polymer chain, but a high density of self-strengthening mechanophores with similar scalability would surely be of practical interest.

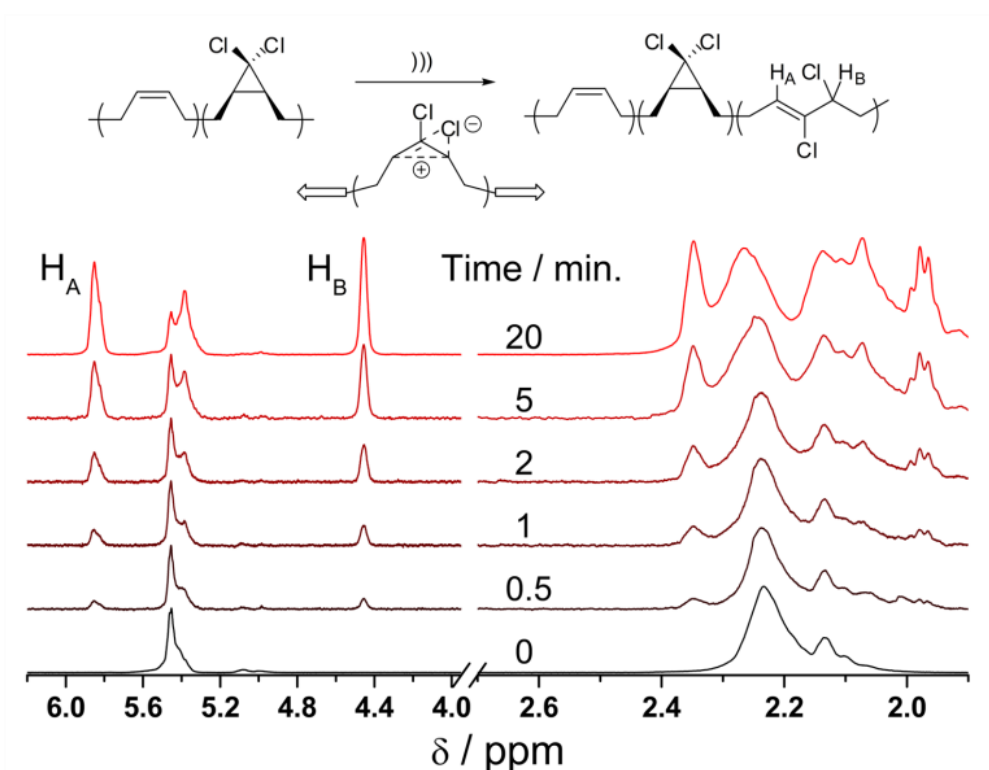


Figure 2.21. Force-induced ring-opening of gem-dichlorocyclopropanes at various time intervals, monitored by $^1\text{H-NMR}$. Reprinted with permission from reference [225].

2.4 Virgin property reduction

In order for self-healing materials to be considered feasible for real applications, it is important to understand how the self-healing components affect the virgin properties of polymers they are meant to heal. But while self-healing studies are very much applied research, and the implications of virgin property reduction are therefore of paramount importance, such information is often lacking in the literature. Here, we summarize and discuss general trends observed with virgin polymer property changes when different types of healing components are added. Table 2.3 outlines much of what is known regarding these property changes.

In most reports of microcapsule-based self-healing mechanisms, increasing loadings of liquid-filled capsules significantly toughens the composite matrix, relative to the neat polymer matrix, until a critical loading is reached, after which point further increases in capsule loading decreases toughness. In DCPD-filled microcapsules, for example, this toughening was attributed to hackle markings and subsurface microcracking at fracture surfaces that were significant only with good capsule-matrix adhesion [226]. But this effect does not seem to be universal, as several microcapsule systems reported minimal changes [85] or decreasing values of fracture toughness [38-41] with increasing capsule loading. However, data in these reports suggests that this behavior may be the result of a complex interplay between the toughening effect of the microcapsules and that of other, toughness-decreasing components (e.g. solid or matrix-dissolved catalysts), resulting in overall decreases in fracture toughness. Reports on the effect of microcapsules on other virgin properties are scarce, but evidence suggests that the capsules have negative effects on modulus [43] and strength [227], which is consistent with what is expected for hollow fillers and voids.

The effect of resin-filled hollow fibers or microvascular networks on virgin polymer properties depends strongly on the placement of the vessels throughout the polymer matrix. For example, hollow fibers with small pitch spacings throughout plies have a detrimental effect on the strength of the composite [132]. Increasing this pitch spacing, or analogously increasing the spacing between vascular channels, can eliminate the effect these vessels have on the polymer's virgin properties, but this often comes at the cost of diminished healing

ability [133-135, 228]. Additionally, an increased mass penalty is observed when incorporating microvascular networks throughout a polymer matrix [153], but mass penalties can potentially be reduced by adjusting the vascular network architecture [144, 145].

Several approaches to self-healing involve the development of new polymer matrices where the healing functionality is inherently part of the virgin material (for example, see the above section on polymers that heal via bond-reformation). While these systems do not contain traditional healing additives, and therefore cannot be discussed in the context of virgin property changes, it is at least important to consider whether or not their virgin properties are adequate enough to substitute for the traditional engineering polymers they intend to replace. The DA-based thermoset polymer shown in Fig. 2.11 is appealing in this respect, given that its Young's modulus and tensile, compression, and flexural strengths are comparable to that of commercial epoxies and unsaturated polyesters [173]. Also, most of the epoxies and common thermoplastic polymers with reversible DA-based crosslinks possess mechanical properties superior to their respective non-crosslinked polymers [180-190]. However, several other custom-made polymer matrices outlined above are either inferred or explicitly stated to have significantly weaker mechanical properties than conventional structural materials and may have limited applications.

Table 2.3. Summary of changes in virgin properties as a result of various self-healing components

	Increase	Minimal change	Decrease
Fracture Toughness	DCPD-filled capsules/solid Grubbs' catalyst [29, 226] Epoxy resin-filled capsules/solid imidazole catalyst [37] Epoxy resin/Mercaptan-filled capsules [43] Phase-separated pEMAA particles [117]	DCPD-filled capsules/solid, wax-encased Tungsten catalyst [85] Shape memory alloy wires [79, 80]	Epoxy resin-filled capsules/matrix-dissolved imidazole catalyst [38, 40, 41] Matrix-dissolved thermoplastic polymer [155]

Table 2.3. (continued)

Strength	Epoxy resin-filled capsules/matrix-dissolved imidazole catalyst (CAI) [42] PDMS-containing capsules (tear) [46]	Epoxy resin-filled hollow fibers – large pitch spacing (flexural) [133-135] Epoxy-resin filled microvascular network (flexural) [153]	Epoxy resin-filled hollow fibers—small pitch spacing (flexural) [132-134] Epoxy resin/Mercaptan-filled capsules (flexural, tensile) [43] DCPD-filled capsules/solid Grubbs' catalyst (tensile, compressive, shear) [227] Epoxy resin-filled capsules/BF ₃ OEt ₂ -infused sisal fiber (flexural, impact) [45]
Modulus		Epoxy resin-filled capsules/BF ₃ OEt ₂ -infused sisal fiber (flexural) [45] Matrix-dissolved thermoplastic polymer (storage) [156]	Epoxy resin/Mercaptan-filled capsules (flexural, Youngs) [43] DCPD-filled capsules/solid Grubbs' catalyst (shear) [227] Phase-separated Epoxy polymer particles (tension) [115,116] Phase-separated pEMAA particles (flexural) [117] Phase-separated poly(caprolactone) (storage) [119]
T_g		Phase-separated poly(caprolactone) [117] Matrix-dissolved thermoplastic polymer (storage) [156]	

Table 2.3. (continued)

Mass penalty	Epoxy-resin filled microvascular network [153]		
---------------------	--	--	--

2.5 Healing evaluation

The quality of healing, generally referred to as “healing efficiency” and denoted as η , is most often defined as the percent recovery of a virgin material property (equation 2.1, P = material property). Details regarding the specific material properties used for this calculation are discussed below, but first it is important to mention some factors that may complicate any direct interpretation of healing efficiency values. First, it should be noted that some results are biased by the fact that very brittle polymers are chosen as reference materials. That is, healing efficiencies using polymers employed in real applications, which often utilize stronger and tougher polymer matrices, will likely be lower due to their superior material properties. Also, the effect of the healing additives on virgin polymer properties may erroneously increase or decrease healing efficiency. As seen in Table 2.3, most healing additives have either a beneficial or detrimental effect on the virgin material properties of the polymers in which they are incorporated, which makes full recovery of these properties either more or less difficult, respectively. This is especially significant when comparing healing efficiencies at different loadings of healing additives. For example, it is often the case that higher loadings of healing components imparts both decreasing virgin properties and increasing healing ability to a polymer, which can greatly exaggerate the effect of adding higher amounts of healing components. For this reason, alternate definitions of healing efficiency are sometimes used that normalize healed material properties by the virgin properties of polymers without added healing components (equation 2.2, P = material property). At any rate, virgin property reduction and material properties of both the virgin and the healed polymer should be reported concurrently with healing efficiency in order to adequately evaluate the quality of healing.

$$\eta = \frac{P^{\text{Healed}}}{P^{\text{Virgin}}} \times 100 \quad (2.1)$$

$$\eta = \frac{P^{\text{Healed}}}{P^{\text{No Healing}}} \times 100 \quad (2.2)$$

In most cases, evaluation of healing requires a controlled and measurable application of damage to the virgin polymer, followed by a similar application of damage to the healed polymer. However, there lacks a unifying standard of how to best apply this damage, and as such, several different damage methods have been used to evaluate healing. Most often, damage is induced through various different tensile, compression or bending test protocols (for example, see Fig. 2.22), but numerous different damage modes have also been utilized—impact, cutting, scratching, sawing, needle puncture, nail puncture, hammering and indentation. Furthermore, different studies employ different extents of damage using these testing protocols, which have ranged from applying only enough stress to induce measurable cracking and delamination to catastrophic failure of specimens into multiple pieces. Healing efficiencies reported on samples that are catastrophically failed are probably a more reliable measure of healing given that the virgin failure and subsequent healing event can be easily controlled along a single fracture path. But causing only partial damage may be the best way to mimic the more frequently-observed and realistic failure conditions such as microcracking and delaminations deep within the material, the healing of which was the original intended purpose for self-healing polymers [28, 229].

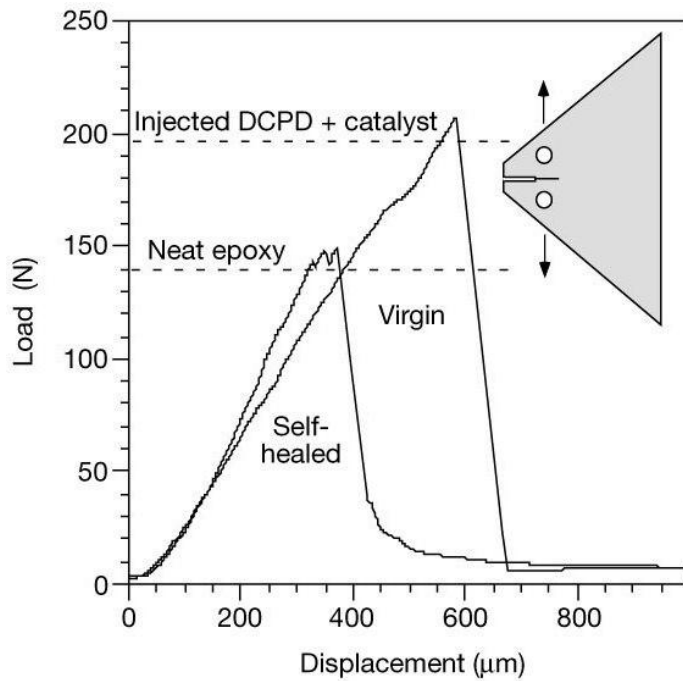


Figure 2.22. Virgin Load-displacement curve of a tapered double-cantilever beam (TDCB) specimen composed of an epoxy matrix with embedded Grubbs' catalyst particles and DCPD-filled microcapsules, along with the load-displacement curve for the subsequently self-healed sample. Reference maximum load value for an otherwise identical neat epoxy matrix (i.e. no embedded healing components) is represented with a dotted line. Reprinted with permission from reference [28].

Table 2.4 lists many of the material properties that have been used to quantify healing efficiency. Which healing efficiency definition is chosen may depend on the virgin polymer properties, desired failure mode, self-healing mechanism, etc. For example, defining healing efficiency as the recovery of fracture toughness allows for a measurement of Mode I crack opening, which is similar to the mechanism of microcrack growth that is often observed in real applications. Healing efficiency based on tear strength or strain energy is a better fit for elastomers or plasticized polymers that undergo highly ductile failure. Recovery of impact, compression-after-impact, or flexural-after-impact strength may be more appropriate metrics for evaluating fiber-reinforced polymers since impact damage is well-suited to target delamination and fiber-matrix debonding failure mechanisms.

Table 2.4. Healing efficiency calculations based on recovery of different material properties.

Material Property	Calculation	Comments
Fracture Toughness	$\eta = \frac{K_{IC}^{Healed}}{K_{IC}^{Virgin}} \times 100$	K_{IC} = Fracture toughness
Strength	$\eta = \frac{\sigma_X^{Healed}}{\sigma_X^{Virgin}} \times 100$	X = Tensile, Compressive, Impact, Tear or Flexural
Strain energy	$\eta = \frac{U_{Healed}/A_{Healed}}{U_{Virgin}/A_{Virgin}} \times 100$	U = Strain Energy; A = Surface area created by fracture
Stiffness	$\eta = \frac{E_{Healed}}{E_{Virgin}} \times 100$	E = Youngs Modulus

As mentioned above, healing efficiencies of specimens only partially failed must be evaluated with some scrutiny since the reported material properties of healed specimens may be a combination of both healed and virgin portions of the polymer. To better illustrate this point, we examine work done by Pang and Bond [131], in which healing agent-filled hollow fibers were incorporated into a fiber-reinforced composite. After low-energy impact indentation and a short healing time, testing specimens were evaluated with a 4-point bend flexural testing protocol. It was observed that samples without impact damage, samples with impact damage but no allotted healing time, and samples with impact damage and healing had mean flexural strengths of 623.9, 548.1, and 603.6 MPa, respectively. The traditional definition of healing efficiency shown in equation 2.1 then yields a value of 97%

$$\left(\eta = \frac{603.6}{623.9} \times 100 = 97\% \right) \text{ whereas only } 73\% \left(\eta = \frac{603.6 - 548.1}{623.9 - 548.1} \times 100 = 73\% \right) \text{ of the strength}$$

that was lost from the impact event was actually recovered. Thus, various methods to calculate healing efficiency have been developed to correct for the residual virgin polymer properties. In one example, Yin et al. used an equation (equation 2.3) similar to the latter one

in the example above to evaluate the healing efficiency based on compression-after-impact strength of a composite containing epoxy-filled microcapsules and a matrix-dissolved imidazole catalyst [42].

$$\eta_{CAI} = \frac{\sigma^{\text{Healed}} - \sigma^{\text{Impact}}}{\sigma^{\text{Virgin}} - \sigma^{\text{Impact}}} \times 100 \quad (2.3)$$

In this equation, σ^{Healed} is the compression strength of the specimen after impact and a subsequent healing cycle, σ^{Impact} is the strength of a sample after impact but prior to healing, and σ^{Virgin} is the compression strength of the virgin sample not subject to any impact damage. Barbero and Ford have developed a continuum healing mechanics approach to quantify the healing of microcracks developed under cyclic shear stress [227, 230, 231]. Their definition of healing efficiency is shown below, where $G_{12}^{d_h}$ is the healed (loading) shear modulus, G_{12}^d is the damaged (unloading) shear modulus, and \bar{G}_{12} is the virgin shear modulus.

$$\eta^d = \frac{G_{12}^{d_h} - G_{12}^d}{\bar{G}_{12} - G_{12}^d} \times 100 \quad (2.4)$$

Jones et al. approached this problem not by evaluating a traditional material property, but instead by quantifying the growth of delamination area [155, 156]. This was accomplished with an image analysis program that, after impacting composite panels, was able to measure the damage area before (A^{Impacted}) and after a healing cycle (A^{Healed}), and healing efficiency was calculated as in equation 2.5:

$$\eta = \frac{A^{\text{Healed}}}{A^{\text{Impacted}}} \quad (2.5)$$

The traditional definition of healing efficiency shown in equation 1 is inappropriate for quantifying fatigue lifetime in self-healing polymers under cyclic fatigue loading; two alternate calculations have been developed. In the first, which is shown in equation 2.6,

fatigue life extension (λ) is evaluated as a function of the total number of cycles to failure for a sample with self-healing capabilities (N_{Healed}) normalized by the number of cycles to failure of an otherwise identical specimen without healing (N_{Control}) [30-32]. The second approach, developed by Lewis and coworkers [33, 34] and shown in equation 2.7, is similar to the first, but instead utilizes the mean fatigue crack propagation rate ($FCPR$).

$$\lambda = \frac{N_{\text{Healed}} - N_{\text{Control}}}{N_{\text{Control}}} \quad (2.6)$$

$$\lambda = \frac{FCPR_{\text{Healed}} - FCPR_{\text{Control}}}{FCPR_{\text{Control}}} \quad (2.7)$$

Several other healing efficiency calculations have been used sporadically in the literature. Beiermann *et al.* and Kalista *et al.* quantified healing by determining the amount of pressure that a healed polymer could withstand before bursting [49, 162, 163]. The efficiencies of many self-healing systems that show promise for coating applications have been measured by depositing the polymer as a film over a metal electrode and measuring the current that can flow through healed polymers [53-56]. Wilson and coworkers developed an approach to calculate the average retention of healing capabilities (ρ_{avg}) of polymers and composites that were initially fabricated at different temperatures [82]. This calculation is shown in equation 2.8, where $\text{Avg}[P_c^{\text{Healed}}]_{T_{\text{postcure}}=35^\circ\text{C}}$ and $\text{Avg}[P_c^{\text{Healed}}]_{T_{\text{postcure}}=125^\circ\text{C}}$ are equal to the average peak load value on load-displacement curves of healed specimens whose polymer matrices' were previously postcured at 35 °C and 125 °C, respectively. While this equation has been used infrequently in the literature thus far, it will be useful to guide the processing of self-healing composites that contain thermally-sensitive components but require curing cycles at elevated temperatures.

$$\rho_{\text{avg}} = \frac{\text{Avg}[P_c^{\text{Healed}}]_{T_{\text{postcure}}=125^\circ\text{C}}}{\text{Avg}[P_c^{\text{Healed}}]_{T_{\text{postcure}}=35^\circ\text{C}}} \times 100 \quad (2.8)$$

2.6 Practical applications of self-healing polymers

2.6.1 Healing in coatings vs. bulk composites

Many of the self-healing systems described in this review are restricted to either thin films and coatings or bulk polymers and composites. For example, polymers that heal via UV-initiated bond-reformation may only be applicable for thin coatings. These polymers require UV-irradiation as a healing stimulus, and practical UV sources, either natural (sunlight) or artificial, may not have penetration depths that can reach the center of bulk polymers. Furthermore, the relatively low healing efficiencies of Chung *et al.*'s UV-healable tricinnamate-based polymers (<25% [192]) and the presumably low stiffness of Ghosh *et al.*'s UV-healable chitosan/polyurethane-based polymers (the mechanical properties of this system were not explicitly stated, but inferred from their ability to readily undergo unassisted crack closure [193]) may further limit them to coating applications, where structural integrity is not of the utmost importance. Similarly, other self-healing polymers known to have relatively low healing efficiencies or weak virgin mechanical properties may also be limited to film or coating applications.

On the other hand, several self-healing systems can only be used in bulk polymers or composites. For the most part, this restriction comes from the mass and volume requirements of certain healing additives being greater than typical thicknesses of thin films. For example, the thinnest reported specimens containing microvascular networks are on the scale of 5-7 mm thick [150, 153], which is at least 1-2 orders of magnitude thicker than required for many thin coatings. Healing agent-filled hollow fibers are also limited to bulk polymers for similar reasons. Microcapsule-based self-healing polymers, however, are not as limited as the microvascular and hollow fibers systems. While microcapsules for self-healing polymers are most efficient on the 100-200 μm size scale [72], which may be too large for thin films, recent reports of healing agent-containing nanoscale sized microcapsules [89] may open the field of microcapsule-based self-healing to thin coating applications.

Although probably best suited for bulk applications, fabricating self-healing systems containing phase-separated thermoplastic polymers as healing agents into thin films may not have as many obstacles as several of the above systems. Although this has not yet been

reported in the literature, the phase-separated EMAA and epoxy particles reported by Meure *et al.* [117] and Zako *et al.* [115,116], respectively, could presumably be reduced to the nano- or micron-size scale using standard melt processing techniques, prior to their incorporation into a self-healing polymer matrix. Luo *et al.*'s epoxy polymers containing reaction-induced phase-separated PCL are especially translatable into thin film applications, as the distribution of the PCL inherently phase-separates on the micron-scale [119], thereby eliminating the need for any additional processing steps to reduce the healing agent size.

2.6.2 Healing in the presence of structural reinforcements

A significant failure mode in fiber-reinforced polymers (FRP's), in addition to the brittle microcracking behavior of their polymer matrices, is their susceptibility to delamination damage. Given that this delamination disrupts the matrix-fiber bonding requisite for composite materials to take advantage of the superior structural properties of their embedded fibers, a self-healing functionality is extremely attractive for composite materials [232]. However, the addition of structural fibers to a polymer often changes the healing performance, relative to that of the neat matrix. Below, we discuss these known effects of structural fibers on healing capabilities. While healing in FRP's is prevalent in many of the different self-healing methodologies presented above (notably those containing epoxy/hardener-filled microcapsules [38-42], phase-separated thermoplastic polymers [115,116], and healing agent-filled hollow fibers [128-135]), the most comprehensive comparisons and discussions of the effect of the presence of structural reinforcements on healing have been reported with systems that heal via embedded DCPD-filled microcapsules and Grubbs' catalyst particles.

One difference between fiber-reinforced polymers and neat polymer matrices containing a healing functionality is the effect of the healing components on the virgin material properties. Generally, adding structural fibers to a neat polymer matrix increases fracture toughness by forcing crack growth to follow a more tortuous path around the fiber architecture. FRP's with self-healing functionality are no exception to this, with higher fracture toughness values for complex fiber weaves than unidirectional fibers [233]. Based on what is known about the toughening that DCPD-filled microcapsules impart to neat

polymers [226], one would initially expect that adding microcapsules to FRP's would further increase their toughness. However, the opposite trend—a marked decrease in fracture toughness—was observed when adding the same microcapsules to FRP's [234]. This was attributed to the microcapsules increasing the thickness of the interlaminar layer, relative to microcapsule-free layers, which has been observed elsewhere to similarly affect composites' fracture toughness [235].

The average fracture toughness-based healing efficiency of a fiber weave-reinforced epoxy polymer containing DCPD-filled microcapsules and Grubbs' catalyst was reported as 38% [234], considerably lower than the 90% healing efficiency reported elsewhere for an otherwise similar neat polymer matrix [29]. While this decrease in healing is likely not as dramatic as a direct comparison of the two values would indicate, due to the virgin property differences between the FRP and neat polymer matrix, it is clear that incorporation of the fiber weave is detrimental to the healing mechanism. It was concluded that the lower healing efficiency was related to a lack of healing additives (catalyst and microcapsules) present at the fiber-matrix interface, where a majority of the damage occurs in the form of delamination. This resulted in less overall healing agent in the damage area, and consequently, lower healing. Furthermore, maximum healing was achieved in the FRP after about 48 hours, which is significantly longer than the time required to reach maximum healing in a neat epoxy polymer (approximately 12 hours [29]). The longer healing time required for FRP's indicates that the curing kinetics of healing agent are much lower than in the neat polymer, which is partially related to the aforementioned lower amounts of catalyst present at the damage surfaces of the delaminations. Also, the slower reaction kinetics may be related to the high thermal mass of the fiber weave contributing to a lower local temperature at the delamination surfaces, relative to the neat polymer's fracture surfaces, where the healing initiated. This longer healing time in FRP's can potentially allow the liquid DCPD healing agent more time to either volatilize or diffuse into the polymer matrix prior to the onset of significant reaction, which may also be contributing to the lower FRP healing efficiency.

Intuitively, smaller-sized healing components with better dispersion throughout the polymer matrix and around the fibers could improve both the healing efficiency and the

healing time in FRP's [234]. Sanada and coworkers attempted to better distribute the self-healing components around the fibers in a unidirectional fiber reinforced epoxy by using a different fabrication technique than in the systems discussed above [236, 237]. The fibers were first coated with an epoxy resin mixture containing Grubbs' catalyst and relatively high loadings of DCPD-filled microcapsules (as high as 40 wt. %). The coated fiber strands were partially cured, placed in a mold, and impregnated with an epoxy/hardener mixture (not containing healing components). This technique allowed for a high concentration of healing components localized around the damage-prone fiber-matrix interfaces without the need for high overall loadings of catalyst and microcapsules throughout the bulk of the polymer. In another approach to this problem, Grubbs' catalyst was not directly embedded in the composite matrix, but instead coated on the outside surface of the fibers [137]. Additionally, recent advances in fabricating smaller microcapsules [89] have already proven fruitful in increasing healing efficiencies in FRP's [238, 239].

2.7 Conclusions

The multidisciplinary field of autonomic healing materials has provided several different techniques to impart a self-repairing function to polymers and composites. In this review, we have summarized these current research thrusts and discussed several issues related to translating the technology to practical applications, such as virgin polymer property changes as a result of the added healing functionality, healing in thin films vs. bulk polymers, and healing in the presence of structural reinforcements. There are a number of variations in the self-healing systems described above that are beginning to garner significant interest, but have thus far been reported infrequently in the literature and therefore was not discussed in great detail herein [240-248]. Additionally, the burgeoning field of computational modeling of the different healing mechanisms is continually providing insights into ideal polymer and composite design parameters for, among other things, improved scalability and healing capabilities [249-267].

While future endeavors will undoubtedly improve current healing mechanisms towards efficient, fully autonomic, and biomimetic healing materials, as well as yield other approaches to imparting autonomic repair, future research thrusts need to concentrate on

issues related to employing self-healing materials in industrial applications. Several companies are beginning to lead the efforts to market and produce self-healing polymers (such as the company Autonomic Materials, which is developing microcapsule-based self-healing elastomers, thermosets and powder coatings [268], and Arkema Inc., which is currently producing polymers that heal via supramolecular assembly [269]), but several issues that are rarely discussed in the literature, such as economic feasibility and long term “healability” of the different healing mechanisms, need to be addressed before self-healing materials can begin to replace current polymers and composites.

2.8 References

- [1] National Research Council Report—Going to Extremes: Meeting the Emerging Demand for Durable Polymer Matrix Composites, 2005.
- [2] D.R. Mulville and I. Wolock: Failure of polymer composites in ‘*Developments in Polymer Fracture -I*’, (ed. E.H. Andrews), 263-316; 1979, London, UK, Applied Science Publishers.
- [3] In ‘*Failure Analysis and Fractography of Polymer Composites*’, (ed. E.S. Greenhalgh), 2009, Cambridge, UK, Woodhead Publishing Limited.
- [4] L. Hollaway: in ‘*Polymer Composites for Civil and Structural Engineering*’, 1993, London, UK, Blackie Academic and Professional, an imprint of Chapman and Hall.
- [5] In ‘*Multi-Scale Modeling of Composite Material Systems: The Art of Predictive Damage Modelling*’, (eds. C. Sourtis and P.W.R. Beaumont), 2005, Cambridge, UK, Woodhead Publishing Limited.
- [6] T.K. O’Brien: ‘Damage and strength of composite materials: trends, predictions, and challenges’, *NASA Conference Publication*, 1994, **3271**, 145-158.
- [7] R.B. Heslehurst: ‘Challenges in the repair of composite structures – Part I’, *SAMPE J.*, 1997, **33**, 11-16.
- [8] R.B. Heslehurst: ‘Challenges in the repair of composite structures – Part II’, *SAMPE J.*, 1997, **33**, 16-21.
- [9] M.F. Ashby, L.J. Gibson, U. Wegst and R. Olive: ‘The mechanical properties of natural materials. I. Material property charts’, *Proc. R. Soc. London, Ser. A*, 1995, **450**, 123-140.
- [10] K.A. Williams, D.R. Dreyer and C.W. Bielawski: ‘The underlying chemistry of self-healing materials’, *MRS Bull.*, 2008, **33**, 759-765.
- [11] R.S. Trask, H.R. Williams and I.P. Bond: ‘Self-healing polymer composite: mimicking nature to enhance performance’, *Bioinsp. Biomim.*, 2007, **2**, 1-9.
- [12] D.Y. Wu, S. Meure and D. Solomon: ‘Self-healing polymeric materials: A review of recent developments’, *Prog. Polym. Sci.*, 2008, **33**, 479-522.

- [13] S. van der Zwaag, N.H. van Dijk, H.M. Jonkers, S.D. Mookhoek and W.G. Sloof: 'Self-healing behaviour in man-made engineering materials: bioinspired but taking into account their intrinsic character', *Phil. Trans. R. Soc. A*, 2009, **367**, 1689-1704.
- [14] M.R. Kessler: 'Self-healing: a new paradigm in materials design', *Proc. Inst. Mech. Eng. G – J. Aer. Eng.*, 2007, **221**, 479-495.
- [15] E. B. Murphy and F. Wudl: 'The world of smart healable materials', *Prog. Polym. Sci.*, 2010, **35**, 223-251.
- [16] Y.C. Yuan, T. Yin, M.Z. Rong and M.Q. Zhang: 'Self-healing in polymers and polymer composites. Concepts, realization and outlook: A review', *Express Polym. Lett.*, 2008, **2**, 238-250.
- [17] S.R. White, M.M. Caruso and J.S. Moore: 'Autonomic healing of polymers', *MRS Bull.*, 2008, **33**, 766-769.
- [18] D. Jung, A. Hegeman, N.R. Sottos, P.H. Geubelle and S.R. White: 'Self-healing composites using embedded microspheres', *Am. Soc. Mech. Eng. Mater. Div. (Publication)*, 1997, **80**, 265-275.
- [19] Stephenson, Larry D. U.S. Army Engineer Research and Development Center-Construction Engineering Research Laboratory (ERDC-CERL), Champaign, IL, U.S. Personal communication regarding work done in the late 1990's, 2008.
- [20] C.W. Bielawski and R.H. Grubbs: 'Living ring-opening metathesis polymerization', *Prog. Polym. Sci.*, 2007, **32**, 1-29.
- [21] S.T. Nguyen, L.K Johnson and R.H. Grubbs: 'Ring-opening metathesis polymerization (ROMP) of norbornene by a group VIII carbene complex in protic media', *J. Am. Chem. Soc.*, 1992, **114**, 3974-3975.
- [22] M.R. Kessler and S.R. White: 'Cure kinetics of the ring-opening metathesis polymerization of dicyclopentadiene', *J. Polym. Sci., Part A: Polym. Chem.*, 2002, **40**, 2373-2383.
- [23] S.T. Nguyen and R.H. Grubbs: 'Syntheses and activities of new single-component, ruthenium-based olefin metathesis catalysis', *J. Am. Chem. Soc.*, 1993, **115**, 9858-9859.
- [24] E.L. Dias, S.T. Nguyen and R.H. Grubbs: 'Well-defined ruthenium olefin metathesis catalysts: mechanism and activity', *J. Am. Chem. Soc.*, 1997, **119**, 3887-3897.
- [25] T.M. Trnka, and R.H. Grubbs: 'The development of L2X2Ru=CHR olefin metathesis catalysts: an organometallic success story', *Acc Chem. Res.*, 2001, **34**, 18-29.
- [26] M.S. Sanford, J.A. Love and R.H. Grubbs: 'Mechanism and activity of ruthenium olefin metathesis catalysis', *J. Am. Chem. Soc.*, 2001, **123**, 6543-6554.
- [27] R.H. Grubbs: 'Olefin-metathesis catalysts for the preparation of molecules and materials', *Angew. Chem. Int. Ed.*, 2006, **45**, 3760-3765.
- [28] S.R. White, N.R. Sottos, P.H. Geubelle, J.S. Moore, M.R. Kessler, S.R. Sriram, E.N. Brown and S. Viswanathan: 'Autonomic healing of polymer composites', *Nature*, 2001, **409**, 794-797.
- [29] E.N. Brown, N.R. Sottos and S.R. White: 'Fracture testing of self-healing polymer composite', *Exp. Mech.*, 2002, **42**, 372-379.

- [30] E.N. Brown, S.R. White and N.R. Sottos: ‘Retardation and repair of fatigue cracks in a microcapsule toughened epoxy composite – Part I: Manual infiltration’, *Compos. Sci. Technol.*, 2005, **65**, 2466-2473.
- [31] E.N. Brown, S.R. White and N.R. Sottos: ‘Retardation and repair of fatigue cracks in a microcapsule toughened epoxy composite – Part II: In situ self-healing’, *Compos. Sci. Technol.*, 2005, **65**, 2474-2480.
- [32] A.S. Jones, J.D. Rule, J.S. Moore, N.R. Sottos and S.R. White: ‘Life extension of self-healing polymers with rapidly growing fatigue cracks’, *J. R. Soc. Interface*, 2007, **4**, 395-403.
- [33] G. Lewis, B. Wellborn, L. Jones II and P. Biggs: ‘A room-temperature autonomically-healing PMMA bone cement: influence of composition on fatigue crack propagation rate’, *J. Appl. Biomater. Biomech.*, 2009, **7**, 90-96.
- [34] P. Biggs, L. Jones II, B. Wellborn and G. Lewis: ‘A self-healing PMMA bone cement: Influence of crystal size of Grubbs’ catalyst’, *IFMBE Proc.*, 2009, **14**, 147-150.
- [35] G.O. Wilson, J.S. Moore, S.R. White, N.R. Sottos and H.M. Andersson: ‘Autonomic healing of epoxy vinyl esters via ring opening metathesis polymerization’, *Adv. Funct. Mater.*, 2008, **18**, 44-52.
- [36] M.D. Chipara, M. Chipara, E. Shansky and J.M. Zaleski, ‘Self-healing of high elasticity block copolymers’, *Polym. Adv. Technol.*, 2009, **20**, 427-431.
- [37] M.Z. Rong, M.Q. Zhang and W. Zhang: ‘A novel self-healing epoxy system with microencapsulated epoxy and imidazole curing agent’, *Adv. Compos. Lett.*, 2007, **16**, 167-172.
- [38] T. Yin, M.Z. Rong, M.Q. Zhang and G.C. Yang: ‘Self-healing epoxy composites-Preparation and effect of the healant consisting of microencapsulated epoxy and latent curing agent’, *Compos. Sci. Technol.*, 2007, **67**, 201-212.
- [39] T. Yin, M.Z. Rong, M.Q. Zhang and J.Q. Zhao: ‘Durability of self-healing woven glass fabric/epoxy composites’, *Smart Mater. Struct.*, 2009, **18**, 1-7.
- [40] T. Yin, M.Z. Rong and M.Q. Zhang: ‘Self-healing of cracks in epoxy composites’, *Adv. Mater. Res.*, 2008, **47-50**, 282-285.
- [41] T. Yin, L. Zhou, M.Z. Rong and M.Q. Zhang: ‘Self-healing woven glass fabric/epoxy composites with the healant consisting of micro-encapsulated epoxy and latent curing agent’, *Smart Mater. Struct.*, 2008, **17**, 1-8.
- [42] T. Yin, M.Z. Rong, J. Wu, H. Chen and M.Q. Zhang: ‘Healing of impact damage in woven glass fabric reinforced epoxy composites’, *Composites Part A.*, 2008, **39**, 1479-1487.
- [43] Y.C. Yuan, M.Z. Rong, M.Q. Zhang, J. Chen, G.C. Yang and X. M. Li: ‘Self-healing polymeric materials using epoxy/mercaptan as the healant’, *Macromolecules*, 2008, **41**, 5197-5202.
- [44] D.Z. Xiao, Y.C. Yuan, M.Z. Rong and M.Q. Zhang: ‘Self-healing epoxy based on cationic chain polymerization’, *Polymer*, 2009, **50**, 2967-2975.
- [45] D.Z. Xiao, Y.C. Yuan, M.Z. Rong and M.Q. Zhang: ‘A facile strategy for preparing self-healing polymer composites by incorporation of cationic catalyst-loaded vegetable fibers’, *Adv. Funct. Mater.*, 2009, **19**, 2289-2296.
- [46] M.W. Keller, S.R. White and N.R. Sottos: ‘A self-healing poly(dimethyl siloxane) elastomer’, *Adv. Funct. Mater.*, 2007, **17**, 2399-2404.

- [47] M.W. Keller, S.R. White and N.R. Sottos: 'Torsion fatigue response of self-healing poly(dimethyl siloxane) elastomers', *Polymer*, 2008, **49**, 3136-3145.
- [48] Y. Haitang, F. Zhengping, F. Xiaoyun and T. Lifang: 'A novel glass fiber-supported platinum catalyst for self-healing polymer composites: Structure and reactivity', *Chin. J. Catal.*, 2007, **28**, 947-952.
- [49] B.A. Beiermann, M.W. Keller and N.R. Sottos: 'Self-healing flexible laminates for resealing of puncture damage', *Smart Mater. Struct.*, 2009, **18**, 1-7.
- [50] D.G. Shchukin and H. Mohwald: 'Self-repairing coatings containing active nanoreservoirs', *Small*, 2007, **3**, 926-943.
- [51] D.V. Andreeva and D.G. Shchukin: 'Smart self-repairing protective coatings', *Mater. Today*, 2008, **11**, 24-30.
- [52] A. Kumar, L.D. Stephenson and J.N. Murray: 'Self-healing coatings for steel', *Prog. Org. Coat.*, 2006, **55**, 244-253.
- [53] V. Sauvant-Moynot, S. Gonzales and J. Kittel: 'Self-healing coating: An alternative route for anticorrosion protection', *Prog. Org. Coat.*, 2008, **63**, 307-315.
- [54] D.G. Shchukin, M. Zheludkevich, K. Yasakau, S. Lamaka, M.G.S. Ferreira and H. Mohwald: 'Layer-by-layer assembled nanocontainers for self-healing corrosion protection', *Adv. Mater.*, 2006, **18**, 1672-1678.
- [55] D.V. Andreeva, D. Fix, H. Mohwald and D.G. Shchukin: 'Self-healing anticorrosion coatings based on pH-sensitive polyelectrolyte/inhibitor sandwichlike nanostructures', *Adv. Mater.*, 2008, **18**, 2789-2794.
- [56] E.V. Skorb, A.G. Skirtach, D.V. Sviridov, D.G. Shchukin and H. Mohwald: 'Laser-controllable coatings for corrosion protection', *ACS Nano*, 2009, **3**, 1753-1760.
- [57] X. Liu, X. Sheng, J.K. Lee and M.R. Kessler: 'Isothermal cure characterization of dicyclopentadiene the glass transition temperature and conversion', *J. Therm. Anal. Calorim.*, 2007, **89**, 453-457.
- [58] E.N. Brown: 'Fracture and fatigue of a self-healing polymer composite material', PhD thesis, University of Illinois Urbana-Champaign, 2003.
- [59] G.L. Nelson and C.-L. Kuo: 'An improved procedure for the preparation of exo-dicyclopentadiene', *Synthesis*, 1975, **105**, 105-106.
- [60] J.D. Rule and J.S. Moore: 'ROMP reactivity endo- and exo-dicyclopentadiene', *Macromolecules*, 2002, **35**, 7878-7882.
- [61] T.C. Mauldin, J.D. Rule, N.R. Sottos, S.R. White and J.S. Moore: 'Self-healing kinetics and stereoisomers of dicyclopentadiene', *J. R. Soc. Interface*, 2007, **4**, 389-393.
- [62] Y.C. Yuan, M.Z. Rong, M.Q. Zhang and G.C. Yang: 'Study of factors related to performance improvement of self-healing epoxy based on dual encapsulated healant', *Polymer*, 2009, **50**, 5771-5781.
- [63] J. K. Lee, S. J. Hong, X. Liu and S. H. Yoon: 'Characterization of dicyclopentadiene and 5- ethylidene-2-norbornene as self-healing agents for polymer composite and its microcapsules', *Macromol. Res.*, 2004, **12**, 478-483.
- [64] G.E. Larin, N. Bernklau, M.R. Kessler and J.C. DiCesare: 'Rheokinetics of ring-opening metathesis polymerization of norbornene-based monomers intended for self-healing applications', *Polym. Eng. Sci.*, 2006, **46**, 1804-1811.

- [65] J.K. Lee, X. Liu, S.H. Yoon and M.R. Kessler: 'Thermal Analysis of ring-opening metathesis polymerized healing agents', *J. Polym. Sci., Part B: Polym. Phys.*, 2007, **45**, 1771-1780.
- [66] X. Liu, J.K. Lee, S.H. Yoon and M.R. Kessler: 'Characterization of diene monomers as healing agents for autonomic damage repair', *J. Appl. Polym. Sci.*, 2006, **101**, 1266-1272.
- [67] X. Liu, X. Sheng, M.R. Kessler and J.K. Lee: 'Rheokinetic evaluation of self-healing agents polymerized by Grubbs' catalyst embedded in various thermosetting systems', *Compos. Sci. Technol.*, 2009, **69**, 2101-2107.
- [68] X. Sheng, M.R. Kessler and J.K. Lee: 'The influence of cross-linking agents on ring-opening metathesis polymerized thermosets', *J. Therm. Anal. Calorim.*, 2007, **89**, 459-464.
- [69] X. Sheng, J.K. Lee and M.R. Kessler: 'Influence of cross-link density on the properties of ROMP thermosets', *Polymer*, 2009, **50**, 1264-1269.
- [70] W. Jeong and M.R. Kessler: 'Toughness enhancement in ROMP functionalized carbon nanotube/polydicyclopentadiene composites', *Chem. Mater.*, 2008, **20**, 7060-7068.
- [71] W. Jeong and M.R. Kessler: 'Effect of functionalized MWCNTs on the thermo-mechanical properties of poly(5-ethylidene-2-norbornene) composites produced by ring-opening metathesis polymerization', *Carbon*, 2009, **47**, 2406-2412.
- [72] J.D. Rule, N.R. Sottos and S.R. White: 'Effect of microcapsule size on the performance of self-healing polymers', *Polymer*, 2007, **48**, 3520-3529.
- [73] D.S. Burton, X. Gao and L.C. Brinson: 'Finite element simulation of a self-healing shape memory alloy composite', *Mech. Mater.*, 2006, **38**, 525-537.
- [74] S. Araki, H. Ono and K. Saito: 'Micromechanical analysis of crack closure mechanism for intelligent material containing TiNi fibers', *JSME Int. J. A, Solid Mech. Mater. Eng.*, 2002, **45**, 208-216.
- [75] K. Hamada, F. Kawano, and K. Asaoka: 'Shape recovery of shape memory alloy fiber embedded resin matrix smart composite after crack repair', *Dent. Mater. J.*, 2003, **22**, 160-167.
- [76] X. Wang: 'Shape memory alloy volume fraction of pre-stretched shape memory alloy wire-reinforced composites for structural damage repair', *Smart Mater. Struct.*, 2002, **11**, 590-595.
- [77] G. Li and M. John: 'A self-healing smart syntactic foam under multiple impacts', *Compos. Sci. Technol.*, 2008, **68**, 3337-3343.
- [78] G. Li and D. Nettles: 'Thermomechanical characterization of a shape memory polymer based self-repairing syntactic foam', *Polymer*, 2010, **51**, 755-762.
- [79] E.L. Kirkby, J.D. Rule, V.J. Michaud, N.R. Sottos, S.R. White and J.-A.E. Manson: 'Embedded shape-memory alloy wires for improved performance of self-healing polymers', *Adv. Funct. Mater.*, 2008, **18**, 2253-2260.
- [80] E.L. Kirkby, V.J. Michaud, J.-A.E. Manson, N.R. Sottos and S.R. White: 'Performance of self-healing epoxy with microencapsulated healing agent and shape memory alloy wires', *Polymer*, 2009, **50**, 5533-5538.
- [81] A.S. Jones, J.D. Rule, J.S. Moore, S.R. White and N.R. Sottos: 'Catalyst morphology and dissolution kinetics of self-healing polymers', *Chem. Mater.*, 2006, **18**, 1312-1317.

- [82] G.O. Wilson, M.M. Caruso, N.T. Reimer, S.R. White, N.R. Sottos and J.S. Moore: 'Evaluation of ruthenium catalysts for ring-opening metathesis polymerization-based self-healing applications', *Chem. Mater.*, 2008, **20**, 3288-3297.
- [83] T.C. Mauldin and M.R. Kessler: 'Enhanced bulk catalyst dissolution for self-healing materials', *J. Mater. Chem.*, 2010, **20**, 4198-4206.
- [84] J.D. Rule, E.N. Brown, N.R. Sottos, S.R. White and J.S. Moore: 'Wax-protected catalyst microspheres for efficient self-healing materials', *Adv. Mater.*, 2005, **17**, 205-208.
- [85] J.M. Kamphaus, J.D. Rule, J.S. Moore, N.R. Sottos and S.R. White: 'A new self-healing epoxy with tungsten (VI) chloride catalyst', *J. R. Soc. Interface*, 2008, **5**, 95-103.
- [86] E.N. Brown, M.R. Kessler, N.R. Sottos and S.R. White: 'In situ poly(urea-formaldehyde) microencapsulation of dicyclopentadiene', *J. Microencapsulation*, 2003, **20**, 719-730.
- [87] R.G. Wang, W.B. Liu, H.Y. Li, X.D. He and F.H. Zhang: 'Preparation and characterization of properties of microcapsules for polymeric composites self-repairing', *Key Eng. Mater.*, 2007, **334-335**, 569-572.
- [88] M.W. Keller and N.R. Sottos: 'Mechanical properties of microcapsules used in a self-healing polymer', *Exp. Mech.*, 2006, **46**, 725-733.
- [89] B.J. Blaiszik, N.R. Sottos and S.R. White: 'Nanocapsules for self-healing materials', *Compos. Sci. Technol.*, 2008, **68**, 978-986.
- [90] H. Li, R. Wang, H. Hu and W. Liu: 'Surface modification of self-healing poly(urea-formaldehyde) microcapsules using silane-coupling agent', *Appl. Surf. Sci.*, 2008, **255**, 1894-1900.
- [91] R. Wang, H. Li, H. Hu, X. He and W. Liu: 'Preparation and characterization of self-healing microcapsules with poly(urea-formaldehyde) grafted epoxy functional group shell', *J. Appl. Polym. Sci.*, 2009, **113**, 1501-1506.
- [92] S.D. Mookhoek, B. J. Blaiszik, H.R. Fischer, N.R. Sottos, S.R. White and S. van der Zwaag: 'Peripherally decorated binary microcapsules containing two liquids', *J. Mater. Chem.*, 2008, **18**, 5390-5394.
- [93] Mookhoek, Steven D. Delft University of Technology, Delft, NL. Personal communication, 2009.
- [94] L. Yuan, G.-Z. Liang and J.-Q. Xie: 'Synthesis and characterization of microencapsulated dicyclopentadiene with melamine-formaldehyde resins', *Colloid Polym. Sci.*, 2007, **285**, 781-791.
- [95] J. Hu, H.-Q. Chen and Z. Zhang: 'Mechanical properties of melamine formaldehyde microcapsules for self-healing materials', *Mater. Chem. Phys.*, 2009, **118**, 63-70.
- [96] X. Liu, X. Sheng, J.K. Lee and M.R. Kessler: 'Synthesis and characterization of melamine-urea-formaldehyde microcapsules containing ENB-based self-healing agents', *Macromol. Mater. Eng.*, 2009, **294**, 389-395.
- [97] S. Cosco, V. Ambrogi, P. Musto and C. Carfagna: 'Properties of poly(urea-formaldehyde) microcapsules containing an epoxy resin', *J. Appl. Polym. Sci.*, 2007, **105**, 1400-1411.
- [98] L. Yuan, G.-Z. Liang, J.-Q. Xie, L. Li and J. Guo: 'The permeability and stability of microencapsulated epoxy resins', *J. Mater. Sci.*, 2007, **42**, 4390-4397.

- [99] L. Yuan, A. Gu and G. Liang: 'Preparation and properties of poly(urea-formaldehyde) microcapsules filled with epoxy resins', *Mater. Chem. Phys.*, 2008, **110**, 417-425.
- [100] Z. Ting, Z. Min, T. Xiao-Mei, C. Feng, Q. Jian-Hui: 'Optimal preparation and characterization of poly(urea-formaldehyde) microcapsules', *J. Appl. Polym. Sci.*, 2010, **115**, 2162-2169.
- [101] D.S. Xiao, M.Z. Rong and M.Q. Zhang: 'A novel method for preparing epoxy-containing microcapsules via UV irradiation-induced interfacial copolymerization in emulsions', *Polymer*, 2007, **48**, 4765-4776.
- [102] D.S. Xiao, Y.C. Yuan, M.Z. Rong and M.Q. Zhang: 'Hollow polymeric microcapsules: preparation, characterization and application in holding boron trifluoride diethyl etherate', *Polymer*, 2009, **50**, 560-568.
- [103] B.J. Blaiszik, M.M. Caruso, D.A. McIlroy, J.S. Moore, S.R. White and N.R. Sottos: 'Microcapsules filled with reactive solutions for self-healing materials', *Polymer*, 2009, **50**, 990-997.
- [104] M.M. Caruso, S.R. Schelkopf, A.C. Jackson, A.M. Landry, P.V. Braun and J.S. Moore: 'Microcapsules containing suspensions of carbon nanotubes', *J. Mater. Chem.*, 2009, **19**, 6093-6096.
- [105] X. Yi, Z. Wei, Z. Shu and X. Binshi: 'Evaluation and analysis for the surface morphology and mechanism properties of the self-repair microcapsule', *Key. Eng. Mater.*, 2008, **373-374**, 714-717.
- [106] H.P. Wang, Y.C. Yuan, M.Z. Rong and M.Q. Zhang: 'Melamine resin-walled microcapsules containing styrene: preparation and characterization', *Adv. Mater. Res.*, 2008, **47-50**, 286-289.
- [107] H. Wang, Y. Yuan, M. Rong and M. Zhang: 'Microencapsulation of styrene with melamine-formaldehyde resin', *Colloid Polym. Sci.*, 2009, **287**, 1089-1097.
- [108] Y.C. Yuan, M.Z. Rong and M.Q. Zhang: 'Preparation and characterization of microencapsulated polythiol', *Polymer*, 2008, **49**, 2531-2541.
- [109] D.A. McIlroy, B.J. Blaiszik, M.M. Caruso, S.R. White, J.S. Moore and N.R. Sottos: 'Microencapsulation of a reactive liquid-phase amine for self-healing epoxy composites', *Macromolecules*, 2010, **43**, 1855-1859.
- [110] J. Yang, M.W. Keller, J.S. Moore, S.R. White and N.R. Sottos: 'Microencapsulation of isocyanates for self-healing polymers', *Macromolecules*, 2008, **41**, 9650-9655.
- [111] J.G. Kirk, S. Naik, J.C. Noosbrugger, D.J. Morrison, D. Volkov and I. Sokolov: 'Self-healing epoxy composites based on the use of nanoporous silica capsules', *Int. J. Fract.*, 2009, **159**, 101-102.
- [112] S.J. Pastine, D. Okawa, A. Zettl and J.M.J. Frechet: 'Chemicals on demand with phototriggerable microcapsules', *J. Am. Chem. Soc.*, 2009, **131**, 13586-13587.
- [113] M. Zako, N. Takano and H. Fujioka: 'Intelligent materials system using epoxy particles for self-repair', *Proc. eighth Japan-US conference on composite materials*, 1999, 841-849.
- [114] M. Zako and N. Takano: 'Intelligent material systems using epoxy particles to repair microcracks and delamination damage in GFRP', *J. Intell. Mater. Syst. Struct.*, 1999, **10**, 836-841.

- [115] S.H. Cho, H.M. Andersson, S.R. White, N.R. Sottos and P.V. Braun: 'Polydimethylsiloxane-based self-healing materials', *Adv. Mater.*, 2006, **18**, 997-1000.
- [116] S.H. Cho, S.R. White and P.V. Braun: 'Self-healing polymer coatings', *Adv. Mater.*, 2009, **21**, 645-649.
- [117] S. Meure, D.Y. Wu and S. Furman: 'Polyethylene-co-methacrylic acid healing agents for mendable epoxy resins', *Acta Mater.*, 2009, **57**, 4312-4320.
- [118] S. Meure, D.-Y. Wu and S. Furman: 'FTIR study of bonding between a thermoplastic healing agent and a mendable epoxy resin', *Vib. Spectrosc.*, 2010, **52**, 10-15.
- [119] X. Luo, R. Ou, D.E. Eberly, A. Singhal, W. Viratyaporn and P.T. Mather: 'A thermoplastic/thermoset blend exhibiting thermal mending and reversible adhesion', *ACS Appl. Mater. Interfaces*, 2009, **1**, 612-620.
- [120] C.M. Dry and N.R. Sottos: 'Passive smart self-repair in polymer matrix composite materials', In: *Smart structures and materials 1995: smart materials*, 3rd edition, (Ed. K. Varadian), *Proc. SPIE*, 1993, **1916**, 438-444.
- [121] C. M. Dry and W. McMillan, 'Crack and damage assessment in concrete and polymer matrices using liquids released internally from hollow optical fibers', *Proc. SPIE - Int. Soc. Opt. Eng.*, 1996, **2718**, 448-451.
- [122] C. M. Dry: 'Adhesive liquid core optical fibers for crack detection and repairs in polymer and concrete matrices. *Proc. SPIE - Int. Soc. Opt. Eng.*, 1995, **2444**, 410-413.
- [123] C. Dry: 'Procedures developed for self-repair of polymer matrix composite materials', *Compos. Struct.*, 1996, **35**, 263-269.
- [124] M. Motuku, U.K. Vaidya and G.M. Janowski: 'Parametric studies on self-repairing approaches for resin infused composites subjected to low velocity impact', *Smart Mater. Struct.*, 1999, **8**, 623-638.
- [125] C. Dry: 'Testing of self-repairing composite airplanes components by use of CAI and the release of the repair chemicals from carefully inserted small tubes', In: *Industrial and commercial applications of smart structures technologies 2007*, (Eds. L.P. Davis, B.K. Henderson and M.B. McMickell), *Proc. of SPIE*, 2007, **6527**, 65270M-1-65270M-4.
- [126] C. Dry: 'Passive self-repairing and active self-sensing in multifunctional polymer composites', In: *Active and passive smart structures and integrated systems 2008*, (Ed. M. Ahmadian), *Proc. of SPIE*, 2008, **6928**, 69281J-1-69281J-9.
- [127] C. Dry: 'Self repairing composites for airplane components', In: *Sensors and smart structures technologies for civil, mechanical, and aerospace systems 2008*, (Ed. M. Tomizuka), *Proc. of SPIE*, 2008, **6932**, 693212-1-693212-13.
- [128] S.M. Bleay, C.B. Loader, V.J. Hawyes, L. Humberstone and P.T. Curtis: 'A smart repair system for polymer matrix composites', *Composites Part A*, 2001, **32**, 1767-1776.
- [129] M. Hucker, I. Bond, A. Foreman and J. Hudd: 'Optimisation of hollow glass fibers and their composites', *Adv. Compos. Lett.*, 1999, **8**, 181-189.
- [130] J.W.C. Pang and I.P. Bond: 'A hollow fibre reinforced polymer composite encompassing self-healing and enhanced damage visibility', *Compos. Sci. Technol.*, 2005, **65**, 1791-1799.
- [131] J.W.C. Pang and I.P. Bond: 'Bleeding composites' – damage detection and self-repair using a biomimetic approach', *Composites Part A*, 2005, **36**, 183-188.

- [132] R.S. Trask and I.P. Bond: 'Biomimetic self-healing of advanced composite structures using hollow glass fibres', *Smart Mater. Struct.*, 2006, **15**, 704-710.
- [133] R.S. Trask, G.J. Williams and I.P. Bond: 'Bioinspired self-healing of advanced composite structures using hollow glass fibres', *J. R. Soc. Interface*, 2007, **4**, 363-371.
- [134] G. Williams, R. Trask and I. Bond: 'A self-healing carbon fibre reinforced polymer for aerospace applications', *Composites Part A*, 2007, **38**, 1525-1532.
- [135] G.J. Williams, I.P. Bond and R.S. Trask: 'Compression after impact assessment of self-healing CFRP', *Composites Part A*, 2009, **40**, 1399-1406.
- [136] H.A. Liu, B.E. Gnade and K.J. Balkus, Jr.: 'A delivery system for self-healing inorganic films', *Adv. Funct. Mater.*, 2008, **18**, 3620-3629.
- [137] N. Fikru: 'Self-healing of fiber reinforced polymer composites', Masters Thesis, Louisiana State University, 2009.
- [138] S. Kim, S. Lorente and A. Bejan: 'Vascularized materials: tree-shaped flow architectures matched canopy to canopy', *J. Appl. Phys.*, 2006, **100**, article no. 063525, 8 pp.
- [139] A. Bejan, S. Lorente and K.-M. Wang: 'Networks of channels for self-healing composite materials', *J. Appl. Phys.*, 2006, **100**, article no. 033528, 6 pp.
- [140] K.-M. Wang, S. Lorente and A. Bejan: 'Vascularized networks with two optimized channel sizes', *J. Phys. D: Appl. Phys.*, 2006, **39**, 3086-3096.
- [141] K.-M. Wang, S. Lorente and A. Bejan: 'Vascularization with grids of channels: multiple scales, loops and body shapes', *J. Phys. D: Appl. Phys.*, 2007, **40**, 4740-4749.
- [142] S. Kim, S. Lorente, A. Bejan, W. Miller and J. Morse: 'The emergence of vascular design in three dimensions', *J. Appl. Phys.*, 2008, **103**, article no. 123511, 9 pp.
- [143] K.-M. Wang, S. Lorente and A. Bejan: 'Vascular materials cooled with grids and radial channels', *Int. J. Heat Mass Transfer*, 2009, **52**, 1230-1239.
- [144] H.R. Williams, R.S. Trask, A.C. Knights, E.R. Williams and I.P. Bond: 'Biomimetic reliability strategies for self-healing vascular networks in engineering materials', *J. R. Soc. Interface*, 2008, **5**, 735-747.
- [145] H.R. Williams, R.S. Trask, P.M. Weaver and I.P. Bond: 'Minimum mass vascular networks in multifunctional materials', *J. R. Soc. Interface*, 2008, **5**, 55-65.
- [146] D. Therriault, S.R. White and J.A. Lewis: 'Chaotic mixing in three-dimensional microvascular networks fabricated by direct-write assembly', *Nat. Mater.*, 2003, **2**, 265-271.
- [147] D. Therriault, R.F. Shepherd, S.R. White and J.A. Lewis: 'Fugitive inks for direct-write assembly of three-dimensional microvascular networks', *Adv. Mater.*, 2005, **17**, 395-399.
- [148] J.A. Lewis and G.M. Gratson: 'Direct writing in three dimensions', *Mater. Today*, 2004, **7**, 32-39.
- [149] K.S. Toohy, N.R. Sottos, J.A. Lewis, J.S. Moore and S.R. White: 'Self-healing materials with microvascular networks', *Nat. Mater.*, 2007, **6**, 581-585.
- [150] K.S. Toohy, N.R. Sottos and S.R. White: 'Characterization of microvascular-based self-healing coatings', *Exp. Mech.*, 2009, **49**, 707-717.
- [151] K.S. Toohy, C.J. Hansen, J.A. Lewis, S.R. White and N.R. Sottos: 'Delivery of two-part self-healing chemistry via microvascular networks', *Adv. Funct. Mater.*, 2009, **19**, 1399-1405.

- [152] C.J. Hansen, W. Wu, K.S. Toohey, N.R. Sottos, S.R. White and J.A. Lewis: 'Self-healing materials with interpenetrating microvascular networks', *Adv. Mater.*, 2009, **21**, 1-5.
- [153] H.R. Williams, R.S. Trask and I.P. Bond: 'Self-healing composite sandwich structures', *Smart. Mater. Struct.*, 2007, **16**, 1198-1207.
- [154] H.R. Williams, R.S. Trask and I.P. Bond: 'Self-healing sandwich panels: restoration of compressive strength after impact', *Compos. Sci. Technol.*, 2008, **68**, 3171-3177.
- [155] S.A. Hayes, F.R. Jones, K. Marshiya and W. Zhang: 'A self-healing thermosetting composite material', *Composites Part A*, 2007, **38**, 1116-1120.
- [156] S.A. Hayes, W. Zhang, M. Branthwaite and F.R. Jones: 'Self-healing of damage in fibre-reinforced polymer-matrix composites', *J. R. Soc. Interface*, 2007, **4**, 381-387.
- [157] M. Yamaguchi, S. Ono and M. Terano: 'Self-repairing property of polymer network with dangling chains', *Mater. Lett.*, 2007, **61**, 1396-1399.
- [158] M. Yamaguchi, S. Ono and K. Okamoto: 'Interdiffusion of dangling chains in weak gel and its application to self-repairing material', *Mater. Sci. Eng., B*, 2009, **162**, 189-194.
- [159] M.A.M. Rahmathullah and G.R. Palmese: 'Crack-healing behavior of epoxy-amine thermosets', *J. Appl. Polym. Sci.*, 2009, **113**, 2191-2201.
- [160] M.M. Caruso, D.A. Delafuente, V. Ho, N.R. Sottos, J.S. Moore and S.R. White: 'Solvent-promoted self-healing epoxy materials', *Macromolecules*, 2007, **40**, 8830-8832.
- [161] M.M. Caruso, B.J. Blaiszik, S.R. White, N.R. Sottos and J.S. Moore: 'Full recovery of fracture toughness using a nontoxic solvent-based self-healing system', *Adv. Funct. Mater.*, 2008, **18**, 1898-1904.
- [162] S.J. Kalista, Jr., T.C. Ward and Z. Oyetunji: 'Self-healing of poly(ethylene-co-methacrylic acid) copolymers following projectile puncture', *Mech. Adv. Mater. Struct.*, 2007, **14**, 391-397.
- [163] S.J. Kalista, Jr. and T.C. Ward: 'Thermal characteristics of the self-healing response in poly(ethylene-co-methacrylic acid) copolymers', *J. R. Soc. Interface*, 2007, **4**, 405-411.
- [164] R.J. Varley and S. van der Zwaag: 'Development of a quasi-static test method to investigate the origin of self-healing in ionomers under ballistic conditions', *Polym. Test.*, 2008, **27**, 11-19.
- [165] R.J. Varley and S. van der Zwaag: 'Towards an understanding of thermally activated self-healing of an ionomer system during ballistic penetration', *Acta Mater.*, 2008, **56**, 5737-5750.
- [166] J.-M. Lehn: 'Dynamers: dynamic molecular and supramolecular polymers', *Prog. Polym. Sci.*, 2005, **30**, 814-831.
- [167] L. Bouteiller: 'Assembly via hydrogen bonds of low molar mass compounds into supramolecular polymers', *Adv. Polym. Sci.*, 2007, **207**, 79-112.
- [168] S.D. Bergman and F. Wudl: 'Mendable polymers', *J. Mater. Chem.*, 2008, **18**, 41-62.
- [169] T. Maeda, H. Otsuka and A. Takahara: 'Dynamic covalent polymers: reorganizable polymers with dynamic covalent bonds', *Prog. Polym. Sci.*, 2009, **34**, 581-604.
- [170] M.W. Urban: 'Stratification, stimuli-responsiveness, self-healing, and signaling in polymer networks', *Prog. Polym. Sci.*, 2009, **34**, 679-687.

- [171] J.S. Park, K. Takahashi, Z. Guo, Y. Wang, E. Bolanos, C. Hamann-Schaffner, E. Murphy, F. Wudl and H.T. Hahn: 'Towards development of a self-healing composite using a mendable polymer and resistive heating', *J. Compos. Mater.*, 2008, **42**, 2869-2881.
- [172] J.S. Park, H.S. Kim and H.T. Hahn: 'Healing behavior of a matrix crack on a carbon fiber/mendomer composite', *Compos. Sci. Technol.*, 2009, **69**, 1082-1087.
- [173] X. Chen, M.A. Dam, K. Ono, A. Mal, H. Shen, S.R. Nutt, K. Sheran and F. Wudl: 'A thermally re-mendable cross-linked polymeric material', *Science*, 2002, **295**, 1698-1702.
- [174] X. Chen, F. Wudl, A.K. Mal, H. Shen and S.R. Nutt: 'New thermally remendable highly cross-linked polymeric materials', *Macromolecules*, 2003, **36**, 1802-1807.
- [175] T.A. Plaisted and S. Nemat-Nasser: 'Quantitative evaluation of fracture, healing and re-healing of a reversibly cross-linked polymer', *Acta Mater.*, 2007, **55**, 5684-5696.
- [176] Y.-L. Liu and C.-Y. Hsieh: 'Crosslinked epoxy materials exhibiting thermal remendability and removability from multifunctional maleimide and furan compounds', *J. Polym. Sci., Part A: Polym. Chem.*, 2006, **44**, 905-913.
- [177] B. Gotsmann, U. Duerig, J. Frommer and C.J. Hawker: 'Exploiting chemical switching in a Diels-Alder polymer for nanoscale probe lithography and data storage', *Adv. Funct. Mater.*, 2006, **16**, 1499-1505.
- [178] B.J. Adzima, H.A. Aguirre, C.J. Kloxin, T.F. Scott and C.N. Bowman: 'Rheological and chemical analysis of reverse gelation in a covalently cross-linked Diels-Alder polymer network', *Macromolecules*, 2008, **41**, 9112-9117.
- [179] E.B. Murphy, E. Bolanos, C. Schaffner-Hamann, F. Wudl, S.R. Nutt and M.L. Auad: 'Synthesis and characterization of a single-component thermally remendable polymer network: Staudinger and Stille revisited', *Macromolecules*, 2008, **41**, 5203-5209.
- [180] Y.-L. Liu and Y.-W. Chen: 'Thermally reversible cross-linked polyamides with high toughness and self-repairing ability from maleimide- and furan-functionalized aromatic polyamides', *Macromol. Chem. Phys.*, 2007, **208**, 224-232.
- [181] Y. Zhang, A.A. Broekhuis and F. Picchioni: 'Thermally self-healing polymeric materials: the next step to recycling thermoset polymers?', *Macromolecules*, 2009, **42**, 1906-1912.
- [182] A.A. Kavitha and N.K. Singha: 'Atom-transfer radical copolymerization of furfuryl methacrylate (FMA) and methyl methacrylate (MMA): a thermally-amendable copolymer', *Macromol. Chem. Phys.*, 2007, **208**, 2569-2577.
- [183] A.A. Kavitha and N.K. Singha: 'A tailor-made polymethacrylate bearing a reactive diene in reversible Diels-Alder reaction', *J. Polym. Sci., Part A: Polym. Chem.*, 2007, **45**, 4441-4449.
- [184] A.A. Kavitha and N.K. Singha: "'Click chemistry" in tailor-made polymethacrylates bearing reactive furfuryl functionality: a new class of self-healing polymeric material', *ACS Appl. Mater. Interfaces*, 2009, **1**, 1427-1436.
- [185] M. Wouters, E. Craenmehr, K. Tempelaars, H. Fischer, N. Stroeks and J. van Zanten: 'Preparation and properties of a novel remendable coating concept', *Prog. Org. Coat.*, 2009, **64**, 156-162.

- [186] M. Watanabe and N. Yoshie: 'Synthesis and properties of readily recyclable polymers from bisfuranic terminated poly(ethylene adipate) and multi-maleimide linkers', *Polymer*, 2006, **47**, 4946-4952.
- [187] K. Ishida and N. Yoshie: 'Synthesis of readily recyclable biobased plastics by Diels-Alder reaction', *Macromol. Biosci.*, 2008, **8**, 916-922.
- [188] Q. Tian, Y.C. Yuan, M.Z. Rong and M.Q. Zhang: 'A thermally remendable epoxy resin', *J. Mater. Chem.*, 2009, **19**, 1289-1296.
- [189] G.R. Palmese, A.M. Peterson and R.E. Jensen: 'Remendable polymeric materials using reversible covalent bonds', In Proceedings of 26th Army Science Conference, Orlando, Florida, USA, 1-4 December 2008.
- [190] A.M. Peterson, R.E. Jensen and G.R. Palmese: 'Reversibly cross-linked polymer gels as healing agents for epoxy-amine thermosets', *ACS Appl. Mater. Interfaces*, 2009, **1**, 992-995.
- [191] S.-Y. Cho, J.-G. Kim and C.-M. Chung: 'A fluorescent crack sensor based on cyclobuane-containing crosslinked polymers of tricinnamates', *Sens. Actuators, B*, 2008, **134**, 822-825.
- [192] C.-M. Chung, Y.-S. Roh, S.-Y. Cho and J.-G. Kim: 'Crack healing in polymeric materials via photochemical [2+2] cycloaddition', *Chem. Mater.*, 2004, **16**, 3982-3984.
- [193] B. Ghosh and M.W. Urban: 'Self-repairing oxetane-substituted chitosan polyurethane networks', *Science*, 2009, **323**, 1458-1460.
- [194] F.R. Kersey, W.C. Yount and S.L. Craig: 'Single-molecule force spectroscopy of bimolecular reactions: system homology in the mechanical activation of ligand substitution reactions', *J. Am. Chem. Soc.*, 2006, **128**, 3886-3887.
- [195] S. Karthikeyan, S.L. Potisek, A. Piermattei and R.P. Sijbesma: 'Highly efficient mechanochemical scission of silver-carbene coordination polymers', *J. Am. Chem. Soc.*, 2008, **130**, 14968-14969.
- [196] A. Piermattei, S. Karthikeyan and R.P. Sijbesma: 'Activating catalysts with mechanical force', *Nat. Chem.*, 2009, **1**, 133-137.
- [197] L. Jafarpour and S.P. Nolan: 'Transition-metal systems bearing a nucleophilic carbene ancillary ligand: from thermochemistry to catalysis', *Adv. Organomet. Chem.*, 2001, **46**, 181.
- [198] W.A. Herrmann, T. Weskamp and V.P.W. Bohm: 'Metal complexes of stable carbenes', *Adv. Organomet. Chem.*, 2001, **48**, 1.
- [199] W.A. Herrmann: 'N-Heterocyclic carbenes: a new concept in organometallic catalysis', *Angew. Chem. Int. Ed.*, 2002, **41**, 1290.
- [200] J.M.J. Paulusse and R.P. Sijbesma: 'Reversible mechanochemistry of a PdII coordination polymer', *Angew. Chem. Int. Ed.*, 2004, **43**, 4460-4462.
- [201] J.M.J. Paulusse, J.P.J. Huijbers and R.P. Sijbesma: 'Quantification of ultrasound-induced chain scission in PdII-phosphine coordination polymers', *Chem. Eur. J.*, 2006, **12**, 4928-4934.
- [202] J.M.J. Paulusse and R.P. Sijbesma: 'Selectivity of mechanochemical chain scission in mixed palladium(II) and platinum(II) coordination polymers', *Chem. Commun.*, 2008, **37**, 4416-4418.

- [203] F.R. Kersey, D.M. Loveless and S.L. Craig: 'A hybrid polymer gel with controlled rates of cross-link rupture and self-repair', *J. R. Soc. Interface*, 2007, **4**, 373-380.
- [204] S. Varghese, A. Lele and R. Mashelkar: 'Metal-ion-mediated healing of gels', *J. Polym. Sci., Part A: Polym. Chem.*, 2006, **44**, 666-670.
- [205] J.W. Kamplain and C.W. Bielawski: 'Dynamic covalent polymers based on carbene dimerization', *Chem. Commun.*, 2006, **16**, 1727-1729.
- [206] K.A. Williams, A.J. Boydston and C.W. Bielawski: 'Towards electrically conductive, self-healing materials', *J. R. Soc. Interface*, 2007, **4**, 359-362.
- [207] D. Montarnal, P. Cordier, C. Soulie-Ziakovic, F. Tournilhac and L. Leibler: 'Synthesis of self-healing supramolecular rubbers from fatty acid derivatives, diethylene triamine, urea', *J. Polym. Sci., Part A: Polym. Chem.*, 2008, **46**, 7925-7936.
- [208] D. Montarnal, F. Tournilhac, M. Hidalgo, J.-L. Couturier and L. Leibler: 'Versatile one-pot synthesis of supramolecular plastics and self-healing rubbers', *J. Am. Chem. Soc.*, 2009, **131**, 7966-7967.
- [209] P. Cordier, F. Tournilhac, C. Soulie-Ziakovic and L. Leibler: 'Self-healing and thermoreversible rubber from supramolecular assembly', *Nature*, 2008, **451**, 977-980.
- [210] S.K. Kundu, T. Matsunaga, M. Yoshida and M. Shibayama: 'Rheological study on rapid recovery of hydrogel based on oligomeric electrolyte', *J. Phys. Chem. B*, 2008, **112**, 11537-11541.
- [211] B.W. Greenland, S. Burattini, W. Hayes and H.M. Colquhoun: 'Design, synthesis and computational modeling of aromatic tweezer-molecules as models for chain-folding polymer blends', *Tetrahedron*, 2008, **64**, 8346-8354.
- [212] S. Burattini, H.M. Colquhoun, B.W. Greenland and W. Hayes: 'A novel self-healing supramolecular polymer system', *Faraday Discuss.*, 2009, **143**, 251-264.
- [213] S. Burattini, H.M. Colquhoun, J.D. Fox, D. Friedmann, B.W. Greenland, P.J.F. Harris, W. Hayes, M.E. Mackay and S.J. Rowan: 'A self-repairing, supramolecular polymer system: healability as a consequence of donor-acceptor π - π stacking interactions', *Chem. Commun.*, 2009, **44**, 6717-6719.
- [214] M.K. Beyer and H. Clausen-Schaumann: 'Mechanochemistry: the mechanical activation of covalent bonds', *Chem. Rev.*, 2005, **105**, 2921-2948.
- [215] M.M. Caruso, D.A. Davis, Q. Shen, S.A. Odom, N.R. Sottos, S.R. White and J.S. Moore: 'Mechanically-induced chemical changes in polymeric materials', *Chem. Rev.*, 2009, **109**, 5755-5798.
- [216] J. Liang and J.M. Fernandez: 'Mechanochemistry: one bond at a time', *ACS Nano*, 2009, **3**, 1628-1645.
- [217] J.D. Rule, S.R. Wilson and J.S. Moore: 'Radical polymerization initiated by the Bergman Cyclization', *J. Am. Chem. Soc.*, 2003, **125**, 12992-12993.
- [218] J.D. Rule and J.S. Moore: 'Polymerizations initiated by diradicals from cycloaromatization reactions', *Macromolecules*, 2005, **38**, 7266-7273.
- [219] C.R. Hickenboth, J.D. Rule and J.S. Moore: 'Preparation of enediyne-crosslinked networks and their reactivity under thermal and mechanical conditions', *Tetrahedron*, 2008, **64**, 8435-8448.

- [220] K.L. Berkowski, S.L. Potisek, C.R. Hickenboth and J.S. Moore: 'Ultrasound-induced site-specific cleavage of azo-functionalized poly(ethylene glycol)', *Macromolecules*, 2005, **38**, 8975-8978.
- [221] S.L. Potisek, D.A. Davis, N.R. Sottos, S.R. White and J.S. Moore: 'Mechanophore-linked addition polymers', *J. Am. Chem. Soc.*, 2007, **129**, 13808-13809.
- [222] D.A. Davis, A. Hamilton, J. Yang, L.D. Cremar, D. Van Gough, S. L. Potisek, M.T. Ong, P.V. Braun, T.J. Martinez, S.R. White, J.S. Moore and N.R. Sottos: 'Force-induced activation of covalent bonds in mechanoresponsive polymeric materials', *Nature*, 2009, **459**, 68-72.
- [223] A.M. Basedow and K.H. Ebert: 'Ultrasonic degradation of polymers in solution', *Adv. Polym. Sci.*, 1977, **22**, 83-148.
- [224] K.S. Suslick and G.J. Price: 'Applications of ultrasound to materials chemistry', *Annu. Rev. Mater. Sci.*, 1999, **29**, 295-326.
- [225] J.M. Lenhardt, A.L. Black and S.L. Craig: '*gem*-dichlorocyclopropanes as abundant and efficient mechanophores in polybutadiene copolymers under mechanical stress', *J. Am. Chem. Soc.*, 2009, **131**, 10818-10819.
- [226] E.N. Brown, S.R. White and N.R. Sottos: 'Microcapsule induced toughening in a self-healing polymer composite', *J. Mater. Sci.*, 2004, **39**, 1703-1710.
- [227] E.J. Barbero and K.J. Ford: 'Characterization of self-healing fiber-reinforced polymer-matrix composite with distributed damage', *J. Adv. Mater.*, 2007, **39**, 20-27.
- [228] A.R. Hamilton, N.R. Sottos and S.R. White: 'Local strain concentrations in a microvascular network', *Exp. Mech.*, 2010, **50**, 255-263.
- [229] R.P. Wool: 'Self-healing materials: a review', *Soft Matter*, 2008, **4**, 400-418.
- [230] Barbero, E. J., Greco, F., and Lonetti, P.: 'Continuum damage-healing mechanics with application to self-healing composites', *Int. J. Damage Mech.*, 2005, **14**, 51-81.
- [231] Barbero, E. J. and Lonetti, P.: 'Application of continuum damage healing mechanics to self-healing composites', *Am. Soc. Mech. Eng., Aerosp. Div. (Publication) AD*, 2003, **68**, 515-519.
- [232] I.P. Bond, R.S. Trask and H.R. Williams: 'Self-healing fiber-reinforced polymer composites', *MRS Bull.*, 2008, **33**, 770-774.
- [233] M.R. Kessler and S.R. White: 'Self-activated healing of delamination damage in woven composites', *Composites Part A*, 2001, **32**, 683-699.
- [234] M.R. Kessler, N.R. Sottos and S.R. White: 'Self-healing structural composite materials', *Composites Part A*, 2003, **34**, 743-753.
- [235] L.T. Drzal and M. Madhukar: 'Fiber-matrix adhesion and its relationship to composite mechanical properties', *J. Mater. Sci.*, 1993, **28**, 569-610.
- [236] K. Sanada, I. Yasuda and Y. Shindo: 'Transverse tensile strength of unidirectional fibre-reinforced polymers and self-healing of interfacial debonding', *Plast. Rubber Compos.*, 2005, **35**, 67-72.
- [237] K. Sanada, N. Itaya and Y. Shindo: 'Effect of microstructure on the performance of unidirectional fiber composites encompassing self-healing of interfacial debonding', In: *Advances in Heterogeneous Material Mechanics (2008)*, 736-739, *Proc. of ICHMM-2008*, 2008, Huangshan, China, 3-8 June 2008.

- [238] J.L. Moll, S.R. White and N.R. Sottos: 'A self-sealing fiber-reinforced composite', *J. Compos. Mater.*, 2010, DOI:10.1177/0021998309356605
- [239] A.J. Patel, N.R. Sottos, E.D. Wetzel and S.R. White: 'Autonomic healing of low-velocity impact damage in fiber-reinforced composites', *Composites Part A*, 2010, **41**, 360-368.
- [240] J.A. Carlson, J.M. English and D.J. Coe: 'A flexible, self-healing sensor skin', *Smart Mater. Struct.*, 2006, **15**, N129-N135.
- [241] C. Suryanarayana, K. Chowdoji Rao and D. Kumar: 'Preparation and characterization of microcapsules containing linseed oil and its use in self-healing coatings', *Prog. Org. Coat.*, 2008, **63**, 72-78.
- [242] C. Andersson, L. Jarnstrom, A. Fogden, I. Mira, W. Voit, S. Zywicki and A. Bartkowiak: 'Preparation and incorporation of microcapsules in functional coatings for self-healing packaging board', *Packag. Technol. Sci.*, 2009, **22**, 275-291.
- [243] J.-H. Park and P.V. Braun: 'Coaxial electrospinning of self-healing coatings', *Adv. Mater.*, 2009, **21**, 1-4.
- [244] C.C. Corten and M.W. Urban: 'Repairing polymers using an oscillating magnetic field', *Adv. Mater.*, 2009, **21**, 5011-5015.
- [245] A.S. Iyer and L.A. Lyon: 'Self-healing colloidal crystals', *Angew. Chem. Int. Ed.*, 2009, **48**, 4562-4566.
- [246] A.B. South and L.A. Lyon: 'Autonomic self-healing of hydrogel thin films', *Angew. Chem. Int. Ed.*, 2010, **49**, 767-771.
- [247] G. Deng, C. Tang, F. Li, H. Jiang and Y. Chen: 'Covalent cross-linked polymer gels with reversible sol-gel transition and self-healing properties', *Macromolecules*, 2010, **43**, 1191-1194.
- [248] H.P. Wang, Y.C. Yuan, M.Z. Rong and M.Q. Zhang: 'Self-healing of thermoplastics via living polymerization', *Macromolecules*, 2010, **43**, 595-598.
- [249] A.C. Balazs: 'Modeling self-healing materials', *Mater. Today*, 2007, **10**, 18-23.
- [250] S. Maiti, C. Shankar, P.H. Geubelle and J. Kieffer: 'Continuum and molecular-level modeling of fatigue crack retardation in self-healing polymers', *J. Eng. Mater. Technol.*, 2006, **128**, 595-602.
- [251] S. Maiti and P.H. Geubelle: 'Cohesive modeling of fatigue crack retardation in polymers: crack closure effect', *Eng. Fract. Mech.*, 2006, **73**, 22-41.
- [252] J.Y. Lee, G.A. Buxton and A.C. Balazs: 'Using nanoparticles to create self-healing composites', *J. Chem. Phys.*, 2004, **121**, 5531-5540.
- [253] S. Tyagi, J.Y. Lee, G.A. Buxton and A.C. Balazs: 'Using nanocomposite coatings to heal surface defects', *Macromolecules*, 2004, **37**, 9160-9168.
- [254] K.A. Smith, S. Tyagi and A.C. Balazs: 'Healing surface defects with nanoparticle-filled polymer coatings: effect of particle geometry', 2005, **38**, 10138-10147.
- [255] S. Gupta, Q. Zhang, T. Emrick, A.C. Balazs and T.P. Russell: 'Entropy-driven segregation of nanoparticles to cracks in multilayered composite polymer structures', *Nat. Mater.*, 2006, **5**, 229-233.

- [256] R. Verberg, A.T. Dale, P. Kumar, A. Alexeev and A.C. Balazs: 'Healing substrates with mobile, particle-filled microcapsules: designing a 'repair and go' system', *J. R. Soc. Interface*, 2007, **4**, 349-357.
- [257] G.V. Kolmakov, K. Matyjeszewski and A.C. Balazs: 'Harnessing labile bonds between nanogel particles to create self-healing materials', *ACS Nano*, 2009, **3**, 885-892.
- [258] G.V. Kolmakov, R. Revanur, R. Tangirala, T. Emrick, T.P. Russell, A.J. Crosby and A.C. Balazs: 'Using nanoparticle-filled microcapsules for site-specific healing of damaged substrates: creating a 'repair-and-go' system', *ACS Nano*, 2010, **4**, 1115-1123.
- [259] G. Lanzara, Y. Yoon, H. Liu, S. Peng and W.-I. Lee: 'Carbon nanotube reservoirs for self-healing materials', *Nanotechnology*, 2009, **20**, article no. 335704, 7 pp.
- [260] O. Herbst and S. Luding: 'Modeling particulate self-healing materials and application to uni-axial compression', *Int. J. Fract.*, 2008, **154**, 87-103.
- [261] A. Ural, V.R. Krishnan and K.D. Papoulia: 'A cohesive zone model for fatigue crack growth allowing for crack retardation', *Int. J. Solids Struct.*, 2009, **46**, 2453-2462.
- [262] A. Dementsov and V. Privman: 'Percolation modeling of conductance of self-healing composites', *Physica A*, 2007, **385**, 543-550.
- [263] V. Privman, A. Dementsov and I. Sokolov: 'Modeling of self-healing polymer composites reinforced with nanoporous glass fibers', *J. Comput. Theor. Nanosci.*, 2007, **4**, 190-193.
- [264] A. Dementsov and V. Privman: 'Three-dimensional percolation modeling of self-healing composites', *Phys. Rev. E.*, 2008, **78**, article no. 021104, 6pp.
- [265] J.M. Lucci, R.S. Amano and P. Rohatgi: 'Computational analysis of self-healing in a polymer matrix with microvascular networks', In *Proc. ASME 2008 International Design Engineering Technical Conferences & Computers and Information in Engineering Conference (IDETC/CIE 2008)*, Brooklyn, New York, USA, 3-6 August 2008.
- [266] S. Luding and A.S.J. Suiker: 'Self-healing of damaged particulate materials through sintering', *Philos. Mag.*, 2008, **88**, 3445-3457.
- [267] S.D. Mookhoek, H.R. Fischer and S. van der Zwaag: 'A numerical study into the effects of elongated capsules on the healing efficiency of liquid-based systems', *Comput. Mater. Sci.*, 2009, **47**, 506-511.
- [268] <http://www.autonomicmaterials.com>
- [269] <http://www.arkema-inc.com>

CHAPTER 3: LATENT CATALYTIC SYSTEMS FOR RING-OPENING METATHESIS-BASED THERMOSETS

A paper published in *Journal of Thermal Analysis and Calorimetry**

Timothy C. Mauldin¹ and Michael R. Kessler²

3.1 Abstract

Synthesis and curing activity of latent ring-opening metathesis polymerization (ROMP)-based catalytic systems are reported using polydicyclopentadiene (pDCPD) as a model system. Differential scanning calorimetry (DSC) is used to monitor the ROMP reactions and to characterize the cured networks. These systems are either slow or completely inactive at ambient temperatures, yet at high temperatures the superior curing activity of other ROMP catalysts are retained. The resulting thermosets show glass transition temperatures from 10-25 °C higher than when cured with other ROMP catalysts.

3.2 Introduction

Thermosets made via ring-opening metathesis polymerization (ROMP) [1,2] are commercially available under the trade names Telene®, Metton®, and Vestenamer®, among others, and they generally are lightweight, possess high glass transition temperatures and have high impact strengths. These commercial systems are made with early transition metal-based catalysts such as tungsten, molybdenum or tantalum [3-5], all of which provide processing problems owing to their air-instability, variable curing activity, and occasional requirement of solvent. In the last several years, however, a series of air-stable, functional group tolerant, and highly active ruthenium ROMP catalysts have been developed, but they are not yet widely used for commercial applications. These ruthenium catalysts, often

* Reprinted with permission of *Journal of Thermal Analysis and Calorimetry*.

¹ Department of Chemistry, Iowa State University, Ames, IA 50011, USA.

² Department of Materials Science and Engineering, Iowa State University, Ames, IA 50011, USA.

dubbed “Grubbs’ catalysts,” [6-9] show promise in developing ROMP thermosets, but probably fall short of requirements for prepreg resins or for reaction injection molding (RIM) due to their extremely high activity, even at sub-ambient temperatures.

In this study, we develop two novel Grubbs’-type catalytic systems that demonstrate latent curing behavior at low temperatures while retaining the high activity of other ruthenium-based catalysts at elevated temperatures. The first system consists of a catalyst designed to inherently disfavor initiation of polymerization, therefore requiring higher temperatures, and the second system uses the commercially available 2nd generation Grubbs’ catalyst [10] along with additives that externally inhibit ligand dissociation. The monomer dicyclopentadiene (DCPD) is used as a model system, and the kinetics of its cure is studied by differential scanning calorimetry and analyzed further using the Ozawa-Flynn-Wall isoconversional model-free approach.

3.3 Experimental

3.3.1 Materials

Trimethylphosphine and all solvents were purchased from Aldrich and, unless otherwise specified, used without further purification. Grubbs’ 2nd generation catalyst, (IMesH₂)(PCy₃)(Cl)₂Ru(=CHPh) **1** (Figure 3.2), was lyophilized according to the literature [11] to assist its solubility. Dicyclopentadiene (>95% *endo*-isomer) was purchased from Alpha Aesar, and the chemical structure is shown in Figure 3.1.

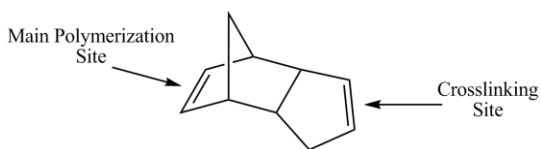


Fig. 3.1 Chemical structure of Dicyclopentadiene (DCPD).

3.3.2 (H₂IMes)(PMe₃)(Cl)₂Ru(=CHPh) (**3**)

Complex **2** was synthesized according to the literature [12], and its manipulation was performed using standard Schlenk techniques under an atmosphere of dry nitrogen gas.

Complex **3** was synthesized by a modified procedure in the literature [13]. To a solution of complex **2** (20 mg, 0.0275 mmol) dissolved in 2 ml dry benzene was added trimethylphosphine (4.18 mg, 0.055 mmol), and the reaction mixture was stirred for 10 minutes. The solvent was evaporated *in vacuo*, washed with cold pentanes (4 x 5 ml), and dried under vacuum for 2 hours to yield a brown powder (13.5 mg, 76% yield), shown in Figure 3.2. $^1\text{H NMR}$ (CDCl_3): δ 19.06 (s, 1H, =CHPh), 7.90 (d, $J = 7.5$ Hz, 2H, ortho CH), 7.47 (t, $J = 7.5$ Hz, 1H, para CH), 7.16 (t, $J = 7.5$ Hz, 2H, meta CH), 7.00 (s, 2H, Mes CH), 6.40 (s, 2H, Mes CH), 4.10 (m, 4H, $\text{NCH}_2\text{CH}_2\text{N}$), 2.64 (s, 6H, ortho CH_3), 2.37 (s, 6H, ortho CH_3), 2.31 (s, 3H, para CH_3), 2.02 (s, 3H, para CH_3), 0.90 (d, $J = 9.6$ Hz, 9H, PCH_3).

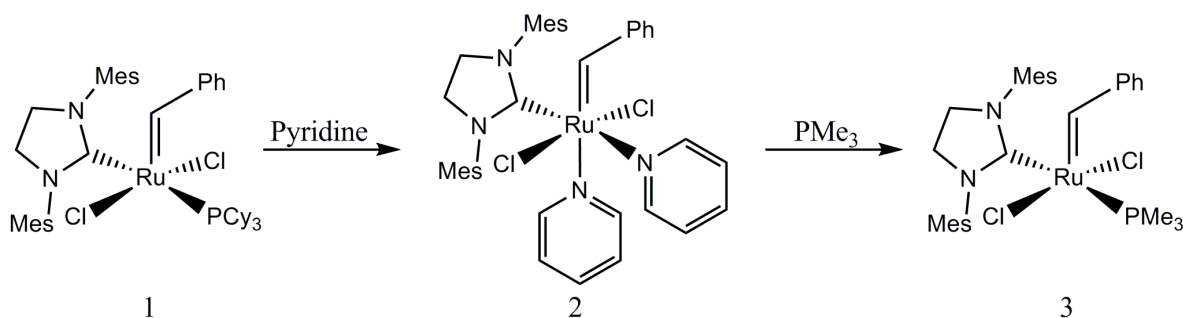


Fig. 3.2 Synthetic route to latent catalyst **3**.

3.3.3 General DSC Technique

Dicyclopentadiene, used either neat or containing dissolved triphenylphosphine, was added to the ruthenium-based ROMP catalyst, stirred quickly until complete catalyst dissolution, and flash-frozen in liquid nitrogen. The resulting solid was slightly melted to remove sample for experiments and refrozen in liquid nitrogen between tests. Samples were loaded into a DSC (Model Q20, TA Instruments) at a standby temperature of -50 °C. DSC experiments for all catalyst systems were under a flow of nitrogen at a constant rate of 50 ml/min. Dynamic curing experiments were performed over a temperature range of -50 to 200 °C at heating rates of 3, 7, 10, 15, and 20 °C/min.

3.4 Isoconversional Model-Free Approach

Degree of cure (α) measured by differential scanning calorimetry is defined as the fraction of heat or enthalpy at a given time:

$$\alpha = \Delta H_t / \Delta H_{\text{rxn}} \quad (3.1)$$

where ΔH_t is the heat evolved at time t and ΔH_{rxn} is the total heat evolution during the curing process. Curing kinetics can then be modeled using the typical curing equation

$$\delta\alpha/\delta t = k(T) f(\alpha) \quad (3.2)$$

that includes reaction model $f(\alpha)$ and the temperature-dependant rate constant $k(T)$. The latter can be further expanded

$$k = A e^{(E_a/RT)} \quad (3.3)$$

to reveal the activation parameters A (pre-exponential factor) and E_a (activation energy). The isoconversional model-free approach assumes that both of these activation parameters are a function of degree of cure (α), and they can be calculated by performing dynamic DSC scans and monitoring how the temperature to reach different degrees of cure changes with different heating rates. To achieve this, Ozawa [14] and Flynn and Wall [15] developed an approach by which equation 3.2 is integrated, and the resulting integral partially solved to give an equation of the form:

$$\ln \beta = -1.052(E_a/RT_i) + C \quad (3.4)$$

where β is the heating rate, T_i is the temperature required to reach a specific conversion, and C is a combination of other terms, including the pre-exponential factor (A). At a given conversion i , a plot of $\ln \beta$ vs. $1/T_i$ over all heating rates then yields a straight line with a slope proportional to E_a .

3.5 Results and Discussion

The mechanism for ring-opening metathesis polymerization of dicyclopentadiene with a ruthenium complex is shown in Figure 3.3. DCPD first replaces the phosphine via dissociative substitution, followed by rearrangement of electrons between the coordinated olefin and carbene to form the metallocyclobutane intermediate, and finally a similar rearrangement of electrons to open the ring and add a penultimate unit to the polymer chain. This gives rise to a new carbene with a neighboring open coordination site to which another monomer can bind and further propagate the growing active chain end. The fact that the only ligands known to be labile on Grubbs'-type catalysts are the phosphine, and their dissociation is necessary for the catalyst to activate and begin propagating, allows this dissociation to be considered an initiation step while the remainder of the catalytic cycle is propagation. This bodes well for designing catalysts with a long pot-life since the degree of latency should be tunable by varying the phosphine moiety in order to inhibit initiation at lower temperatures. Intuitively, these catalysts with various different phosphines should preserve the high catalytic activity of 2nd generation Grubbs' catalyst **1** since the propagating metal species, sans phosphine, are identical.

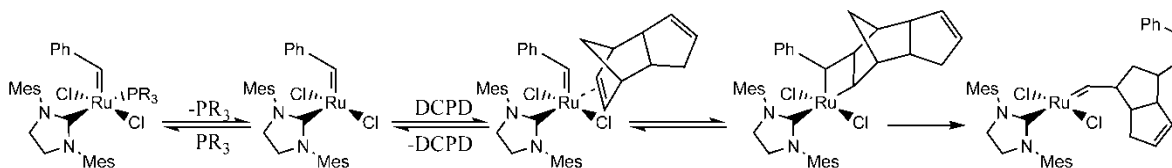


Fig. 3.3 ROMP of dicyclopentadiene by a 2nd generation Grubbs'-type catalyst.

Complex **3** was synthesized by indirectly replacing the PCy₃ ligand in complex **1** with PMe₃ (Figure 3.2). As shown in Figure 3.4, curing of dicyclopentadiene with complex **3** is clearly more latent than with complex **1** at various mole % loadings of each catalyst.

The degree of latency for the two catalysts is well-explained by the electronic and steric parameters of their respective phosphines. Electronically, the more nucleophilic a ligand, the slower dissociation tends to be. Ligands that act as strong nucleophiles have a high affinity for electrophiles like transition metals, and the bonds formed generally have high bond strengths that require a significant input of energy to break. Also, smaller ligands

are typically known to have slower dissociation kinetics. Larger ligands maximize steric congestion on the metal center, and reduction of this steric strain via dissociation helps to facilitate the dissociation process. Smaller ligands, however, do not have such a driving force and, from an enthalpic standpoint, are favored to remain coordinated to the metal.

Table 3.1 shows that the conjugate acid of PCy_3 has a pK_a (a common measure of electronic character of phosphines) making it slightly more nucleophilic than PMe_3 , which would imply that from an electronic standpoint PCy_3 is more latent. However the size of PMe_3 , expressed by its cone angle, is significantly smaller than PCy_3 . Seeing as catalyst **3** is considerably more latent than catalyst **1**, it appears that this greatly reduced size of PMe_3 offsets the minor electronic advantage towards latency that PCy_3 would be expected to have. Considerable effort in the literature dedicated to studying other Grubbs'-type metathesis catalysts has shown a wide range of solution phosphine dissociation rates by varying the phosphine used [16], which suggests that the curing latency of these systems can also be so tuned.

The second approach investigated to improve the latency of Grubbs'-type ROMP catalysts is by addition of free phosphine to the monomer. Figure 3.5 shows dynamic DSC scans of catalyst **1** with neat DCPD and catalyst **1** with 30, 60, and 120 molar equivalents (relative to catalyst) of PPh_3 initially dissolved in the DCPD. Analysis of the DSC plots confirms that addition of triphenylphosphine also inhibits dissociation of complex **1**, and the extent of the shift in the DSC curves appears proportional to the amount of free phosphine added.

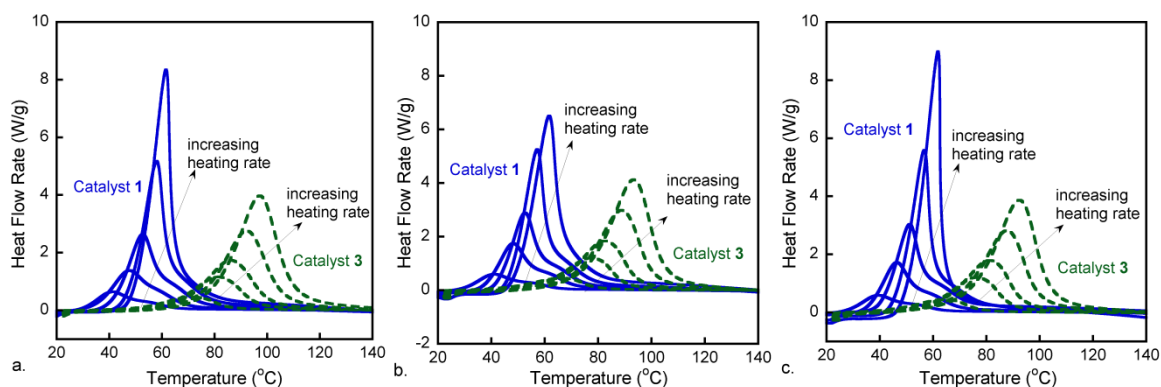


Fig. 3.4 DSC curves of samples with a) 4000:1, b) 3000:1, and c) 2000:1 molar ratio of [DCPD]:[catalyst] for catalysts **1** (blue) and **3** (green) at five different heating rates: 3, 7, 10, 15, and 20 °C/min.

This improved latency is attributed to Grubbs'-type catalysts dissociation existing in equilibrium with their respective dissociated species (Figure 3.6). Addition of a large excess of free phosphine to the curing system pushes this equilibrium towards the ROMP-inactive precatalyst and increase the latency of the system. It seems that only at elevated temperatures is this equilibrium pushed towards the ROMP-active dissociated complex where appreciable amounts of reaction can occur.

Table 3.1 pKa and cone angle of phosphines in catalysts **1** and **3**.

Phosphine	Cone angle	pKa
PCy ₃	170°	9.7
PMe ₃	118°	8.65
PPh ₃	145	2.73

Another hypothesis to explain these results is degradation of the ruthenium catalyst, facilitated by free phosphine, which has been reported elsewhere [17,18]. This would render much catalyst inactive and effectively reduce its concentration which could, in theory, increase latency. However, our results (vide infra, Figure 3.7) show that the degree of latency of catalyst **1** seems somewhat indiscriminate of catalyst loading, but very sensitive to

amount of free phosphine. Hence, the latter hypothesis is not given much weight here, but the potential for a combination of both effects cannot be ignored.

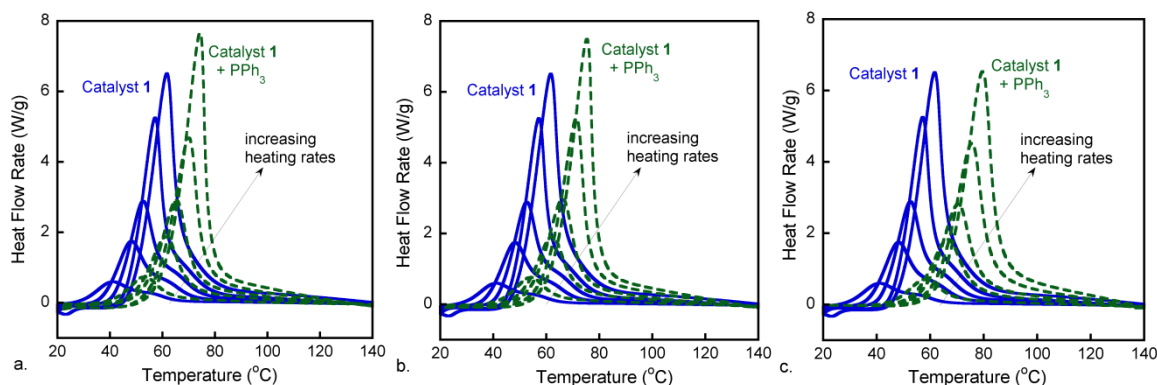


Fig. 3.5 DSC curves of samples with a 3000:1 molar ratio of [DCPD]:[catalyst **1**] (blue) and a) 3000:1:30, b) 3000:1:60, and c) 3000:1:120 molar ratio of [DCPD]:[catalyst **1**]:[PPh₃] (green) at five different heating rates: 3, 7, 10, 15, and 20 °C/min.

A comparison of the three catalyst system's peak temperatures (T_p) and temperatures at 10% cure ($T_{\alpha=0.1}$) are shown in Figure 3.7. While measurement of onset temperatures for each system would probably be the best approach to quantitatively evaluate the latency of each system, comparisons are often difficult owing to the different curvature in their DSC plots. However, it is believed that a comparison of two points of reference—peak temperatures and temperatures at a low degree of cure—should at least provide some insight into the degree of latency for each system.

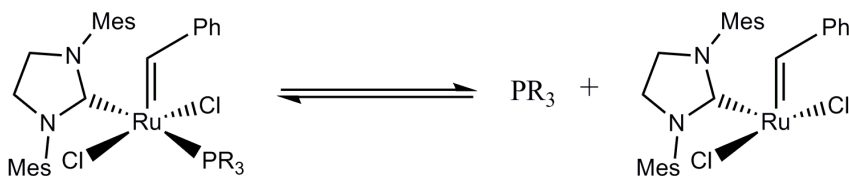


Fig. 3.6 Equilibrium of phosphine dissociation.

The difference between data sets containing 30 and 60 equivalents of free phosphine is small, but both T_p and $T_{\alpha=0.1}$ are consistently higher with 60 eq. PPh₃. Addition of 120

equivalents gives temperatures that are clearly higher overall heating rates. Since the same catalyst concentration was used in all experiments where free PPh_3 was added, it is reasonable to claim that addition of free phosphine can act as a means to “fine tune” the latency of ROMP-based systems. This trend is also in good agreement with the above argument of phosphine dissociation occurring in equilibrium—the more free phosphine initially added, the further the equilibrium will be pushed towards the ROMP-inactive pre-catalyst, consequently requiring higher temperatures to shift the equilibrium towards the ROMP-active catalyst. The exact dependency of this latency on free phosphine loading, however, is not very clear. The difference in the T_p and $T_{\alpha=0.1}$ values between data sets containing 30 and 60 equivalents of free phosphine ranges from 1.0-1.5 °C over all heating rates, and the range of differences between systems containing 60 and 120 equivalents of free phosphine is 3.7-4.4 °C. This seems like a consistent trend, but the difference in T_p and $T_{\alpha=0.1}$ between data sets containing 0 and 30 equivalents of free phosphine (the data set represented by 3000:1 [DCPD]:[catalyst **1**], \circ in Figure 3.7, can also be considered as a 3000:1:0 molar ratio of [DCPD]:[catalyst **1**]:[PPh_3]) is anomalously large—they range from 9.2-13.0 °C. A conclusive theory has not yet been formulated to explain this phenomenon, but it may be the aforementioned possibility of free phosphine both degrading catalyst, therefore reducing effective catalyst concentration and increasing latency, and existing in the equilibrium represented in Figure 3.6, also increasing latency. Both effects may be active in increasing latency when small amounts of free phosphine are added until perhaps a maximum amount of catalyst degradation is reached, and the trend between data sets including 30, 60 and 120 equivalents of free phosphine is solely representative of the equilibrium in Figure 3.6.

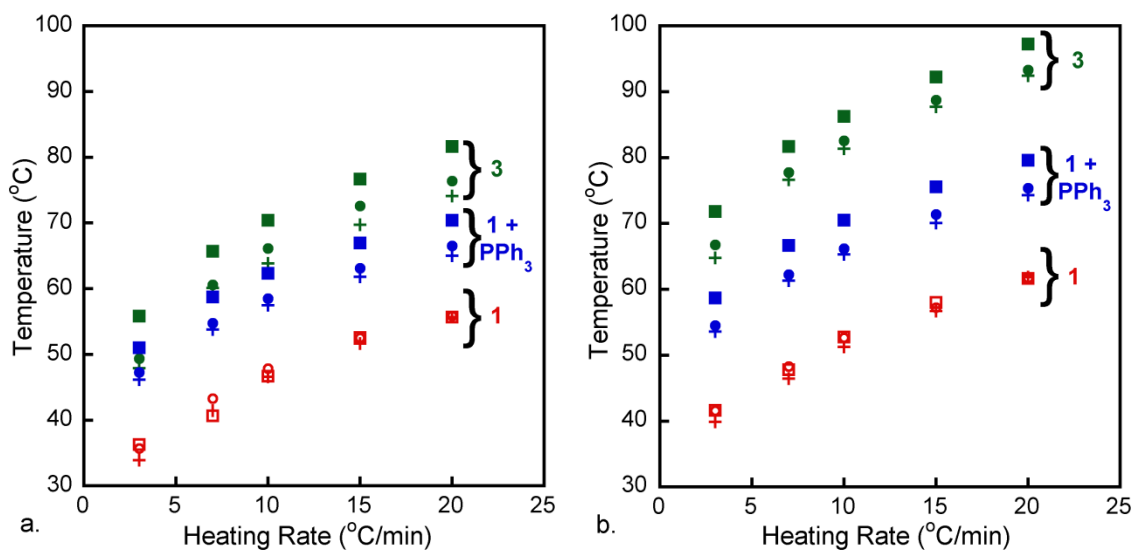


Fig. 3.7 a) Temperatures at 10% cure ($T_{\alpha=0.1}$) and b) peak temperatures (T_p) for all catalyst systems. Both plots contain data using catalyst **1** (2000:1 +, 3000:1 ○, and 4000:1 □ molar ratio [DCPD]:[Ru]), catalyst **3** (2000:1 +, 3000:1 ●, and 4000:1 ■ molar ratio [DCPD]:[Ru]), and catalyst **1** + PPh₃ (3000:1:30 +, 3000:1:60 ●, and 3000:1:120 ■ molar ratio [DCPD]:[Ru]:[PPh₃]).

Exothermic peaks from reaction with catalyst **3** shows shifts to higher temperatures with decreasing catalyst loading. At all heating rates, the highest catalyst loading, 2000:1 [DCPD]:[catalyst], clearly have the lowest T_p and $T_{\alpha=0.1}$ values, followed by 3000:1, then 4000:1. With a higher amount of catalyst, relative to monomer, there are more polymer chains propagating at any time, and a given degree of cure can be achieved at lower temperatures. This trend is generally expected and has been observed for many different systems [19]. Catalyst **1** may show a similar trend, but it is not as apparent as with catalyst **3**. While some data points in Figure 3.7 show no dependency of the exothermic peak's position on catalyst loading, most seem to follow the same trend as catalyst **3**. However, since all T_p and $T_{\alpha=0.1}$ values at each heating rate are very similar, this apparent trend cannot be conclusively distinguished from experimental error. In either case, it is at least evident that the dependency of the position of the exothermic peak is more sensitive to catalyst loading with catalyst **3** than with catalyst **1**.

Another note of interest is the material properties of the resulting polymer formed from each catalyst system. The typical glass transition temperatures, T_g , of each system is shown in Table 3.2. Catalyst **1** and catalyst **3** form polymers with very similar glass transition temperatures, consistently around 160 °C and 164°C, respectively. These T_g values are considerably higher than that reported for commercial pDCPD systems of about 140-150 °C [20], most likely because the more active catalysts **1** and **3** are able to polymerize more of the less-reactive crosslinking sites on DCPD (Figure 3.1) than other catalysts. Polymers made from catalyst **1** + PPh₃ have drastically reduced T_g 's that drop with a higher loading of free phosphine. In samples made with catalyst **1** + PPh₃, a reduced glass transition temperature is expected, since the large amount of free phosphine can act as a plasticizer in the polymer matrix. Also presented in Table 3.2 is the ΔH_{rxn} for all of the catalyst systems, evaluated by taking the integral under the DSC peak corresponding to exothermic reaction. All T_g and ΔH_{rxn} values presented are very consistent and repeatable, implying that their differences are not a result of experimental error. Reasons for these differences are discussed in detail below.

Table 3.2 Representative Glass transition temperatures (T_g) and reaction enthalpies (ΔH_{rxn}) for polymers formed from different catalyst systems. Glass transition temperatures presented here were taken from samples cured at $\beta = 15$ °C/min, and T_g values were measured at a heating rate of $\beta = 15$ °C/min.

Catalyst system	T_g (°C)	ΔH_{rxn} (J/g)
1	160.3	342.3 ± 7.2
3	164.1	311.0 ± 7.7
1 + 30 eq. PPh ₃	145.3	351.8 ± 2.4
1 + 60 eq. PPh ₃	139.7	347.8 ± 4.8
1 + 120 eq. PPh ₃	121.2	336.8 ± 3.9

The propagation of each catalyst system ideally should retain the high catalytic activity known for the 2nd generation Grubbs' catalyst [21,22], so the dynamic scans were examined via an Ozawa-Flynn-Wall analysis to determine activation energies. This data is

shown in Figure 3.8. Activation energy seems to be independent of catalyst concentration, and the general shape of the plots for all three systems shows typical diffusion control—activation energy stays relatively constant at low conversions, followed by what appears to be an exponential increase, presumably near or after the gel point. This behavior has been observed in other ROMP curing studies [23]. Assuming the nearly constant activation energy at low degrees of cure is the best representation of the propagation activity of each catalyst, it appears that both catalyst **1** and catalyst **3** have similar propagation activity, within experimental error. This effect is expected, considering both catalysts have the same propagating metal center.

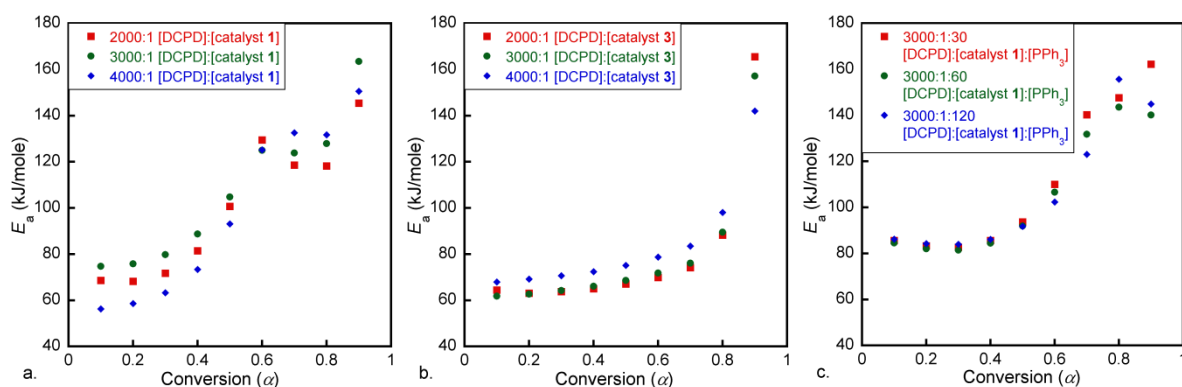


Fig. 3.8 Activation Energy (E_a) profiles of a) catalyst **1**, b) catalyst **3**, and c) catalyst **1** + PPh_3 .

The higher activation energy at low conversions for the system containing catalyst **1** + PPh_3 probably results directly from the equilibrium shown in Figure 3.6. Even at higher temperatures when the equilibrium is expected to favor the ROMP-active species, the mere presence of at most 120 equivalents of free phosphine should be statistically likely to rebind with some propagating catalyst molecules, forcing them back into their dormant, precatalyst state. The aggregate energy required to both activate the polymerization and to frequently re-dissociate phosphine from the catalyst is then expected to be higher than the other systems.

Figure 3.8a and 3.8b, activation energy profiles for catalysts **1** and **3**, respectively, show similar activation energies at conversions from 0-0.3 and 0.9. From 0.4-0.8, however, the two plots deviate significantly. All best-fit lines in the plots of $\ln \beta$ vs. $1/T_i$, from which

Figure 3.8 was derived, were good fits to the experimental data with correlation coefficients (r^2) typically greater than 0.993 (a representative plot is shown in Figure 3.9), so the deviations between Figures 3.8a and 3.8b are not attributed to experimental error.

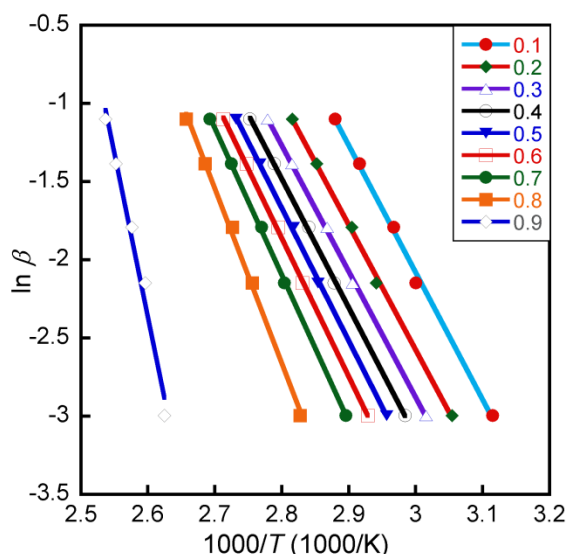


Fig. 3.9 A representative plot of $\ln \beta$ vs. $1/T_i$. Data presented here is taken from 2000:1 [DCPD]:[catalyst **3**].

A hypothesis has been formulated to explain this result. It is assumed that since the activation energy in Figure 3.8b remains fairly linear up to high conversions, followed by classic diffusion control, that heat evolved using catalyst **3** is solely a result of the ROMP reaction, while catalyst **1** undergoes one or more heat-evolving processes other than ROMP, thereby causing the deviations at conversions of $\alpha=0.4-0.8$.

That the activation energy in Figure 3.8a deviates from Figure 3.8b only at middle-to-high conversions implies that whatever process may be occurring at $\alpha=0.4-0.8$ is autocatalytic in nature. It is probably not truly autocatalytic in the sense that it does not help to propagate further polymerization (as evidenced by the lower T_g value for catalyst **1**), but instead initiates some other reaction on the polymer chain. This is consistent with the ΔH_{rxn} of catalyst **1** being about 30 J/g higher than with catalyst **3**, since this extra autocatalytic process would increase the heat evolved per unit mass.

This then leaves the question of what process besides ROMP could be evolving heat via reaction on the polymer chain, slightly reducing the T_g of the overall polymer, and why this process would occur with catalyst **1**, but not catalyst **3**. Highly active catalysts, including catalyst **1**, are known to sometimes undergo cross-metathesis on the acyclic double bonds of the polymer chain, especially at high temperatures [24], in a process known as back biting, which could explain these results. An example of back biting on a pDCPD chain is shown in Figure 3.10. This process is not nearly as exothermic as is the opening of a strained ring in ROMP, which explains why only a minor increase in ΔH_{rxn} is observed; it would cleave crosslinks on the polymer chain to leave either macrocyclic sidegroups or free molecules, which explains the drop in T_g ; and the back biting would be most prominent at high degrees of cure where the amount of acyclic olefins are maximized, which explains why the anomalous peak does not occur at low conversions.

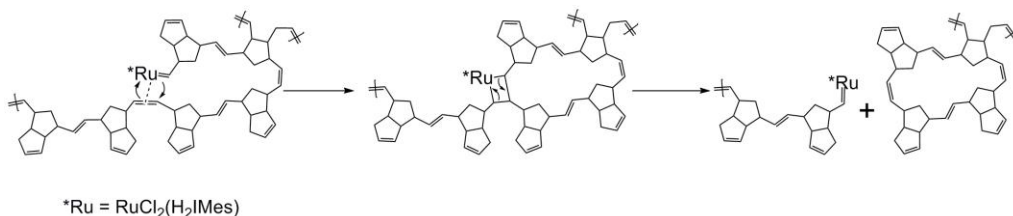


Fig. 3.10 An example of back biting on a pDCPD matrix.

Back biting does not appear to be prominent in catalyst **3**, marked by a lack of an extra peak in Figure 3.8b. When one turnover of ROMP is completed, the ruthenium catalyst exists as a 14-electron, 4-coordinate complex, shown as the last product in Figure 3.3. A nearby sigma-donor, in the case of this study either olefin or phosphine, should quickly coordinate to this high energy, transient intermediate. If an olefin coordinates at high conversions where a large amount of acyclic double bonds are present, it is likely that the coordinating olefin will be acyclic, which means the back biting interaction would be favored. If instead phosphine coordinates, the catalyst is stabilized and, upon re-dissociation of that phosphine, can be more selective to undergo the more kinetically and thermodynamically favorable reaction with a cyclic monomer. It would then appear that the extent of back biting could potentially be related to the catalyst's relative binding affinity to

olefin and phosphine. Both catalysts **1** and **3** should have equivalent binding affinities to olefin, since they are the same propagating metal center reacting with the same olefin monomer, but different binding affinities to their respective free phosphines, PCy₃ and PMe₃. Since binding affinity of a ligand to a substrate is typically inversely related to its rate of dissociation from that substrate [25], PMe₃ is expected to have a much higher binding affinity to its catalyst than PCy₃, and this higher affinity for phosphine in catalyst **3** would disfavor back biting reactions, relative to catalyst **1**.

Also lending evidence to this theory is the appearance of the anomalous peak occurring at high conversions in Figure 3.8c. The free phosphine used here, PPh₃, is expected to have a much lower binding affinity to catalyst than either PCy₃ or PMe₃, as suggested by its low pK_a (Table 3.2), and back biting reactions should be favored. However the binding affinity of PPh₃ to catalyst in these systems should effectively be higher than the pK_a implies since such a large excess (30, 60, or 120 eq.) is present. This can potentially explain why the anomalous peak occurs at higher conversions for Figure 3.8c than in Figure 3.8a—a larger amount of acyclic double bonds, created at higher conversions, is necessary to statistically outweigh the increased amount of free phosphine.

Furthermore, with higher loadings of free phosphine to increase the effective binding affinity to catalyst, less back biting is expected to occur. This is corroborated by the ΔH_{rxn} decreasing with increasing phosphine loading.

3.6 Conclusions

In this study, several different ROMP-based catalytic systems were used to cure dicyclopentadiene, and the resulting curing behavior was analyzed by DSC. It was shown that, compared to the 2nd generation Grubbs' catalyst **1**, catalyst **3** was much more latent and is potentially useful to increase the pot-life of polymers made by ruthenium-based ROMP. Also, dicyclopentadiene cured with catalyst **1** + free phosphine had an increased latency over catalyst **1** alone, but with much higher activation energy and a much lower T_g . Reasons for the differences in latency, activation energy, ΔH_{rxn} , and glass transition temperature of all systems were discussed in detail.

3.7 Acknowledgements

Financial support for this work was provided by the donors of The American Chemical Society Petroleum Research Fund (ACS PRF# 47700-AC7). We kindly thank Dr. Richard Larock for his donation of triphenylphosphine.

3.8 References

- [1] K.J Ivin and J.C. Mol, *J. Olefin metathesis and metathesis polymerization*. 1997, San Diego, CA: Academic Press.
- [2] C.W. Bielawski and R.H. Grubbs, *Prog. Polym. Sci.*, 32 (2007) 1.
- [3] R.H. Grubbs and W. Tumas, *Science*, 243 (1989) 907.
- [4] A.M. Rouhi, *Chem. Eng. News*, 80 (2002) 29.
- [5] A.M. Rouhi, *Chem. Eng. News*, 80 (2002) 34.
- [6] S.T. Nguyen, L.K. Johnson and R.H. Grubbs, *J. Am. Chem. Soc.*, 114 (1992) 3974.
- [7] S.T. Nguyen and R.H. Grubbs, *J. Am. Chem. Soc.*, 115 (1993) 9858.
- [8] E.L. Dias, S.T. Nguyen and R.H. Grubbs, *J. Am. Chem. Soc.*, 119 (1997) 3887.
- [9] R.H. Grubbs, *Angew. Chem. Int. Ed.*, 45 (2006) 3760.
- [10] M. Scholl, S. Ding, W.L. Choon and R.H. Grubbs, *Org. Lett.*, 1 (1999) 953.
- [11] A.S. Jones, J.D. Rule, J.S. Moore, S.R. White and N.R. Sottos, *Chem. Mater.*, 18 (2006) 1312.
- [12] M.S. Sanford, J.A. Love and R.H. Grubbs, *Organometallics*, 20 (2001) 5314.
- [13] S.L. Bolton, J.E. Williams, and M.B. Sponsler, *Organometallics*, 26 (2007) 2485.
- [14] T. Ozawa, *Bull. Chem. Soc. Jpn.*, 38 (1965) 1881.
- [15] J.H. Flynn and L.A. Wall, *Polym. Lett.*, 4 (1966) 323.
- [16] M.S. Sanford, J.A. Love, and R.H. Grubbs, *J. Am. Chem. Soc.*, 123 (2001) 6543.
- [17] S.H. Hong, M.W. Day and R.H. Grubbs, *J. Am. Chem. Soc.*, 126 (2004) 7414.
- [18] S.H. Hong, A.G. Wenzel, T.T. Salguero, M.W. Day and R.H. Grubbs, *J. Am. Chem. Soc.*, 129 (2007) 7961.
- [19] Xia Sheng, personal communication.
- [20] Metton® and Telene® brochures.
- [21] M.S. Sanford, M. Ulman and R.H. Grubbs, *J. Am. Chem. Soc.*, 123 (2001) 749.
- [22] C.W. Bielawski and R.H. Grubbs, *Angew. Chem. Int. Ed.*, 39 (2000) 2903.
- [23] M.R. Kessler and S.R. White, *J. Polym. Sci. Part A*, 34 (2002) 743.
- [24] T.-L. Choi, and R.H. Grubbs, *Angew. Chem. Int. Ed.*, 42 (2003) 1743.
- [25] R.H. Crabtree (ed.), *The Organometallic Chemistry of the Transition Metals*, 4th edition, John Wiley and Sons, New York 2005, p. 104-111.

CHAPTER 4: ENHANCED BULK CATALYST DISSOLUTION FOR SELF-HEALING MATERIALS

A paper published in *Journal of Materials Chemistry* *

Timothy C. Mauldin¹ and Michael R. Kessler²

4.1 Abstract

A model was developed to aid in the selection of healing monomers that can rapidly dissolve catalysts in self-healing materials. Predictions are made regarding dissolution rates of Grubbs' catalyst in a small library of ring-opening metathesis polymerization (ROMP)-active norbornenyl-based healing monomers. The Grubbs' catalyst and the healing monomers were experimentally assigned sets of Hansen parameters, and it was observed that healing monomers and blends of monomers with parameters similar to the catalyst were able to rapidly dissolve the catalyst. The model is limited in its ability to predict dissolution trends of healing monomers with substantially differently viscosities.

4.2 Introduction

In the past decade, polymers and composites that can repair themselves with complete, or nearly complete, autonomy have been extensively studied in academia and received significant commercial interest [1-3]. Perhaps the most ubiquitous self-healing mechanism developed to date incorporates liquid monomer-filled vessels and catalyst particles into a polymer matrix. Upon material fracture, vessels rupture, followed by flow of the liquid monomer into the crack volume. When the monomer contacts the catalyst particles it polymerizes and adheres the crack faces together (Figure 4.1) [4-7]. The first and most well-studied monomer/catalyst combination used thus far in self-healing systems is

* Reprinted with permission of *Journal of Materials Chemistry*.

¹ Department of Chemistry, Iowa State University, Ames, IA 50011, USA.

² Department of Materials Science and Engineering, Iowa State University, Ames, IA 50011, USA.

dicyclopentadiene (DCPD) and Grubbs' catalyst, the former of which undergoes ring-opening metathesis polymerization (ROMP) [8-10] in the presence of the latter [11-17]. This system worked well to first demonstrate self-healing as both the catalyst and DCPD satisfy many of the unique and complex requirements of this healing mechanism, but owing to the price of Grubbs' catalyst, the research community has been slowly moving away from ROMP-based self-healing in favor of healing based on other chemistries. But while healing with these other chemistries (notably siloxane polycondensation [18], epoxy ring-opening polymerization [19], solvent activation of residual matrix reaction [20], and click chemistry [21], among others) has indeed proven fruitful, the superior healing precedent set by the seminal Grubbs' catalyst should disallow it from being deemed impractical for self-healing applications simply due to economic considerations.

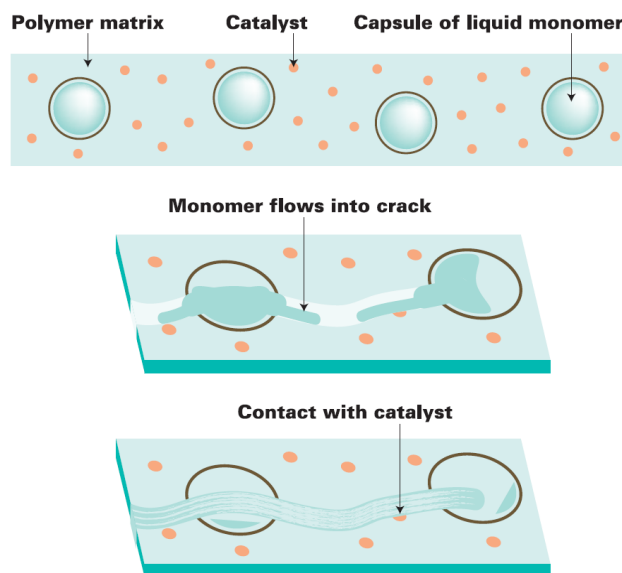


Figure 4.1. Schematic representing self-healing of a polymer

One approach to minimize the economic obstacle of using Grubbs' catalyst is to reduce the amount of catalyst required to achieve maximum healing potential. Unfortunately, efficient use of the catalyst in a self-healing system is often difficult due to the fact that the monomer needs to dissolve the catalyst in a very non-ideal mixing scenario; that is, elevated temperatures or external agitation cannot realistically be applied to aid catalyst

dissolution during the healing event. In addition, sluggish catalyst dissolution can also likely be attributed to the fact that the catalyst particle is embedded in the crack surface, limiting the surface area of catalyst exposed to the liquid monomer during healing to one cross-sectional area of the particle. Nevertheless, others have developed rather clever techniques to promote efficient use of Grubbs' catalyst during healing. For example, Rule et al. showed that by first encapsulating Grubbs' catalyst particles in wax microspheres, a 10-fold decrease in catalyst loading can achieve similar or better healing relative to the original, wax-free self-healing systems [22]. Catalyst was used more efficiently due to the catalyst particles being smaller in size in the wax microspheres, which increases the surface area of catalyst exposed to liquid monomer. Furthermore, the Grubbs' catalyst was protected by the wax casing from surface layer decomposition caused by contact with the polymer matrix resin during composite fabrication. Another approach to more efficiently use catalyst is to incorporate different healing monomers and monomer blends that inherently require less catalyst to achieve a high degree of polymerization, and therefore require lower loadings of catalyst in the self-healing polymer. For example, Liu et al. have identified a low viscosity, highly-reactive ROMP monomer called ethylidene norbornene that can be used either neat or in blends with DCPD to, among other things, significantly reduce the required catalyst loading in a self-healing polymer [23-27].

An alternate approach to efficiently using the catalyst in a self-healing polymer is to increase the rate at which catalyst is dissolved into the liquid monomer. Presumably, the reason why such a large amount of Grubbs' catalyst, relative to DCPD, is necessary in self-healing polymers is because the catalyst particles exposed on the crack surface are not entirely dissolved before DCPD undergoes appreciable amounts of polymerization, and therefore cannot easily dissolve more catalyst. Hence, the effective catalyst concentration is considerably lower than the feed concentration that is initially added to the self-healing polymer. So to reach maximum healing capabilities, comparatively large amounts of catalyst are necessary. Increasing the dissolution rate of the catalyst would then cause the effective concentration to approach the feed catalyst concentration, thus requiring less overall catalyst to achieve similar levels of healing. Jones et al. attempted to increase dissolution kinetics by grinding, freeze-drying, and recrystallizing catalyst particles to smaller sizes, thereby

increasing their surface area [28]. Smaller catalyst particles were shown to dissolve faster in the healing monomer than the large, as-received Grubbs' catalyst particles. In some cases, this faster dissolution also improved healing by ensuring a relatively even distribution of dissolved catalyst throughout the monomer, which led to a continuous polymer film in the crack volume. This was unlike early self-healing systems with large, slow-dissolving catalyst particles, whose reaction with monomer was largely heterogeneous, leading to intermittent patches of polymer surrounding catalyst embedded in the crack plane. However, reducing catalyst particle size and increasing catalyst surface area is not without drawbacks. For example, as mentioned above, the extent of catalyst surface layer decomposition is increased with a greater surface area, and the smaller size potentially leads to catalyst dissolution in the polymer matrix resin in which it is embedded.

In addition to decreasing the amount of catalyst required for self-healing polymers, improving the bulk catalyst dissolution kinetics can also increase the speed of healing, which greatly expands self-healing polymer's potential application base. Ideally, self-repair should be as rapid as possible, especially for applications where the polymer may be subject to rapid or periodic stress. But it was recently observed that healing kinetics is not a simple phenomenon and dependent on many factors, notably the sensitive interplay between catalyst dissolution kinetics and bulk polymerization kinetics of the healing monomer [29]. In particular, it was noted that the bulk polymerization kinetics of the healing monomer should not greatly exceed the catalyst dissolution kinetics. Otherwise the system would result in a polymer with poor properties and "spotty" healing, similar to the aforementioned case of healing with large, slow-dissolving catalyst particles. Thus, catalyst dissolution kinetics is a significant (but often ignored) consideration when determining the speed and quality of self-healing.

In this paper, we create a small library of healing monomers and develop a model to make predictions regarding their ability to dissolve a catalyst in a self-healing polymer. While we anticipate our model can be versatile enough to be applicable to any type of healing chemistry, due to the robust and well-studied healing performance of ROMP-based self-healing, we focus our discussion here only on the dissolution of Grubbs' catalyst in ROMP-active healing monomers. In order to create this model, we borrow several ideas

from the concept of solubility parameters, otherwise widely known in the realm of polymer physics as a means to make predictions regarding solute-solvent interactions and the thermodynamics of polymer mixing [30]. Details of the calculations and the strengths and limitations of the model are discussed in detail. And finally, the model is experimentally validated by directly measuring the dissolution rate of a structurally-modified Grubbs' catalyst in various monomers and monomer blends. The structurally-modified catalyst was used to inhibit polymerization of the ROMP-active monomers during the course of the dissolution.

4.3 Experimental

4.3.1 General considerations

Bis(tricyclohexylphosphine)benzylideneruthenium dichloride (1st generation Grubbs' catalyst), bicyclo[2.2.1]hept-2-ene (norbornene), dicyclopentadiene, 5-vinyl-2-norbornene, 5-ethylidene-2-norbornene, 5-norbornene-2-carboxylic acid, 5-norbornene-2-methanol, tetramethylsilane, ethyl vinyl ether, and all solvents/starting materials/reagents used for synthesis were purchased from Aldrich and, unless stated otherwise, used as-received. While determining Grubbs' catalyst's parameters, all solvents known to not readily absorb atmospheric moisture were used as-received from freshly-opened bottles. All other solvents were either purchased anhydrous or dried accordingly and were handled under a nitrogen gas purge. 5-norbornene-2-carboxaldehyde [31], 2-(chloromethyl)-5-norbornene [32], 2-(bromomethyl)-5-norbornene [33], ethyl 5-norbornene-2-carboxylate [34], 5-(methoxymethyl)-2-norbornene [35], and 2-acetyl-5-norbornene [36] were synthesized according to literature procedures. All 5-substituted norbornenyl-derivatives, either purchased or synthesized, were obtained as a mixture of *exo*- and *endo*-isomers. All other syntheses are described below. ¹H-NMR spectra were recorded at either 300 or 400 MHz with a Varian Spectrometer (Palo Alta, CA) using CDCl₃ as a solvent and residual chloroform as an internal reference. HR-MS was done on a Finnigan TSQ700 mass spectrometer (San Jose, CA). Unless otherwise stated, room temperature is defined as 23-24 °C.

4.3.2 Synthesis of phenyl vinyl ether

A modified version of the original preparation [37] was used. β -Bromophenetole (15 g, 75 mmol) was added to KOH (20 g, 0.36 mol), which had been ground into a fine powder. The suspension was heated to a reflux (~ 150 °C) for 12 hours. The crude product was isolated by vacuum filtration and purified by silica gel column chromatography (hexanes) to yield a clear, colorless liquid (3.1 g, 35%). $^1\text{H-NMR}$ (300 MHz, CDCl_3) δ ppm 7.35 (apparent t, $J = 9$ Hz, 2H), 7.10, (t, $J = 9$ Hz, 1H), 7.04 (d, $J = 9$ Hz, 2H), 6.68 (dd, $J = 6, 15$ Hz, 1H), 4.79 (dd, $J = 3, 15$ Hz, 1H), 4.45 (dd, $J = 3, 6$ Hz, 1H). High-resolution mass spectrometry (HRMS) expected 120.0575, found 120.0571.

4.3.3 Synthesis of $(\text{PCy}_3)_2\text{Cl}_2\text{Ru}=\text{C}(\text{H})\text{OPh}$

Phenyl vinyl ether (2.5g, 21 mmol) was slowly added to a CH_2Cl_2 (10 ml) solution of Grubbs' 1st generation catalyst, $(\text{PCy}_3)_2\text{Cl}_2\text{Ru}=\text{C}(\text{H})\text{Ph}$, (2 g, 2.4 mmol). This solution was allowed to stir at room temperature for 30 minutes, during which time the purple solution changed to a dark red color. The solvent was evaporated *in vacuo*, and the resulting solid was washed with 4 x 10 ml of cold (-25 °C) pentane to reveal a red solid (1.90 g, 93%). $^1\text{H-NMR}$ (300 MHz, CDCl_3) δ ppm 14.84 (s, 1H), 7.36 (apparent t, $J = 7.8$ Hz, 2H), 7.21 (t, $J = 7.5$ Hz, 1H), 7.09 (d, $J = 7.8$ Hz, 2H), 2.72-2.64 (m, 6H), 2.01-1.97(m, 12H), 1.81-1.71 (m, 19H), 1.61-1.51 (m, 13H), 1.35-1.20 (m, 16H).

4.3.4 Synthesis of *N,N*-dimethyl-5-norbornene-2-carboxamide

N,N-dimethylacrylamide (15 g, 0.15 mole) was added to 250 ml ethyl acetate. Over the course of 30 minutes, freshly-distilled cyclopentadiene (11 g, 0.17 mol) was added dropwise. After complete addition, the solution was brought to a gentle reflux and allowed to stir for 5 days in the dark, with an additional 1 ml of cyclopentadiene being added daily. Complete consumption of *N,N*-dimethylacrylamide was observed by silica gel thin-layer chromatography (ethyl acetate, $R_f = 0.6$), and volatiles were removed *in vacuo*. The resulting crude product was cooled to ~ 5 °C and triturated three times with pentane (1x250 ml, 2x100 ml). Upon warming to room temperature, a dark brown, viscous liquid was isolated (19.5 g, 78%) with sufficient purity ($>95\%$). Product was a mixture of *endo/exo*-

isomers (~4/1). ¹H-NMR (300 MHz, CDCl₃) for the *endo* isomer: δ ppm 6.15 (dd, J = 3.0, 5.7 Hz, 1H), 6.02 (dd, J = 3.0, 5.7 Hz, 1H), 3.10-3.01 (m, 2H), 3.07 (s, 3H), 2.90-2.83 (m, 1H), 2.88 (s, 3H), 1.97-1.89 (m, 1H), 1.41-1.32 (m, 2H), 1.28 (apparent d, J = 8.1 Hz, 1H). High-resolution mass spectrometry (HRMS) expected 165.1154, found 165.1160.

4.3.5 Dissolving Grubbs' Catalyst in solvent

5 mg of Grubbs' 1st generation catalyst was weighed into a small, flame-dried vial, and the catalyst particles were evenly distributed throughout the bottom area of the vial. A given solvent was added to the vial via syringe (0.5 ml). The solvent addition was rapid enough to quickly cover the catalyst layer, but not so rapid that the even distribution of the catalyst along the bottom of the vial was disturbed. For those solvents whose saturation point was not reached after dissolving the 5 mg of catalyst (i.e. solubility of catalyst in solvent > 5mg/0.5ml), the approximate time for complete dissolution was recorded. For solvents that became saturated prior to completely dissolving the 5 mg catalyst, the saturation level was determined, and a similar dissolution experiment was rerun with half the amount of catalyst that can saturate the solvent (e.g. if the saturation level of Grubbs' catalyst in a solvent was determined to be 4 mg catalyst/0.5 ml solvent, the subsequent dissolution test was done with 2 mg catalyst in 0.5 ml solvent). Three dissolution experiments were performed with each solvent. Each solvent's dissolution rate was categorized as either rapid, moderate, slow or deficient, based on the table below:

Table 4.1. Ranking system for dissolution of Grubbs' catalyst in various solvents

Category	Description
Rapid	Fully dissolved during, or within a few seconds after, solvent addition.
Moderate	30 – 90 seconds
Slow	2-5 minutes
Deficient	>5 minutes

Additionally, an extra dissolution experiment was performed with double the amount of each solvent in order to determine the dependence of the dissolution rate on the degree of undersaturation.

4.3.6 Dissolving Grubbs' Catalyst in monomer

250 ± 1 mg of modified Grubbs' 1st generation catalyst, (PCy₃)₂Cl₂Ru=C(H)OPh, was weighed into a flame-dried vial, and the catalyst particles were evenly distributed throughout the area of the bottom of the vial. Exactly 5 ml of monomer or monomer blend containing 0.2 ml tetramethylsilane internal standard was quickly added to the catalyst in a manner that did not disturb the even distribution of catalyst on the bottom of the vial. At 5-minute intervals up to 30 minutes, 0.1 ml of liquid was withdrawn from the center of the solution. To these aliquots was added 10 µl of ethyl vinyl ether to ensure minimal or no polymerization during further characterization. ¹H-NMR spectra (400 MHz, CDCl₃, 64 scans) were taken of the aliquots, and the amount of dissolved catalyst is defined as the molar ratio of catalyst to TMS internal standard, denoted herein as "relative intensity." Relative intensity was calculated by

$$\text{Relative Intensity} = \frac{\sum I_{Ru=C(H)R}}{I_{TMS} / 12} \quad (4.1)$$

where $\sum I_{Ru=C(H)R}$ is the sum of all ruthenium carbene integrations, and I_{TMS} is the integration value of tetramethylsilane. Reported relative intensity values are the average of three dissolution experiments.

4.4 Results and Discussion

4.4.1 Healing monomer library dissolution parameters

For each monomer in the healing monomer library (shown in Figure 4.2) we calculated a set of Hansen parameters, which were originally developed to provide a semi-quantitative model for predicting cohesive compatibility between solvents, plasticizers,

polymers, dyes, etc. [38]. Hansen parameters, denoted as δ_x , are defined as the square root of the cohesive energy density related to an x-type intermolecular attraction, where chemicals with similar parameters have both similar cohesive energies and, more importantly for the present work, greater chemical compatibility. A conceptual explanation of Hansen parameters and their calculation is discussed briefly here, and in much greater detail in reference 39.

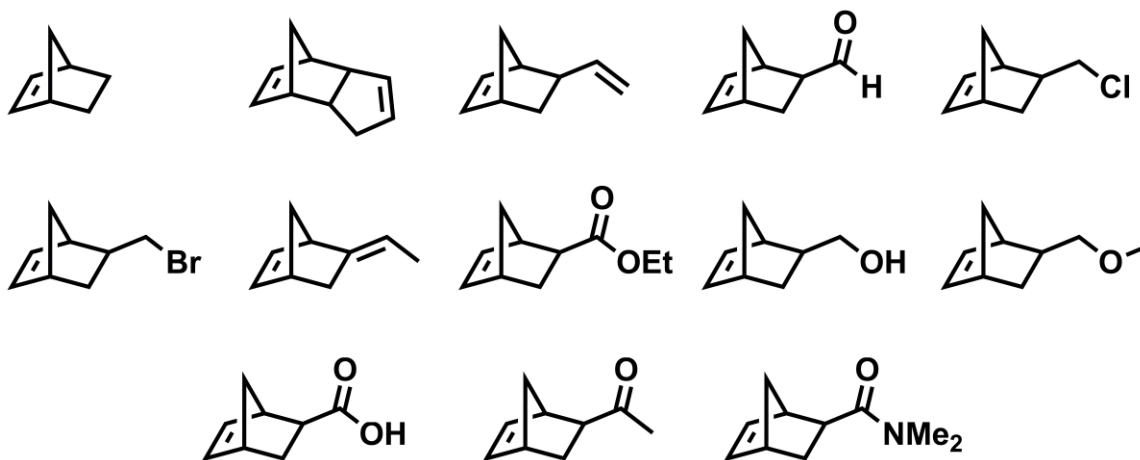


Figure 4.2. ROMP-active, healing monomer library.

A Hansen parameter of a chemical's x-type cohesive force can be directly calculated from the x-type force's contribution to the total cohesive energy of a chemical, E_x , normalized by its molar volume, V :

$$\delta_x = \sqrt{\frac{E_x}{V}} \quad (4.2)$$

There are three parameters historically defined as Hansen parameters: δ_D , the parameter related to intermolecular dispersion forces; δ_P , the parameter related to fixed-dipole forces; and δ_H , a parameter classically known as the hydrogen-bonding parameter, but often regarded as an electron-transfer parameter. As shown in equation 4.3, the sum of the squares of the Hansen parameters is equivalent to the total parameter, δ_T , which is known as the one-

dimensional, Hildebrand parameter. Additionally, using equations 4.2 and 4.3, the relationship can be rewritten directly as a function of cohesive energy densities (equation 4.4), although dealing with the smaller Hansen parameters is often more convenient.

$$\delta_T^2 = \delta_D^2 + \delta_P^2 + \delta_H^2 \quad (4.3)$$

$$\frac{E_T}{V} = \frac{E_D}{V} + \frac{E_P}{V} + \frac{E_H}{V} \quad (4.4)$$

Then, chemicals with similar parameters can be considered chemically compatible and have some favorable intermolecular interactions. While Hansen parameters are most often used to make predictions regarding thermodynamic-based interactions of two or more chemicals (e.g. solubility, polymer swelling in a solvent, polymer mixing, etc.), it has been shown that they can also potentially be useful in linking together chemicals' kinetic processes [40], but to the best of our knowledge, have never been used to make predictions on dissolution. However, it should be noted that these parameters are only meant to be a useful guide for making predictions, and their specific values should be considered approximations that cannot predict minor differences in behavior.

While Hansen parameters can be calculated experimentally, reasonably accurate values can be obtained using the Beerbower group contribution method, where atomic groups (e.g. $-\text{CH}_2-$, $=\text{CH}-$, $-\text{OH}$, $-\text{C}_6\text{H}_5$, $-\text{NH}_2$, etc.) have fixed cohesive energy contributions related to a specific Hansen intermolecular force (i.e. dispersion, fixed-dipole or hydrogen-bonding). Lists of the Beerbower group contributions can be found in numerous sources [39]. In order to determine E_X for a given chemical, the sum of the appropriate atomic group contributions for that chemical is determined, and the corresponding Hansen parameters are calculated using equation 4.2. However, our initial efforts to directly use this group contribution approach were unsuccessful, presumably a result of the norbornenyl functionality present on all of our healing monomers being a highly-strained, bicyclic structure, while group contributions are generally intended for use with small, linear, and strain-free molecules. Hence, we experimentally calculated the “atomic group contribution”

for the 2-norbornenyl-group with covalent connectivity at the 5-position (the functionalized position in the majority of our 2-norbornenyl-based library). Then, our 2-norbornenyl “group contribution” was used concurrently with the Beerbower group contributions to build Hansen parameters for our healing monomer library. Further details regarding the calculation of the 2-norbornenyl “group contribution” are available in the supplementary information for this paper, and the full set of Hansen parameters for all healing monomers is shown in table 4.2.

Table 4.2. Complete Hansen Parameters for the healing monomer library

Monomer ^a	δ_T	δ_D	δ_P	δ_H
-H	16.0	15.5	1.4	3.7
-CH=CH-CH ₂ -	17.8	17.1	1.8	4.7
-CH=CH ₂	16.2	15.4	1.7	4.6
=CH-CH ₃	16.7	15.9	2.0	4.7
-COOEt	16.9	15.3	3.2	6.4
-CH ₂ -OH	22.9	18.0	5.1	13.2
-COOH	21.4	18.5	3.5	10.3
-COCH ₃	19.3	17.5	5.7	6.0
-CHO	20.4	16.1	10.4	6.9
-CH ₂ -Cl	18.2	16.7	6.3	3.7
-CH ₂ -Br	18.5	16.7	6.2	5.0
-CH ₂ -O-CH ₃	16.9	15.7	3.9	4.8
-CON(CH ₃) ₂	22.7	18.5	9.8	8.8

^athe functional group listed refers to a derivative of 2-norbornene functionalized with this group at the 5-position.

The parameters for the healing monomer library are shown in Figure 4.3, expressed as a 2-dimensional Hansen Parameter Map, which we refer to as a Healing Monomer Map. Since the δ_D Hansen parameters for all of the healing monomers are very similar (16.7 ± 1.1 MPa^{1/2}), they are intentionally ignored both in Figure 4.3 and when comparing the parameters of different chemicals (*vide infra*), which is commonly done with Hansen parameters. It is

noteworthy that, for all healing monomers, $\delta_H > 3$. This is true even of the hydrocarbon monomers that are not expected to show significant hydrogen bonding. But as mentioned above, the “hydrogen-bonding” parameter nomenclature is something of a misnomer, used largely due to historical precedent, and instead should be considered as a parameter related to electron-transfer intermolecular forces. Therefore, the unexpectedly large δ_H values can be explained by the norbornenyl-group’s double bond acting as a Lewis base, which is essentially defined as a species that can undergo electron-transfer. Furthermore, the lewis basicity of the norbornenyl double bond is especially high, relative to other double bonds, because donation of its π -bonding electrons would result in a moderate relief of ring-strain in the highly-strained norbornenyl functionality. All other Hansen parameters for the healing monomers fall within expected ranges for the functional groups on each monomer (i.e. hydrocarbons have low δ_P values, the amide has a high δ_P value, monomers with a removable hydrogen have high δ_H values, etc.).

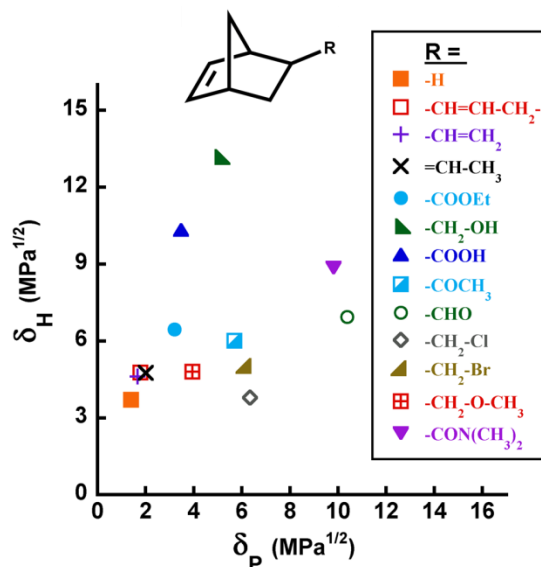


Figure 4.3. Healing Monomer Map for the ROMP-active library used in this study.

4.4.2 Catalyst dissolution parameters

The Hansen parameters for Grubbs’ Catalyst were determined by qualitatively measuring dissolution of the catalyst in various common organic solvents with well-known

parameters. A total of 34 solvents with a wide array of Hansen parameters were chosen (Hansen parameters for common solvents can be found in numerous sources, for example reference 39), which are plotted in Figure 4.4a. While it was difficult to quantify dissolution rate of the catalyst in the solvents for a variety of reasons (some extremely rapid dissolution, some extremely slow dissolution, and an overall great deal of scatter in quantitative measurements), it was surprisingly easy and reliable to qualitatively determine dissolution rates. Dissolution rates of the catalyst in the solvents naturally fell into four categories, which we denote herein as rapid, moderate, slow and deficient (Figure 4.4b), which are described in more detail in the experimental section of this paper. Assignment of the solvents into these four categories was straightforward, and very few solvents were at the “borderline” of two categories, but any type of ranking of the solvents within each category is futile due to the amount of scatter during attempts to quantify dissolution. On a side note, several of the solvents used in this study are known to react with Grubbs’ catalyst (e.g. acetonitrile, acrylonitrile, aniline, pyridine, piperidine and pyrrole), and can potentially skew their inherent dissolution kinetics. However, we found that our interpretation of the Hansen Parameter Map both including and excluding the data points accrued from these solvents was essentially identical.

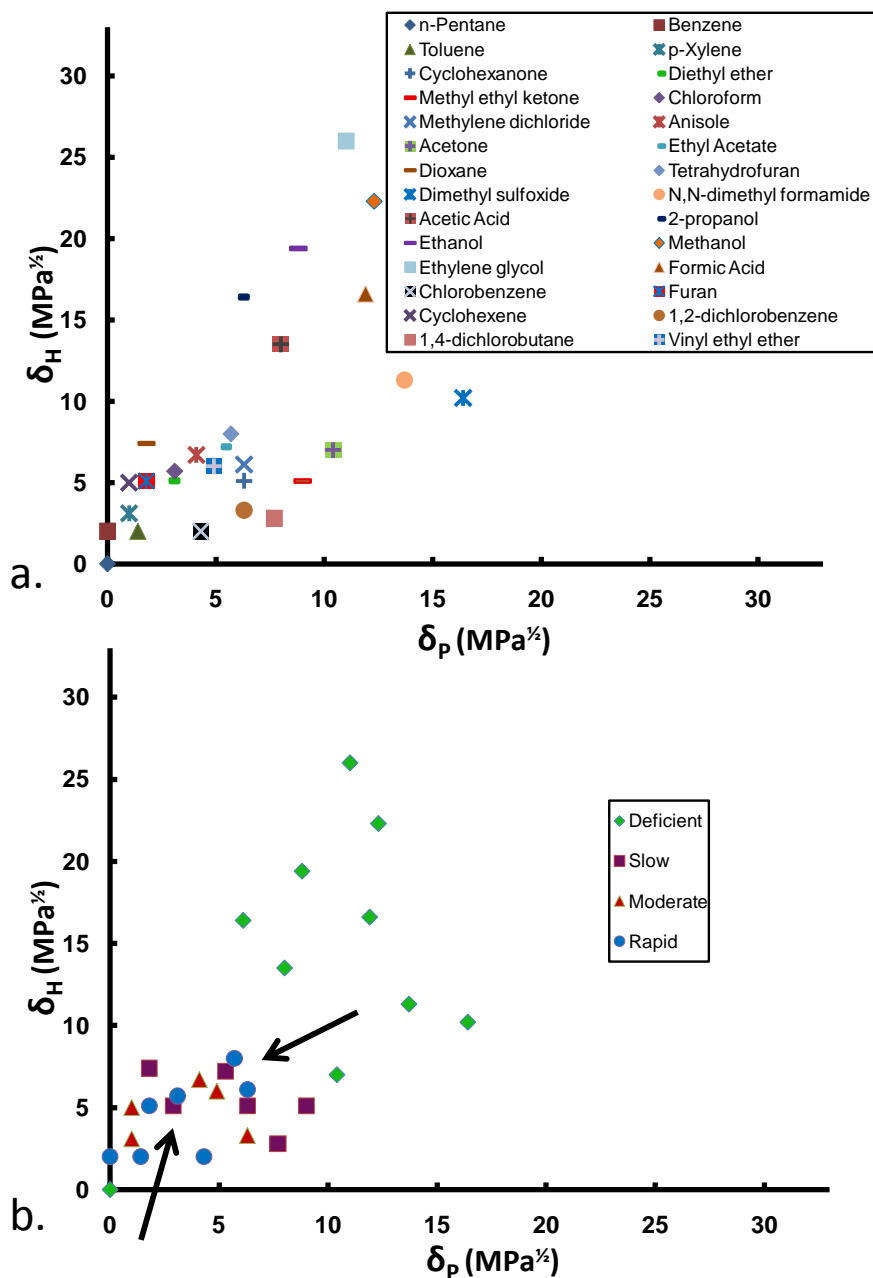


Figure 4.4. a) Solvent parameter map and b) results of dissolution measurements of Grubbs' catalyst in each solvent. The arrows denote regions of superior dissolution.

During dissolution measurements, which are described in more detail in the experimental section of this paper, temperature (room temperature), agitation rate (no agitation), and interfacial area of the catalyst available to the monomer were kept constant, forcing the dissolution rate to be dependant solely on chemical compatibility between the

solvents and the catalyst. However, one potential concern while taking dissolving measurements is that the degree of undersaturation may affect the dissolution rate. But increasing the amount of solvent available to dissolve the catalyst, which would increase the degree of undersaturation, seemed to have minimal effect on the dissolution. At the very least, the different degrees of undersaturation did not create ambiguity as to which of the four qualitative dissolution categories the solvents should be placed.

It is clear from Figure 4.4b that there are localized regions of rapid, moderate, slow and deficient dissolution on the Hansen Parameter Map; the regions of rapid dissolution are marked by arrows. Additionally, the regions of rapid dissolution seem to be roughly circular in shape, and proceeding outside the “rapid” dissolving circle are sequential regions of moderate, slow, and deficient dissolution. This is consistent with what is observed for polymers, which commonly have “spheres” on their Hansen Parameter Maps that correspond to regions of good solubility, swelling, etc. in solvents whose parameters are within the “sphere,” and the center coordinates of the “sphere” correlates to the polymer’s Hansen parameters [39]. While the existence of multiple spheres, as in this work, is very uncommon with polymers, there is some precedent for multiple spheres in a Hansen Parameter Map for other organometallic compounds [41]. Therefore, we confidently assign Grubbs’ catalyst two sets of Hansen parameters, which are roughly calculated to be ($\delta_P = 2.9$, $\delta_H = 3.3$) and ($\delta_P = 7.0$, $\delta_H = 7.1$).

4.4.3 Model Validation

By comparing Figures 4.3 and 4.4b, it is apparent that no healing monomer’s Hansen parameters coincide very well with Grubbs’ catalyst’s parameters, implying that the maximum dissolution kinetics cannot be achieved with a one-component healing monomer. However, Hansen parameters are known to obey a simple rule of mixing; in other words, any miscible blend of liquids takes on the Hansen parameters intermediate between the separate components of the blend [39], as shown in equation 4.5.

$$\delta_{X,blend} = \sum \theta_i \delta_{X,i} \quad (4.5)$$

In this equation, $\delta_{x,blend}$ is the Hansen parameter of the x-type cohesive force (i.e. Dispersion, Dipole or Hydrogen bonding forces) in the blend of liquids, θ_i is the volume fraction of the i -th liquid in the blend, and $\delta_{x,i}$ is the Hansen parameter of the x-type cohesive force for the i -th liquid in the blend. Therefore, to experimentally validate our model, various healing monomers were blended in the appropriate volume fractions that would cause the blend to have Hansen parameters similar to the catalyst's parameters. The two healing monomer blends chosen for this study (one blend to match each of the Grubbs' catalyst's two Hansen parameters) are shown in tables 4.3 and 4.4. It should be noted that the blend represented in table 4.3 (Hansen parameters: ($\delta_P = 2.9$, $\delta_H = 4.6$)) does not exactly match the estimated Hansen parameters of Grubbs' catalyst ($\delta_P = 2.9$, $\delta_H = 3.3$). This is because this set of Grubbs' catalyst parameters falls out of the range of the parameters of our healing monomer library, making it mathematically impossible to find a monomer blend that precisely matches the catalyst's parameters. Hence, a blend was chosen whose overall Hansen parameters are reasonably close to that of the Grubbs' catalyst; possible errors resulting from this modification are discussed below.

An obvious problem with measuring the dissolution rate of Grubbs' catalyst with a ROMP-reactive monomer is the ensuing polymerization reaction affecting dissolution. While the dynamic structural and rheological environment resulting from bulk polymerization is indeed indicative of what is actually occurring during the complex self-healing process, for the purposes of this study where we focus solely on dissolution rates (and need a suitable method to measure dissolution), the polymerization reaction must be temporarily stopped. To achieve this, a modified version of Grubbs' catalyst with extremely low ROMP-reactivity was synthesized (shown in Figure 4.5 along with the structure of the Grubbs' catalyst). While this catalyst is not exactly inactive, the placement of an oxygen atom between the carbene and the phenyl group places the catalyst into a thermodynamic well, which was sufficient to inhibit an appreciable amount of polymerization in the time-scale of our experiments. In fact, for other alkoxy carbene-derivatives of Grubbs' catalyst, this ROMP-inhibition was observed for higher catalyst concentrations, longer times, and higher temperatures than those in this study [42]. Of course, this structural modification should not come at the expense of significantly changing the Hansen parameters of the

catalyst. Thus, dissolution tests of the modified catalyst in solvent similar to those described in the previous section were done, which yielded similar results as the unmodified catalyst. Therefore the modified Grubbs' catalyst shown in Figure 4.5 was used in all dissolution tests of catalyst in healing monomer.

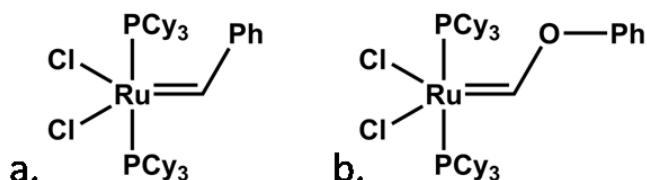


Figure 4.5. a) Grubbs 1st generation catalyst and b) a ROMP-inactive, modified version of Grubbs' catalyst.

Ideally, monomers and monomer blends with parameters closer to the catalyst's parameters would dissolve the catalyst fastest. NMR-based dissolution tests (see experimental section) of the first monomer blend ($\delta_P = 2.9$, $\delta_H = 4.6$; shown in table 4.3) and the individual components of this blend are shown in Figure 4.6. As mentioned earlier, it was not possible to construct a monomer blend with Hansen parameters that equaled the catalyst's first set of parameters, so the blend in table 4.3 was chosen as having parameters close to the catalyst; at the very least, the blend's parameters were closer to the catalyst than any of the components of the blend. As seen in Figure 4.6, the dissolution rate of the catalyst by the blend and by norbornene (R = H) were approximately equal, followed by the acetyl-functionalized norbornenyl derivative (R = COCH₃) and the ester-functionalized derivative (R = COOEt). However, it is important to note that because norbornene is a solid at room temperature, its dissolution experiments had to be carried out at elevated temperatures (~50 °C). Although it is hard to distinguish differences in the dissolution rates of the blend and of norbornene from experimental error, it is definitely reasonable to presume that norbornene's theoretical room temperature dissolution rate would be slower than that of the blend, which is in agreement with our model predictions. Furthermore, the proximity of norbornene's Hansen parameters to the catalyst is not too dissimilar from the proximity of the blend's parameters to the catalyst. So even if the reduction in norbornene's dissolution rate from ~50

°C to room temperature was small enough to still be indistinguishable from that of the blend, our model would still predict dissolution behavior reasonably well. The slower dissolution rates of the acetyl and ester-functionalized norbornenyl groups are also in agreement with predictions—both monomers have Hansen parameters that are, comparably, far from that of the catalyst. In fact, the catalyst's parameters ($\delta_P = 2.9$, $\delta_H = 3.3$) are slightly closer to that of the acetyl-functionalized derivative than the ester-derivative. This predicts that the dissolution rate of the catalyst by the acetyl-derivative would be slightly faster than the ester, which is also in agreement with what is experimentally observed.

Table 4.3. Hansen parameters for three healing monomers and their volume fractions required to make a blend that approximately matches one of the Hansen parameters of the Grubbs' catalyst ($\delta_P = 2.9$, $\delta_H = 3.3$). The “R =” corresponds to the functional group at the 5-position of the norbornenyl-based monomer.

Entry	Volume Fraction			δ_P ($MPa^{1/2}$)	δ_H ($MPa^{1/2}$)
	R = H	R = COOEt	R = COCH ₃		
1 ^a	1	0	0	1.4	3.7
2	0	1	0	3.2	6.5
3	0	0	1	5.7	6.0
4	.62	.06	.32	2.9	4.6

^atest conducted at ~50 °C

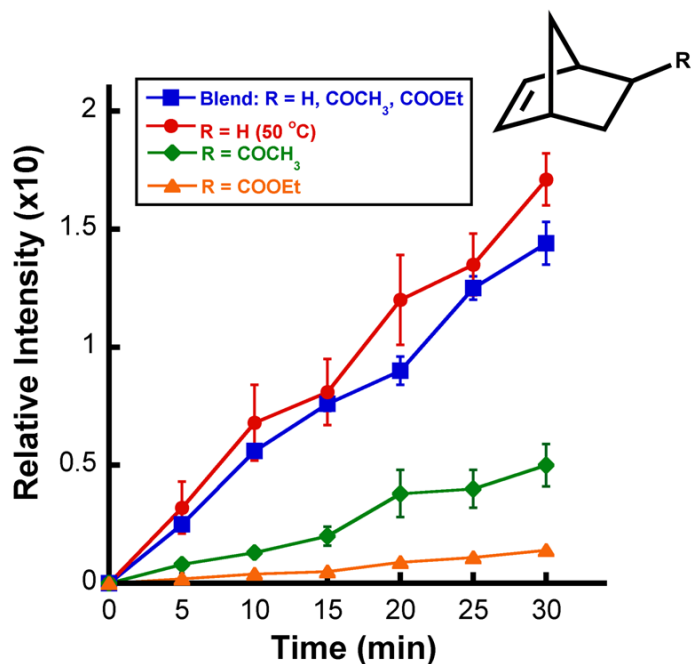


Figure 4.6. Dissolution of a modified Grubbs' catalyst in various monomers and monomer blends. The "R =" group in the legend denotes the functionality at the 5-position of the norbornenyl group. The monomer blend has Hansen parameters of ($\delta_P = 2.9$, $\delta_H = 4.6$), which is similar to that of the catalyst.

A blend whose Hansen parameters matched the second set of Grubbs' catalyst's parameters ($\delta_P = 7.0$, $\delta_H = 7.1$) was constructed from three of the healing monomers, which are shown in table 4.4. Dissolution experiments of the modified Grubbs' catalyst with this blend and the individual components of the blend were conducted, and this data is shown in Figure 4.7. The acid-functionalized norbornenyl-derivative ($R = \text{COOH}$) was obviously the slowest to dissolve the catalyst, which is expected from the large distance of the acid's Hansen parameters from that of the catalyst. The aldehyde-functionalized monomer ($R = \text{CHO}$) was much faster to dissolve the catalyst than the acid, but slower than both the blend and the bromomethyl-functionalized norbornene ($R = \text{CH}_2\text{Br}$). This is also predicted with our Hansen parameter-based model, as the aldehyde-derivative's Hansen parameters are closer to the catalyst's parameters than the acid, but further than both the blend and the bromomethyl-derivative. However, the dissolution rates of the catalyst by the blend and the bromomethyl-norbornene monomer are nearly identical. The Hansen parameters of the

bromomethyl-derivative are closer to the catalyst's parameters than almost all of the other components in the healing monomer library, so a relatively rapid dissolution rate is expected, but the fact that it has a dissolution rate as rapid as the blend (which exactly matches the catalyst's parameters) falls outside of what is expected with our model. There are several possible explanations for this behavior. First, the possibility that the second set of Grubbs' catalyst Hansen parameters ($\delta_P = 7.0$, $\delta_H = 7.1$) is not entirely accurate cannot be ignored. As mentioned earlier, Hansen parameters are a semi-quantitative technique in that the large degree of error in their calculation makes it difficult to predict minor differences in behavior. Perhaps the difference in the proximities of the parameters between the catalyst/blend and the catalyst/bromomethyl-derivative is too small, thereby causing the inaccuracies in parameter calculations to become more evident. But the most likely explanation for the blend's dissolution rate being closer than expected to the bromomethyl-derivative's dissolution rate is viscosity. Dissolution rates are known to be viscosity-dependant [43], with trends of generally slower dissolution with increasing viscosity. It is easily observed that the blend, which contains 27% of the highly viscous acid-functionalized norbornene, is of a higher viscosity than the bromomethyl norbornenyl-derivative. Hence, it is reasonable to assume that the blend's rate of dissolving catalyst is being effectively reduced as a result of its higher viscosity, and the model predictions were not necessarily incorrect. Nonetheless, it should be noted in future utilizations of this model that dissolution rates will probably fall short of Hansen parameter-based predictions when using healing monomers of higher viscosities. While this is indeed a limitation of using the model presented here, most of the healing monomers in the library of figure 4.1 were liquids of relatively low viscosity. In fact, this viscosity effect probably has not manifested itself in the other experiments presented in this paper because all of the other healing monomers tested have similar viscosities, at least by visual inspection. Furthermore, high-viscosity healing monomers and monomer blends are already considered unfavorable for self-healing for a number of reasons, and they would therefore likely be prematurely excluded as a possibility when considering a feasible healing monomer/catalyst combination.

Table 4.4. Hansen parameters for three healing monomers and their volume fractions required to make a blend that matches one of the Hansen parameters of the Grubbs' catalyst ($\delta_P = 7.0$, $\delta_H = 7.1$). The "R =" corresponds to the functional group at the 5-position of the norbornenyl-based monomer.

Entry	Volume Fraction			δ_P ($MPa^{1/2}$)	δ_H ($MPa^{1/2}$)
	R = COOH	R = CHO	R = CH ₂ Br		
1	1	0	0	3.5	10.3
2	0	1	0	10.4	6.9
3	0	0	1	6.2	5.0
4	0.27	0.36	0.37	7.0	7.1

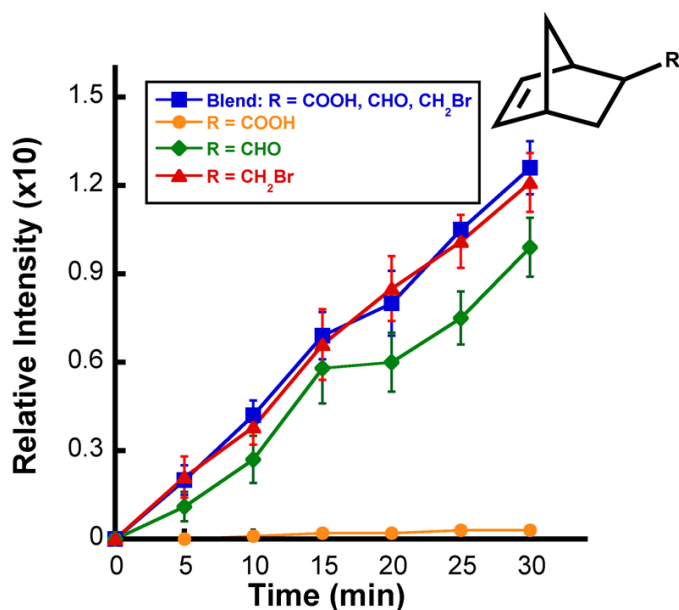


Figure 4.7. Dissolution of a modified Grubbs' catalyst in various monomers and monomer blends. The "R =" group in the legend denotes the functionality at the 5-position of the norbornenyl group. The monomer blend has Hansen parameters of ($\delta_P = 7.0$, $\delta_H = 7.1$), which matches that of the catalyst.

4.5 Conclusions

In this paper, a model was developed using the concept of Hansen parameters in order to make predictions regarding the dissolution of a solid catalyst in liquid monomers for self-healing applications. More specifically, we developed our model in reference to the dissolution of Grubbs' catalyst in a library of ROMP-active monomers, which are often used as a catalyst/healing monomer combination in other self-healing works. Hansen parameters were calculated for a small library of norbornenyl-based monomers, which are generally reactive via the ROMP reaction. The Grubbs' catalyst was found to have two sets of Hansen parameters, and blends of healing monomers created to match these parameters were found to dissolve the catalyst rapidly. However, the model is limited in its ability to predict and compare dissolution rates of liquids with significantly different viscosities. While our model was developed for a ROMP-based self-healing system, we believe this Hansen parameter technique is fundamental and versatile enough to be applied to other types of self-healing chemistries.

4.6 Acknowledgements

This work was supported by The American Chemical Society Petroleum Research Fund (ACS PRF# 47700-AC7). The authors gratefully acknowledge Dr. Xia Sheng, Dr. Wonje Jeong, and Dr. Malika Jeffries-EL for helpful discussions.

4.7 References

- [1] Kessler, M.R. Self-healing: a new paradigm in materials design. *Proc. IMechE Part G-J. Aero.* **2007**, 221(G4), 479-495.
- [2] Wool, R.P. Self-healing materials: a review. *Soft Matter* **2008**, 4, 400-418.
- [3] Bergman, S.D. and Wudl, F. Mendable Polymers. *J. Mater. Chem.* **2008**, 18, 41-62.
- [4] White, S.R., Sottos, N.R., Geubelle, P.H., Moore, J.S., Kessler, M.R., Sriram, S.R., Brown, E.N. and Viswanathan, S. Autonomic healing of polymer composites. *Nature*, **2001**, 409, 794-797.
- [5] Kessler, M. R.; Sottos, N. R. and White, S. R. Self-healing Structural Composite Materials. *Compos. Part A-Appl. Sci.* **2003**, 34, 743-753.
- [6] Toohey, K.S., Sottos, N.R., Lewis, J.A., Moore, J.S. and White, S.R. Self-healing materials with microvascular networks. *Nat. Mater.* **2007**, 6, 581-585.

- [7] Toohey, K.S.; Hansen, C.; Sottos, N.R.; Lewis, J.A. and White, S.R. Delivery of two-part self-healing chemistry via microvascular networks. *Adv. Funct. Mater.* **2009**, *19*, 1399-1405
- [8] Dias, E.L.; Nguyen, S.T.; Grubbs, R.H. Well-defined ruthenium olefin metathesis catalysts: mechanism and activity. *J. Am. Chem. Soc.* **1997**, *119*, 3887-3897.
- [9] Trnka, T.M., Grubbs, R.H. The development of L2X2Ru=CHR olefin metathesis catalysts: an organometallic success story. *Acc Chem. Res.* **2001**, *34*, 18-29.
- [10] Bielawski, C.W.; Grubbs, R.H. Living ring-opening metathesis polymerization. *Prog. Polym. Sci.* **2007**, *32*, 1-29.
- [11] Kirkby, E.; Michaud, V.; Manson, J.A.; Rule, J.D.; Sottos, N.R. and White, S.R. Embedded shape-memory allow wires for improved performance of self-healing polymers. *Adv. Funct. Mater.* **2008**, *18*, 2253-2260
- [12] Sheng, X.; Lee, J.K. and Kessler, M.R. The influence of cross-link density on the properties of ROMP thermosets. *Polymer* **2009**, *50*, 1264-1269.
- [13] Wilson, G.O.; Moore, J.S.; White, S.R.; Sottos, N.R. and Andersson, H.M. *Adv. Funct. Mater.* **2008**, *18*, 44-52.
- [14] Kessler, M.R. and White, S.R. Cure kinetics of ring-opening metathesis polymerization of dicyclopentadiene. *J. Polym. Sci., Part A: Polym. Chem.* **2002**, *40*, 2373-2383.
- [15] Larin, G.E.; Kessler, M.R., Bernklau, N. and DiCesare Rheokinetics of ring-opening metathesis polymerization of norbornene based monomers intended for self-healing applications. *J.C. Polym. Eng. Sci.* **2006**, *46*, 1804-1811.
- [16] Mauldin, T.C. and Kessler, M.R. Latent catalytic systems for ring-opening metathesis-based thermosets. *J. Therm. Anal. Calorim.* **2009**, *96*, 705-713.
- [17] Kessler, M.R. and White, S.R. Self-activated healing of delamination damage in woven composites. *Compos. Part A-Appl. Sci.* **2001**, *32*, 683-699.
- [18] Cho, S.H., Andersson, H.M., White, S.R., Sottos, N.R. and Braun, P.V. Polydimethylsiloxane-based self-healing materials. *Adv. Mater.*, **2006**, *18*(8), 997-1000.
- [19] Yuan, Y.C., Rong, M.Z., Zhang, M.Q., Chen, J., Yang, G.C. and Li, X.M. Self-healing polymeric materials using epoxy/mercaptan as the healant. *Macromolecules*, **2008**, *41*(14), 5197-5202.
- [20] Caruso, M.M.; Blaiszik, B.J.; White, S.R.; Sottos, N.R. and Moore, J.S. Full recovery of fracture toughness using a nontoxic solvent-based self-healing system. *Adv. Funct. Mater.* **2008**, *18*, 1898-1904.
- [21] Sheng, X.; Mauldin, T.C. and Kessler, M.R. manuscript in preparation.
- [22] Rule, J.D.; Brown, E.N.; Sottos, N.R.; White, S.R. and Moore, J.S. Wax-protected catalyst microspheres for efficient self-healing materials. *Adv. Mater.* **2005**, *17*, 205-208.
- [23] Liu, X.; Lee, J.K.; Yoon, S.H. and Kessler, M.R. Characterization of diene monomers as healing agents for autonomic damage repair. *J. Appl. Polym. Sci.* **2006**, *101*, 1266-1272.
- [24] Lee, J.K.; Liu, X.; Yoon, S.H. and Kessler, M.R. Thermal analysis of ring-opening metathesis polymerized healing agents. *J. Polym. Sci., Part B: Polym. Phys.* **2007**, *45*, 1771-1780.
- [25] Liu, X.; Sheng, X.; Lee, J.K.; Kessler, M.R. and Kim, J.S. Rheokinetic evaluation of self-healing agents polymerized by Grubbs' catalyst embedded in various thermosetting resins. *Compos. Sci. Technol.* **2009**, *69*, 2102-2107.

- [26] Liu, X.; Sheng, X.; Kessler, M.R. and Lee, J.K. Isothermal cure characterization of ROMP healing agents for autonomic damage repair: the glass transition temperature and conversion. *J. Therm. Anal. Calorim.* **2007**, *89*, 453-457.
- [27] Liu, X.; Sheng, X.; Lee, J.K. and Kessler, M.R. Synthesis and characterization of melamine-urea-formaldehyde microcapsules containing ENB-based self-healing agents. *Macromol. Mater. Eng.* **2009**, *294*, 389-395.
- [28] Jones, A.S.; Rule, J.D.; Moore, J.S., White, S.R. and Sottos, N.R. Catalyst morphology and dissolution kinetics of self-healing polymers. *Chem. Mater.* **2006**, *18*, 1312-1317.
- [29] Mauldin, T.C.; Rule, J.D.; Sottos, N.R.; White, S.R. and Moore, J.S. Self-healing kinetics and the stereoisomers of dicyclopentadiene. *J. R. Soc. Interface* **2007**, *4*, 389-393.
- [30] Hildebrand, J. and Scott, R.L. *The Solubility of Nonelectrolytes*, 3rd Ed., Reinhold, New York, 1950.
- [31] Bonnesen, P.V.; Puckett, C.L.; Honeychuck, R.V. and Hersh, W.H. Catalysis of diels-alder reactions by low oxidation state transition-metal lewis acids: fact and fiction. *J. Am. Chem. Soc.* **1989**, *111*, 6070-6081.
- [32] Freeman, P.K.; Rao, V.N. Mallikarjuna.; George, D.E. and Fenwick, G.L. The reactions of exo- and endo-5-chloromethylnorbornene with sodium. *J. Org. Chem.* **1967**, *32*, 3958-3963.
- [33] Dolman, S.J.; Hultsch, K.C.; Pezet, F.; Teng, X.; Hoveyda, A.H. and Schrock, R.R. Supported chiral Mo-based complexes as efficient catalysts for enantioselective olefin metathesis. *J. Am. Chem. Soc.* **2004**, *126*, 10945-10953.
- [34] Ponticello, I.S. The preparation of α -substituted acrylic esters. *J. Polym. Sci., Polym. Chem. Ed.* **1979**, *17*, 3509-3518.
- [35] Oh, S.; Lee, J.-K.; Theato, P. and Char, K. Nanoporous thin films based on polylactide-grafted norbornene copolymers. *Chem. Mater.* **2008**, *20*, 6974-6984.
- [36] Beslin, P.; Lagain, D.; Vialle, J. and Minot, C. Preparation of α -unsaturated acyclic thioketones – regioselective dimerization of 4H-1,3-dithiin. *Tetrahedron Lett.* **1981**, *37*, 3839-3845.
- [37] Lauer, W.M. and Spielman, M.A. Synthesis of α,β -unsaturated ethers. *J. Am. Chem. Soc.* **1931**, *53*, 1533-1536.
- [38] a) Hansen, C.M. The three dimensional solubility parameter – key to paint component affinities I. Solvents, plasticizers, polymers, and resins. *J. Paint Technol.* **1967**, *39*, 104-117. b) Hansen, C.M. The three dimensional solubility parameter – key to paint component affinities II. Dyes, emulsifiers, mutual solubility and compatability, and pigments. *J. Paint Technol.* **1967**, *39*, 505-510. c) Hansen, C.M. and Skaarup, K. The three dimensional solubility parameter – key to paint component affinities III. Independent calculation of the parameter components. *J. Paint Technol.* **1967**, *39*, 11-514.
- [39] Hansen, C.M. *Hansen Solubility Parameters: A User's Handbook*, 2nd ed.; CRC Press: Boca Raton, FL, 2007.
- [40] Barton, A.F.M. Applications of solubility parameters and other cohesion parameters in polymer science and technology *Pure Appl. Chem.* **1985**, *57*, 905-912.
- [41] Personal communication between Alan Beerbower and Charles Hansen, which revealed two distinct solubility spheres for lithium stearate (further details in Reference 39).

[42] Louie, J. and Grubbs, R.H. Metathesis of electron-rich olefins: structure and reactivity of electron-rich carbene complexes. *Organometallics* **2002**, *21*, 2153-2164.

[43] Banakar, U.V. *Pharmaceutical Dissolution Testing*, Vol. 49; Marcel Dekker, Inc.: New York, 1992.

CHAPTER 5: A MODIFIED RHEOKINETIC TECHNIQUE DESIGNED TO ENHANCE THE UNDERSTANDING OF MICROCAPSULE-BASED SELF-HEALING POLYMERS

Timothy C. Mauldin,¹ Joshua Leonard,² Kelly Earl,² Jong Keun Lee,³ and Michael R. Kessler²

5.1 Abstract

A modified rheokinetic technique was developed to monitor the polymerization of healing monomers in a microcapsule-based self-healing mimic environment. Using this modified technique, monomers active towards ring-opening metathesis polymerization (ROMP) were either identified or disregarded as candidates for incorporation in self-healing polymers. The effect of initiator loading on the quality and speed of healing was also studied. It was observed that self-healing polymers have upper and lower temperature limits between which the healing mechanism performs at optimal levels. Also, a study of the quality of healing cracks of different thicknesses was performed, and it was discovered that above a critical crack thickness value, the quality of self-healing diminishes substantially; reasons for this phenomenon are discussed in detail.

5.2 Introduction

In recent years, the development and refinement of self-healing polymers has garnered significant interest in both academic and industrial communities. Perhaps most indicative of the immense interest in this still relatively young field of research is the large number of review articles that have appeared in the literature, most within the last half-decade [1-18]. Several fundamentally different healing mechanisms have been developed,

¹ Department of Chemistry, Iowa State University, Ames, IA 50011, USA

² Department of Materials Science and Engineering, Iowa State University, Ames, IA 50011, USA.

³ Department of Polymer Science and Engineering, Kumoh National Institute of Technology, Gumi, Gyungbuk 731-701, Republic of Korea.

all of which have their own commercial niche, but self-healing polymers containing microencapsulated healing components [19-23] have received a significant amount of the attention. In this healing mechanism, microcapsules containing liquid ring-opening metathesis-based monomer are embedded within a polymer matrix, along with ruthenium olefin metathesis catalyst particles. When damage occurs, cracks propagate through the polymer matrix, rupturing the embedded microcapsules. The previously encapsulated liquid monomer is then able to flow into the damage region and contact the catalyst particles, polymerize, and adhere the crack surfaces together.

While this mechanism of healing may initially seem straightforward, significant optimization of the healing components is required before these materials can be considered for commercial use. For example, the microcapsules and catalyst must be compatible with standard polymer processing techniques (e.g. the high pressures of some melt-processing techniques, high-temperature curing cycles, etc.). The physical properties of the liquid healing monomer must allow for easy flow into the damage region (i.e. low viscosity), for minimal loss due to volatilization or diffusion into the polymer matrix, and for good wetting of the crack surface. Dissolution of catalyst in liquid monomer, as well as the subsequent polymerization kinetics, must also be tailored accordingly. And finally, the resulting polymer must have sufficient adhesive and mechanical properties to mitigate further damage. With this daunting set of requirements in mind, much of our previous work has focused on evaluation of healing monomers through thermal analysis and mechanical testing [24-31]. These techniques are designed to be versatile, relatively quick and easy to use, and they often yield the copious amounts of quantitative data necessary to adequately design and screen different healing components. However, due to several complexities of the self-healing mechanism, these ex-situ analytical techniques are only a complement to, and not a substitute for, the evaluation of healing formulations through actual fabrication and testing of self-healing materials. Direct evaluation of self-healing materials is most often done by fabricating fracture specimens containing the embedded healing components. Upon initially failing the specimens under mechanical load, the fracture halves are brought into contact and allowed to heal, after which point the resulting healed specimens can be subsequently retested. Tapered double-cantilever beam geometry fracture specimens were first used for

this purpose [32-34] as this geometry yields some fracture properties that are independent of crack length, which otherwise may vary from a pristine sample to its healed sample [35]. While these techniques are probably more laborious and wasteful of materials than the ex-situ analyses mentioned above, they are crucial in that they provide an actual demonstration of healing, as well as providing some quantitative description of that healing by virtue of comparison of mechanical properties of virgin vs. healed specimens.

The goal of this work is to develop an analytical technique that collapses the dichotomy between the ex-situ and direct evaluation methods of self-healing polymers. In other words, we have developed a novel technique that simulates the self-healing mechanism, but is nonetheless quick, easy to perform, requires very little material, and yields large amounts of quantitative data. To do this, we modified a traditional parallel plate rheological technique in such a way that mimics a self-healing polymer, as shown in Figure 5.1. The center image represents a bottom rheometer parallel plate, on top of which a material can be layered. Then by adding a top rheometer plate and applying a shear force, rheological properties of the material under various stimuli (e.g. time, temperature, shear rate, etc.) can be measured. For example, the left arrow in Figure 5.1 shows a traditional rheokinetic setup in which the developing rheological properties of a polymerizing monomer/catalyst solution can be determined. In our modified rheokinetic technique, however, we use the rheometer bottom plate as a scaffold to build a pseudo self-healing polymer. This is done by first coating the bottom plate with a catalyst-embedded polymer, and then polishing the surface of the modified plate to reveal catalyst particles. Then upon injecting liquid monomer on the surface of the modified plate, catalyst dissolution and polymerization must occur concurrently in a confined environment (Figure 5.1, right arrow), roughly in the same manner as occurs during the self-healing mechanism. Preliminary efforts have already been successful in using this technique to rapidly screen different healing monomers, catalysts and polymer matrices suitable for self-healing materials [36, 37]. Here, we expand this modified rheokinetic further to identify its limitations as well as probe the effect of self-healing material design parameters (e.g. monomer identity, catalyst identity, amount of healing components used, etc.) on the self-healing mechanism. Also, successful implementation of this technique has led to the discovery of unexpected and, to the best of our knowledge,

previously unknown limitations to self-healing related to an extreme sensitivity both to temperature and to the thickness of the damage region that requires healing.

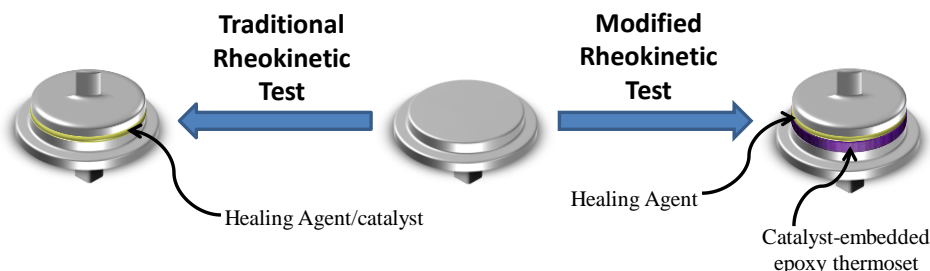


Figure 5.1. Schematic representation of a traditional rheokinetic experiment (left arrow) and our modified rheokinetic experiments with a polymer-coated bottom plate (right arrow)

5.3 Experimental

5.3.1 General Considerations

Dicyclopentadiene (DCPD), benzylidene-bis(tricyclohexylphosphine) dichlororuthenium (1st generation Grubbs' Catalyst), and 5-ethylidene-2-norbornene (ENB) were all purchased from Aldrich and use as received. EPON 828 Epoxy Resin, and EPIKURE 3223 Curing Agent (diethylenetriamine) were bought from Miller-Stephenson and also used as received. Literature methods were used to prepare 5-chloromethyl-2-norbornene [38], 5-bromomethyl-2-norbornene [39], and ethyl 5-norbornene-2-carboxylate [40]. Rheology was performed using an AR2000ex stress-controlled rheometer (TA Instruments) with parallel plate geometry. Aluminum parallel plates with a 25 mm diameter were purchased from TA Instruments. Bottom parallel plates with a drip channel were used.

5.3.2 Rheometer bottom plate modification

EPON 828 epoxy resin was vigorously hand-stirred with 14 pph diethylenetriamine and degassed at ambient temperature under high vacuum for 15 minutes. In most cases, 1st Generation Grubbs' Catalyst was gently hand-stirred into the solution until the catalyst particles were well dispersed, by visual inspection. Unless otherwise noted, 2.5 wt/wt% catalyst particles were added to the epoxy resin. The suspension was poured into custom-designed, open silicone rubber molds with center-bored cylinders and one vent hole, and

rheometer bottom parallel plates were inverted and fixed into the cylinder so that the drip channel rested snug on the top of the mold (see supplementary information for custom-designed mold schematics). Molds were placed in a 65 °C preheated oven for 1 hour, after which time the epoxy resin was sufficiently cured, resulting in an epoxy-based disc coating on the rheometer plate surface with precise dimensions of 25 mm diameter and 2 mm thickness. Catalyst was revealed on the surface of the plates by hand-polishing the coating, immediately before each experiment, first with 600 grit sandpaper and second with 2000 grit sandpaper. Catalyst particles showed excellent dispersion in the final samples (shown in the supplementary information).

5.3.3 Rheology procedure

Rheological experiments were conducted as follows, unless otherwise noted in the text. Top and bottom rheometer plates were fixed to the instrument, and 0.25 ml of 5 vol/vol% ENB in DCPD mixture was injected on the bottom plate with a 1-ml syringe. The 5% ENB was used as a reactive diluent to lower DCPD's melting point to 8-9 °C, and will be referred to simply as DCPD. In some cases, a premixed catalyst and monomer solution was added to unmodified bottom plates. In either case, the time from which the monomer first contacted the catalyst particles until data collection had begun was recorded with a stop watch, and that time was artificially added to the start of each test (e.g. if the monomer was in contact with the catalyst for 10 seconds prior to the start of data collection, then the data point at which $t=0$ sec was shifted to $t=10$ sec, and all other data points were shifted accordingly). Oscillatory shear experiments were used to monitor changes in shear dynamic mechanical properties (G' = shear storage modulus, G'' = shear loss modulus, and $\tan \delta$). Initially, experiments were run in a strain-controlled setting at a strain of 5% and frequency of 1 Hz. A strain of 5% was chosen as an optimal value that provides enough torque to collect data on low-viscosity liquids with an acceptable level of noise, but also a small enough shear rate so as not to artificially aid catalyst dissolution in monomer. Once the modulus of the material developed to require a shear stress of 1000 Pa to attain the 5% strain, the experiment was programmed to switch to a stress-controlled setting with a constant shear stress of 1000 Pa and a frequency of 1 Hz. This change in testing mode was done to

accommodate for the high sample moduli reached at the end of each experiment, which in a strain-controlled setting would otherwise require shear stresses outside of instrument limits to attain a shear strain of 5%. Also unless noted otherwise, all tests were performed at 23 °C. Gelation time is loosely defined as the time at which the G' and G'' curves crossover, and vitrification time is defined as the time after the gelation time at which $\tan \delta$ is at a maximum. Figure 5.2 graphically depicts how each of these variables are chosen in a representative rheokinetic plot. All reported values of gelation time, vitrification time, and G'_{final} are an average of three experiments.

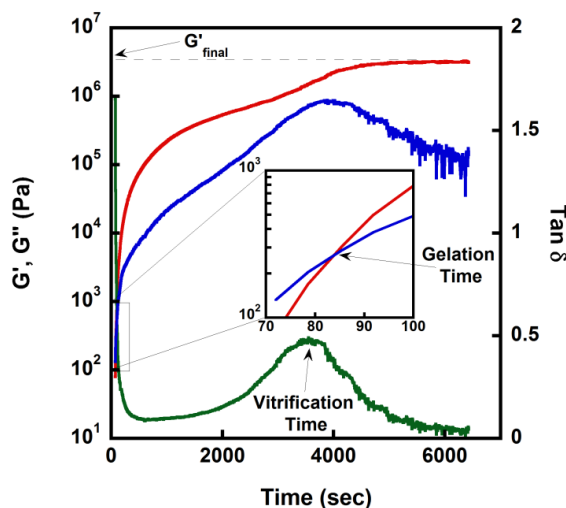


Figure 5.2. A representative rheokinetic plot showing the evolution of G' (red), G'' (blue), and $\tan \delta$ (green). Gelation time was taken as the crossover between the G' and G'' plots, Vitrification time was defined at the maximum of the $\tan \delta$ curve, and G'_{final} is modulus at which G' reaches a steady-state.

5.4 Results and Discussion

Microcapsule-based self-healing polymers have utilized a number of different healing chemistries, such as epoxide ring opening [41-48], “click” chemistry [49, 50], siloxane polycondensation [51, 52], radical polymerization [53-55], and ring-opening metathesis polymerization (ROMP) [56-65]. Ring-opening metathesis polymerization of dicyclopentadiene (DCPD) with Grubbs’ olefin metathesis catalyst [66-68] is notable as one of the first polymerization mechanisms demonstrated to work well in self-healing polymers

[69]. For this reason, ROMP with the 1st generation Grubbs' catalyst was chosen as a healing chemistry for this work, but we envision that the rheokinetic technique presented herein is versatile enough to be applied to any other type of healing chemistry desired.

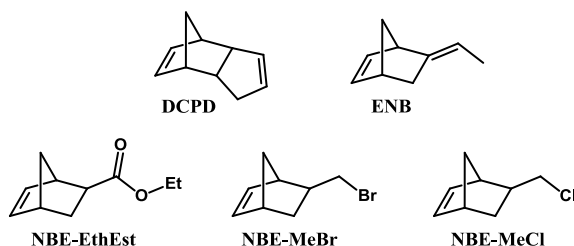


Figure 5.3. Chemical structures and abbreviations of several ROMP-active monomers.

The original motivation for developing this modified rheokinetic technique was to rapidly screen different healing monomers in order to identify ideal candidates with a good balance of catalyst dissolution kinetics and polymerization kinetics. To this end, evolution of dynamic mechanical properties in the modified rheokinetic technique was monitored for several ROMP-active monomers, the chemical structures of which are shown in Figure 5.3. Specifically, Figure 5.4 shows the evolution of G' with respect to time during the polymerization reaction of each of these monomers. Monomers ENB, NBE-MeBr, and NBE-MeCl show superior rheokinetics, with gelation times of 170 ± 10 , 181 ± 15 , and 281 ± 18 seconds, respectively. All three of these monomers gel considerably faster than DCPD (gelation time of 682 ± 45 seconds), which is notable since DCPD is often considered as a “benchmark” healing monomer for its superior healing precedent in previous work [69]. ENB seems particularly attractive as a healing monomer candidate, as it attains its maximum G' value in roughly 30 minutes, nearly an order of magnitude faster than all other monomers studied here. NBE-EthEst showed the slowest rheokinetics of the five monomers studied, with any measurable growth of storage modulus occurring only after approximately 90 minutes and no gelation (i.e. no G' , G'' crossover) over the course of this experiment. While this data implies that NBE-EthEst would likely not be a successful healing monomer, this demonstrates that our modified rheokinetic technique is not only useful to select promising healing monomer candidates, but also useful to quickly discard less favorably candidates.

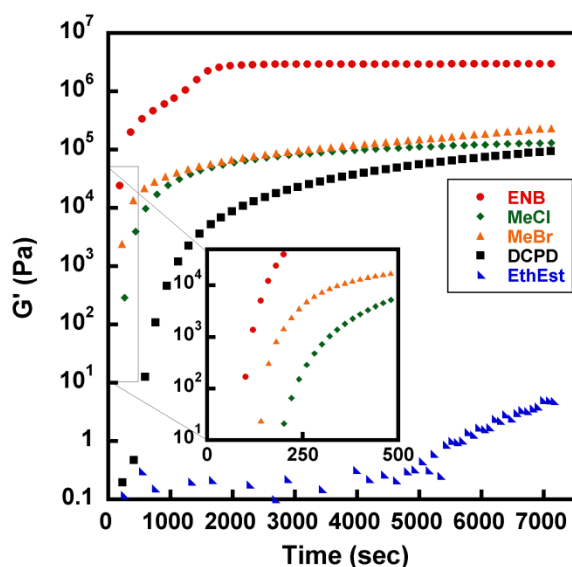


Figure 5.4. Evolution of shear storage modulus (G') of several ROMP-active healing monomer candidates.

One important consideration in developing microcapsule-based self-healing materials is the amount of healing additives that should be added to the overall polymer matrix. On one hand, lower loadings of healing additives are preferred in order to reduce overall material cost and inhibit reduction in the virgin polymer's properties. But loadings should not be so low that the quality and speed of healing is negatively affected. While traditional techniques to determine optimal loadings of healing additives in self-healing polymers would likely include the sometimes long and tedious tasks of fabricating and testing fracture specimens with various combinations and loadings of healing components, the present modified rheokinetic technique is ideally suited to quickly and efficiently answer these types of questions. For example, Figure 5.5 shows the effect of catalyst particle loading in the modified rheometer plate setup on the evolution DCPD's of storage modulus. As expected, increasing loadings of the catalyst clearly accelerates the polymerization reaction, and higher loadings of catalyst yield polymer with a higher overall G' at any given time.

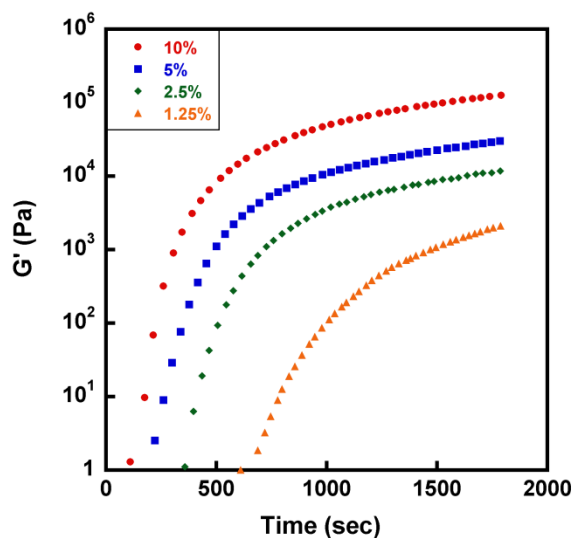


Figure 5.5. Evolution of G' during polymerization of DCPD with different loadings of Grubbs' catalyst in the modified rheometer plate coating. Percentage loadings of catalyst are wt/wt% with respect to the epoxy coating.

Given that self-healing polymers could be envisioned for outdoor applications, in which temperatures significantly fluctuate based on the time of day, season, and global location, it is of interest to have a detailed understanding of how the quality and kinetics of self-healing changes with temperature. Figure 5.6 shows the change in G' of DCPD at a range of different isothermal temperatures, chosen to mimic what may be experienced in outdoor environments. At 0 °C, there is no observable growth of G' throughout the course of this experiment. This is likely because 0 °C is below the melting temperature of DCPD (8-9 °C), and thus DCPD is a solid at this temperature. Presumably, solid DCPD does not have the ability to dissolve catalyst from the modified rheometer plate, and therefore no reaction is expected to take place. Upon increasing the temperature above DCPD's melting temperature to 13 °C, growth in G' is observed, although with a relatively long gelation time of 1027 ± 48 seconds. Increasing temperature to 28 °C further accelerates the polymerization to have a gelation time of 364 ± 41 seconds. However, increasing the temperature to 40 °C initially appears to slow the polymerization, contrary to what may be expected at elevated temperatures. Visual observation of the bottom rheometer plate after immediate removal from the instrument revealed a layer of polymer film directly covering the modified bottom

plate, on top of which was a layer of liquid monomer DCPD (Figure 5.7). It is believed that the rheological inference that the kinetics decreases at higher temperatures is not correct, and instead that the polymerization reaction is in fact so rapid that it quickly gels around catalyst particles, preventing both further dissolution of catalyst and slowing diffusion of catalyst into the upper layer of liquid. The fact that samples at elevated temperatures exhibits obvious property gradients through the sample thickness complicates any rheological interpretation of this data, but these results demonstrate that the self-healing mechanism has a heightened sensitivity to moderately high healing temperatures.

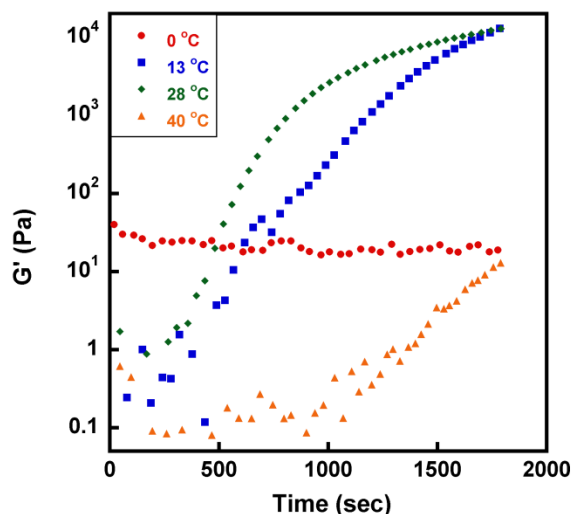


Figure 5.6. Evolution of G' during the polymerization of DCPD on modified rheometer plates at different isothermal temperatures.

By visual inspection, Figure 5.7 shows that the stiffest layers of polymer exists in close proximity to the bottom rheometer plate, which serves as a catalyst source, and stiffness decreases further from the modified plate surface. Presumably, the reason for the direction of the property gradient is that catalyst dissolved from the modified rheometer plate begins in the bottom layers of the monomer and must diffuse towards the top layers of monomer. This led to the question of whether healing would be significantly affected based on the thickness of the liquid monomer sample, in which it was postulated that thicker samples may require more time to diffuse catalyst through to the top layers of monomer. With respect to self-

healing polymers, this question has implications towards the capability of healing cracks of different thickness. To test these hypotheses, rheological experiments were performed with varying the gap sizes (i.e. the distance from the top rheometer plate surface to the modified bottom plate surface), which required varying amounts of monomer to fill the different sized gaps. Gap size was varied by adjusting the volume of monomer delivered to the gap region. Delivering 0.1, 0.3, and 0.5 ml of DCPD to the gap region yielded average starting gap sizes (i.e. gap sizes immediately after monomer injection, prior to any gap shrinkage upon polymerization) of 180 ± 9 , 534 ± 41 , 839 ± 58 μm , respectively. Figure 5.8 shows how gelation time, vitrification time, and G'_{final} change with changing gap size. Also, as a control test, Figure 5.8 shows the dependence of these three variables on gap size in unmodified rheology experiments, in which catalyst and monomer was premixed (2mg/ml catalyst/monomer) and injected on an unmodified bottom rheometer plate.

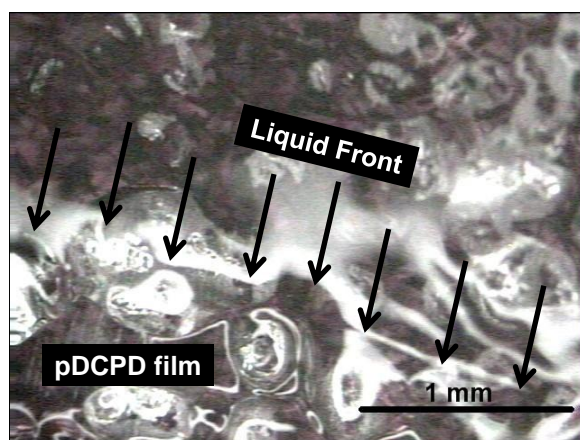


Figure 5.7. Optical microscope image of a rheometer bottom plate showing a layer of liquid DCPD above a layer of polymerized DCPD. Image was taken immediately after a 30 minute rheokinetic test at an isothermal temperature of 40 °C.

The values measured in the modified and unmodified rheokinetic tests cannot be directly compared, since the amount of catalyst dissolved in monomer during the modified rheokinetic tests is unknown, but interpretations can be made based on the sensitivity of rheological property development to gap size. Seen in Figures 5.8a and 5.8b, gelation time and vitrification time change considerably with different gap sizes when using the modified

rheometer plates. Considering that, when using unmodified plates, these times show almost no dependence on gap size, it is very likely that this effect is related to through-thickness property gradients resulting from slow diffusion of catalyst from the modified plate through to the upper layers of monomer. This was visually confirmed by removing the parallel plates from the instrument after gelation, but prior to vitrification; the DCPD samples on the modified bottom parallel plates were very tacky on the surface, but the subsurface layers just above the modified plate surface were solid polymer. However, it is seen in Figure 5.8c that final shear storage modulus, G'_{final} , seems to be mostly insensitive to gap size with both the modified and unmodified parallel plates. This implies that sufficient amount of catalyst will eventually permeate throughout the entire sample thickness, which is reasonable considering the fact that diffusion is a kinetic event only and is not expected to affect the thermodynamically-dominated steady state storage modulus.

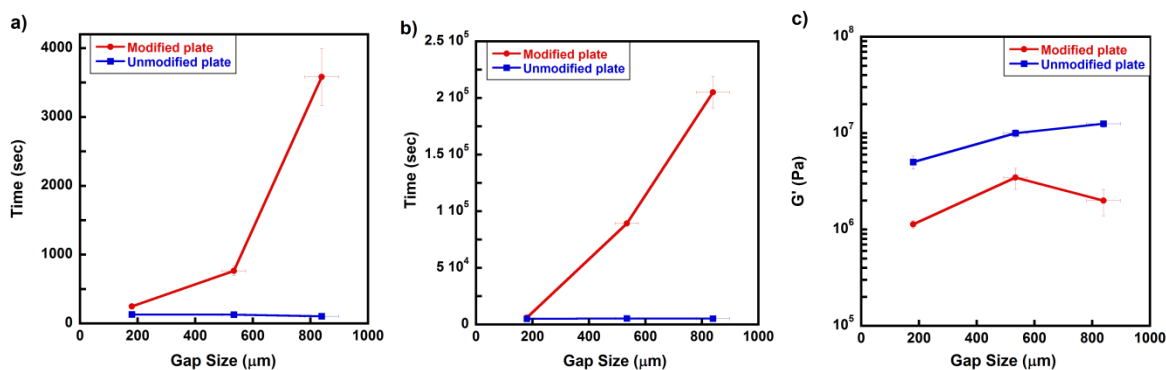


Figure 5.8. Dependence of (a) gel time, (b) vitrification time, and (c) G'_{final} on gap size during modified and unmodified rheological experiments.

What is most surprising here is how extremely sensitive gelation and vitrification is to gap size, especially at gap sizes $>200 \mu\text{m}$, in which the time increase seems to be exponential with gap size. It does appear that at gap sizes $<200 \mu\text{m}$, however, there is minimal deviation between data obtained from modified and unmodified plates. One plausible explanation for this is that catalyst can diffuse relatively quickly through the liquid monomer until a significant increase in monomer viscosity occurs due to onset of polymerization, at which time catalyst diffusion is retarded. When interpreting this data with respect the self-healing

mechanism, it must be taken into consideration that only the bottom rheometer parallel plate (i.e. not the top parallel plate) is coated with a catalyst/epoxy layer, while in a self-healing polymer presumably both crack surfaces would contain embedded catalyst particles that can contribute to the chemical reaction. Therefore, the behavior observed in the rheometer gap is assumed to be roughly equivalent to that which would occur in half of the crack thickness in a self-healing polymer. If this assumption is correct, then it would appear that crack thicknesses $<400 \mu\text{m}$ would be mostly unaffected by this catalyst diffusion phenomenon, while the healing kinetics of cracks with thicknesses $>400 \mu\text{m}$ could be significantly affected by crack size. While a crack thickness value of $\sim 400 \mu\text{m}$ can hardly be considered a universal critical value, (surely, this value would change with different monomers, catalysts, temperatures, etc.), it is important because it is on the approximate size scale expected for larger delamination thicknesses in fiber-reinforced composite materials and moderate-sized macrocracks. Rule and coworkers also noted the benefits of healing smaller crack sizes [70], but their conclusions were based on issues related to ensuring a sufficient supply of healing monomer to damage volumes; to the best of our knowledge, this work is the first observation of catalyst diffusion-based property gradients in healing monomers resulting from larger crack thicknesses.

5.5 Conclusions

Rheometer bottom parallel plates were modified with a catalyst-embedded epoxy coating in order to mimic a crack surface of a fractured microcapsule-based self-healing polymer. Using these modified rheometer plates, rheokinetic analyses were performed on healing monomers in a pseudo self-healing environment. It was demonstrated that this technique could be used to quickly and efficiently develop a tailored self-healing polymer by rapidly screening the effect of various design parameters (e.g. monomer and catalyst identity, catalyst loading, etc.) on the quality and speed of healing. Additionally, the simplicity and versatility of this technique, coupled with its substantial quantitative outputs, enabled two previously unknown limitations to the self-healing mechanism—upper/lower temperature limits and large crack thicknesses—to be identified and studied.

5.6 Acknowledgements

This work was supported by The American Chemical Society Petroleum Research Fund (ACS PRF# 47700-AC7). The authors gratefully acknowledge Dr. Xing Liu and Dr. Xia Sheng for rheometer assistance and helpful discussions.

5.7 References

- [1] K.A. Williams, D.R. Dreyer and C.W. Bielawski, *MRS Bull.*, 2008, **33**, 759-765.
- [2] R.S. Trask, H.R. Williams and I.P. Bond, *Bioinsp. Biomim.*, 2007, **2**, 1-9.
- [3] T.C. Mauldin and M.R. Kessler, *Int. Mater. Rev.*, 2010, **55**, 317-346.
- [4] D.Y. Wu, S. Meure and D. Solomon, *Prog. Polym. Sci.*, 2008, **33**, 479-522.
- [5] S. van der Zwaag, N.H. van Dijk, H.M. Jonkers, S.D. Mookhoek and W.G. Sloof, *Phil. Trans. R. Soc. A*, 2009, **367**, 1689-1704.
- [6] M.R. Kessler, *Proc. Inst. Mech. Eng. G – J. Aer. Eng.*, 2007, **221**, 479-495.
- [7] E. B. Murphy and F. Wudl, *Prog. Polym. Sci.*, 2010, **35**, 223-251.
- [8] Y.C. Yuan, T. Yin, M.Z. Rong and M.Q. Zhang, *Express Polym. Lett.*, 2008, **2**, 238-250.
- [9] S.R. White, M.M. Caruso and J.S. Moore, *MRS Bull.*, 2008, **33**, 766-769.
- [10] R.P. Wool, *Soft Matter*, 2008, **4**, 400-418.
- [11] A.B.W. Brochu, S.L. Craig and W.M. Reichert, *J. Biomed. Mater. Res. Part A*, 2011, **96A**, 492-506.
- [12] H.P. Wang, M.Z. Rong and M.Q. Zhang, *Prog. Chem.*, 2010, **22**, 2397-2407.
- [13] J.A. Syrett, C.R. Becer and D.M. Haddleton, *Polym. Chem.*, 2010, **1**, 978-987.
- [14] M. Samadzadeh, S.H. Boura, M. Peikari, S.M. Kasiriha and A. Ashrafi, *Prog. Org. Coat.*, 2010, **68**, 159-164.
- [15] B.J. Blaiszik, S.L.B. Kramer, S.C. Olugebefola, J.S. Moore, N.R. Sottos and S.R. White, *Annu. Rev. Mater. Res.*, 2010, **40**, 179-211.
- [16] S.D. Bergman and F. Wudl, *J. Mater. Chem.*, 2008, **18**, 41-62.
- [17] M.W. Urban, *Prog. Polym. Sci.*, 2009, **34**, 679-687.
- [18] S. Burattini, B.W. Greenland, D. Chappell, H.M. Colquhoun and W. Hayes, *Chem. Soc. Rev.*, 2010, **39**, 1973-1985.
- [19] E.N. Brown, M.R. Kessler, N.R. Sottos and S.R. White, *J. Microencapsulation*, 2003, **20**, 719-730.
- [20] X. Liu, X. Sheng, J.K. Lee and M.R. Kessler, *Macromol. Mater. Eng.*, 2009, **294**, 389-395.
- [21] E.N. Brown, S.R. White and N.R. Sottos, *J. Mater. Sci.*, 2004, **39**, 1703-1710.
- [22] M.R. Kessler, N.R. Sottos and S.R. White, **34**, 743-753.
- [23] M.R. Kessler and S.R. White, *Composites Part A*, 2001, **32**, 683-699.
- [24] X. Liu, X. Sheng, J.K. Lee and M.R. Kessler, *J. Therm. Anal. Calorim.*, 2007, **89**, 453-457.
- [25] G.E. Larin, N. Bernklau, M.R. Kessler and J.C. DiCesare, *Polym. Eng. Sci.*, 2006, **46**, 1804-1811.

- [26] X. Liu, J.K. Lee, S.H. Yoon and M.R. Kessler, *J. Appl. Polym. Sci.*, 2006, **101**, 1266-1272.
- [27] X. Sheng, M.R. Kessler and J.K. Lee, *J. Therm. Anal. Calorim.*, 2007, **89**, 459-464.
- [28] X. Sheng, J.K. Lee and M.R. Kessler, *Polymer*, 2009, **50**, 1264-1269.
- [29] W. Jeong and M.R. Kessler, *Chem. Mater.*, 2008, **20**, 7060-7068.
- [30] W. Jeong and M.R. Kessler, *Carbon*, 2009, **47**, 2406-2412.
- [31] T.C. Mauldin and M.R. Kessler, *J. Mater. Chem.*, 2010, **20**, 4198-4206.
- [32] E.N. Brown, N.R. Sottos and S.R. White, *Exp. Mech.*, 2002, **42**, 372-379.
- [33] E.N. Brown, S.R. White and N.R. Sottos, *Compos. Sci. Technol.*, 2005, **65**, 2466-2473.
- [34] E.N. Brown, S.R. White and N.R. Sottos, *Compos. Sci. Technol.*, 2005, **65**, 2474-2480.
- [35] E.N. Brown, *J. Strain. Anal. Eng. Des.*, 2011, **46**, 167-186.
- [36] J.K. Lee, X. Liu, S.H. Yoon and M.R. Kessler, *J. Polym. Sci., Part B: Polym. Phys.*, 2007, **45**, 1771-1780.
- [37] X. Liu, X. Sheng, M.R. Kessler and J.K. Lee, *Compos. Sci. Technol.*, 2009, **69**, 2101-2107.
- [38] P.K. Freeman, V.N. Rao, V.N.M. Rao; D.E. George, and G.L. Fenwick, G.L., *J. Org. Chem.*, 1967, **32**, 3958-3963.
- [39] S.J. Dolman, K.C. Hultsch, F. Pezet, X. Teng, A.H. Hoveyda and R.R. Schrock, *J. Am. Chem. Soc.*, 2004, **126**, 10945-10953.
- [40] I.S. Ponticello, *J. Polym. Sci., Polym. Chem. Ed.*, 1979, **17**, 3509-3518.
- [41] M.Z. Rong, M.Q. Zhang and W. Zhang, *Adv. Compos. Lett.*, 2007, **16**, 167-172.
- [42] T. Yin, M.Z. Rong, M.Q. Zhang and G.C. Yang, 2007, **67**, 201-212.
- [43] T. Yin, M.Z. Rong, M.Q. Zhang and J.Q. Zhao, *Smart Mater. Struct.*, 2009, **18**, 1-7.
- [44] T. Yin, M.Z. Rong and M.Q. Zhang, *Adv. Mater. Res.*, 2008, **47-50**, 282-285.
- [45] T. Yin, L. Zhou, M.Z. Rong and M.Q. Zhang, *Smart Mater. Struct.*, 2008, **17**, 1-8.
- [46] T. Yin, M.Z. Rong, J. Wu, H. Chen and M.Q. Zhang, *Composites Part A.*, 2008, **39**, 1479-1487.
- [47] Y.C. Yuan, M.Z. Rong, M.Q. Zhang, J. Chen, G.C. Yang and X. M. Li, *Macromolecules*, 2008, **41**, 5197-5202.
- [48] D.Z. Xiao, Y.C. Yuan, M.Z. Rong and M.Q. Zhang, *Polymer*, 2009, **50**, 2967-2975.
- [49] X. Sheng, T.C. Mauldin and M.R. Kessler, *J. Polym. Sci., Part A: Polym. Chem.*, 2010, **48**, 4093-4102.
- [50] M. Gragert, M. Schunack and W.H. Binder, *Macromol. Rapid Commun.*, 2011, **32**, 2011.
- [51] M.W. Keller, S.R. White and N.R. Sottos, *Adv. Funct. Mater.*, 2007, **17**, 2399-2404.
- [52] M.W. Keller, S.R. White and N.R. Sottos, *Polymer*, 2008, **49**, 3136-3145.
- [53] L. Yao, Y.C. Yuan, M.Z. Rong and M.Q. Zhang, *Polymer*, 2011, **52**, 3137-3145.
- [54] L. Yao, M.Z. Rong, M.Q. Zhang and Y.C. Yuan, *J. Mater. Chem.*, 2011, **21**, 9060-9065.
- [55] H.P. Wang, Y.C. Yuan, M.Z. Rong and M.Q. Zhang, *Macromolecules*, 2010, **43**, 595-598.
- [56] M.R. Kessler and S.R. White, *J. Polym. Sci., Part A: Polym. Chem.*, 2002, **40**, 2373-2383.

- [57] A.S. Jones, J.D. Rule, J.S. Moore, N.R. Sottos and S.R. White, *J. R. Soc. Interface*, 2007, **4**, 395-403.
- [58] G.O. Wilson, J.S. Moore, S.R. White, N.R. Sottos and H.M. Andersson, *Adv. Funct. Mater.*, 2008, **18**, 44-52.
- [59] J.D. Rule and J.S. Moore, *Macromolecules*, 2002, **35**, 7878-7882.
- [60] T.C. Mauldin, J.D. Rule, N.R. Sottos, S.R. White and J.S. Moore, *J. R. Soc. Interface*, 2007, **4**, 389-393.
- [61] J. K. Lee, S. J. Hong, X. Liu and S. H. Yoon, *Macromol. Res.*, 2004, **12**, 478-483.
- [62] A.S. Jones, J.D. Rule, J.S. Moore, S.R. White and N.R. Sottos, *Chem. Mater.*, 2006, **18**, 1312-1317.
- [63] G.O. Wilson, M.M. Caruso, N.T. Reimer, S.R. White, N.R. Sottos and J.S. Moore, *Chem. Mater.*, 2008, **20**, 3288-3297.
- [64] J.D. Rule, E.N. Brown, N.R. Sottos, S.R. White and J.S. Moore, *Adv. Mater.*, 2005, **17**, 205-208.
- [65] J.M. Kamphaus, J.D. Rule, J.S. Moore, N.R. Sottos and S.R. White, *J. R. Soc. Interface*, 2008, **5**, 95-103.
- [66] R.H. Grubbs, *Angew. Chem. Int. Ed.*, 2006, **45**, 3760-3765.
- [67] S.T. Nguyen and R.H. Grubbs, *J. Am. Chem. Soc.*, 1993, **115**, 9858-9859.
- [68] E.L. Dias, S.T. Nguyen and R.H. Grubbs, *J. Am. Chem. Soc.*, 1997, **119**, 3887-3897.
- [69] S.R. White, N.R. Sottos, P.H. Geubelle, J.S. Moore, M.R. Kessler, S.R. Sriram, E.N. Brown and S. Viswanathan, *Nature*, 2001, **409**, 794-797.
- [70] J.D. Rule, N.R. Sottos and S.R. White, *Polymer*, 2007, **48**, 3520-3529.

CHAPTER 6: RING-OPENING METATHESIS POLYMERIZATION OF A MODIFIED LINSEED OIL WITH VARYING LEVELS OF CROSSLINKING

A paper published in *Journal of Polymer Science Part A: Polymer Chemistry**

Timothy C. Mauldin,¹ Karen Haman,² Xia Sheng,² Phillip Henna,¹ Richard C. Larock,¹ and Michael R. Kessler²

6.1 Abstract

A commercial norbornyl-functionalized linseed oil, blended with a bicyclic norbornene-based crosslinking agent (at loadings ranging from 0 to 50 wt. %) undergoes ring-opening metathesis polymerization (ROMP) with the 1st generation Grubbs' catalyst to form a biorenewable polymer network. Co-monomers are characterized, the thermal and mechanical properties of the cured systems are investigated by dynamic mechanical analysis (DMA), and thermal decomposition is evaluated by thermogravimetric analysis (TGA). The resin is shown to consist of a modified linseed oil and small oligomers of cyclopentadiene. Broad tan delta peaks suggest inhomogeneous phase morphologies, which result in complex crosslinking behaviors. The thermal stability of the polymers increases with increasing crosslinker content.

6.2 Introduction

In recent years there has been a surge of interest in bio-based materials, specifically those resulting from commercially available and biorenewable vegetable oils, in an effort to reduce our dependency on conventional petroleum-based polymers. Historically, vegetable oils have been used in the paint and coating industry [1-2] for their ability to react with

* Reprinted with permission of *Journal of Polymer Science Part A: Polymer Chemistry*.

¹ Department of Chemistry, Iowa State University, Ames, IA 50011, USA.

² Department of Materials Science and Engineering, Iowa State University, Ames, IA 50011, USA.

oxygen and act as drying agents, but recent work has shown that derivatives of these vegetable oils can form bulk polymers and composites with similar or better thermal/mechanical properties than their petrochemical counterparts [3-4]. Vegetable oil-based materials also have the advantage of lower cost, minimal VOC emissions, and biodegradative tendencies.

Most common vegetable oils consist of a triglyceride unit with three fatty acid-based ester chains. With some exceptions, individual chains are generally linear, ranging from 14 to 22 carbons in length, and containing 0-3 double bonds. This high degree of unsaturation gives these macromolecules potential for functionalization and subsequent polymerization to form a highly crosslinked polymer matrix. Polymers have been made from soybean [5-8], corn [9], tung [10-11], linseed [12-15], and castor oil [16-17], among others, and many approaches to polymerization have been utilized including cationic [18-20], free radical [21-22], thermal [23-24], UV-initiated [25] and ring-opening polymerization [26]. Strangely, transition metal-based catalysts have yet to assert themselves as a force in vegetable oil bulk polymerization, despite the continual development of novel catalyst complexes that can produce high-yielding, stereoregular, regioregular, monodisperse and living polymers, often under mild reaction conditions.

One type of reaction that has become very popular over the last several years is ring-opening metathesis polymerization (ROMP), initiated by organometallic carbenes [27-33]. Most of the well-defined ROMP catalysts are grouped in the category of either Grubbs [34-36] or Schrock-type [37-39] complexes, named after their Nobel laureate inventors [40-41]. The former show great practicality due to their high reactivity, functional group tolerance, and air/moisture insensitivity. An example of a catalytic turnover of a ROMP propagation step with Grubbs' 1st generation catalyst is shown in Figure 6.1.

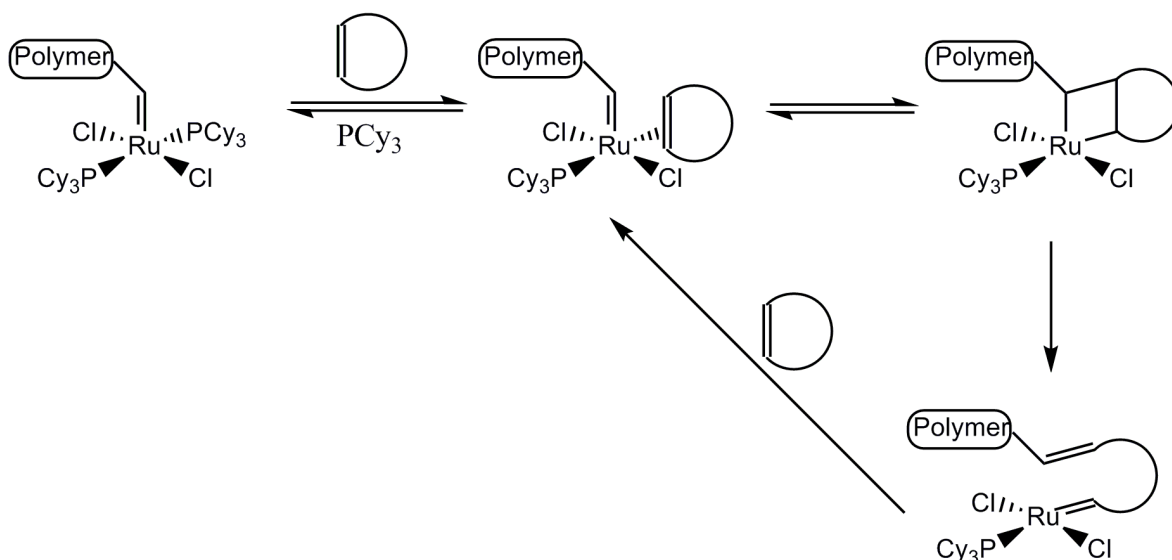


Figure 6.1. Ring-opening metathesis polymerization of a cyclic alkene with the 1st generation Grubbs' catalyst.

While highly reactive ROMP catalysts have been developed to initiate the polymerization of low-strain cycloalkenes, most complexes show greatest reactivity with high-strain cyclic olefins [42-43], notably norbornene [44-46], cyclobutene [47-48] and cyclooctene [49-50] functionalities. In fact, to the best of our knowledge, the only report of a ROMP-based vegetable oil polymer was recently published with a norbornyl-functionalized castor oil copolymerized with cyclooctene by the 2nd generation Grubbs' catalyst [51]. With a wide array of conceivable ROMP-reactive comonomers, polyunsaturated vegetable oils, metathesis catalysts, and cyclic olefin functionalities, this subfield of vegetable oil polymers can be expanded towards the synthesis of new and exciting materials.

In this work, we investigate a commercially available, norbornyl-functionalized linseed oil (DilulinTM), copolymerized with a ROMP-reactive crosslinking agent (Figure 6.2) using the 1st generation Grubbs' catalyst. The complex chemical structure of DilulinTM is characterized and the mechanical properties of the resulting copolymers are studied via dynamic mechanical analysis (DMA) and thermal stability by thermogravimetric analysis (TGA) at various loadings of crosslinker. Complex crosslinker behavior is observed and discussed in detail.

6.3 Experimental

Bicyclo[2.2.1]hepta-2,5-diene (Aldrich), hydroquinone (Aldrich), *endo*-dicyclopentadiene (Acros Organics), and all solvents (Aldrich) were used without purification. Norbornyl-functionalized linseed oil, purchased from Cargill under the trade name Dilulin™, was also used as received.

Bis(tricyclohexylphosphine)benzylideneruthenium(II) dichloride (Grubbs' catalyst) was purchased from Aldrich and recrystallized using a modified lyophilization method [52]: Grubbs' catalyst was dissolved in benzene (50 mg/ml), flash-frozen in a liquid nitrogen bath for 5 minutes, and the benzene was allowed to sublime under vacuum overnight. An isomeric mixture of 1,4,4a,5,8,8a-hexahydro-1,4,5,8-*exo*,-*endo*-dimethanonaphthalene (*exo*-*endo* isomer, 87 mol. %) and 1,4,4a,5,8,8a-hexahydro-1,4,5,8-*exo*,-*exo*-dimethanonaphthalene (*exo*-*exo* isomer, 13 mol. %) were synthesized as reported in the literature [53] and used as a mixture. This mixture will herein be referred to as the crosslinker or CL. The isomeric chemical structures are shown in Figure 6.2.

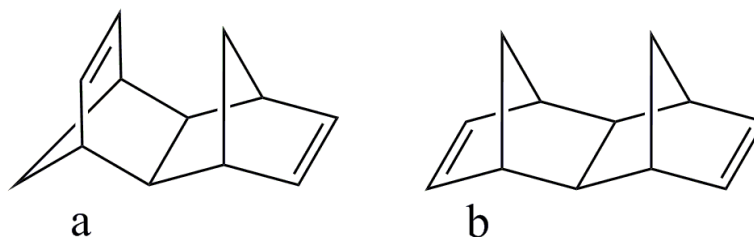


Figure 6.2. Mixture of a) *exo*-*endo* and b) *exo*-*exo* isomers that comprise the crosslinker.

Polymer samples were prepared by dispersing various loadings of crosslinker in Dilulin™ with six to eight brief pulses from a sonic probe. The resulting mixture was cooled to 0 °C and stirred vigorously with Grubbs' catalyst (2 mg/ml) for about 30 seconds or until complete dissolution. The solution was injected into a rectangular glass mold to form thin strip samples. The curing schedule applied is described in detail in Table 6.1. After curing had completed, the polymer samples were removed from their molds, cut, and polished to uniform dimensions of 1 x 5 x 20 mm.

Table 6.1. Curing Schedule for DilulinTM/CL/Grubbs' Catalyst Samples.

Step	Procedure	Time
1	Ramp to 70°C at 5 °C/min	10 minutes
2	Isothermal at 70 °C	2 hours
3	Ramp to 170°C at 5 °C/min	20 minutes
4	Isothermal at 170 °C	1 hour
5	Cool to Room Temperature	3-4 hours

Soxhlet extraction of the polymer samples was carried out with refluxing methylene chloride for 24 hours. The solvent was evaporated from the extracts *in vacuo*, and both the extracts and the remaining solid were dried under a high vacuum for 24 hours. Weight-based swelling tests were done in methylene chloride with an allowed swelling time of 48 hours.

¹H NMR spectra were taken with a 400 MHz Varian Spectrometer (Palo Alto, CA) using d-trichloromethane as the solvent. EI-MS spectra of monomers dissolved in THF were taken with a Finnigan TSQ instrument. Dynamic mechanical analysis was performed on thin strip samples using a Q800 DMA (TA Instruments). Samples were loaded into tension clamps with a torque of 3 in-lb. Controlled strain tests were carried out at a dynamic amplitude of 5 μm and a frequency of 1 Hz with 0.001 N pre-load force, 120% force track, and a heating rate of 3 °C/minute from -120 °C to 200 °C. The thermal decomposition of the polymer samples was measured using a Q50 TGA (TA instruments) under air (50 ml/min) at 25 °C/min from room temperature to 500 °C. Polymer fractions weighing approximately 15 mg were cut from the thin strip samples for thermogravimetric analysis.

6.4 Results and Discussion

6.4.1 Structural characterization of DilulinTM

DilulinTM is a mixture of norbornyl-functionalized linseed oil and cyclopentadiene (CPD) oligomers. Soucek and coworkers have reported some synthetic details and structural elucidation of DilulinTM [54-56], but a more detailed characterization is necessary to explain our results. Two distinct components are isolable from DilulinTM by simple silica gel column

chromatography (SiO₂, hexanes) [57], one fraction consisting of modified linseed oil (70% by weight) and the other of cyclopentadiene (CPD) oligomers (30% by weight).

The individual CPD oligomers were difficult to separate, but EI-MS of the bulk mixture shows prominent *m/z* peaks at intervals of 66 (66, 132, 198, 264, 330, 396 and 462; see supplementary information), evidence of observable amounts of monomer to 7-mer. ¹H NMR spectral analysis of the oligomer mixture shows complex groups of multiplets corresponding to significant and equivalent amounts of norbornyl and cyclopentadienyl protons at $\delta = 5.9\text{-}6.3$ ppm and $5.4\text{-}5.7$ ppm, respectively (data not shown). The presence of olefins corresponding to these peaks makes radical oligomerization unlikely since these double bonds, especially norbornyl, react very rapidly through such mechanisms. Instead, the existence of these olefinic protons is likely the result of a thermal Diels-Alder oligomerization. Gas phase thermal oligomerization of cyclopentadiene is known to be very facile at high temperatures and pressures [58], both being conditions by which linseed oil's norbornylation occurs. Due to the ROMP-reactive norbornene groups on these oligomers, they were not removed from DilulinTM prior to polymerization.

A ¹H NMR and a mass spectrum of the oil fraction of DilulinTM is shown in Figure 6.3 and in the supplementary information, respectively. All sp³ methyl, methylene and methine proton peaks in Figure 6.3 are in agreement with what is expected for triglyceride-based linseed oil [59]. The mass spectrum data (available in the supplementary information) shows both a group of molecular ion peaks at 860-880 Da corresponding to the molecular weight of linseed oil (the "group" of molecular ions is a function of the natural variance in fatty acid chains on vegetable oils, creating several oil molecules differing in the number of double bonds), and small groups of peaks at 924-944 and 990-1100 Da corresponding to linseed oil functionalized with one or two molecules of cyclopentadiene. Integration of the sp² proton peaks shows about 3.9 linear olefins and 0.6 norbornyl olefins, resulting in an average of 4.5 total olefins per molecule of modified linseed oil. This is unusual, since linseed oil contains an average of approximately 6 double bonds per molecule, and most common types of pericyclic additions of cyclopentadiene (or oligomers of CPD) to oil would not result in a reduction in the total number of double bonds formed in the product. It is likely that during the synthesis of DilulinTM a significant amount of thermally-initiated

intramolecular cyclizations of the oil occurs to add allylic carbons and allylic protons across double bonds—a reaction well-represented in the literature over the past 30 years [60-65]. This reaction is known for all unsaturated fatty acids, but is particularly favorable in linolenic chains, which comprise over 50% of linseed oil [66]. The most common type of intramolecular cyclization of a linolenic chain is shown mechanistically in Figure 6.4. The initial oil (I), upon heating, undergoes a [1,6] prototropic migration to form a cyclopentenyl unit (II). Further heating of this intermediate induces a rearrangement to form a cyclohexenyl group (III) in the oil chain [67]. In Figure 6.3, there is a small, but noticeable, peak occurring in the range of $\delta = 5.6\text{-}5.7$ ppm (marked with an arrow) that could arise from either or both of the cyclized products illustrated in Figure 6.4.

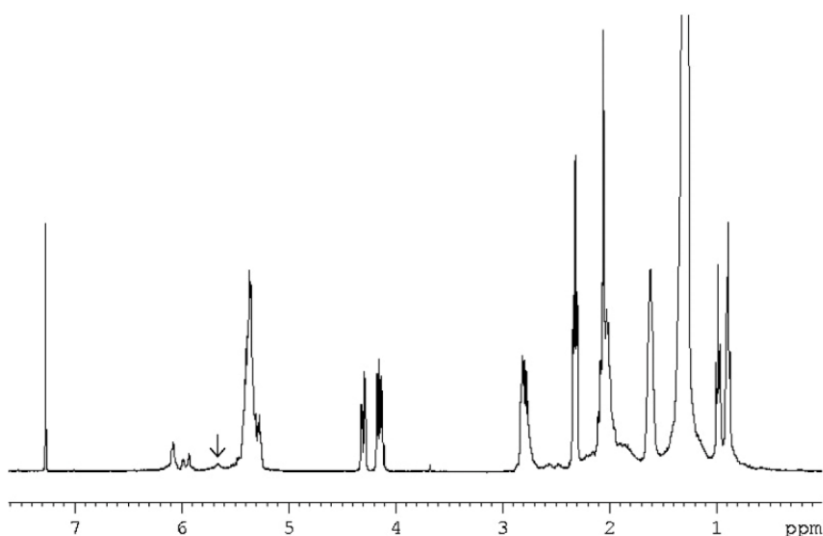
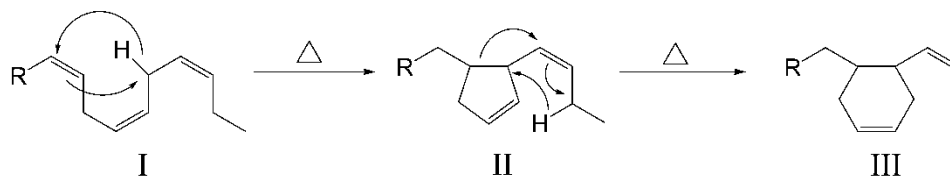


Figure 6.3. ^1H NMR spectra of oil fraction isolated from DilulinTM.

Two important observations can be made from analysis of the oil fraction. First, it is clear that the intramolecular cyclization of linseed oil is the dominant reaction in the synthesis of DilulinTM, occurring possibly multiple times per molecule (a reduction of about 1.5 double bonds per molecule from linseed oil to DilulinTM's oil fraction corresponds to at least an average of 1.5 cyclizations per molecule). Second, the major products expected to be observed upon these cyclizations—cyclopentenyl and cyclohexenyl groups—are minor. The aforementioned peaks in Figure 6.3 ranging from $\delta = 5.6\text{-}5.7$ ppm integrate to only 0.3

protons, corresponding to only 0.15 total cyclopentenyl and cyclohexenyl groups per molecule. While other types of intramolecular rearrangements are known to be minor reactions upon heating vegetable oils, we believe the reduction of cyclopentenyl/cyclohexenyl groups results from the addition of cyclopentadiene during heating of the linseed oil. The double bonds of linseed oil are linear, unstrained, non-conjugated, and alkyl-substituted, making them poor dienophiles. Their Diels-Alder reaction with cyclopentadiene is expected to be slow and low-yielding, even at high temperatures and pressures. But upon intramolecular cyclization, to form intermediate II in Figure 6.4, these olefins become slightly activated by the introduction of ring strain, and they become better dienophiles than their linear precursors. Cyclopentadiene conceivably acts as an intermediate trap by forming a norbornyl unit by Diels-Alder cycloaddition on to the cyclopentenyl group. The newly formed, norbornyl-substituted cyclopentenyl group could still undergo the expected rearrangement, but this would probably be somewhat inhibited by both the slight deactivation of the formerly bis-allylic carbon to a monoallylic carbon and the bulkiness of the norbornyl group, thus preventing the large degree of molecular ordering required for pericyclic reactions. A proposed chemical structure for the modified oil fraction of DilulinTM is presented in Figure 6.5, but the natural variance in the fatty acid chains of linseed oil along with the unpredictability of intramolecular cyclizations makes this structure merely a guide for the types of functionalities that may exist in the oils. A more detailed structure elucidation of DilulinTM and similar modified vegetable oils is currently underway in our labs.



R = remainder of triglyceride

Figure 6.4. Mechanism of the thermally-initiated intramolecular cyclization of a linolenic acid chain of linseed oil.

6.4.2 Microphase Analysis

When the DilulinTM and CL are blended, they form a homogeneous transparent mixture. However, as the resin mixture begins to cure (after the addition of Grubbs' catalyst), the materials become cloudy (especially for CL loadings of 30 wt. % and higher). This change in transparency with cure is an indication of a reaction induced phase separation (RIPS), which is commonly seen in reactive polymer blends [68]. The difference in ROMP reactivity and structure between the CL component and the DilulinTM may cause the more reactive CL monomer to be consumed faster, causing polymer that is formed later in the reaction to have a higher composition of the slower reacting monomer, which in turn results in microphase heterogeneity and property gradients throughout the structure [69]. Cured polymer samples with various crosslinker loadings are shown in Figure 6.6. These show a trend towards increased cloudiness (and more microphase separation in the copolymers) with higher crosslinker content. DMA plots for crosslinker loadings of 30, 40 and 50 wt. % (Figure 6.7a) show very broad step changes in the storage modulus drop and broad $\tan \delta$ peaks containing as many as three identifiable peaks and shoulders, also indicative of microphase separation. The broad glass transition region may be due to a combination of the large number of relaxation modes available to triglyceride-based polymers [70] and to the overlapping of the relaxation regions from the immiscible phases. A complex system containing three ROMP-reactive components—norbornyl-functionalized oil, oligomers of CPD, and crosslinker—would intuitively have multiple phases rich in specific comonomers, but detailed interpretation is not straightforward.

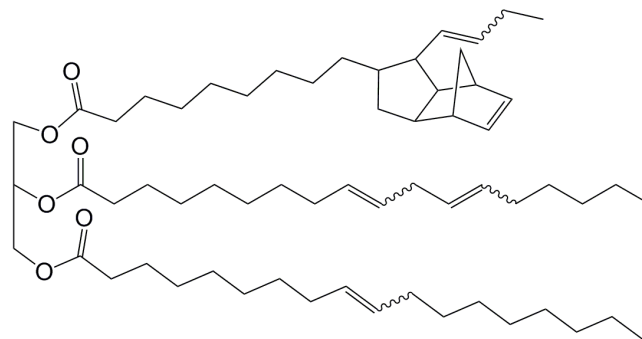


Figure 6.5. A representative structure of the oil fraction of DilulinTM.

For homogeneous polymers, the glass transition is often defined from a DMA curve as either the onset in the storage modulus drop ($T_g^{E' \text{ onset}}$), the peak in the loss modulus curve ($T_g^{E'' \text{ peak}}$), or the peak in the $\tan \delta$ curve ($T_g^{\tan \delta \text{ peak}}$). The T_g values obtained from these methods is different and, especially for highly crosslinked thermosets with a broad transition range, can vary by up to 25 °C with $T_g^{E' \text{ onset}} < T_g^{E'' \text{ peak}} < T_g^{\tan \delta \text{ peak}}$ [71]. For non-homogeneous systems, when more than one phase exists, the material may exhibit multiple glass transition temperatures represented by multiple peaks (or shoulders) in the loss modulus or $\tan \delta$ curves, which correspond to the glass transition temperatures of the various phases. However, peaks and shoulders below the primary glass transition temperature also show up in homogeneous systems as sub- T_g transitions (T_β) related to very localized main or side chain movement [71]. Thus, it is difficult to say conclusively that the additional shoulders in the $\tan \delta$ curves relate to the glass transition temperatures of the various phases and not simply to sub- T_g transitions. Nonetheless, because of the evidence for phase separation from the change in transparency (Fig. 6.6), we postulate that the additional shoulders in the $\tan \delta$ peaks are related to the primary glass transition temperatures of at least three phases (with distinct T_g temperature ranges) and that these somewhat overlapping transitions are responsible for the broad range in the overall glass transition relaxation. Assigning T_g values from the DMA plot alone is difficult, so the three phases will be referred to simply as the low T_g , medium T_g , and high T_g phase.

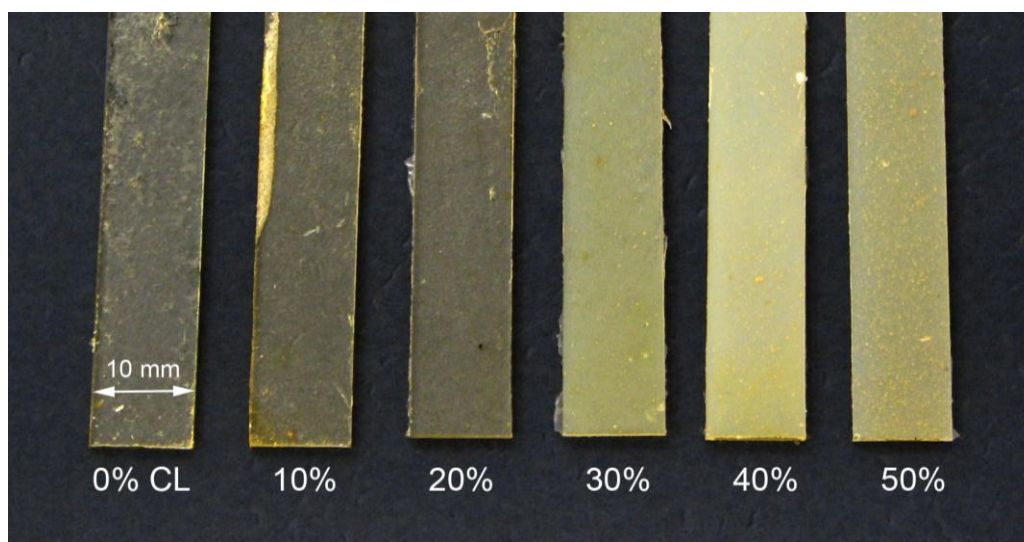


Figure 6.6. Thin strip samples of Dilulin[™]/CL copolymer at various crosslinker loadings.

The glass transition temperature of the low T_g phase is expected to be near the temperature corresponding to the onset of the storage modulus drop. The $\tan \delta$ peak of the low T_g phase manifests itself in the overall $\tan \delta$ curve as a shoulder with a peak that appears to roughly correspond to this drop at all three crosslinker loadings, so the T_g can be estimated by the onset temperature from the storage modulus curve. This predicts that the glass transition temperatures for the low T_g phase are -52.1 , -43.2 , and -42.0 °C at 30, 40, and 50% CL loading, respectively. It is likely that this phase is oil-rich. The crosslinker is expected to have the highest glass transition temperature of the comonomers, and the T_g of the CPD oligomers, all of which have similar structure and reactivity to the dimer, should not deviate significantly from that of DCPD, which was measured to be 140 °C at identical loadings of 1st generation Grubbs' catalyst [72]. Also, extremely low T_g values are expected for a phase that consists of large amounts of unreacted oil (25 wt% of Dilulin[™] is not norbornylized) and a polymer chain with large molecular weight triglyceride side groups.

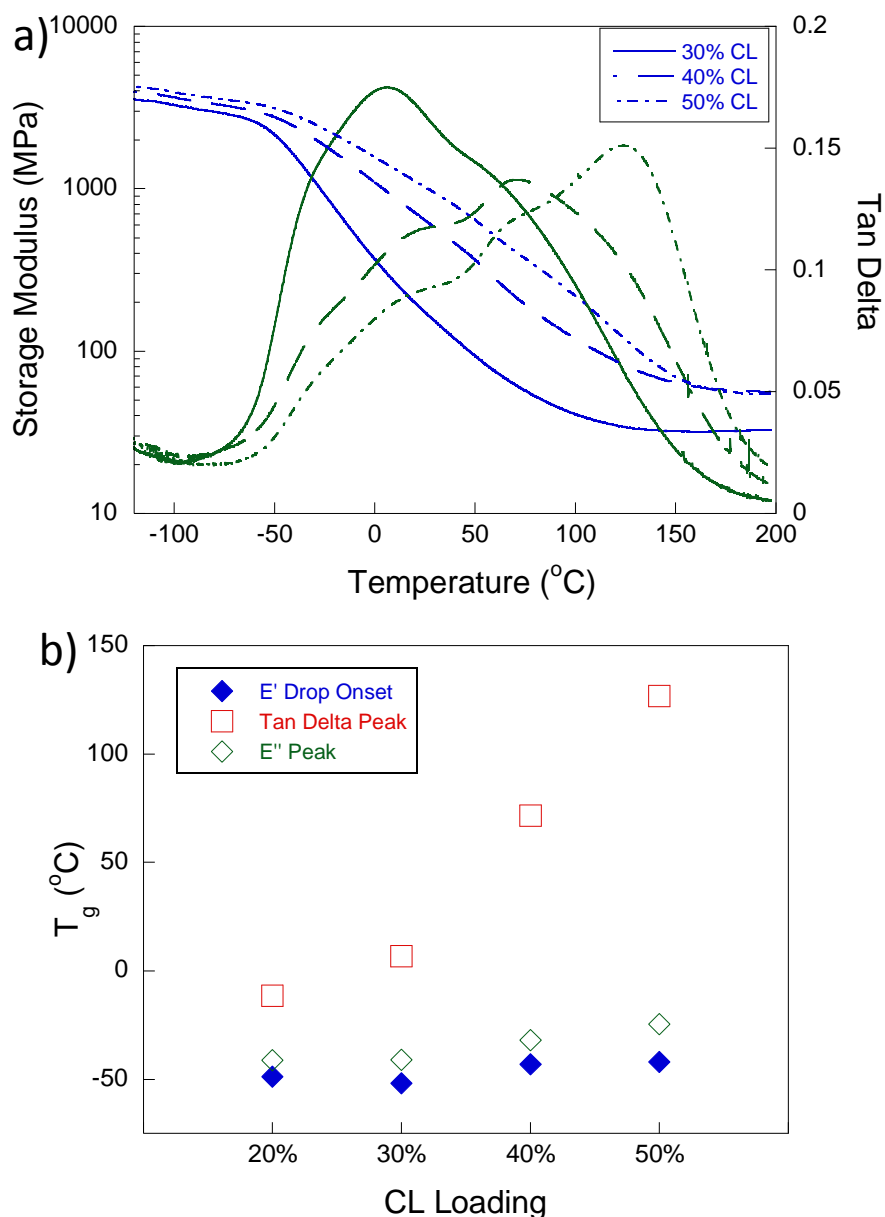


Figure 6.7. Thermal-mechanical behavior from DMA experiments of DilulinTM/CL copolymers (a) temperature dependence of storage modulus and tan δ , (b) major transition temperature as measured by E' onset, tan δ peak, and E'' peak.

Without further knowledge of the glass transition temperatures of the medium and high T_g phases, it is difficult to interpret the composition of those phases. Due to the high reactivity of CL with Grubbs' catalyst, sample preparation of the homopolymer is difficult, but it is estimated that the T_g of pure CL polymer is approximately 300 °C [73]. Because of

this extremely high theoretical glass transition temperature for CL, we can make an assumption that the medium T_g phase is rich in oligomers of CPD and the high T_g phase is crosslinker rich. However, the high T_g phase has a glass transition temperature that is no greater than 150 °C, so calling it “rich” in crosslinker may be an overstatement. A high degree of miscibility between the crosslinker and CPD oligomers is expected in the high T_g phase since all molecules are structurally similar polycyclic dienes with equally reactive norbornene groups.

Figure 6.7b shows the overall effective glass transition temperatures as measured by the E' onset, E'' peak, and $\tan \delta$ peak for DilulinTM/CL copolymers with CL loadings ranging from 20-50% (we were not able to evaluate specimens with lower loadings of CL, because of the fragile nature of the samples at these compositions). There is a very large difference between $T_g^{E' \text{ onset}}$ and $T_g^{\tan \delta \text{ peak}}$, which increases substantially with increasing CL loading. Similar behavior, showing a strong divergence between the $T_g^{E'' \text{ peak}}$ and $T_g^{\tan \delta \text{ peak}}$ with increasing co-monomer concentration, has also been observed for acrylated epoxidized soybean oil (AESO)-styrene based systems by Wool and Sun [69].

6.4.3 Crosslink Efficiency

The efficiency of CL in crosslinking the polymer network has been analyzed by Soxhlet extraction for DilulinTM/CL samples at all loadings of CL. Figure 6.8 (left y-axis) shows that when DilulinTM is polymerized without the addition of crosslinker, over 30% by weight of material is removed, and, as the amount of crosslinker in the matrix increases, the weight percent of material extracted steadily drops in a non-linear fashion. Table 6.2 shows the data from Figure 6.8 along with the calculated percent of non-norbornyl-functionalized linseed oil for all crosslinker loadings.

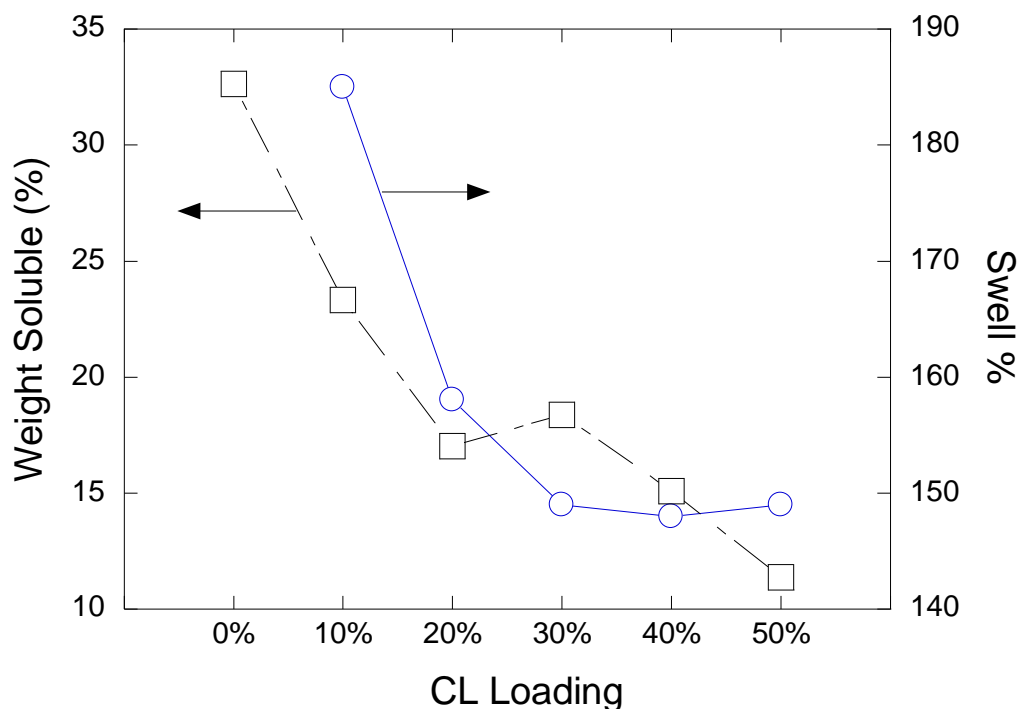


Figure 6.8. Soxhlet extraction with methylene chloride (Y1 axis) and weight-based swelling (Y2 axis) of Dilulin/CL polymers at various comonomer volume fractions.

From Table 6.2, it appears the extract weight percent of all polymer samples containing crosslinker is comparable to the calculated weight percent of the non-norbornyl-functionalized oil that is not expected to be incorporated into the polymer matrix. In a sample of pure DilulinTM polymer, however, the weight percent of extracts is considerably higher than the calculated percent of non-norbornyl-functionalized oil, the difference being low molecular weight oligomers extracted by the hot solvent. These low molecular weight Dilulin oligomers consist of both oil and the CPD oligomers that are not incorporated into the bulk thermoset due to the low levels of crosslinking. This shows that even at low loadings, the crosslinker is efficient enough to incorporate nearly all small oligomers into the crosslinked polymer matrix.

Table 6.2. Comparison of Extract Weight Percent and Calculated Amount of Non-Norbornyl-Functionalized Linseed Oil at Various Crosslinker Loadings.

Crosslinker Loading	% Extracted	% Dilulin without norbornyl group ^a
0%	32.6 ± 2.4%	25.4%
10%	23.3 ± 1.4%	22.9%
20%	17.0 ± 1.1%	20.3%
30%	18.4 ± 2.4%	18.8%
40%	15.1 ± 1.7%	15.2%
50%	11.4 ± 4.5%	12.7%

^a DilulinTM calculated to contain 30% CPD oligomers, 45% norbornyl-functionalized oil, and 25% non-norbornyl-functionalized oil.

6.4.4 Crosslink Density

Swelling tests were conducted on samples of all CL loadings to qualitatively determine crosslink density (Figure 6.8, right y-axis). DilulinTM polymer with 10% CL loading swells to nearly double its original weight in methylene chloride after 48 hours. Swell percentage decreases with increased crosslinker content until it levels off at about 150% using 30% crosslinker. This implies a non-linear relationship between crosslink density and crosslinker loading. This is corroborated by comparing the storage modulus at the rubbery plateaus in Figure 6.8a, which also has a non-linear relationship with crosslink density. The plateau for 30% crosslinker loading occurs at 31.96 MPa, while the plateau for 40% and 50% loadings are essentially equivalent at 56.19 MPa and 54.17 MPa, respectively.

It is likely that this trend results from the complexity of the microphase separation at different comonomer compositions. The composition of each phase (especially the phase presumed to be rich in CL) clearly changes with crosslinker loading, as evidenced by their changing glass transition temperatures, which can be roughly estimated from the $\tan \delta$ curves. Since the high T_g phase glass transition temperature increases with CL content, the volume fraction of CL in this phase is also likely increasing, but probably not increasing in the other phases where the majority of the swelling is likely occurring. This effect should

increase the crosslink density of the high T_g phase with increasing crosslinker content, and not increase the crosslink density of possibly both the low and middle T_g phases with increasing crosslinker content. Further analysis without detailed information of individual phase compositions and crosslink densities is difficult, but for such complex behavior, it is reasonable to expect that the weighted average of each phase's crosslink density (which manifests itself in the storage modulus of the rubbery plateau) shows a nonlinear dependence on CL loading.

6.4.5 Thermal Stability

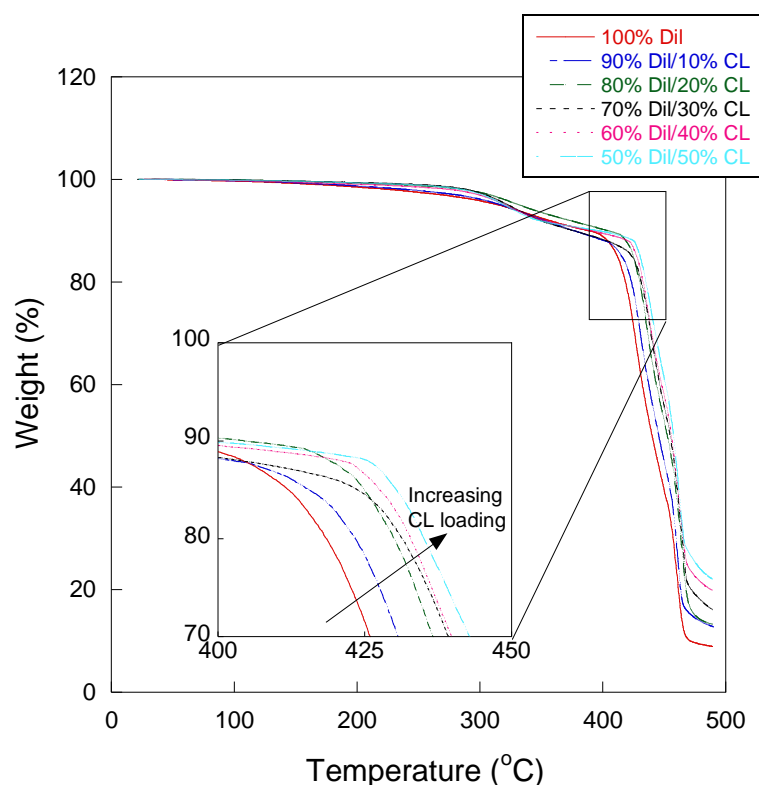


Figure 6.9. Thermogravimetric analysis of DilulinTM and crosslinker.

DilulinTM/CL copolymers show good thermal stability over the complete composition ranges investigated. All crosslinker loadings lose less than 5% by weight up to 315 °C and lose less than 10% by weight up to 380 °C (Table 6.3). A 5% weight loss occurs in a small

step in the range of 300-330°C for all CL loadings. This temperature range is in good agreement with the approximate boiling point for fatty acid triglyceride vegetable oils. Major degradation mechanisms occur over 400 °C for all samples. Careful analysis of the inset in Figure 6.9 shows the onset temperature of the large step drop slightly increases with higher crosslinker loadings. The onset temperature ranges from about 400 °C for pure DilulinTM polymers to nearly 430 °C for 50% CL loading.

Table 6.3. Thermal Stability of DilulinTM/CL Copolymers.

Crosslinker Loading	T _{max loss} (°C)	T _{5% loss} (°C)	T _{10% loss} (°C)
0%	460.02	317.70	390.85
10%	460.11	319.13	378.17
20%	463.49	334.00	406.09
30%	463.30	324.14	378.00
40%	461.86	322.14	393.20
50%	461.33	320.89	394.42

6.5 Conclusions

Herein, we characterize a norbornyl-functionalized linseed oil monomer, DilulinTM, and its ROM-initiated copolymer with a crosslinking agent. DilulinTM consists of several small thermal oligomers of cyclopentadiene and a cyclized oil chain containing a norbornyl pendant group. The resulting polymer shows complex phase behavior at high loadings of crosslinker, consisting of at least three total phases. Only small amounts of crosslinker are required to incorporate nearly all small oligomers into the polymer matrix, and increasing the crosslinker content increases the thermal stability and crosslink density, but the dependence of the latter on CL loading is complex.

6.6 Acknowledgements

This work was conducted with the financial support of collaboration between Women in Science and Engineering (WISE) and the Department of Materials Science and

Engineering. Thanks to Wonje Jeong and Will Goertzen for technical assistance and helpful discussions.

6.7 References

- [1] Wexler, H. *Encycl. Polym. Sci. Technol.* 1966, 5, 216.
- [2] Gallagher, E.C. *ASTM Special Technical Publication* 1972, STP 500, 53-70.
- [3] Li, F.; Larock, R. C. *Polym. Mater. Sci. Eng.* 2002, 86, 379-380.
- [4] Li, F.; Larock, R. C. In *Natural Fibers, Biopolymers, and Their Biocomposites*; Mohanty, A.K.; Misra, M.; Drzal L.T., Eds.; CRC Press: Boca Raton, FL, 2005, pp 727.
- [5] Li, F.; Hanson, M.V.; Larock, R.C. *Polymer* 2001, 42, 1567-1579.
- [6] Li, F.; Larock, R.C. *J. Appl. Polym. Sci.* 2001, 80, 658-670.
- [7] Li, F.; Larock, R. C. *J. Polym. Sci., Part B: Polym. Phys.* 2000, 38, 2721-2738.
- [8] Li, F.; Larock, R. C. *J. Polym. Sci., Part B: Polym. Phys.* 2001, 39, 60-77.
- [9] Li, F.; Hasjim, J.; Larock, R.C. *J. Appl. Polym. Sci.* 2003, 90, 1830-1838.
- [10] Li, F.; Larock, R.C. *J. Appl. Polym. Sci.* 2000, 78, 1044-1056.
- [11] Li, F.; Larock R.C. *Biomacromolecules* 2003, 4, 1018-1025.
- [12] Motawie, A.M.; Hassan, F.A.; Manich, A.; Aboul-Fetouh, M.E.; El-din, A.F. *J. Appl. Polym. Sci.* 1995, 55, 1725-1732.
- [13] Meneghetti, S.M.P.; de Souza, R.F.; Monteiro, A.L.; de Souza, M.O. *Prog. Org. Coat.* 1998, 33, 219-224.
- [14] Tuman, S.J.; Chamberlain, D.; Scholsky, K.M.; Soucek, M.D. *Prog. Org. Coat.* 1996, 28, 251-258.
- [15] Henna, P.; Andjelkovic, D. D.; Kundu, P. P.; Larock, R. C. *J. Appl. Polym. Sci.* 2007, 104, 979-985.
- [16] Yin, Y.; Yao, S.; Zhou, X. *J. Appl. Polym. Sci.* 2003, 88, 1840-1842.
- [17] Cassidy, P.E.; Schwank, G.D. *J. Appl. Polym. Sci.* 1974, 18, 2517-2526.
- [18] Khot, S.N.; Lascala, J.J.; Can, E.; Morye, S.S.; Williams, G.I.; Palmese, G.R.; Kusefoglu, S.H.; Wool, R.P. *J. Appl. Polym. Sci.* 2001, 82, 703-723.
- [19] Li, F.; Perounoud, A.; Larock, R. C. *Polymer* 2001, 42, 10133-10145.
- [20] Andjelkovic, D. D.; Valverde, M.; Henna, P.; Li, F.; Larock, R. C. *Polymer* 2005, 46, 9674-9685.
- [21] Frankel, E.N. *Prog. Lipid Res.* 1980, 19, 1-22.
- [22] Valverde, M.; Andjelkovic, D. D.; Kundu, P. P.; Larock, R. C. *J. Appl. Polym. Sci.* 2008, 107, 423-430.
- [23] Wang, C.; Erhan, S. J. *Am. Oil Chem. Soc.* 1999, 76, 1211-1216.
- [24] Kundu P.; Larock, R. C. *Biomacromolecules* 2005, 6, 797-806.
- [25] Thames, S.F.; Yu, H. *Surf. Coat. Technol.* 1999, 115, 208-214.
- [26] Eren, T.; Kuesefoglu, S.H.; Wool, R. *J. Appl. Polym. Sci.* 2003, 90, 197-202.
- [27] Bielawski, C.W.; Grubbs, R.H. *Prog. Polym. Sci.* 2007, 32, 1-29.
- [28] Han, H.; Chen, F.; Yu, J.; Dang, J.; Ma, Z.; Zhang, Y.; Xie, M. *J. Polym. Sci., Part A:*

Polym. Chem. 2007, 45, 3986-3993.

[29] Gstrein, X.; Burtscher, D.; Szadkowska, A.; Barbasiewicz, M.; Stelzer, F.; Grela, K.; Slugovc, C. J. Polym. Sci., Part A: Polym. Chem. 2007, 45, 3494-3500.

[30] Biagini, S.C.G.; Parry, A.L. J. Polym. Sci., Part A: Polym. Chem. 2007, 45, 3178-3190.

[31] Liaw, D.-J.; Wang, K.-L.; Lee, K.-R.; Lai, J.-Y. J. Polym. Sci., Part A: Polym. Chem. 2007, 45, 3022-3031.

[32] Hayano, S.; Sugawara, T.; Tsunogae, Y. J. Polym. Sci., Part A: Polym. Chem. 2006, 44, 3153-3158.

[33] Switek, K.A.; Chang, K.; Bates, F.S.; Hillmyer, M.A. J. Polym. Sci., Part A: Polym. Chem. 2007, 45, 361-373.

[34] Dias, E.L.; Nguyen, S.T.; Grubbs, R.H. J. Am. Chem. Soc. 1997, 119, 3887-3897.

[35] Trnka, T.M.; Grubbs, R.H. Acc Chem. Res. 2001, 34, 18-29.

[36] Sanford, M.S.; Love, J.A.; Grubbs, R.H. J. Am. Chem. Soc. 2001, 123, 6543-6554.

[37] Knoll, K.; Krouse, S. A.; Schrock, R. R. J. Am. Chem. Soc. 1988, 110, 4424-4425.

[38] Krouse, S. A.; Schrock, R. R. Macromolecules 1988, 21, 1885-1888.

[39] Knoll, K.; Schrock, R. R. J. Am. Chem. Soc. 1989, 111, 7989-8004.

[40] Schrock, R.R. Angew. Chem. Int. Ed. 2006, 45, 3748-3759.

[41] Grubbs, R.H. Angew. Chem. Int. Ed. 2006, 45, 3760-3765.

[42] Demonceau, A.; Stumpf, A.W.; Saive, E.; Noels, A.F. Macromolecules 1997, 30, 3127-3136.

[43] Nguyen, S.T.; Grubbs, R.H. J. Am. Chem. Soc. 1993, 115, 9858-9859.

[44] Nguyen, S.T.; Johnson, L.K.; Grubbs, R.H. J. Am. Chem. Soc. 1992, 114, 3974-3975.

[45] Nishihara, Y.; Inoue, Y.; Nakayama, Y.; Shiono, T.; Takagi, K. Macromolecules 2006, 39, 7458-7460.

[46] Nishihara, Y.; Izawa, S.; Inoue, Y.; Nakayama, Y.; Shiono, T.; Takagi, K. J. Polym. Sci.,

Part A: Polym. Chem. 2008, 46, 3314-3325.

[47] Perrott, M.G.; Novak, B.M. Macromolecules 1996, 29, 1817-18236.

[48] Maughon, B.R.; Grubbs, R.H. Macromolecules 1997, 30, 3459-3569.

[49] Schwab, P.; Grubbs, R.H.; Ziller, J.W. J. Am. Chem. Soc. 1996, 118, 100-110.

[50] Winkler, B.; Rehab, A.; Ungerank, M.; Stelzer, F. Macromol. Chem. Phys. 1997, 198, 1417-1425.

[51] Henna, P.H.; Larock, R.C. Macromol. Mater. Eng. 2007, 292, 1201-1209.

[52] Jones, A.S.; Rule, J.D.; Moore, J.S.; White, S.R.; Sottos, N.R. Chem. Mater. 2006, 18, 1312-1317.

[53] Stille, J.K.; Frey, D.A. J. Am. Chem. Soc. 1959, 81, 4273-4275.

[54] Zong, Z.; Soucek, M.D.; Liu, Y.; Hu, J. J. Polym. Sci., Part A: Polym. Chem. 2003, 41, 3440-3456.

[55] Chen, J.; Soucek, M.D.; Simonsick, W.J.; Celikay, R.W. Polymer 2002, 43, 5379-5389.

[56] Chen, J.; Soucek, M.D.; Simonsick, W.J.; Celikay, R.W. Macromol. Chem. Phys. 2002, 203, 2042-2057.

[57] Henna, P.; Larock R.C. To be submitted.

[58] Xiong, Z.; Mi, Z.; Zhang, X. React. Kinet. Catal. Lett. 2005, 85, 89-97.

- [59] Gunstone, F. In *Fatty Acid and Lipid Chemistry*; Blackie Academic and Professional: New York, 1996; pp 252.
- [60] Sébédio, J.-L.; Grandgirard, A. *Prog. Lipid Res.* 1989, 28, 303-336.
- [61] Christie, W.W.; Dobson, G. *Eur. J. Lipid. Sci. Technol.* 2000, 102, 515-520.
- [62] Dobson, G. In *Recent Developments in the Synthesis of Fatty Acid Derivatives*; AOCS Press: Champaign, IL, 1999; pp. 196.
- [63] Perkins, E.G.; Rojo, J.A. *J. Am. Oil Chem. Soc.* 1987, 64, 414-421.
- [64] Sébédio J.-L.; Prevost, J.; Grandgirard, A. *J. Am. Oil Chem. Soc.* 1987, 64, 1026-1032.
- [65] Le Quéré, J.-L.; Sébédio, J.-L. In *Frying Fats*; AOCS Press, Champaign, IL, 1995; pp 49.
- [66] Gunstone, F.D.; Padley, F.B. In *Lipid Technologies and Applications*; Marcel Dekker, Inc.: New York, 1997; pp 714.
- [67] Destailats, F.; Angers, P. *Eur. J. Lipid Sci. Technol.* 2005, 107, 767-772.
- [68] Williams, R. J.; Rozenberg, B. A.; Pascault, J.-P. *Adv. Polym. Sci.* 1997, 128, 95-156.
- [69] Wool, R. P.; Sun X.S. In *Bio-Based Polymers and Composites*; Elsevier Academic Press: Boston, 2005; pp 85.
- [70] Khot S.N.; La Scala, J.J.; Can E.; Morye, S.S.; Williams, G.I.; Palmese, G.R.; Kusefoglu, S.; Wool, R.P. *J. Appl. Polym. Sci.* 2001, 82, 703-723.
- [71] Menard, K.P. In *Dynamic Mechanical Analysis: A Practical Introduction*; CRC Press LLC: Boca Raton, FL, 1999.
- [72] Liu, X.; Sheng, X.; Lee, J.K.; Kessler, M.R. *J. Thermal Anal. Cal.* 2007, 89, 453-457.
- [73] Sheng, X., Kessler, M.R.; Lee, J.K. *J. Thermal Anal. Cal.* 2007, 89, 459-464.

CHAPTER 7: BLOCK COPOLYMERS DERIVED FROM THE ACYCLIC DIENE METATHESIS (ADMET) POLYMERIZATION OF A MODIFIED VEGETABLE OIL

Timothy C. Mauldin,¹ Ella F. Spiegel,² and Michael R. Kessler²

7.1 Abstract

Acyclic diene metathesis (ADMET) of an α,ω -diene, in the presence of a small amount of monoene, derived from a vegetable oil was used to synthesize new telechelic polymers with hydroxyl endgroups. These polymers were synthesized in good yields (generally greater than 90%) with number-average molecular weights greater than 30,000 g/mole and PDI values near 2.0. Ring-opening polymerization of lactide was grown with the ADMET polymer endgroups serving as initiator sites, from which ABA triblock copolymer were synthesized.

7.2 Introduction

In recent years there has been a surge of interest in engineering block copolymers with custom material properties, achievable by varying block structure and chain length. Notably, block copolymers exhibiting microphase separation have found a commercial niche as a valuable class of materials known as thermoplastic elastomers [1], but several new applications—such as uses in adhesives, surfactants, drug delivery, templating materials, nanocomposite fabrication and lithographic techniques—also show promise for commercial use. However, the growing industrial demand for these materials is beginning to conflict with the now ubiquitous goal to reduce our dependency on petroleum-based monomers (e.g. styrene, butadiene, isoprene, etc.) from which many commercial polymers are derived. Olefin metathesis polymerization [2, 3] of renewable chemicals—such as the unsaturated fatty acids of vegetable oils—are ideally suited to form biopolymers capable of mimicking commercial polymers based on petrochemicals. Ring-opening metathesis polymerization

¹ Department of Chemistry, Iowa State University, Ames, IA 50011, USA.

² Department of Materials Science and Engineering, Iowa State University, Ames, IA 50011, USA.

(ROMP) [4-6] in particular has seen enormous use as a route to block copolymers, due to its “living” chain-growth reaction. However, ROMP’s mechanism towards producing block copolymers stems from polymer growth from a single chain end, whereas growing polymer from the endgroups of telechelic polymers is often a more straightforward and direct route to the commercially useful ABA-type block copolymers. Acyclic Diene Metathesis polymerization (ADMET) [7-9] of α,ω -dienes, on the other hand, has shown much precedent as a versatile route to telechelic polymers [10, 11]. Here, we develop a bio-derived, telechelic polymers made via ADMET polymerization of a modified vegetable oil; use this polymer to grow triblock copolymer materials from lactic acid, another bioderivative; and characterize the resulting copolymer properties.

7.3 Experimental

7.3.1 General Considerations

All reagents were purchased from Aldrich Chemical Co. Toluene and tetrahydrofuran (THF) were distilled over Na/benzophenone immediately prior to use, pyridine was purchased anhydrous and stored over molecular sieves (4Å), and all other chemicals were used without further purification. Molecular weight measurements were determined either by size exclusion chromatography (SEC) with polystyrene standards in HPLC-grade tetrahydrofuran. $^1\text{H-NMR}$ spectra were recorded with a 300 MHz spectrometer using *d*-trichloromethane as solvent and residual chloroform as an internal standard. Differential Scanning Calorimetry was performed with a Q2000 Model DSC (TA Instruments) under a flow of dry nitrogen gas (50 ml/min) at heating/cooling rates of 15 K/min. Thermogravimetry of polymers was done with a Q50 Model TGA (TA Instruments) under air (60 ml/min) at a rate of 20 K/min.

7.3.2 Synthesis of ethane-1,2-diyl bis(undec-10-enoate) (**1**)

Thionyl Chloride (50 ml, 0.42 mol) was added dropwise to a solution of toluene (50 ml) and 10-undecenoic acid (36.9 g, 0.20 mol) in an oven-dried flask under dry nitrogen gas. After stirring for 6 hours at room temperature, toluene and excess thionyl chloride were

removed by vacuum distillation. To the resulting product, 25 ml of fresh toluene was twice added and removed under vacuum to eliminate residual thionyl chloride. Without further purification, 100 ml THF was added to the product, to which a solution of pyridine (17.7 ml, 0.22 mol) and ethylene glycol (6.2 g, 0.10 mol) in 25 ml of THF was added dropwise. After 14 hours stirring at room temperature, the reaction mixture was concentrated to ~75 ml, diluted with 200 ml diethyl ether, and washed with water (2 x 100 ml) and brine (1 x 100 ml). Volatiles were evaporated, and the crude product was purified by silica gel chromatography (hexane/ethyl acetate = 7/1 (v/v)) to reveal a clear liquid (83%). ¹H-NMR (300 MHz, CDCl₃) δ: 5.73-5.86 (m, 2H); 4.89-5.04 (m, 4H); 4.26 (s, 4H); 2.31 (t, 4H, J = 7.2 Hz); 1.99-2.06 (m, 4H); 1.55-1.67 (m, 4H); 1.15-1.43 (m, 20H) ppm.

7.3.3 ADMET Polymerization.

A typical polymerization was as follows: 1st generation Grubbs' catalyst (5 mg, 6.1 x 10⁻³ mmol) was lyophilized [12] in a 10 ml, oven-dried flask to aid its dissolution in the ADMET monomer. ADMET monomer (0.5 g, 1.25 mmol), either neat or containing 1 wt. % dissolved monoene, was added to the catalyst at ambient temperature, which was stirred rapidly under mild vacuum. After ~30 minutes the viscosity of the reaction rapidly increased, at which point the heat was increased to 80 °C and the reaction flask opened to heavy vacuum. After 24 hours, vacuum was broken and the bulk solid was dissolved in 10 ml THF, precipitated with 50 ml methanol, and vacuum filtered. The resulting polymer was dried under vacuum at 90 °C until constant mass to reveal a tan, opaque film, shown in Figure 7.1.

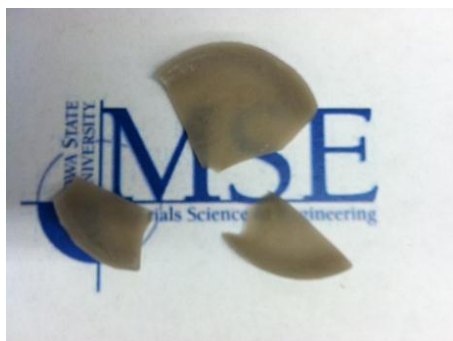


Figure 7.1. Bioderived polymer made from ADMET polymerization.

7.3.4 Ring-opening polymerization of lactide.

Alcohol end-capped ADMET polymer (0.25 g), L-lactide (0.3 g, 2.08 mmol), and a stirbar were added to a 7.4 ml vial and dried at 25 °C under vacuum overnight. The vial was flushed with N₂ for 20 minutes and 20 µl of a 1 M solution of stannous octoate in toluene was added. The vial was immersed in a 130 °C oil bath. After 12 hours, the vial was removed from heat and allowed to cool under N₂, dissolved in 10 ml THF, precipitated with 50 ml methanol. The product was vacuum filtered, and the resulting solid was dried at 50 °C under vacuum overnight.

7.4 Results and Discussion

Acyclic Diene Metathesis is a condensation polymerization of an α,ω -diene, which in this study was synthesized from a vinyl-terminated fatty acid, derived from the steam-cracking of castor oil, and shown in Figure 7.2. ADMET is an especially well-suited polymerization technique for fatty acids, which typically contain a high degree of unsaturation; ADMET polymerizations of fatty acid derivatives have yielded a wide array of polymers with different properties [13-15].

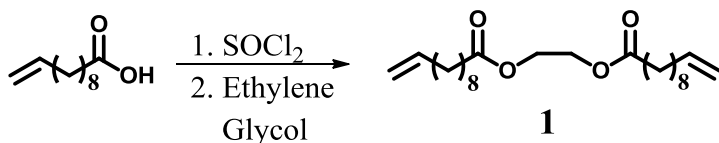


Figure 7.2. Synthesis of ADMET monomer.

The olefin metathesis catalyst Bis(tricyclohexylphosphine)benzylidene ruthenium dichloride, (1st generation Grubbs' catalyst), was used to perform the ADMET reaction. The polymerization was run at elevated temperatures and under vacuum in order to remove ethylene gas byproduct, hence driving the reaction to form polymer. All polymerizations (Figure 7.3) performed in this study were done in bulk (i.e. solvent-free) conditions.

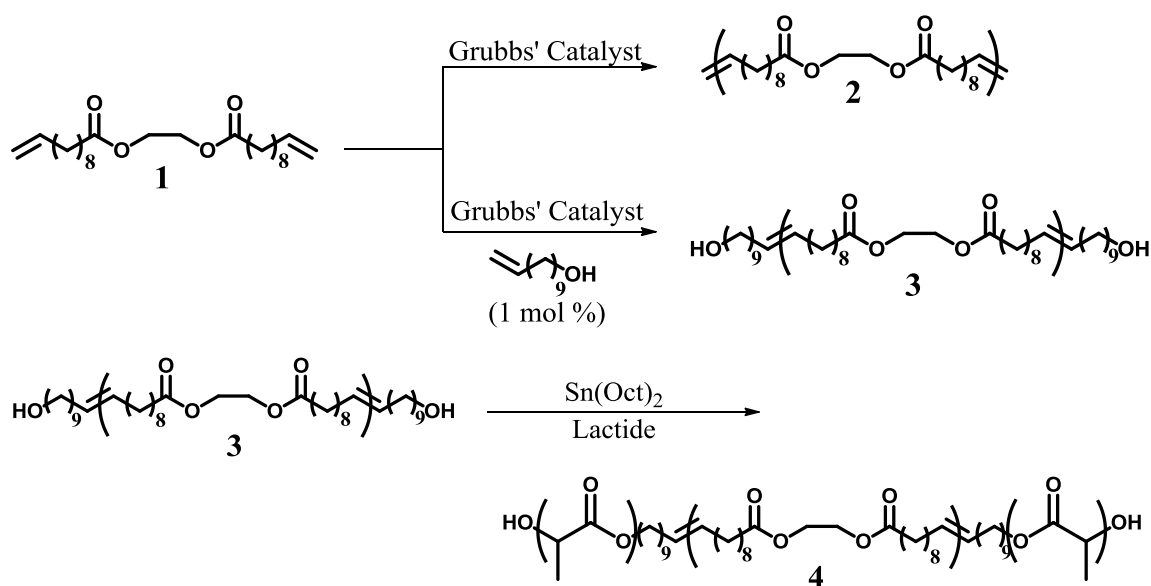


Figure 7.3. Synthesis of ADMET and triblock polymers.

Before attempting to form block copolymers, it was necessary to find the optimal conditions under which polymer 2 forms; Table 1 outlines these efforts. Yields for the ADMET polymerization were typically high (89-95%), and PDI values for most entries were moderately low (1.47-1.90) for step-growth polymerization mechanisms. Significant drop-offs in molecular weight were observed after 24 hours reaction time, presumably due to undesired cross-metathesis or back-biting reactions on the polymer chain once internal olefins began to significantly outnumber terminal olefins. Optimal reaction temperature was found to be 80 °C with significantly lower molecular weights and higher polydispersity indices above this temperature. Temperatures lower than 80 °C also yielded lower molecular weight polymers. The reason for this is related to the fact that once the polymer reaches a sufficient molecular weight, it begins to crystallize and therefore lacks the molecular mobility to further react. Visual inspection of entry 5 in table 1 clearly revealed that this polymer was a solid after ~1 hour reaction time, while all other entries existed as polymer melts throughout the course of the reaction. Hence, entry 3 in table 5 was chosen as the optimal reaction conditions and was used for all subsequent polymerizations.

Table 1. ADMET reaction optimization of **1**.

Trial	Rxn time (h)	Rxn temp. (°C)	Yield	M _n (g/mol)	PDI
1	2.5	80	86%	24700	1.90
2	6	80	89%	33500	1.89
3	24	80	90%	33700	1.81
4	48	80	90%	28500	6.82
5	24	70	93%	13400	1.47
6	24	90	95%	25500	1.47
7	24	100	91%	9400	2.23

The conversion of terminal monomer to internal polymer olefins allows for easy monitoring of the polymerization reaction via ¹H-NMR (Figure 7.4). Three proton peaks resulting from terminal olefins are observed in the ADMET monomer in the ranges of 5.73-5.86 (H_c of the monomer) and 4.89-5.04 ppm (H_a and H_b of the monomer). These peaks are absent in polymer **1** and are instead replaced with peaks representative of two internal vinylic protons (H_a and H_b of the polymer).

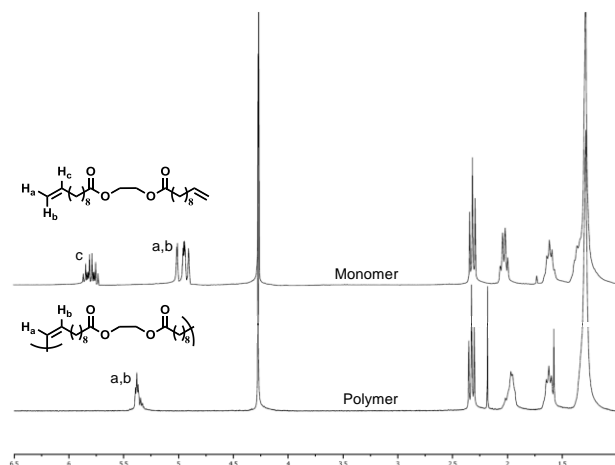


Figure 7.4. ¹H-NMR spectra (300 MHz, CDCl₃) of ADMET monomer (top spectra) and ADMET polymer (bottom spectra) with vinyl protons peaks assignments denoted as H_a, H_b, or H_c.

ADMET polymer **2** was characterized by Differential Scanning Calorimetry (DSC) and Thermogravimetry (TG), the results of which are summarized in Table 1. DSC revealed that polymer **1** is a semi-crystalline polymer, undergoing both a glass transition (42 °C) and a melting transition (55 °C). Thermogravimetry revealed good thermal stability, with only 5% weight by 388 °C.

Table 2. Molecular weight characterization and thermal properties for polymers **2**, **3** and **4**.

Polymer	M _n (g/mol)	PDI	T _g (°C)	T _m (°C)	T _D ^a (°C)
2	33700	1.81	42	55	388
3	28500	1.93	41	56	374
4	54600	2.14	42	55	331

In order to synthesize block copolymers, a telechelic polymer with endgroups capable of initiating polymerization mechanisms is needed. To achieve this, the ADMET polymerization was ran on **1** in the presence of 1 mol. % of a terminal monoene, (which can react via ADMET, end-capping the polymer) that also contained an alcohol (Figure 7.3), capable of initiating ring-opening polymerizations of cyclic esters [16]. The resulting polymer **3** had a slightly lower molecular weight and slightly higher PDI, which is expected for a polymerization containing an end-capping monoene. This drop in molecular weight was sufficiently small for our purposes, and polymer **3** was used for subsequent growth of block copolymer. Thermal properties of polymer **3** were very similar to polymer **2**.

From polymer **2**, triblock copolymers were formed under standard ring-opening polymerization (ROP) conditions of lactide monomer, yielding an ABA tri-block copolymer with roughly equivalent A- and B-block weight fractions (estimated from polymer **3**'s roughly double molecular weight of polymer **2**, shown in table 2). ¹H-NMR of the triblock copolymer in Figure 7.5 confirms structure of the two blocks. Interestingly, the DSC analysis of the triblock copolymer yielded nearly identical data as from the ADMET homopolymer. It is believe that the glass transition of the poly(lactic acid) blocks, which is

typically ~ 60 °C [17], is indeed present in the copolymer, but unobservable by DSC as it overlaps with the melting transition of the center, ADMET-based block. Poly(lactic acid) is generally known as a semi-crystalline polymer, with a melting temperature ranging from 130-180 °C [17], but no melting transition was observed at or near this temperature range.

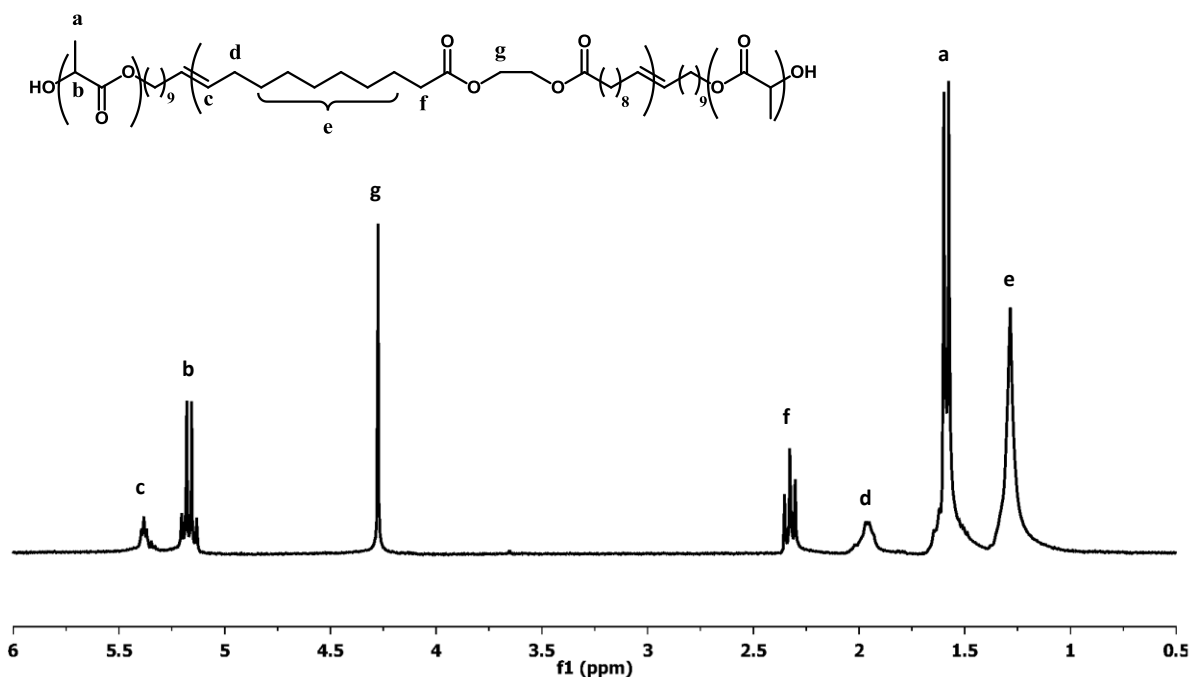


Figure 7.5. ^1H -NMR of triblock copolymer **3**.

7.5 Conclusions

ADMET polymerization of an α,ω -diene derived from a renewable resource (castor oil) was used to synthesize the center block of a triblock copolymer. The center block copolymer was synthesized in good yield to form a semi-crystalline polymer with a molecular weight of 33,700 g/mol. At the expense of a minor loss in molecular weight, the ADMET polymer was made in the presence of an end-capping monoene, which was able to form a telechelic polymer with endgroups capable of initiating further polymerization. Ring-opening polymerization of lactide was grown from these endgroups to synthesize an ABA triblock copolymer.

7.6 Acknowledgements

The authors kindly acknowledge Dr. Xia Sheng and Dr. Mahendra Thunga for their helpful discussions.

7.7 References

- [1] Spontak, R.J. and Patel, N.P. *Curr. Opin. Colloid Interface Sci.* **2000**, *5*, 334.
- [2] Baughman, T.W. and Wagener, K.B. *Adv. Polym. Sci.* **2005**, *176*, 1.
- [3] Bielawski, C.W. and Grubbs, R.H. *Prog. Polym. Sci.* **2007**, *32*, 1.
- [4] Kessler, M.R. and White, S.R. *J. Polym. Sci., Part A: Polym. Chem.* **2002**, *40*, 2373.
- [5] Nguyen, S.T.; Johnson, L.K. and Grubbs, R.H. *J. Am. Chem. Soc.* **1992**, *114*, 3974.
- [6] Nguyen, S.T. and Grubbs, R.H. *J. Am. Chem. Soc.* **1993**, *115*, 9858.
- [7] Wagener, K.B.; Boncella, J.M. and Nel, J.G. *Macromolecules* **1991**, *24*, 2649.
- [8] Wagener, K.B. and Smith, D.W. *Macromolecules* **1991**, *24*, 6073.
- [9] Schwendeman, J.E.; Church, A.C. and Wagener, K.B. *Adv. Synth. Catal.* **2002**, *344*, 597.
- [10] Marmo, J.C. and Wagener, K.B. *Macromolecules* **1993**, *26*, 2137.
- [11] Marmo, J.C. and Wagener, K.B. *Macromolecules* **1995**, *28*, 2602.
- [12] Jones, A.S.; Rule, J.D.; Moore, J.S.; White, S.R. and Sottos, N.R. *Chem. Mater.* **2006**, *18*, 1312.
- [13] Rybak, A. and Meier, M.A.R. *ChemSusChem* **2008**, *1*, 542.
- [14] Fokou, P.A. and Meier, M.A.R. *Macromol. Rapid Commun.* **2008**, *29*, 1620.
- [15] Fokou, P.A. and Meier, M.A.R. *J. Am. Chem. Soc.* **2009**, *131*, 1664.
- [16] O'Keefe, B.J., Hillymer, M.A. and Tolman, W.B. *J. Chem. Soc., Dalton Trans.* **2001**, 2215.
- [17] Drumright, R.E.; Gruber, P.R. and Henton, D.E. *Adv. Mater.* **2000**, *12*, 1841.

CHAPTER 8: GENERAL CONCLUSIONS

8.1 General Discussions

The first topic of this thesis reports on the investigation of a number of factors influencing the mechanism of self-healing with encapsulated healing additives. Self-healing is influenced by several kinetic events, such as polymerization kinetics of the encapsulated healing monomer, dissolution kinetics of catalyst in monomer, and diffusion of dissolved catalyst throughout the dynamic rheological environment of a polymerizing monomer. This thesis presents one of the first thorough investigations of all of these kinetic parameters, en route to the development of practical self-healing materials.

Initial efforts focused on manipulating the latency of the ring-opening metathesis polymerization (ROMP) of dicyclopentadiene with a ruthenium metathesis catalyst, which in a self-healing polymer could be used to allow for time for a buildup of other kinetic events, such as dissolution and diffusion of catalyst through monomer, prior to chemical reaction. An analogue of the 1st generation Grubbs' catalyst was prepared with a less labile coordinated ligand, which was shown to significantly delay the initiation of polymerization. Also, it was observed that, in the presence of a varying amount of free phosphine ligand, olefin metathesis could be tuned to a desired extent of latency.

A model was developed to predict the dissolution rates of Grubbs' catalyst in various ROMP-active monomers. This model, borrowing ideas from the concept of solubility parameters, was shown to be reasonably efficient in providing a quick and convenient method to design monomers and blends of monomers capable of rapid catalyst dissolution. It is expected that this model can aid in the selection of reactive "dissolution additives" to be combined with other healing monomers that are otherwise known to produce polymers possessing superior adhesive and mechanical properties. Successful implementation of this technique is expected to accelerated the healing process and promote a more efficient use of catalyst, both of which can aid in reducing the amount of potentially costly catalyst required self-healing polymers.

Finally, a novel rheokinetic technique was developed in which reaction progress of a monomer, as well as the resulting polymer's material properties, could be monitored in a

self-healing mimic environment. Our efforts in this technique were twofold. First, from a purely analytical perspective, we demonstrated the utility of this technique to identify various healing monomer properties under a wide variety of reaction conditions that could potentially be experienced in self-healing (e.g. different healing monomers, catalyst loadings, temperatures, crack sizes, etc.). Second, we used this technique to identify a previously unknown phenomenon affecting the self-healing mechanism—property gradients through thickness of polymerizing healing monomer, related to slow diffusion of catalyst from its source (i.e. the self-healing crack surface) throughout the monomer.

The second topic of this thesis involved the synthesis and characterization of polymers initially derived from vegetable oils. Early efforts demonstrated that a derivative of linseed oil, modified to contain norbornenyl groups, could be polymerized in the presence of an olefin metathesis catalyst to form a series of highly crosslinked thermoset polymers with ambient temperature storage moduli (~1 GPa), glass transition temperatures (70-125 °C) and decomposition temperatures (320-330 °C) comparable to petroleum-based plastics. Additionally, a new class of linear, telechelic biopolyester was developed from the acyclic diene metathesis (ADMET) polymerization of a modified vegetable. Synthesis of near fully bio-derived ABA triblock copolymers were formed by growth of poly(lactic acid) from the endgroups of the telechelic polymers.

8.2 Recommendations for future research

The implementation of self-healing polymers in commercial applications seems to be limited by a combination of the quality and economics of its healing chemistry. For example, ROMP with Grubbs'-type catalysts has always worked quite well as a healing chemistry since its inception [1], but incorporating ruthenium catalysts into large-scale polymer production paradigms is probably not economically feasible. Our hope is that the research presented herein has provided a basis for improvements in self-healing polymers that can, among other things, aid in the reduction of catalyst loadings, but olefin metathesis chemistry with ruthenium catalysts is still probably only limited to small, specialized applications. On the other hand, healing chemistries that are attractive from an economic standpoint, such as the ring-opening of epoxy resins and amine curing agents that are widely

available, often require reaction conditions (e.g. elevated temperatures, external agitation) unrealistic for practical applications [2-4]. Hence, the discovery and development of a new healing chemistry is the most logical recommendation for future research in this field.

In late 2007, we had the epiphany that a set of reaction characteristics presumed to be “ideal” for a self-healing chemistry was nearly identical to that of another chemical reaction methodology called “click” chemistry (Table 8.1), the initial report of which was coincidentally first published a mere few months prior to the first report of self-healing polymers [5]. Considering that “click” chemistry was, at that time, dominated by one specific reaction—the copper-catalyzed azide-alkyne [2+3] cycloaddition (CuAAC)—we proceeded to synthesize a variety of azide- and alkyne-based monomers and test these monomers’ reactivity in the presence of a copper catalyst under the solvent-free conditions that would be required in self-healing. These initial results were met with moderate success [6], but unfortunately azide substrates that were safe enough to isolate and handle neat exhibited unexpectedly slow bulk “click” reaction kinetics. While our interest has somewhat waned, others have followed our example and attempted to implement the CuAAC in self-healing polymers [7]. But perhaps identification of the ideal self-healing chemistry is intertwined with the fate of new fundamental discoveries in the field of “click” chemistry.

Table 8.1. Lists of reaction characteristics of the ideal healing agent chemistry (left column) and “click” chemistry (right column). Conceptually similar characteristics are marked with arrows. List contents were taken directly from seminal papers in both fields [1, 5].

<u>Healing chemistry requirements</u>	<u>“Click” chemistry requirements</u>
Quantitative yields ←	→ High-yielding reactions
Ambient and sub-ambient reactivity ←	→ Reactive in ambient conditions
Bulk polymerization ←	→ No or benign (e.g. water) solvents
Rapid polymerization ←	→ Fast reaction kinetics
Non-condensation polymerization ←	→ Minimal or inoffensive byproducts
Long shelf life	Harmless reagents
Low viscosity, volatility	High atom economy

With regards to the second part of this project, it is recommended that efforts be refocused on yielding useful polymers and composite materials ultimately derived from highly sustainable vegetable oils (e.g. soy and corn oil in North America, palm oil in Asia, etc.). The work presented in this thesis uses linseed oil (chapter 6) and castor oil (chapter 7) as sources, each of which do have their own commercial niche, but are produced on considerably smaller scales than some other plant oils. Although the plant oils used here are extremely attractive in that they have high olefin contents (linseed oil) and some synthetically useful naturally occurring functional groups (castor oil contains hydroxyl groups), wide scale use of these oils may still be limited by relatively low worldwide production levels. Conversely, production of polymers from more abundant vegetable oils would probably require more elaborate synthetic routes towards useful monomer, but large-scale use of these oils in the polymer industry would converge, and not conflict, with worldwide trends of agricultural oil production that, for example, has seen roughly 10-fold increases in soy and palm oil over the last 30 years [8].

8.3 References

- [1] White, S.R.; Sottos, N.R.; Geubelle, P.H.; Moore, J.S.; Kessler, M.R.; Sriram, S.R.; Brown, E.N. and Viswanathan, S. *Nature* **2001**, *409*, 794.
- [2] Rong, M.Z.; Zhang, M.Q. and Zhang W. *Adv. Compos. Lett.*, **2007**, *16*, 167.
- [3] Yin, T.; Rong, M.Z.; Zhang, M.Q. and Yang, G.C. *Compos. Sci. Technol.*, **2007**, *67*, 201.
- [4] Yin, T.; Rong, M.Z.; Zhang, M.Q. and Zhao, J.Q. *Smart Mater. Struct.*, **2009**, *18*, 1.
- [5] Kolb, H.C.; Finn, M.G. and Sharpless, K.B. *Angew. Chem. Int. Ed.* **2001**, *40*, 2004.
- [6] Sheng, X.; Mauldin, T.C. and Kessler, M.R. *J. Polym. Sci., Part A: Polym. Chem.* **2010**, *48*, 4093.
- [7] Gragert, M.; Schunack, M. and Binder, W.H. *Macromol. Rapid Commun.* **2011**, *32*, 419.
- [8] United States Department of Agriculture – foreign agricultural service. Production, supply and distribution online. <http://www.fas.usda.gov/psdonline/> (accessed Sep 01, 2004).

APPENDIX A: SUPPLEMENTARY INFORMATION FOR CHAPTER 4

A.1 Calculation of Norbornene's Group Contributions

The four Beerbower “group contributions” of norbornene are identical to the four corresponding cohesive energies of norbornene (E_T , total cohesive energy; E_D , cohesive energy related to dispersion forces; E_P , cohesive energy related to fixed dipole forces; and E_H , cohesive energy related to hydrogen bonding forces), which were determined using previously established methods [1]. Their calculation is detailed in the subsections below:

A.2 Calculation of E_T for norbornene

Total cohesive energy, E_T , is defined as the energy of vaporization (ΔE_{vap}), which can be calculated from enthalpy of vaporization (ΔH_{vap}) at room temperature using equation A.1 (where R is the ideal gas constant and T is room temperature, taken as 25 °C).

$$E_T = \Delta E_{\text{vap}} = \Delta H_{\text{vap}} - RT \quad (\text{A.1})$$

Enthalpy of vaporization (ΔH_{vap}) was measured with a differential scanning calorimeter (DSC, Model Q20, TA instruments). All DSC experiments were conducted under a flow of nitrogen gas at a constant rate of 50 ml/min. In a typical experiment approximately 10 mg of solid monomer was loaded into a DSC sample pan, and the pan was covered and pressed with a sample lid containing a pinhole-sized puncture. A dynamic scan was performed on the sample at a heating rate of 40 K/min over a temperature range of 50 °C – 175 °C. The average of 5 experiments yielded a ΔH_{vap} for norbornene of 292 ± 13.2 J/g. Then, E_T was determined from equation S4.1 to be 28.55 ± 1.4 kJ/mole.

A.3 Calculation of E_D for norbornene

The cohesive energy related to dispersion forces for a chemical is defined as the total cohesive energy for that chemical's homomorph (saturated, hydrocarbon analogue). Hence, the same DSC measurements outlined above for calculating the total cohesive energy for norbornene was applied to norbornene's homomorph—norbornane (Aldrich, used as

received). For norbornane, ΔH_{vap} was measured as 268 ± 4.0 J/g, and E_D for norbornene was then determined to be 26.85 ± 0.4 kJ/mole. A typical DSC plot showing the vaporization of norbornene and norbornane is shown in Figure A.1.

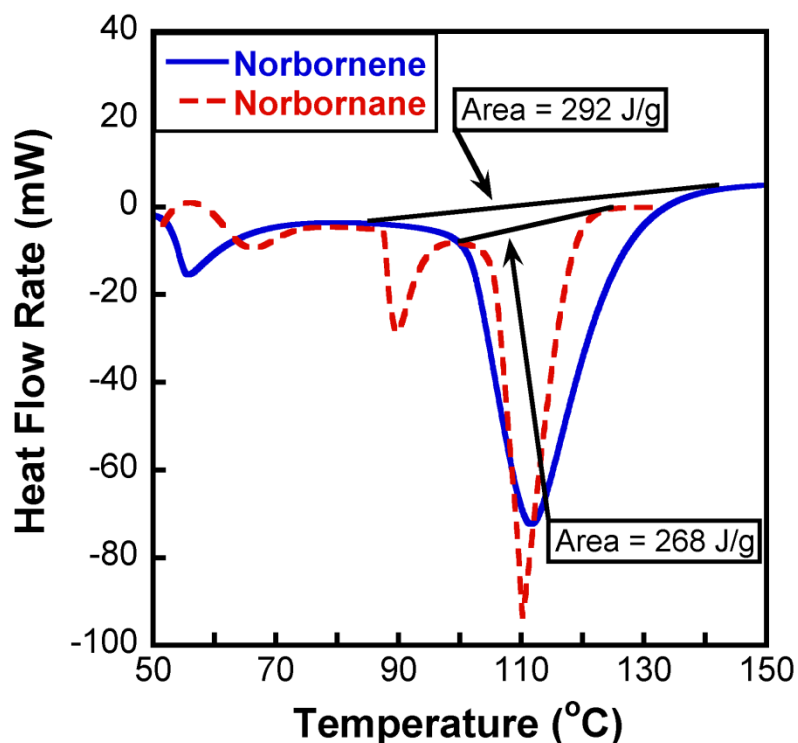


Figure A.1. Vaporization of norbornene and norbornane measured by DSC. The enthalpy of vaporization (ΔH_{vap}) is defined as the area under the endothermic vaporization peak, denoted by arrows.

A.4 Calculation of E_p for norbornene

E_p of a chemical is conveniently calculated by the Hansen-Beerbower equation:

$$E_p = 1398.76 \cdot \mu^2 \quad (\text{A.2})$$

where μ is the chemical's dipole moment and the constant 1398.76 gives the parameter in SI units. With a dipole moment of 0.396 D [2], E_p for norbornene was calculated to be 0.22 kJ/mole.

A.5 Calculation of E_H for norbornene

There is no way to directly measure E_H for a chemical. Instead, E_H is generally determined by first calculating the other three cohesive energy densities (E_T , E_D , and E_P) and using equation A.3.

$$E_T = E_D + E_P + E_H \quad (\text{A.3})$$

E_H was determined to be 1.47 kJ/mole.

A.6 Summary

E_x	Equation	Value (kJ/mole)	E_x/V (MPa)	δ_T (MPa ^{1/2})
E_T	$E_T = \Delta E_{\text{vap}} = \Delta H_{\text{vap}} - RT$	28.55 ± 1.4	256.2	16.0
E_D	$E_D = \Delta E_{\text{vap,norbornane}} = \Delta H_{\text{vap,norbornane}} - RT$	26.85 ± 0.4	241.0	15.5
E_P	$E_P = 1398.76 \cdot \mu^2$	0.22	2.0	1.4
E_H	$E_T = E_D + E_P + E_H$	1.47	13.2	3.7

A.7 References

- [1] Hansen, C.M. *Hansen Solubility Parameters: A User's Handbook*, 2nd ed.; CRC Press: Boca Raton, FL, 2007
- [2] TOPAS Advanced Polymers Technical Datasheet for norbornene

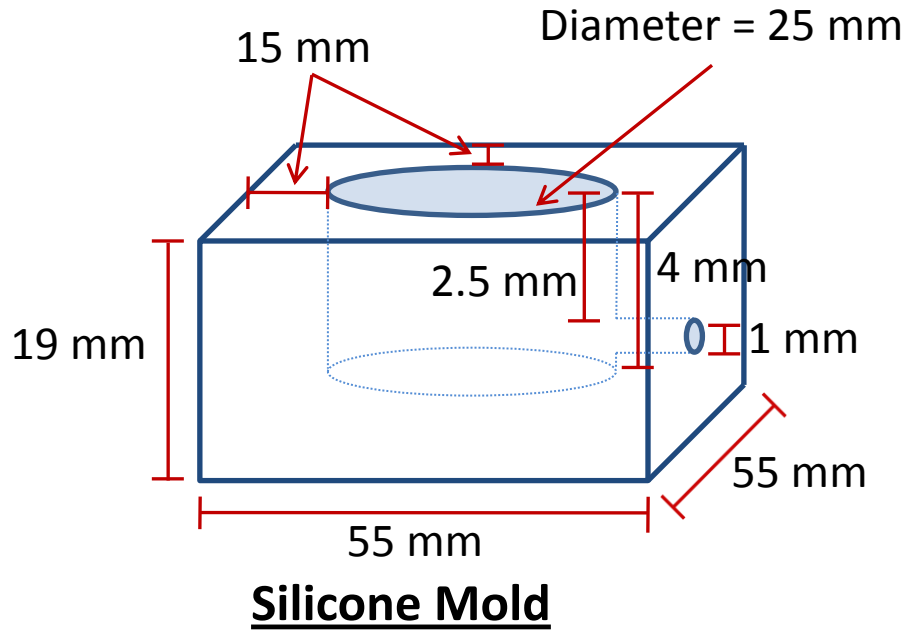
APPENDIX B: SUPPLEMENTARY INFORMATION FOR CHAPTER 5

Figure B.1. Schematics of custom designed mold to coat rheometer bottom parallel plate.

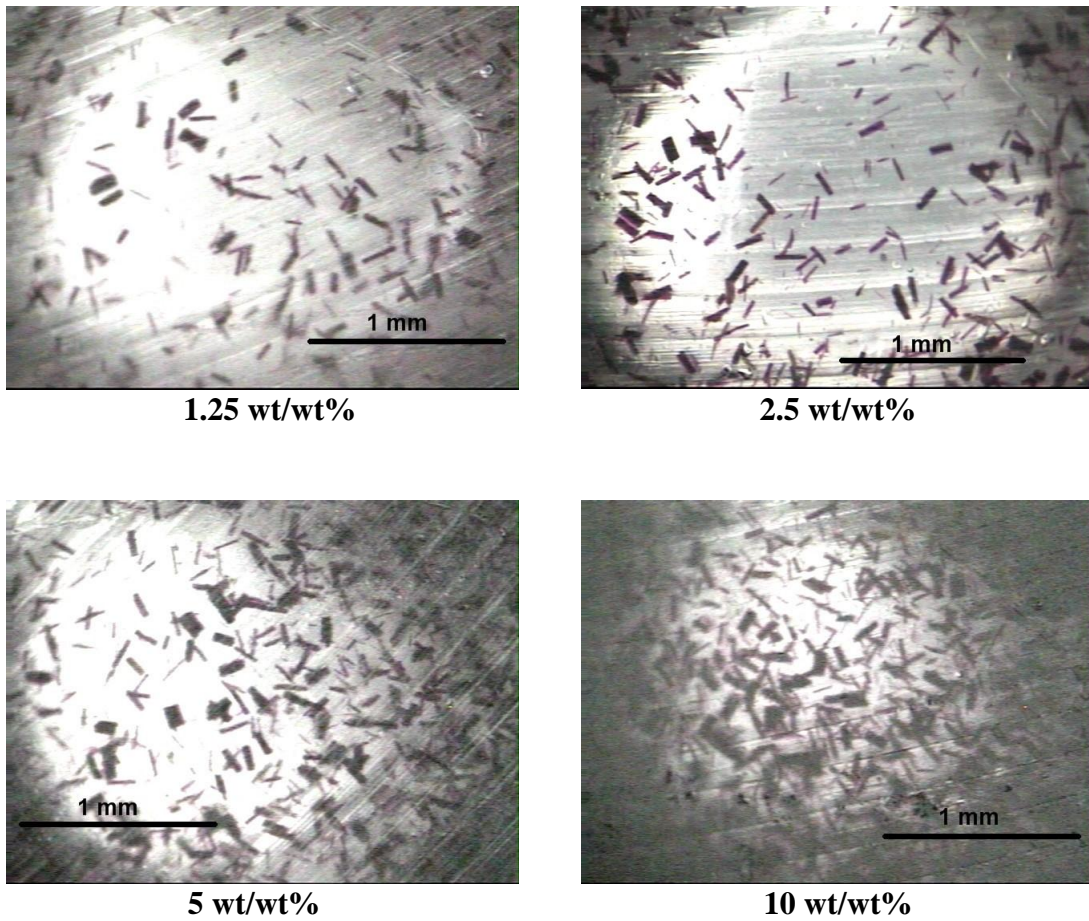


Figure B.2. Dispersion of various loadings of 1st Generation Grubbs' Catalyst in fully cured epoxy polymer.

APPENDIX C: SUPPLEMENTARY INFORMATION FOR CHAPTER 6

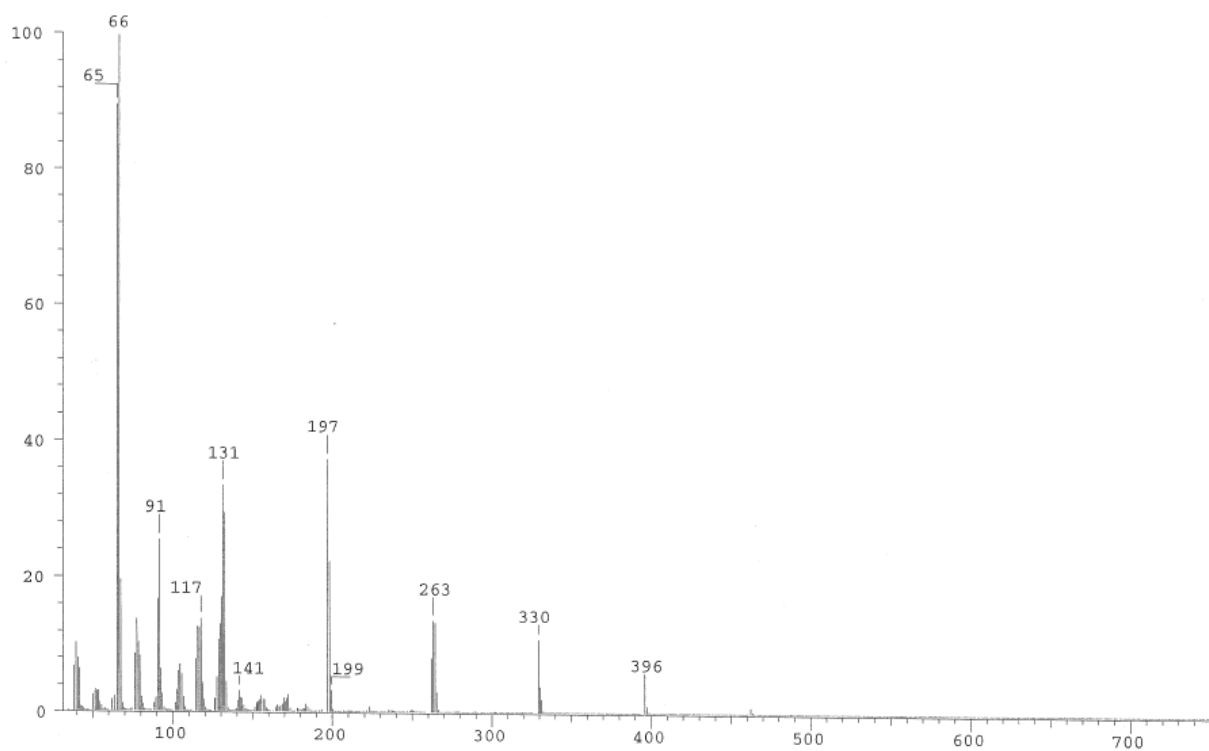


Figure C.1. EI-MS of the CPD oligomers isolated from Dilulin

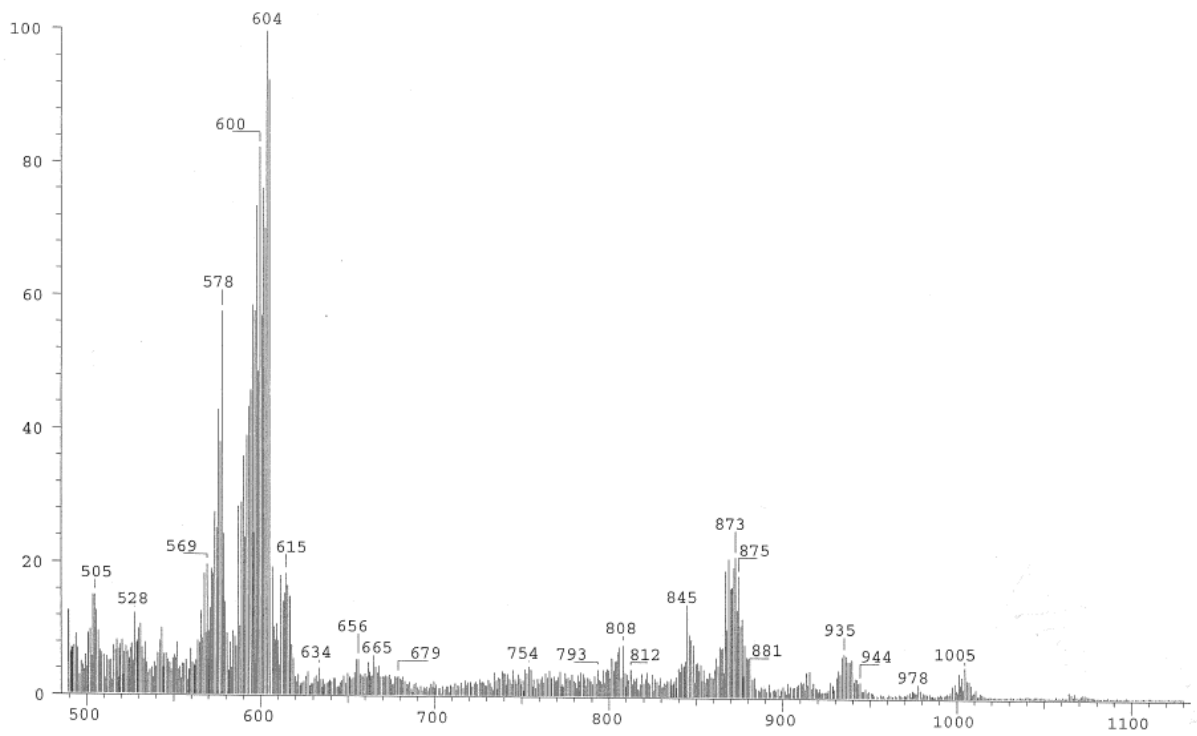


Figure C.2. EI-MS of the oil fraction isolated from Dilulin.

**APPENDIX D: DIFFERENTIAL SCANNING CALORIMETER-BASED CURING
KINETIC ANALYSES OF THE RING-OPENING METATHESIS
POLYMERIZATION OF SUBSTITUTED NORBORNENYL DERIVATIVES.**

D.1 Introduction

Successful completion of the work presented herein, especially chapters 3-5, required a general knowledge of the bulk reaction kinetics of various ring-opening metathesis (ROM)-based monomers. Differential scanning calorimetry (DSC), which can measure heat evolution as a function of time or temperature, is a well-suited technique to achieve this goal. Hence, reaction kinetics of a small library of norbornenyl-based monomers (chosen for their typical high reactivity towards ROM) was monitored by DSC. The monomers studied here, shown in Figure D.1, were selected on the basis of their physical properties (liquids at ambient temperature were favored over solids, for ease of sample processing) and known functional group compatibilities with Grubbs' olefin metathesis catalyst. Reaction kinetics was monitored via the Ozawa-Flynn-Wall Isoconversional model free method [1, 2], described in more detail below.

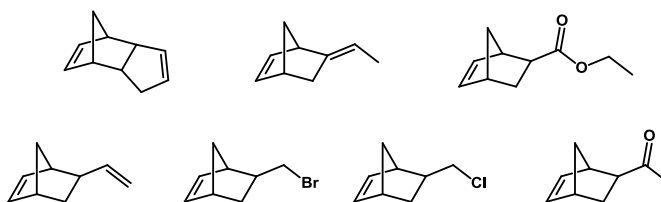


Figure D.1. Chemical structures of monomers used in this study.

D.2 Experimental

D.2.1 General Considerations

Dicyclopentadiene, 5-ethylidene-2-norbornene, 5-vinyl-2-norbornene, and Bis(tricyclohexylphosphine)benzylideneruthenium dichloride (1st generation Grubbs' catalyst) were purchased from Aldrich and used as-received. Literature procedures were used to prepare 2-(chloromethyl)-5-norbornene [3], 2-(bromomethyl)-5-norbornene [4], ethyl

5-norbornene-2-carboxylate [5], and 2-acetyl-5-norbornene [6] without modification. Prior to use, Grubbs' catalyst was freeze-dried [7] to aid in rapid dissolution in all monomers.

D.2.2 General DSC technique

Liquid monomer was added to the 1st generation Grubbs' catalyst at a loading of 2mg/ml. Catalyst was able to completely dissolve in monomer by the end of monomer addition. The solution was immediately flash-frozen in liquid nitrogen. A small amount of the resulting solid was slightly melted to remove sample for experiments and refrozen in liquid nitrogen between tests. Samples were loaded into a DSC (Model Q20, TA Instruments) at a standby temperature of -50 °C. DSC experiments for all catalyst systems were under a flow of nitrogen at a constant rate of 50 ml/min. Dynamic curing experiments were performed over a temperature range of -50 to 200 °C at heating rates of 5, 10, 15, and 20 K/min.

D.2.3 Ozawa-Flynn-Wall Isoconversional Model Free analysis

Degree of cure (α) measured by differential scanning calorimetry is defined as the fraction of heat or enthalpy at a given time:

$$\alpha = \Delta H_t / \Delta H_{\text{rxn}} \quad (\text{D.1})$$

where ΔH_t is the heat evolved at time t and ΔH_{rxn} is the total heat evolution during the curing process. Curing kinetics can then be modeled using the typical curing equation

$$\delta\alpha/\delta t = k(T) f(\alpha) \quad (\text{D.2})$$

that includes reaction model $f(\alpha)$ and the temperature-dependant rate constant $k(T)$. The latter can be further expanded

$$k = A e^{(E_a/RT)} \quad (\text{D.3})$$

to reveal the activation parameters A (pre-exponential factor) and E_a (activation energy). The isoconversional model-free approach assumes that both of these activation parameters are a function of degree of cure (α), and they can be calculated by performing dynamic DSC scans and monitoring how the temperature to reach different degrees of cure changes with different heating rates. To achieve this, Ozawa [8] and Flynn and Wall [9] developed an approach by which equation D.2 is integrated, and the resulting integral partially solved to give an equation of the form:

$$\ln \beta = -1.052(E_a/RT_i) + C \quad (\text{D.4})$$

where β is the heating rate, T_i is the temperature required to reach a specific conversion, and C is a combination of other terms, including the pre-exponential factor (A). At a given conversion i , a plot of $\ln \beta$ vs. $1/T_i$ over all heating rates then yields a straight line with a slope proportional to E_a .

D.3 Results

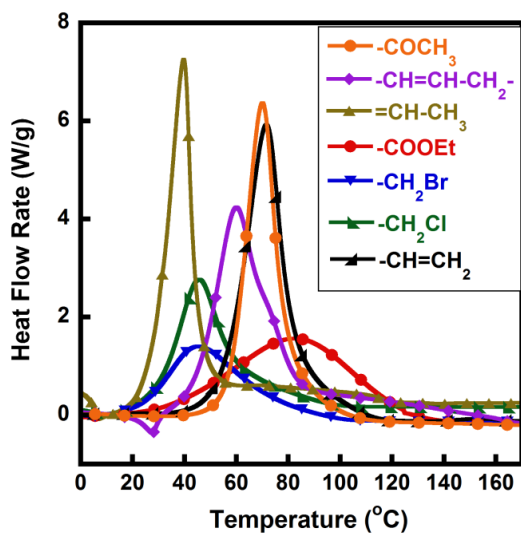


Figure D.2. Heat evolution of various ROMP-active monomers measured by DSC. Each plot represents a 2-norbornene derivative functionalized in the 5-position with the chemical moiety listed in the legend. Data shown represents the dynamic scan at 10 K/min.

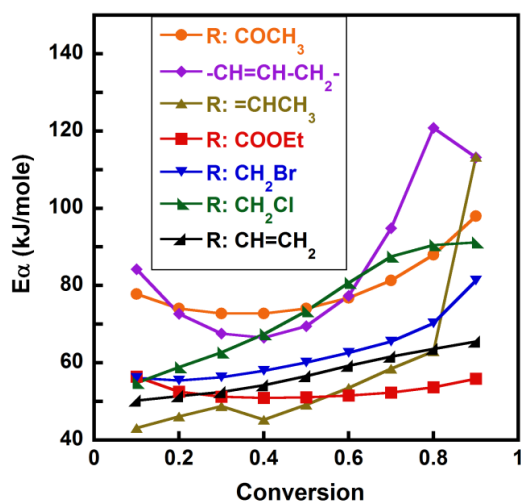


Figure D.3. Conversion-dependant activation energy (E_{α}) for various ROMP-active monomers, determined by the Ozawa-Flynn-Wall approach. Each plot represents a 2-norbornene derivative functionalized in the 5-position with the chemical moiety listed in the legend.

D.4 Conclusions

Based on the above results, dicyclopentadiene, 5-ethylidene-2-norbornene, 2-(bromomethyl)-5-norbornene and 2-(chloromethyl)-5-norbornene were identified as monomers with relatively rapid reaction kinetics. Given that bulk reaction kinetics is linked to the speed of healing in self-healing polymers (see Chapter 2.3.1), these monomers were chosen for additional screening in Chapter 5. Also chosen for further screening in Chapter 5 was ethyl 5-norbornene-2-carboxylate, due to its slower reaction kinetics, for proof of concept of the technique described in that chapter. All monomers were selected for use in Chapter 4, in which a moderately sized norbornenyl-derivative library was necessary for experimentation.

D.5 References

- [1] Ozawa, T. *Bull. Chem. Soc. Jpn.* **1965**, 38, 1881.
- [2] Flynn, J.H. and Wall, L.A. *Polym. Lett.* **1966**, 4, 323.

- [3] Freeman, P.K.; Rao, V.N. Mallikarjuna.; George, D.E. and Fenwick, G.L. *J. Org. Chem.* **1967**, *32*, 3958-3963.
- [4] Dolman, S.J.; Hultsch, K.C.; Pezet, F.; Teng, X.; Hoveyda, A.H. and Schrock, R.R. *J. Am. Chem. Soc.* **2004**, *126*, 10945-10953.
- [5] Ponticello, I.S. *J. Polym. Sci., Polym. Chem. Ed.* **1979**, *17*, 3509-3518.
- [6] Beslin, P.; Lagain, D.; Vialle, J. and Minot, C. *Tetrahedron Lett.* **1981**, *37*, 3839-3845.
- [7] Jones, A.S.; Rule, J.D.; Moore, J.S.; White, S.R. and Sottos, N.R. *Chem. Mater.* **2006**, *18*, 1312.
- [8] T. Ozawa, *Bull. Chem. Soc. Jpn.*, 38 (1965) 1881.
- [9] J.H. Flynn and L.A. Wall, *Polym. Lett.*, 4 (1966) 323.